ISTANBUL TECHNICAL UNIVERSITY ★ GRADUATE SCHOOL OF SCIENCE ENGINEERING AND TECHNOLOGY

AN INVESTIGATION ON STRUCTURAL IDENTIFICATION (ST-ID) OF A LONG-SPAN BRIDGE FOR PERFORMANCE PREDICTION

Ph. D. THESIS

Selçuk BAŞ

Department of Civil Engineering

Structural Engineering Programme

JUNE 2017

ISTANBUL TECHNICAL UNIVERSITY ★ GRADUATE SCHOOL OF SCIENCE ENGINEERING AND TECHNOLOGY

AN INVESTIGATION ON STRUCTURAL IDENTIFICATION (ST-ID) OF A LONG-SPAN BRIDGE FOR PERFORMANCE PREDICTION

Ph. D. THESIS

Selçuk BAŞ
(501122009)

Department of Civil Engineering

Structural Engineering Programme

Thesis Advisor: Prof. Dr. Alper İLKİ
Thesis Co-Advisor: Assoc. Prof. Dr. Nurdan M. APAYDIN

JUNE 2017

İSTANBUL TEKNİK ÜNİVERSİTESİ ★ FEN BİLİMLERİ ENSTİTÜSÜ

UZUN AÇIKLIKLI BİR KÖPRÜNÜN PERFORMANS TAHMİNİ İÇİN YAPISAL TANILANMASI ÜZERİNE BİR ARAŞTIRMA

DOKTORA TEZİ

Selçuk BAŞ
(501122009)

İnşaat Mühendisliği Anabilim Dalı

Yapı Mühendisliği Programı

Tez Danışmanı: Prof. Dr. Alper İLKİ
Eş Danışman: Doç. Dr. Nurdan M. APAYDIN

HAZİRAN 2017

Selçuk BAŞ, a Ph.D. student of ITU Graduate School of Science, Engineering and Technology student ID 501122009, successfully defended the dissertation entitled "AN INVESTIGATION ON STRUCTURAL IDENTIFICATION (ST-ID) OF A LONG-SPAN BRIDGE FOR PERFORMANCE PREDICTION", which he prepared after fulfilling the requirements specified in the associated legislations, before the jury whose signatures are below.

Thesis Advisor:	**Prof. Dr. Alper İLKİ** Istanbul Technical University	.....
Co-advisor:	**Assoc. Pof. Dr. Nurdan M. APAYDIN** General Directorate of Turkish State Highways	.....
Jury Members:	**Assoc. Prof. Dr. A. Necmettin GÜNDÜZ** Istanbul Technical University	.....
	Prof. Dr. Kutlu DARILMAZ Istanbul Technical University	.....
	Prof. Dr. F. Necati ÇATBAŞ University of Central Florida	.....
	Prof. Dr. Metin AYDOĞAN Istanbul Technical University	.....
	Prof. Dr. Hilmi LUŞ Boğaziçi University	.....

Date of Submission : 05 June 2017
Date of Defense : 21 June 2017

To my spouse and my little baby for their endless support, understanding and patience

To my mother and father for their endless support and encouragement

FOREWORD

First and foremost, I would like to express my deepest gratitude and my thanks to my supervisor, Dr. Alper İlki, co-advisors Dr. Nurdan M. Apaydın and Dr. F. Necati Çatbaş for their unending supports, guidance, recommendations and friendships throughout the PhD study. For publishing articles and the collaboration with internationally distinguished researchers and highly renowned professional engineers in the field of bridge and structural engineering, I would also like to state my additional special thanks to Dr. Nurdan M. Apaydin and Dr. F. Necati Çatbaş. Without their invaluable mentorship and experiences on bridge engineering, this study would not be possible.

I am also thankful to the members of my dissertation committee, Dr. A. Necmettin Gündüz and Dr. Kutlu Darılmaz for their instructive comments and recommendations that provide to make this study relatively qualitative. Besides, I would like to greatly appreciate Dr. Ebru Harmandar and Dr. Mustafa Gül for their recommendations, helps and feedbacks.

Finally, many gratefully special thanks to my mother and father for their gratuitous supports and endless understanding in my life. And last, but most certainly not least, I would like to express my deepest love and gratitude to my lovely family: my spouse Seda and my little baby Berra for their endless supports, patience and encouragements in several difficult times of this study.

Thanks to you all in my life…

June 2017

Selçuk BAŞ
Structural Engineer

TABLE OF CONTENTS

Page

ABBREVIATIONS

ANNs : Artificial Neural Networks
ASTM : American Standards for Testing and Material
ATH : Acceleration Time-History
AVT : Ambient Vibration Test
CAD : Computer-aided Design
DD-1 : Earthquake level with a 2 % probability of exceedance in 50 years corresponding to return period of 2475 years.
DD-2 : Earthquake level with a 10 % probability of exceedance in 50 years corresponding to return period of 475 years.
DOF : Degree-Of-Freedom
DTH : Displacement Time-History
EQ : Earthquake
FE : Finite Element
FEM : Finite Element Model
FFT : Fast Fourier Transform
FINSIM : FINite fault SIMulation program
GPS : Global Positioning System
H30-S24 : Heavy Truck Load for Bridges
KGM : General Directorate of Turkish State Highways
LL : Live Load
LRFD : Load and Resistant Factor Design
LVDT : Linear Variable Differential Transformer
Mp : Multi-point Earthquake Analysis/Multi-point Earthquake Motion
NNL : Non-Linear
NNLGEO : Non-linear Geometric Analysis
PSD : Power Spectral Density
SHM : Structural Health Monitoring
St-Id : Structural Identification
Sys-Id : System Identification
Up : Uniform-point Earthquake Analysis/Uniform-point
TMDs : Tuned Mass Dampers
WASHMS : Wind and Structural Health Monitoring System

SYMBOLS

a_0	: Combination constant for Mass Matrix
a_1	: Combination constant for Stiffness Matrix
[c]	: Damping matrix
f	: Frequency
F_{sample}	: Sampling frequency
F_s	: Local site effect coefficient for S_s
F_1	: Local site effect coefficient for S_1
[k]	: Stiffness matrix
L_w	: Window length
[m]	: Mass matrix
M_{xy}	: Yield bending moment in x-direction
M_{xp}	: Plastic bending moment in x-direction
M_{yy}	: Yield bending moment in y-direction
M_{yp}	: Plastic bending moment in y-direction
P_c	: Axial force
S_{ae}	: Elastic design spectral acceleration (g)
S_s	: Short period spectral accelaration constant
S_{DS}	: Design spectral acceleration constant for short period range
S_1	: T=1.0 s period spectral acceleration constant
S_{D1}	: Design spectral acceleration constant for 1.0 sec period range
T	: Period
T_A	: Corner period of elastic design spectrum
T_B	: Corner period of elastic design spectrum
ω_i, ω_j	: i^{th} and j^{th} mode angular frequency
Δ_f	: Frequency resolution
γ_f	: Near-fault constant
ξ	: Damping ratio
ζ_i, ζ_j	: i^{th} and j^{th} mode damping ratio
$\sigma_{monitored}$	: Monitored stress
σ_{design}	: Design stress

LIST OF TABLES

Page

LIST OF FIGURES

Page

AN INVESTIGATION ON STRUCTURAL IDENTIFICATION (ST-ID) OF A LONG-SPAN BRIDGE FOR PERFORMANCE PREDICTION

SUMMARY

Of all the civil infrastructures, long-span cable-supported bridges are the lifeline structures for the transportation network in a country/state. These bridges are not only a substantial component in transportation system, but also offer a respectable contribution to economic and cultural growth of their regions. Compared to other infrastructures, long-span bridges are not budget-friendly transportation items. Along with the construction cost, the cost of maintenance, management, and safety of long-span bridges is also relatively high. Many long-span bridges in service may also be vulnerable to various unpredicted load events and environmental conditions. Comprehensive investigations on long-span bridges therefore needs to be conducted before and after construction. Structural Identification (St-Id) presents an effective solution to better structural assessment of long-span bridges utilizing Structural Health Monitoring (SHM) data. This approach provides the bridge authorities/owners with an integrated concept consisting of six-step framework: (i) visualization and conceptualization (ii) priori modeling (iii) experimentation (iv) data analysis (v) calibration/verification analysis (vi) utilization. Even though containing limitations, uncertainties and challenges in each step, St-Id process yields to significant decision making-based outcomes for long-span bridges.

The main aim of the dissertation is to make a comprehensive investigation on structural response of the long-span bridges in Turkey adopting the integrated approach of St-Id. For this objective, the Boshporus Suspension Bridge is considered as a real-life civil infrastructure in this dissertation. Based on the conclusions of the investigation on the Bosphorus Bridge, it is also aimed to present a framework for integrated solution to safety and proper structural condition assessment of other existing or new long-span bridges in Turkey. In the first part of the dissertation, the first two steps of St-Id, which are visualization / conceptualization and priori modeling, are presented. For this aim, original project drawings, retrofit projects and experiences from the bridge's official authority KGM (General Directorate of Turkish State Highways) are identified and compiled properly. Taking these documents and experiences into consideration, an elaborate study is conducted to establish priori finite element model (FEM) of the bridge.

Based on the conclusions obtained from the analyses results of the priori model, more advanced FE models of improved spine-beam and 3-D full-scale shell are developed for further investigations on the bridge. In this section of the dissertation, similar efforts are also made for FE modeling of the bridge with vertical hangers. For this purpose, the hanger replacement project considerations that also include certain retrofitting works are precisely specified. New locations of vertical hangers at the deck and main cables are first determined. Besides, physical and technical properties of new rocker bearings, wind tongues, viscous dampers and tower base-section retrofitting are presented in detail. Considering these specifications, improved spine-beam and 3-D

full-scale shell FE model of the Bosphorus Bridge with inclined and vertical hangers are prepared to perform the modal analysis. Making a comparison between the results of the FE models, updates for the models and vertical hanger effects are determined in terms of natural vibration frequency. In the second part of this dissertation, the SHM system of the Bosphorus Bridge is presented in detail in accordance with the requirements of St-Id approach in order to conduct the second steps of St-Id: experimentation and data analysis. General design considerations, monitoring objectives and parameters of the SHM system are clarified depending on the bridge's own characteristics. The monitoring specifications of the bridge are also determined to be in close agreement with those of the well-known long-span bridges in Hong Kong and Japan. Considering these specifications and recommendations of the KGM, critical points and components to be monitored are specified and preliminary performance criteria is proposed for the Bosphorus Bridge. For data analysis, the extreme wind event is considered. Before the data analysis, this event is accurately identified and presented. Depending on the preliminary results, the need to develop a new Matlab code for averaging extreme wind data is stated. The frequency-domain results are then obtained to be clear and the first nine dominant (deck and tower modes) modes of the bridge are identified. Moreover, influence of the extreme wind event on the bridge is determined on the basis of its dynamic properties through SHM data. The last part of the dissertation includes updating of the developed FE models with the experimental frequencies obtained from the extreme wind event through the SHM system and the utilization for seismic performance prediction of the bridge under the multi-point scenario earthquake motion.

The conclusions obtained from St-Id process of the Bosphorus Bridge indicate that the developed FE models can be utilized for advanced analysis and investigations of the bridge. Particularly, the updated 3-D full-scale shell model of the bridge can be considered for various further objectives. The Bosphorus Bridge is determined to show elastic performance under the extreme wind load based on the comparative experimental results obtained from "During" and "After" data analysis. Visual inspection of the Power Spectral Densities (PSDs) of the dynamic response also demonstrates an increase in the damping capacity of the lateral mode under the extreme wind load. This increase can be attributed to activated friction at the expansion joints and the change in the boundary conditions of the rocker bearings that restrained lateral movement. From the multi-point and uniform-point earthquake analyses under the scenario earthquakes for Istanbul, the bridge with both inclined and vertical hangers is not likely to be damaged and no repair and strengthening intervention can be required for the bridge. Under the DD-1 spectrum compatible earthquakes, damage is estimated for the tower base-section and approach viaduct box-section of the bridge with both inclined and vertical hangers. For retrofit strategy, sectional capacity is recommended to be increased with additional longitudinal stiffener of doubly symmetric W100x499 I-beam. The comparative results also yield to necessity of the consideration of the multi-point earthquake analysis rather than the uniform-point earthquake analysis. Using simplified approach, structural response of the bridge to the multi-point earthquakes is identified with the deck and tower vibration modes.

Some recommendations are also made depending on the outcomes of the detailed analyses. With the increase in the number of long-span bridges in Turkey, especially in Istanbul, there is need for a command center where the all SHM systems are integrated for rapid decision-making. Due to high seismicity of Istanbul, the connection of the earthquake warning system with the SHM systems of the bridges

and other important infrastructures should also be integrated. Along with the preliminary attempt to determine the operational performance criteria of the Bosphorus Bridge in this dissertation, developing extended SHM-based operational performance criteria is also necessary to take preventive measures for operational and extreme load events.

UZUN AÇIKLIKLI BİR KÖPRÜNÜN PERFORMANS TAHMİNİ İÇİN YAPISAL TANILANMASI ÜZERİNE BİR ARAŞTIRMA

ÖZET

Tüm inşaat mühendisliği alt yapıları içinde kablo destekli uzun açıklıklı köprüler, bir ülkenin veya bölgenin ulaşım ağı için hayati öneme sahip yapılardır. Bu tür köprü yapıları ulaşım sisteminin önemli bir parçası olmasının yanı sıra aynı zamanda bulundukları şehirlere/bölgelere önemli düzeyde kültürel ve ekonomik katkı da sağlamaktadır. Diğer inşaat mühendisliği yapıları ile karşılaştırıldığında ise, uzun açıklıklı köprüler bütünsel olarak maliyetli yapılardır. Yapım maliyetinin yanı sıra, bu köprülerin bakım, yönetim ve yapısal güvenlik maliyetleride oldukça yüksektir. Aynı zamanda, hali hazırda hizmet veren birçok uzun açıklıklı köprülerin beklenmedik çeşitli yükleme durumlarında ve çevre şartlarına karşı güvenliği yeterli olmayabilir. Bu yüzden, uzun açıklıklı köprülerin yapım öncesi ve sonrası için detaylı ve geniş ölçekli teknik araştırmaların yürütülmesine ihtiyaç vardır. Yapısal Tanılama (St-Id) yaklaşımı, Yapısal Sağlık İzleme (SHM) sistemi yardımıyla uzun açıklıklı köprülerin çok daha iyi yapısal değerlendirilmesi için etkin bir çözüm sunmaktadır. Bu yaklaşım uzun açıklıklı köprülerin yönetiminden sorumlu kurumlara/yetkililere altı aşamadan oluşan bütünleştirilmiş bir konsept sağlamaktadır: (i) görselleştirme/somutlaştırma, (ii) ön modelleme, (iii) deney çalışması, (iv) veri analizi, (v) kalibrasyon/doğrulama analizi ve (vi) kullanma/yararlanma. Bunlardan ilk beş aşama istenilen amaç doğrultusunda yararlanılacak sonuçlar için hazırlık aşamasıdır. Son aşama ise istenilen amaç doğrultusunda yapılan analizlerin veya çalışmaların sonuçlarını almaya yöneliktir. St-Id yaklaşımının bütünüyle uygulanmasının, yaklaşımın kendi özelliği sebebiyle mümkün olmaması ihtimaline karşın yaklaşımın bu kısıtlı versiyonu bile uzun açıklıklı köprüler için karar vermeye dayalı önemli sonuçlar vermektedir.

Tez çalışmasının temel amacı, St-Id yaklaşımından yararlanarak Türkiye'de bulunan uzun açıklıklı köprülerin yapısal davranışı üzerine detaylı ve geniş ölçekli bir araştırma yapmaktır. Bu amaç doğrultusunda tez çalışmasında, Türkiye'de hali hazırda hizmet veren önemli inşaat mühendisliği yapılarından biri olan Boğaziçi Asma Köprüsü dikkate alınmıştır. Aynı zamanda tezde, Boğaziçi Köprüsü üzerine yapılan araştırmalardan elde edilen sonuçlara dayanarak Türkiye'deki mevcut veya yeni yapılacak diğer uzun açıklıklı köprülerin güvenliği ve gerçekçi yapısal durum değerlendirmesi için bütünleştirilmiş bir çözüm getirmek amacıyla bir çerçeve sunulması da amaçlanmaktadır. Tez çalışmasının ilk bölümünde, St-Id yaklaşımının ilk iki aşaması olan (i) görselleştirme/somutlaştırma (ii) ön modelleme çalışmaları yapılmıştır. Bu amaç doğrultusunda, orijinal proje çizimleri, güçlendirme projeleri ve hesap raporları ile köprünün işletmesinden sorumlu yetkili kurum olan Karayolları Genel Müdürlüğü'nün tecrübeleri olabildiğince doğru bir şekilde belirlenmiş ve sunulmuştur. Bu teknik dokümanları ve tecrübeleri göz önünde bulundurarak, köprünün ön sonlu elemanlar modelini oluşturmak için detaylı bir çalışma yürütülmüştür. Bu ön çalışmalardan elde edilen sonuçlara dayanılarak, köprüye ait daha detaylı analizler yapmak amacıyla köprünün ileri düzeyde sonlu elemanlar modeli olan geliştirilmiş üç boyutlu çubuk model ve üç boyutlu tam ölçekli kabuk

model hazırlanmıştır. Tezin bu aşamasında, benzer çalışmalar köprünün düşey halatlı halinin sonlu elemanlar modelinin oluşturulması için de yapılmıştır. Bu nedenle, bazı yapısal güçlendirme çalışmalarını da içeren düşey halat değişim projesinin detayları incelenmiş ve sunulmuştur. Böylece iki halat düzenini dikkate alarak köprünün geliştirilmiş üç boyutlu çubuk ve üç boyutlu tam ölçekli kabuk sonlu elemanlar modelleri modal analizin gerçekleştirilmesi amacıyla hazır hale getirilmiştir. Oluşturulan modellerden elde edilen modal analiz sonuçları karşılaştırılarak modellerin doğrulaması ve düşey halat durumunun yapı üzerine etkileri titreşim frekanslarına göre belirlenmiştir. Tez çalışmasının ikinci kısmında, St-Id yaklaşımının ikinci aşaması olan (iii) deney çalışması (iv) veri analizi çalışmalarını gerçekleştirmek amacıyla St-Id yaklaşımının gerekliliklerine uygun olacak şekilde köprünün SHM sistemi detaylı bir şekilde incelenmiştir. SHM sisteminin genel tasarım kriterleri, amaçları ve izleme parametreleri köprünün kendi karakteristik özellikleri dikkate alınarak belirlenmiştir. Bu çalışmalar sonunda, köprünün izleme özellikleri Hong Kong ve Japonya'daki önemli ve iyi bilinen uzun açıklı köprülerininki ile oldukça yakın bir uyum içinde olduğu belirlenmiştir. Elde edilen bu sonuçları ve Karayolları Genel Müdürlüğü'nün izleme sistemindeki tecrübelerini göz önünde bulundurarak, köprüde izlenmesi gerekli kritik noktalar ve yapısal elemanlar belirlenmiş ve köprü için ön performans kriterleri önerilmiştir. SHM veri analizi için kritik rüzgâr durumu dikkate alınmıştır. Veri analizinde ilk önce kritik rüzgâr etkisi doğru bir şekilde tanımlanmıştır. SHM veri analizinden elde edilen ön sonuçlara göre kritik rüzgâr datasını işlemek amacıyla Matlab programını kullanarak köprünün özelliklerine uygun yeni bir veri analizi kodunun geliştirilmesine olan ihtiyaç vurgulanmıştır. Geliştirilen kodu kullanarak frekans alanındaki sonuçlar çok daha gerçekçi elde edilmiş ve köprünün tabliye ve kule modlarını içeren ilk dokuz titreşim modu belirlenmiştir. Ayrıca, kritik rüzgâr olayının köprüye olan etkisi SHM sistemi verileri ile elde edilen köprünün dinamik özelliklerine göre belirlenmiştir. Tez çalışmasının son kısmı ise oluşturulan köprü sonlu eleman modellerinin SHM sistemi vasıtasıyla kaydedilen kritik rüzgâr verilerinden elde edilen deneysel frekans sonuçları ile (iv) kalibrasyon/doğrulama çalışmalarını ve köprünün çok mesnetli deprem hareketi altında deprem performans tahmini için yararlanma ve karar verme çalışmalarını içermektedir.

Boğaziçi Köprüsü'nün St-Id yaklaşımından elde edilen sonuçlar, oluşturulan üç boyutlu çubuk ve tam ölçekli kabuk sonlu eleman modellerinin köprünün ileri düzeyli yapısal analiz ve araştırmalarında güvenli bir şekilde kullanılabilir olduğunu göstermiştir. Özellikle köprünün doğrulanmış üç boyutlu tam ölçekli kabuk sonlu eleman modelinin, ileri düzeyli analiz ve çalışmalarda güvenli bir şekilde kullanılabileceği belirlenmiştir. "Esnası" ve "Sonrası" zaman aralıklarından elde edilen karşılaştırmalı deneysel sonuçlara dayanarak Boğaziçi Köprüsü'nün kritik rüzgâr yüklemesi altında elastik performans gösterdiği belirlenmiştir. Köprünün dinamik davranışının güç spektral yoğunluklarının gözlemsel olarak incelenmesi aynı zamanda kritik rüzgâr yükü etkisi altında köprünün etkin yanal modunun sönümleme kapasitesinde bir artış olduğunu göstermiştir. Sönümleme kapasitesindeki bu artış, genleşme derzlerinde harekete geçen sürtünmeye ve yanal hareketi kısıtlanmış pandül mesnetlerin mesnetlenme şartlarındaki değişime dayandırılmıştır. İstanbul'da olması muhtemel senaryo depremleri etkisi altında yapılan çok mesnetli ve tek mesnetli deprem analizlerinden elde edilen sonuçlardan, köprünün hasar görmediği tahmin edilmiş ve köprü için onarım ve güçlendirme müdahalelerine ihtiyaç olmadığı belirlenmiştir. Analizlerden elde edilen sonuçlar köprünün muhtemel kritik yapısal elemanlarının kule, tabliye ve genleşme derzlerinin olduğunu göstermiştir. Çok

mesnetli deprem etkisi altında eğik ve düşey halat durumuna göre de köprünün yapısal performansı belirlenmeye çalışılmış ve düşey askı halat durumu için aynı deprem yüklemesi altında eksenel çekme kuvveti değerinde oldukça büyük azalmalar elde edilmiştir. Buna karşın aynı azalma ana halat ve kenar açıklık kablolarında görülmemiştir. Bu sonuçlar köprünün geometrisinin düşey ve orijinal halatlı durumlarda bozulmamasının gerekliliğine dayandırılmıştır. Ayrıca, karşılaştırmalı sonuçlardan köprünün deprem analizlerinde tek mesnetli deprem analizinden ziyade çok mesnetli deprem analizinin dikkate alınmasının gerekliliği sonucu çıkmıştır. Basitleştirilmiş bir yaklaşımdan yararlanarak köprünün çok mesnetli deprem etkisi altındaki yapısal davranışı tabliye ve kulelerin titreşim modları ile açıklanmıştır. Tez çalışmasından elde edilen sonuçlara dayanarak köprü ile alakalı bazı önerilere de yer verilmiştir. İstanbul'da deprem riskinin yüksek olması sebebiyle deprem uyarı sisteminin uzun açıklıklı köprülerin yapısal sağlık izleme sistemleri ve diğer önemli inşaat mühendisliği yapılarının izleme sistemleri ile ortak bütünleştirilmiş bir iletişim içinde olmasının gerekliliği belirtilmiştir. Ayrıca Boğaziçi Köprüsü'nün operasyonel performans kriterlerinin belirlenmesi için tez çalışması kapsamında yapılan ön çalışmaya ek olarak operasyonel ve kritik yük durumlarında köprüde koruyucu önlemler almak amacıyla genişletilmiş SHM tabanlı operasyonel performans kriterlerinin geliştirilmesinin zorunluluğu vurgulanmıştır.

1. INTRODUCTION

Of all the civil-infrastructures, long-span bridges, such as cable-stayed and suspension bridges shown in Figure 1.1 having considerably different structural system compared with other structures are the main component in the transportation network in a country/state. Not only being substantial lifelines in transportations system, but also these bridges make respectable contribution to economic and cultural growth of their regions.

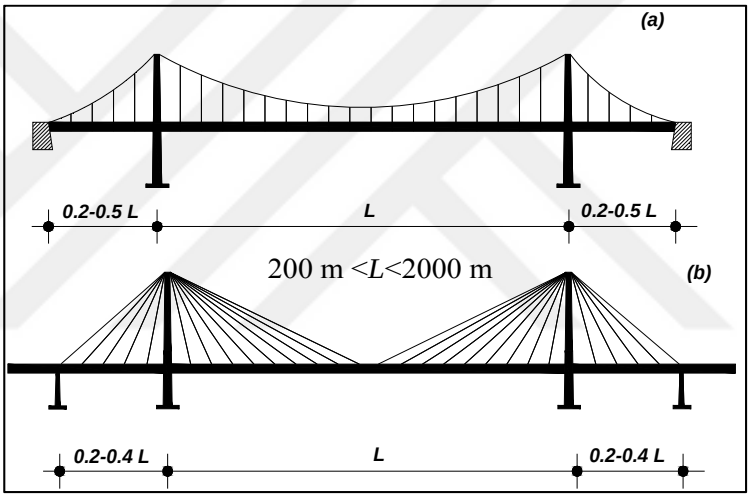

Figure 1.1 : Long span bridges: (a) suspension bridge (b) cable-stayed bridge (Gimsing and Georgakis, 2011).

On the other hand, long span bridges are not budget-friendly structures compared to other structures. In addition to construction cost, the cost of their maintenance, management and safety is also higher. Many long-span bridges in service are also vulnerable to various unpredicted load events and environmental conditions. For example, according to ASCE (2013), one in nine of the bridges in U.S. are rated as either functionally obsolete or structurally deficient. The investment needs to structurally improve performance of bridges in USA are approximately US$20.5 in a short period. Therefore, governments make sizeable investment both for their replacement and maintenance costs as wells as rehabilitation and retrofit projects. Considering such crucial functions of them and various investments for improving their structural performance, it is clear that comprehensive investigations on long-span

bridges are necessary before and after construction since they are out of the scope of general bridge codes.

Despite of the complexity of long-span bridges, they were designed and analyzed depending on the realistic and deterministic approach. To illustrate, most of these bridges were designed based on the allowable stress design method. Over the last decades, the engineers and researchers have focused on both experimental and analytical studies taking their complexity and non-linear characteristics into consideration. For analytical studies, these structures are numerically modeled through finite element model (FE). With utilizing FE method, modal analysis, buckling analysis and earthquake-induced analysis of complex structures are readily carried out. Although sophisticated analytical modeling is a powerful tool for simulating three-dimensional (3-D) local and global behavior of long span bridges, it does not reflect the real behavior owing to uncertainties, idealization and assumption, such as, in material model and analysis method. Therefore, only FE model is not enough for fully understanding the response and behavior of this type of large-scale structures.

Experimental field studies of long-span bridges give reliable consequences for the current performance of them. Therefore, conducting experimental studies are relatively important for comparing the outcomes from FE analysis with those obtained from field studies; however, experimental analysis could not be possible every time, especially for long-span bridges. Additionally, data analysis and management are necessary for interpretation of obtained experimental data. For this objective, Structural Health Monitoring (SHM) is proposed as a complementary experimental technique, including structural condition evaluation, model development and calibrating, and real-time monitoring. With the major leaps in sensing and information technology, utilizing SHM to better assess new designed and existing structures is growing interest worldwide though a standard for SHM is not available.

Consequently, discrepancies between measured and simulated response of long span bridges are available, and the integration of this gap becomes crucial for this type of bridges. To deal with this incompatibility, Structural Identification (St-Id) concept is taken into account in the most studies. Structural identification (St-Id) presents the integration of FE model and experiments for calibration/updating and verification of 3-D model for reliable simulations. In order to utilize St-Id, effective experimental techniques, the most outstanding one of which is structural health monitoring (SHM),

is necessary for long-span bridges. Accordingly, St-Id makes a great contribution to bridging the gap between 3-D model and real structure. The following steps below summarize St-Id framework,

- Visualization and conceptualization
- Priori modeling
- Experimentation
- Data analysis
- Calibration analysis
- Utilization

As can be understood from the stages of St-Id, this procedure provides inclusive assessment process enabling more objective and realistic decision on structural performance of long-span bridges. Accordingly, implementation of structural-identification to long span bridges enables to link the gap between the analytical model and real system. This leads to estimating the performance and vulnerability of structural systems reliably by means of improved simulation. Since restricted experimental studies on long-span bridges are carried out in literature, field-calibrated analytical model provides opportunity to make reliable analysis for any aspect of long span bridges.

1.1 Structural Identification (St-Id)

Structural identification is the process of developing calibrated/updated analytical model (mathematical or geometric) of structures from experiments and observations for reliable performance evaluation, simulation and decision-making. Structural identification (St-Id) and system identification (Sys-Id) are two concepts that are closely related to each other. Therefore, St-Id is a result of translation and application of system identification to mechanical and civil structural system (Catbas et al, 2013). This concept was first presented to engineering mechanics by Hart and Yao (1977) and to civil-structural engineering by Liu and Yao (1978). Although many efforts are made to implement St-Id to structural engineering, applications of this concept are not yet widespread in civil engineering practice (Catbas et al, 2003). Depending upon major leaps in sensing and information technology, St-Id concept becomes more

popular for confidential performance assessment and simulation of structures (Aktan and Yao, 1996). For different aspect of the St-Id concept, a number of studies were conducted by (Catbas et al, 2004; Doebling et al, 1998; Moon and Aktan, 2006; Sohn et al, 2003). In these studies, structural health monitoring (SHM) was utilized for St-Id.

Most comprehensive study for St-Id was carried out by the ASCE SEI Committee on Structural Identification of Constructed Systems (Catbas et al, 2013). In addition to detailed knowledge for this process given in this study, a set of case studies are presented to illustrate the application of St-Id to buildings and bridges. Six chapters are introduced to comprehend St-Id concept properly. The scope of these sections are related to modelling, experimentation, data processing, comparison of model and experiment and decision-making. As schematically shown in Figure 1.2, these stages are given in below;

- Drivers for identification
- A Priori modeling
- Experimentation
- Data analysis
- Model calibration
- Utilization

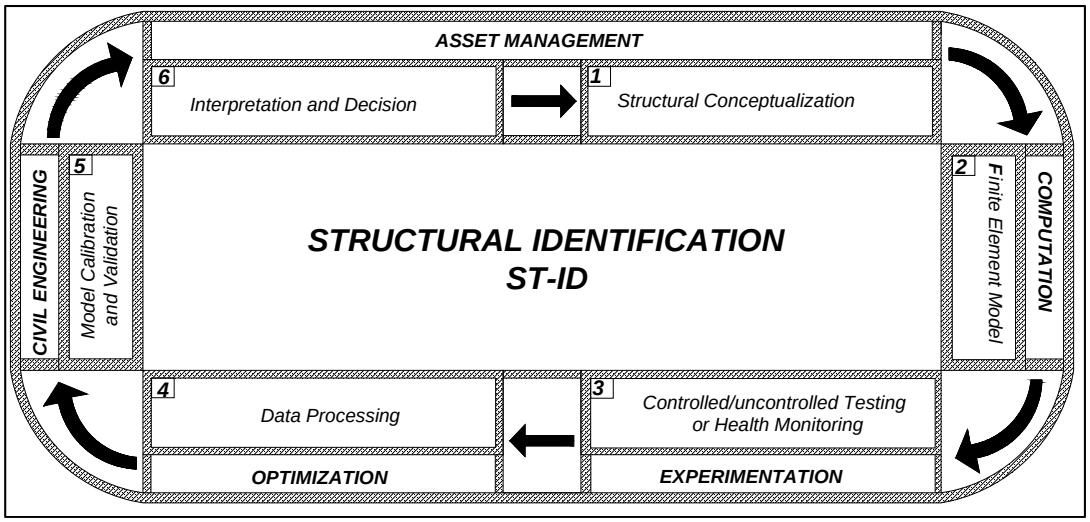

Figure 1.2 : Structural Identification (St-Id) concept.

According the committee, this study aims to link the gap between the analytical model and real system for any aspect of structures by developing reliable analytical model (mathematical or geometric). Similarly, the necessities of describing these stages for implementation of St-Id to structures are presented by other important studies (Aktan et al, 1997; Aktan et al, 1998). In order to integrate analytical model including nominal structural properties and real system for reliable simulation of structures, physics-based/model based (parametric) or non-physics-based/data driven models (non-parametric) may be developed to reach the objective (Catbas et al, 2013) . Detailed properties for these models are given in Table 1.1.

Table 1.1 : Different type of analytical models (Catbas et al, 2013).

Physics-Based Models	**Non-Physics-Based Models**
Mathematical Physics Models • F=ma *Continua Models* • Theory of Elasticity • Field and Wave Eqns • Idealized Diff. Eqns (Bernoulli, Vlasov, etc.) *Discrete Geometric Models* • Smeared-Macro or Element Level Models • FEM-for Solids and Field Problems (*most commonly used by practicing engineers*) • Modal Models: - Modal Parameters - Ritz Vectors *Numerical Models* • K,M,C Coefficients	*Semantic Models* • Ontologies • Semiotic Models *Meta Models* • Input-Output Models • Rule-based Meta Models • Mathematical (Ramberg-Osgood, etc.) *Numerical Models* • Probabilistic Models - Histograms to Frequency Distribution - Standard Prob. Distributions - Independent events - Event-based - Time-based - Symptom-based • Agents • Statistical (Data-Based) - ARMA, ANN, others -Signal/Pattern Analysis, Wavelet, EMD, others

Physics-based model approaches require to conceptualize the structural system accurately. Field observations, CAD drawings, 3-D solid modeling and photographs of structures can be used to accomplish the conceptualizing process (Gokce, 2012). Therefore, this analytical modeling form is utilized to better describe physical conceptualization and to make analysis for any aspect of structures. Since the efforts stated above to develop parametric model require a plenty of time and many experiences, the use of physic-based St-Id becomes difficult (Worden, 1997). Taking the boundary conditions, continuity conditions, equilibrium and kinematics into account, a number of investigations were conducted for parametric-based St-Id in

literature (Aktan et al, 1997; Aktan et al, 1998; Brownjohn, 2003; Brownjohn et al, 2003; Charles and David, 1998; Doebling et al, 1998; Maeck and De Roeck, 2003; Natke and Yao, 1988). It is the main advantage of this approach to reliable simulate structural behavior under critical loading conditions, such as wind, earthquake and impact loading. Depending upon outcomes to be obtained from simulating behavior, physics-based model enables to determine causes of changes in structural behavior and the impact of these changes on structural parameters necessary for predicting the performance of system. Non-linear model is considered in several studies, whereas parametric-based St-Id is commonly based on linear matrix structural analysis (Catbas et al, 2013).

Secondly, non-parametric-based model for St-Id is based on solely training of data obtained from normal operating condition. Accordingly, diagnosing structural behavior of systems is employed with the help of these identified data. Although different methods are introduced in literature for this approach, Artificial Neural Networks (ANNs) (Chang et al, 2001; Hae-Bum and Sami, 2009; Masri, 1996; Masri, 2000; Nakamura et al, 1998; Yun et al, 2009), wavelet decomposition (Gurley and Kareem, 1999; Hou et. al, 2000; Kijewski and Kareem, 2003) and auto-regressive moving average vector models (Bodeux and Golinval, 2001; Gul and Catbas, 2011; Mustafa and Catbas, 2011; Shinozuka and Ghanem, 1995) are the most used ones. These methods have many advantages including automation, real-time St-Id, continuous monitoring, developing advanced phenomena, and minimization of errors owing to user-interaction. Moreover, data driven nature of this approach provides computational ability to deal with large amount of data. The important difference between parametric (physics-based) and non-parametric (non-physics-based) model is that non-parametric model can solely diagnose changes in structural behavior and cannot determine the causes of behavior changes or its effect on overall performance of system (Catbas et al, 2013).

When it comes to the implementation of this St-Id process to long-span bridges, such as cable-stayed and suspension bridges, several studies have carried out for determining the structural dynamic characteristics under various loading conditions owing to wind and traffic-induced loads and for updating analytical model by utilizing measured dynamic properties. In literature, some methods were proposed by (Abdel-Ghaffar, 1978; Abdel-Ghaffar, 1976; Ahmed and Lawrence, 1983) to find the lateral

vibration features of suspension bridge by means of finite elements method. Besides, Ghaffar and Scanlan (1985a, 1985b) performed ambient vibration test to determine the dynamic properties of suspended members and the towers of the Golden Gate. They made a comparison between measured frequencies with those attained from the finite element model. Mazurek and Dewolf studied on determining calibrated analytical model to employ health monitoring on highway bridge by using the laboratory model test. They concluded that same concept employed in the laboratory could be used in the field to attain vibrational features of the bridge. Agbabian et al. (1991) and Nigbor et al. (1991) used updated analytical model for baseline for health monitoring. Brownjohn and Xia (2000) investigated the implementation of sensitivity-based model updating technology to the dynamic assessment of the Safti Link Bridge, a curved cable-stayed bridge in Singapore. For this purpose, they developed a software to calibrate analytical model for the bridge. Chang et al. (2001) developed finite element model and conducted ambient vibration studies to determine the dynamic characteristics of the fairly long cable-stayed bridge in Hong Kong. It was concluded in the study that finite element model should be calibrated if the measurements are relatively dependable. Mottershead and and Friswell (1993) and Natke et al. (1994) carried out detailed review studies on modal updating of bridges. Several suspension bridges in Hong Kong were modeled and instrumented for long term monitoring for seismic, wind, and any purpose of health monitoring by Wong et al. (2000). For the same purpose, Kashima et al. (2001) conducted analytical and experimental studies for the Akashi Strait Bridge. In these studies, the authors aimed at determining modal properties by utilizing ambient vibration monitoring and additional experimental techniques. Moreover, Aktan et al. (2000) conducted research projects for Commodore Barry Bridge, long span truss bridge over the Delaware River. They considered the St-Id concept for structural performance and behavior of the bridge. It was stated in this study that a complete and proper visualization must be employed, especially for long span bridges. In addition to this outcome, they also proposed that a continuous health monitoring system was installed on the bridge for effective concept for experimental studies on long-span bridges. Gokce et al. (2013) carried out a case study on a moveable bridge for performance prediction by using the St-Id concept with uncertainties. In this study, preliminary finite element model of Sunrise movable bridge was updated with Structural Health Monitoring (SHM) data by using Artificial Neural Networks (ANNs) method. To predict load rating and system reliability of the

bridge, the family of models concept was utilized by using the parent (calibrated) FE model. The primary point of the study was to estimate the future performance of the moveable bridge under environmental loading conditions.

With respect to the suspension bridges in Turkey, specifically the Bosphorus Bridge (the 1st Bridge) and the Fatih Sultan Mehmet Bridge (the 2nd Bridge), and ongoing long span bridge projects, the Yavuz Sutan Selim Bridge (the 3rd Bridge) and Osman Gazi Bridge (Izmit Bay Bridge) as shown in Figure 1.3, limited number of studies and research projects involving structural identification (St-Id) of these bridges.

Figure 1.3 : General views from the bridges: (a) the Bosphorus Bridge (b) the Fatih Sultan Mehmet Bridge (c) the Yavuz Sultan Selim Bridge (d) the Osman Gazi Bridge.

For the suspension bridges, several studies were conducted to determine dynamic characteristic under critical loading and environmental conditions by using certain experimental technique and to calibrate analytical model by using measured dynamic

parameters. In this sense, Dumanoglu et al. (1992) and Brownjohn et al. (1992) studied on the natural dynamic properties of the Fatih Sultan Mehmet (the Second Bosphorus) Bridge.

They used auto-power spectrum methods to find the modal frequencies. They indicated that the measured and computed values were relatively compatible with the low frequency range. Nevertheless, they presented an increasing divergence for frequencies with higher value. Brownjohn (1994) also looked into the effect of non-linear behavior on modal properties of the Bosphorus and Fatih Sultan Mehmet Bridges, and determined that non-linear behavior appeared under low-level dynamic excitation. Erdik and Uckan (1989) conducted ambient vibration survey of the Bosphorus Bridge for comparing the values with those of the previous studies. Apaydin and Erdik (1999) installed a structural health monitoring system for ambient vibration of the Bosphorus Bridge and designed a new vibration monitoring system for the Fatih Sultan Mehmet Bridge to diagnose change in structural behavior of the bridge and update analytical model of the bridge by utilizing measured vibrational data. Erdik and Apaydin (2005) determined the natural frequency and corresponding mode shapes of two Bosphorus suspension bridges in their dead and live load. Apaydin et al. (2012) conducted a study on determining free vibration parameters by using ambient vibration test under traffic and no traffic loading conditions. To reveal differences of modal properties between traffic and no traffic condition, they carried out temporal and spectral analyses of recorded motions. This study presented the loading condition on the long-span suspension bridges. Apaydin (2002) performed a detailed study for evaluation of dynamic characteristics of the Fatih Sultan Mehmet Bridge by using the experimental and the analytical methods. This study revealed that the bridge might be damaged at the end spans of the deck under earthquake action. Kosar (2003) evaluated experimentally the dynamical characteristics of the Bosphorus Suspension Bridge by using Ambient Vibration Test (AVT). A detailed 3-D finite element model of the main structure of the bridge without the approach viaducts was developed, and the results from free vibration analysis and those attained by experimental study of AVT are compared and the difference between them are discussed. Furthermore, Apaydin (2010) made an investigation on structural earthquake performance of the Bosphorus and the Fatih Sultan Mehmet Bridges. In the study, free vibration analysis of the bridges was also performed by employing a

sophisticated 3-D finite element model of them. The Bosphorus Bridge was modeled by including the approach-viaducts, which constitute the side span of the bridge. These viaducts were also numerically modeled in Bas et al. (2016a) and Bas et al. (2016b) for the earthquake analysis. The results from the analyses demonstrated that the viaduct with no cable elements should be sperately considered from the main-span of the Bosphorus Bridge to accurately estimate the damage level and thus performance level of them.

As seen from these studies on the suspension bridges in Turkey, approximately no study on the combined assessment of the Boshorus Bridge from experimental, numerical (FE modeling) to decision-making on the bridge's performance under operational and extreme events was carried out. Besides, Structural Identification (St-Id) concept was considered partially in the existing studies. Therefore, the main aim of this dissertation is to carry out detailed experimental data analysis and numerical analysis for the Bosphorus Bridge taking the requirements of St-Id process into account.

1.2 Structural Health Monitoring (SHM)

In order to reduce total life-cycle cost of bridges, recently developed SHM system is also considered the cutting-edge technology. With the help of SHM system, operational and structural performance of them under extreme loads, such as marathon, heavy traffic, wind and earthquake loads are readily detected. The recent developments in sensing and information technology also gets SHM system to higher level. Many researchers (Aktan et al, 2000; Ko and Ni, 2005; Jiang and Adeli, 2005; Brownjohn and Pan, 2008; Xu, 2008) define the main objectives of SHM system as monitoring response of structures under various loading conditions, evaluating operational and structural performance of them, damage or deterioration detection and guiding inspection and maintenance of them. Limited studies conducted in the early 1930s to determine dynamic behavior of Golden Gate and Bay Bridges in San Francisco in US provide an opportunity to develop SHM system for long-span bridges. Besides, the Tacoma Narrows Bridge in Washington State, USA, collapsed entirely under wind load, opened the door to monitoring, inspection, maintenance and safety of suspension bridges. To illustrate, this experience gave rise to conducting retrofit study for the Golden Gate Bridge and other suspension bridges. In order to decrease catastrophic

failures in suspension bridge, Doebling et al. (1996) introduced a comprehensive bridge inspection program. Recently, almost all bridges in service in the world have been assessed structurally in every two years. Due to many benefits of SHM system, a number of long span bridges are equipped with monitoring devices, and these devices are updated in accordance with the advances in technology. Although installation of SHM on long-span bridges increases considerably, no specific, general standards or codes for practitioners are still the lack of SHM system. Some researchers published a valuable handbooks, guidelines and research books (Aktan et al, 2002; Boller et al, 2009; Karbhari and Ansari, 2009; Wenzel, 2009; Xu and Xia, 2011).

In general, the components of a SHM system are given below by Xu and Xia (2011);

- Sensory systems
- Data acquisition system and transmission system
- Data processing and control system
- Data management systems
- Structural evaluation system

Sensory systems includes a number of sensors distributed along bridge for the purpose of obtaining a signal. The signals captured from sensors are collected from data acquisition system and transmitted to database server. Data processing and control systems provide the control of data acquisition and transmissions system, processing, storing and indicating data. For temporal and spatial data management, data management system with database system is needed. Structural evaluation system provides to make a comparison between measured data and bridge's designs limits or its analysis results. Even if SHM system seems to a complete system in operation, in fact, each part of SHM system is independent, which means that there is no detrimental effect on the operation of the remaining part of the entire system. Design of SHM systems is based on clearly describing the objectives of the monitoring. Therefore, working SHM designer together with bridge designer is inevitable to identify the objectives very well. Considering the objectives, monitoring requirements should be identified Aktan et al. (2003). The requirements are as in below;

- The parameters for being monitored (wind, displacement, temperature)
- The design value and measurement range of the parameters

- The spatial and temporal properties of the parameters
- The accuracy requirements
- The environmental condition of the monitoring
- The duration of the monitoring

Following identification of the monitoring parameters, the next step is to determine the number of sensors based on the monitoring objectives. In order to compensate for the requirements of the monitoring, it is important to select which types of sensor are used. For this purpose, technical specifications of the sensors including measurement range, sampling rate, sensitivity, resolution, linearity, stability, accuracy, repeatability, frequency responses should be identified clearly. Considering these main items stated above, advanced structural health monitoring systems have been developed and installed on several suspension bridges in the world to monitor structural health of bridge in real time. Some applications of SHM systems to the important suspension bridges in Hong Kong and Japan are presented in the dissertation. Accordingly, their design objectives and outcomes are compared to those of the Bosphorus Bridge to verify the effectiveness of its SHM system.

Due to the importance of SHM system to conduct experimental study of long-span bridges, a number of applications to in-service long-span bridges were made in literature by (Abe and Amano, 1998; Aktan et al, 2002; Aktan et al, 2000; Fujino et al, 2000; JSCE, 1998; Kashima et al, 2001; Yamada et al, 2000).

For the long-span bridges in Hong-Kong, Flint eat al. (1995), Highways-Department (2002), Lau et al. (1999), Wong (2001), Wong et al. (2000), Xu and Xia (2011) and Yeung et al. (1995) conducted various study/projects on SHM system. The SHM of the bridges in Hong Kong is employed with Wind and Structural Health Monitoring System (WASHMS) consisting of six modulus as shown in Figure 1.4 that are;

- Sensory system
- Data acquisition and transmission system
- Data processing and control system
- Structural health evaluation system
- Structural health data management system

- Inspection and maintenance system

The critical bridges in Hong Kong shown in Figure 1.5 are the Tsing Ma Bridge (suspension), the Kap Shui Mun Bridge (cable-stayed), and the Ting Kau Bridge (cable-stayed). These bridges have been monitored with the WASHMS considering the objectives below;

- to understand the structural behavior under operational loads
- to develop bridge model using monitored data
- to update/calibrate the bridge model for evaluation techniques allowing to make reliable analysis
- to make structural or operational provision against rare events, such as strong earthquakes and typhoons.

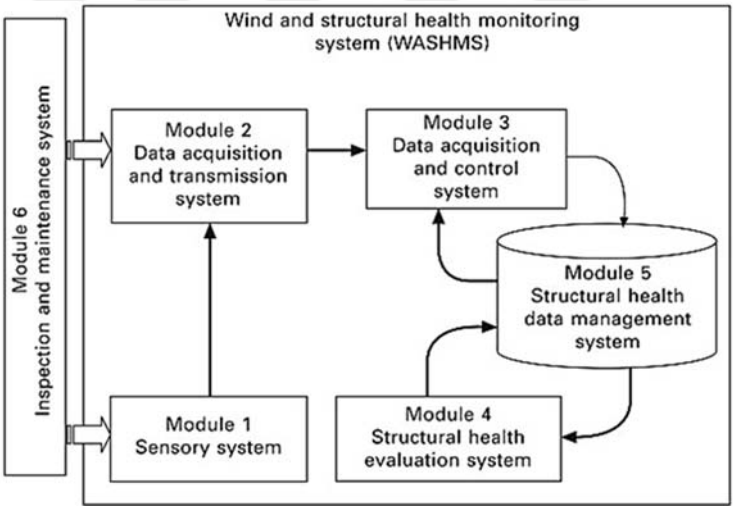

Figure 1.4 : The modules of the WASHMS (Flint et al, 1995; Highways-Department, 2002; Wong, 2001; Xu, 2008).

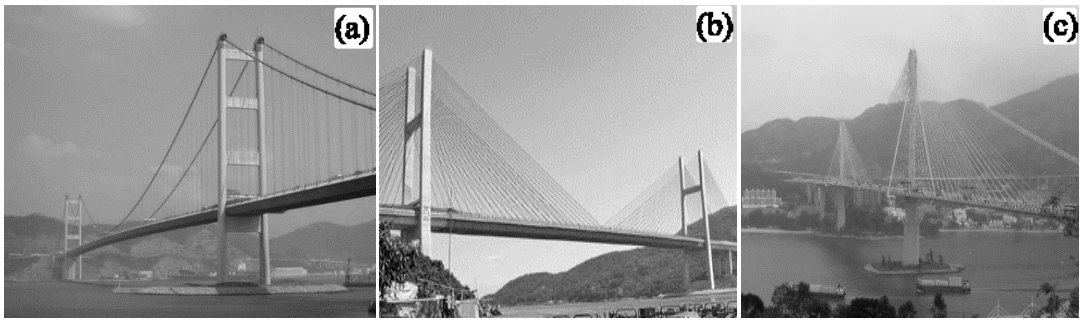

Figure 1.5 : General view of some bridges in Hong Kong: (a) the Tsing Ma Bridge; (b) the Kap Shui Mun Birdge; (c) the Tsing Kau Bridge (Flint et al, 1995; Highways-Department, 2002; Wong, 2001; Xu, 2008).

After determining the main objectives of the WASHMS, identification of the monitoring parameters is the next step for structural health monitoring and evaluation of the bridges. For the Tsing Ma Bridge, the Kap Shui Mun Bridge, and the Ting Kau Bridge, the following parameters are considered;

- Environmental effects: wind, earthquake, temperature, humidity, corrosion
- Service (operational) loads: highway and railway loads
- Bridge characteristics: static features (such as creep/relaxation) and dynamic features (such as modal frequencies, modal damping, mode shapes)
- Bridge responses: the forces in cables, geometrical changes in deck and tower, fatigue damage in key components

Based on the design objectives and the monitoring parameters, the sensory system of the WASHMS including various type of sensors is identified. The sensors are presented Figure 1.6 for the Tsing Ma Bridge, the Kap Shui Mun Bridge and the Ting Kau Bridge.

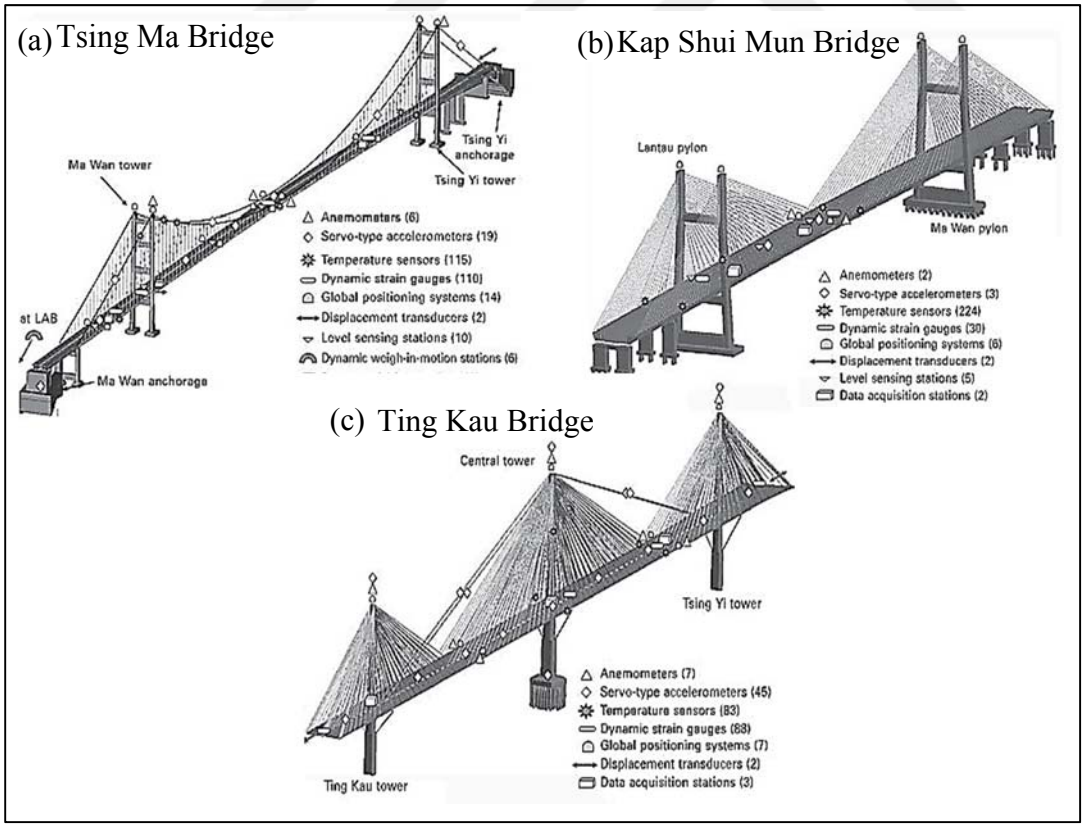

Figure 1.6 : Instrumentation layout: (a) Tsing Ma Bridge (b) Kap Shui Mun Bridge (c) Ting Kau Bridge (Flint et al, 1995; Highways-Department, 2002; Wong, 2001; Xu, 2008).

In accordance with the monitoring objectives, the following criteria are considered for the selection of sensors;

- operational bandwidth
- magnitude and frequency response over that bandwidth
- sensitivity and accuracy
- power supply requirements
- physical characteristics (dimensions, weight and material)
- environmental operating conditions such as temperature ranges
- type of output signal
- any signal conditioning requirements
- costs

Another important feature of the sensory system of the bridges is to be designed in accordance with designated bridge operation criteria at key locations or components of the bridges. These criteria are determined considering load and resistance ratio given in Federation Highway Administration's Bridge Ratings for Operation. These operation criteria are given in Table 1.2.

Design values corresponds to bridge design loads or resistance capacity and response at the serviceability limit states (SLS). SLS means that the bridge is under usual loading condition to which the bridge frequently is subjected, and there is no any damage. To quantitate of the SLS, a safe key point/component is the ratio factor of 1.33 is considered. In fact, this means that the displacement or stress of 75% (monitored value /design value). Operation Level I is normally executed as real-time operation and Operation Level II and III are normally executed as off-time operation. The structural evaluation carried out in Operation strategies II and III requires the implementation of five analysis steps: (i) confirmation of existence of overstress or damage; (ii) determination of overstressed/damaged location; (iii) identification of type and cause of overstress or damage; (iv) quantification of the amount of overstress or damage; and (v) estimation of any adverse effects on global structural performance or prediction of useful life remaining. These steps are presented systematically by a block diagram for the bridges as shown in Figure 1.7.

Table 1.2 : Operational performance criteria for the bridges in Hong Kong.

Operation Level	Limits $\sigma_{monitored}/\sigma_{design}$	Structural Condition	Prevention
Level I	<0.75	Normal	Routine statistical analysis and report of measurements results
Level II	=0.75	Critical	Structural evaluation of measurement results by finite element and/or surrogate models are required to check any over-displaced or over-stressed phenomenon occurring in non-instrumented or key location and/or component. If yes, inform the bridge maintenance team for carrying out detailed inspection on that problematic location or component.
Level III	0.75<	Strcutural degradation	The detailed structural evaluation of measurement results by finite element and/or surrogate models are required to check any damage induced and to assess the adverse effects on SHM of the bridge such damage on global bridge performance. If yes, inform the bridge maintenance team for carrying out detailed inspection and assess the scope and time of remedial action, where necessary

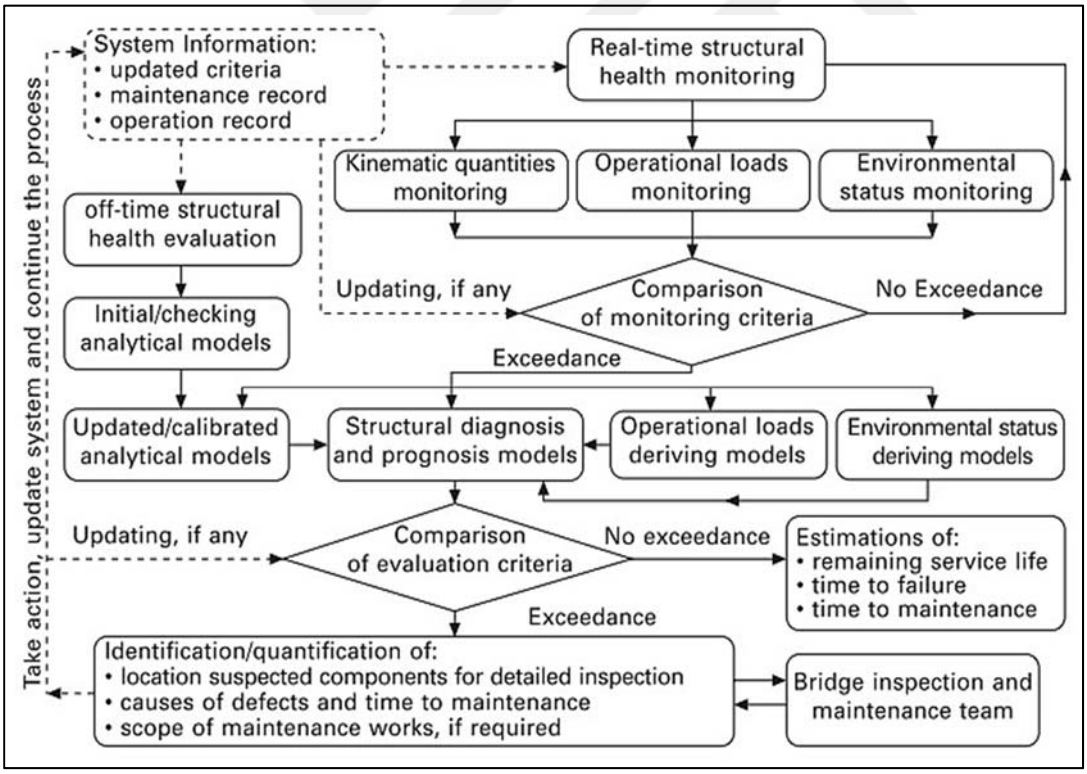

Figure 1.7 : The WASHMS operation block diagram (Flint et al, 1995; Highways-Department, 2002; Wong, 2001; Xu, 2008).

In Figure 1.8, the routine data analysis is presented. In this analysis, using acceleration data in time-domain recorded at different deck points of the Tsing Ma Bridge, the modal characteristics are extracted by frequency domain analysis, the Fast Fourier

Transform (FFT) analysis. The results obtained by FEM are verified by those of FFT analysis. Accordingly, it is concluded that difference between the data analysis and FEM model is very close.

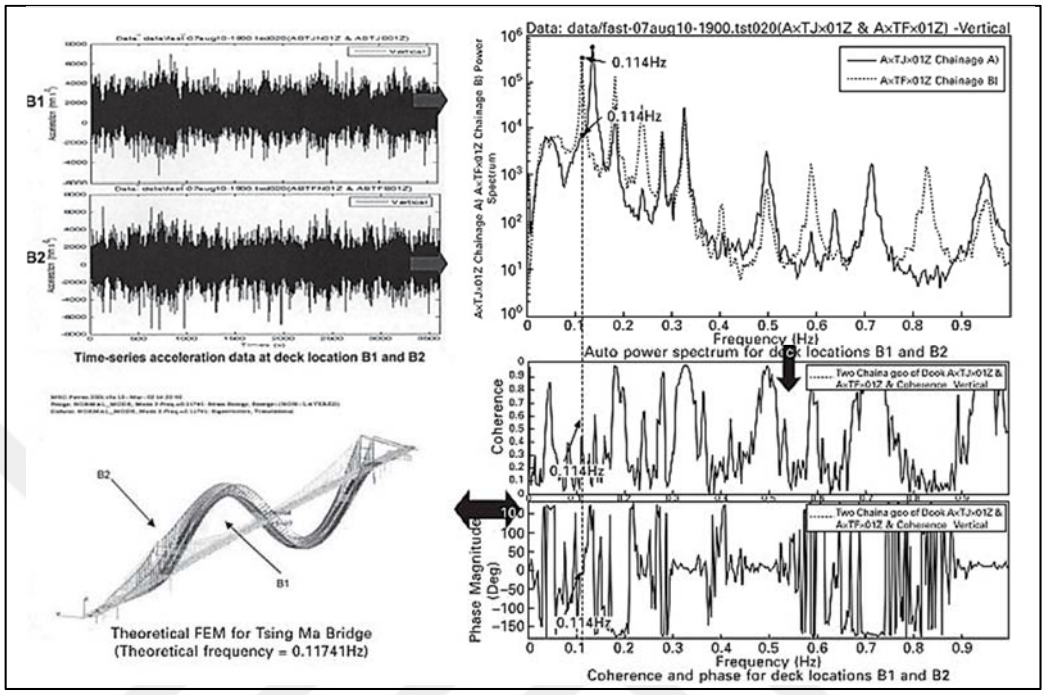

Figure 1.8 : Data analysis for identification of modal characteristics of the Tsing Ma Bridge (Flint et al, 1995; Highways-Department, 2002; Wong, 2001; Xu, 2008).

Figure 1.9 : The Akashi Kaikyo Bridge.

With the main span length of 1991 m and total length of 3911 m, the Akashi Kaikyo Bridge shown in Figure 1.9 is the longest suspension bridge in the world. The bridge crosses over the Seto Inland Sea. Since it is subjected to heavy humidity, a comprehensive corrosion protection system is developed and is implemented to the bridge. In addition to the environmental effects, the bridge is susceptible to various types of loads, especially earthquake and wind. For this reason, the implementation of

real–time SHM system is inevitable for the bridge to understand the global and local performance of the bridge under different loading conditions (Fujino et al, 2000).

Considering the complexity of the Akashi Kaikyo Bridge, the monitoring objectives below are considered;

- ❖ Design verification
- ❖ Structural maintenance
- ❖ Traffic management.

For design verification, it is aimed to verify design consideration under strong wind and earthquakes, to develop a more accurate design for the future bridges, and to develop reliable SHM system with a self-check function to determine the disorder of the system itself. For structural maintenance, it is aimed to analyze and evaluate the SHM of the bridge using the recorded data, and to assess structural deterioration and performance degradation. For traffic management, it is aimed to update the traffic control due to an earthquake or strong wind, and to provide reliable information for managing traffic flow. The design verifications of monitoring items are summarized in Table 1.3.

Table 1.3 : Design verification items of the Akashi-Kaikyo Birdge (Fujino et al, 2000).

Item	Main Focus	Measured Parameter
Earthquake characteristics	Seismic motion and magnitude Earthquake frequency characteristics Ground characteristics Phase difference	Acceleration
Earthquake dynamic response	Acting seismic force Displacement Natural frequency Superstructure seismic motion	Response acceleration (velocity) Displacement Response acceleration (velocity)
Wind characteristics	Basic wind speed Design wind speed Variable wind speed characteristics: - Intensity of turbulence - Spatial correlation - Power spectrum	Wind direction and wind speed
Wind dynamic response	Superstructure natural frequency Vibration mode configuration Structural damping Gust response Action of main tower (TMD)	Response acceleration (velocity) Displacement Predominant frequency Wind speed and response acceleration Response displacement

After identification of the main objectives, the primary focus and corresponding physical parameters, the sensor layout and its location are shown in Figure 1.10. In this configuration, seismometer is utilized to record the earthquake reliably by deploying them at a place that is distant 100 m from the bridge axis. The recorded data is used as an input for structural identification of the bridge. In order to identify the wind vibration characteristics of the bridge, anemometers are used. Another aim of these sensors is to monitor spatial correlation in the horizontal direction. Accelerometers are used to determine and to verify the dynamic behavior of the bridge properly. Velocity gage is installed to monitor the vibration characteristics of the deck and the towers under wind and earthquake loads. With the help of GPS installation, geometric changes in top end of the tower and mid-span point of deck are determined. For the wind stabilization of the tower with the height of 300 m, tuned mass dampers (TMDs) are deployed inside the tower. Thermometers are installed on cable elements and mid-span of deck.

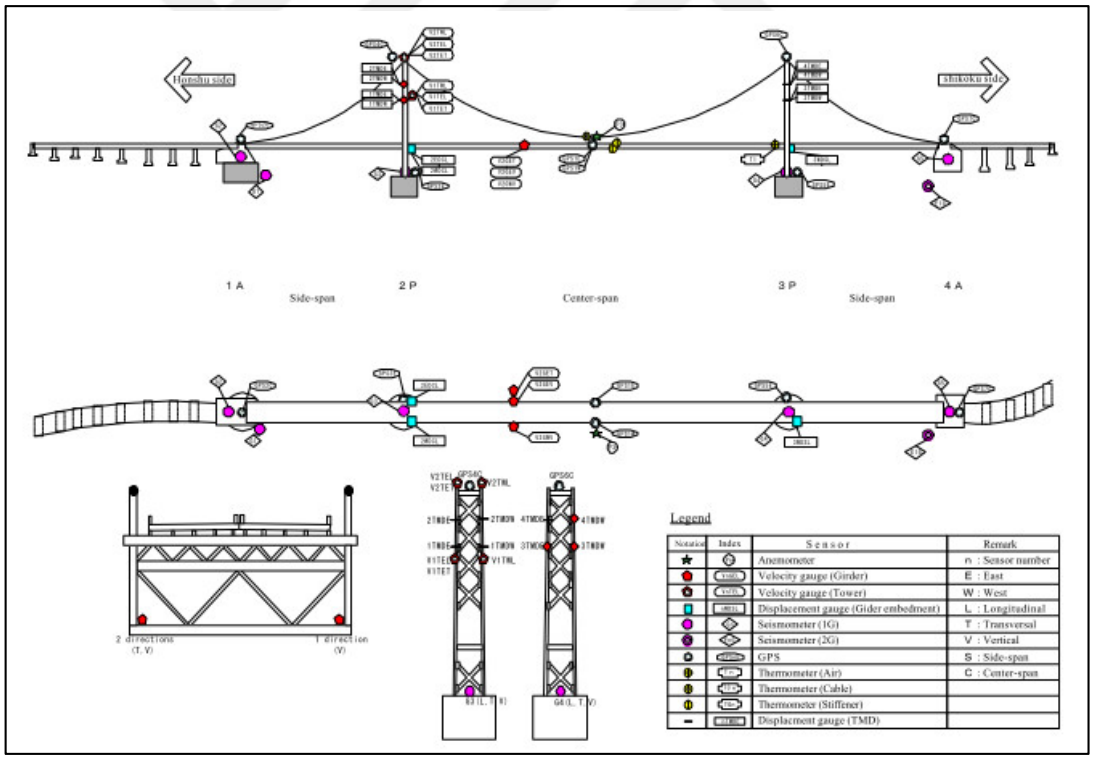

Figure 1.10 : Sensor arrangement of the Akshi-Kaikyo Bridge (Fujino et al, 2000).

From the bridge monitoring systems adopted in Hong Kong and Japan, the implementation of SHM system provides powerful tool to understand the behavior of the bridges under operational and extreme loads. In addition, this system allows the bridges' authority to take prevention for continuing the operation of the bridges. As in

the WASHMS in Hong Kong's bridges, using the monitored data, determination of operational performance criteria for critical components of the bridges plays vital role in their services. Here, the critical issue is interpretation of the performance in the quantitative manner. Another important item is how to formulate the quantification of the performance criteria. In this dissertation, preliminary performance criteria and its formulation are tired to be identified for the Bosphorus Bridge based on the design specifications of the SHM system of the bridge.

1.3 Significance, Objectives and Scope

As shown in Figure 1.11, the Bosphorus Bridge is one of the most important lifeline infrastructure of Istanbul, Turkey. The Bosphorus Suspension Bridge with six lanes serves more than five billion vehicles annually, and was opened to traffic in 1973.

Figure 1.11 : The Bosphorus Bridge and the other long-span bridges in Istanbul.

This bridge has the main span length of 1074m and two side spans with length of 231 m and 255 m, respectively. Instead of suspension system, these side spans are

contemplated as the approach viaducts supported at the base. Accordingly, the bridge serves critical function for traffic flow between two continents, Asia and Europe.Taking the important function of the Bosphorus Bridge into account, comprehensive analytical and experimental studies are inevitable to reliably make decision on its local and global structural performances under various effects including current operation, maintenance and rehabilitation, and bearing system. Although a number of studies were conducted for the bridge to determine dynamic and wind vibration characteristics, St-Id concept was considered partially in these studies. This approach has the ability to characterize local and global behavior of constructed structural system and its environmental conditions by field observations, measurements and controlled experiments in connection with FE model. Thus, the significance of this dissertation is to conduct reliable study on the current and future structural performance of the Bosphorus Bridge considering the steps of St-Id approach as shown in Figure 1.12.

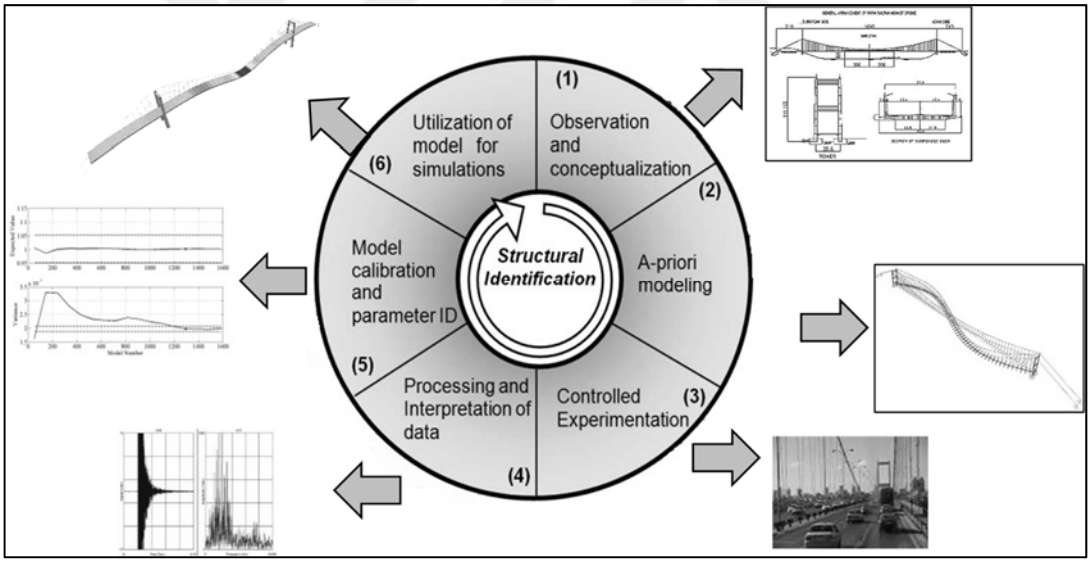

Figure 1.12 : Structural Identification (St-Id) approach.

Depending on the significance of conducting experimental research and developing reliable FE model for long-span bridges, it is clear that St-Id is necessary especially for large-scale structures. The primary objective of the dissertation is to make a comprehensive investigation on structural response of the Bosphorus Bridge adopting the integrated approach of St-Id. Based on the consequences from the Bosphorus Bridge, it is also aimed to present a framework for integrated solution to safety and proper structural condition assessment of other existing or newly constructing long-

span bridges in Turkey. With the help of St-Id, relatively confidential FE model of the bridge will be developed after completion of each step, and the improved FE model allows to make further analyses for any aspect of the bridge. Based on all efforts for St-Id, global and local structural performances of the Bosphorus Bridge will also be predicted. In accordance with the following objectives given below, the scope of the dissertation is schematically summarized as depicted in Figure 1.13.

- to reliably describe and characterize dynamic behavior of the bridges.
- to develop relatively confidential analytical models for further advanced analysis of the suspension bridge.
- to estimate their global and local structural performances.

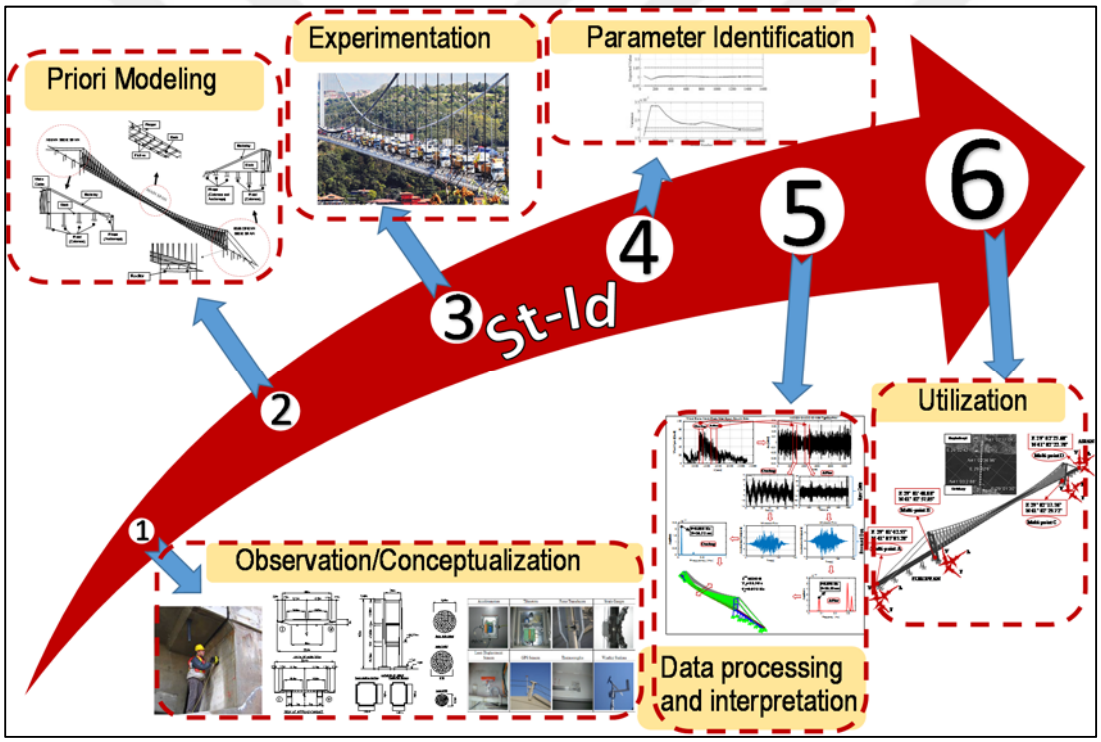

Figure 1.13 : Scope of the dissertation (the steps of St-Id).

1.4 Organization of the Dissertation

The dissertation is organized in accordance with each steps of St-Id as follows:

In Chapter 1, literature survey on the structural identification of the Bosphorus Bridge is conducted and the necessity of implementing this approach to the bridge is stated due to approximately no study on the combined assessment of the Boshorus Bridge from experimental, numerical (FEM) to decision-making on the bridge's performance

under operational and extreme events. Detailed information is also given for each step of St-Id with its implementation to real-life bridges in the world. Similar efforts are also employed for SHM system that is crucial tools for experimentation step of the St-Id. Based on various scientific studies on SHM system of the important long-span bridges in the litearature, a framework is tried to be developed for the Bosphorus Bridge. Accordingly, comprehensive preparatory study is carried out in Chapter 1 for the implementation of St-Id approach to the bridge considering the efforts in the literature for the bridge.

Chapter 2 presents general outline and specifications of the Bosphorus Bridge. Considering the original project drawings and recommendations from the bridge's authority (KGM), detailed sectional and physical properties are obtained for FE modeling efforts of the bridge. In this chapter, the hanger replacement project specifications are also identified in detail and preparatory study on FE modeling of the bridge with vertical hanger.

In Chapter 3, the principle considerations for priori FE modeling of the Bosphorus Bridge are identified based on the outcomes from the Chapter 2. Taking these preliminary considerations into account, elaborate literature survey on finite element modeling of long-span cable support bridges is conducted to specify advanced modeling requirements. Based on all requirements, the spine-beam and 3-D full-scale FE model of the bridge with inclined and vertical hangers are established. Thus, the second step of St-Id is completed.

In Chapter 4, the modal analysis considerations are given and the results from the modal analyses of the developed FE models of the bridge are presented. In order to specify accuracy of the established FE models, these results are compared to each other and those from previous experimental studies in the literature. Comparative results from the modal analyses enable to verify/calibrate the developed FE models for reliable further analysis of the bridge, such as earthquake, strong wind, heavy-truck, human-induced etc., and to identify the effects of vertical hanger replacement on the dynamic response of the bridge. Thus, the fourth step of St-Id is completed after the comparison of experimental data analysis results to be obtained in Chapter 6.

Chapter 5 is dedicated to the SHM system of the Bosphorus Bridge. General design considerations, monitoring objectives and parameters of the SHM system of the bridge

are accurately identified depending on its own characteristics. Sensor specifications, configurations and layout of the SHM system is demonstrated. Considering the principle SHM system specifications of the bridge and the recommendations of the bridge authority (KGM), operational and extreme load events are determined, and monitoring points and critical components are specified. All outcomes from the detailed SHM investigation provide to develop operational performance criteria for the bridge.

Chapter 6 contains the works related to the data analysis step of St-Id. According to the conclusions from Chapter 5, structural identification is decided to be handled with the extreme wind data recorded from the SHM system of the bridge. For this objective, the extreme wind event is first identified properly and the wind direction is corrected with the polar charts. The identified data is then processed for preliminary outcomes. Due to high noise content in the preliminary results, a special average processing for the bridge is carried out and the PSD analysis reveals to have smoother results. Along with natural vibration frequencies of the bridge, data analysis is also conducted to identify the influence of the extreme wind event on the dynamic properties of the bridge. For this aim, the data is separated into the specific time intervals. Accordingly, the first nine vibration frequencies of the bridge are identified accurately and the extreme wind effects are determined with comparative study. Based on these results, the developed FE models are obtained to be in high accordance with the experimental wind data results.

In Chapter 7, the utilization step of St-Id is conducted on the earthquake performance prediction of the bridge with inclined and vertical hangers. Depending on detailed literature survey on the earthquake analysis of long-span bridges, this aim is achieved with the multi-point earthquake analysis (Mp) approach. The first effort to make Mp analysis is to produce spatially varying site-specific scenario earthquake records for Istanbul considering the geographic coordinate of the support points of the bridge. Next, the Mp analysis approach is introduced. In an effort to identity the effects of the Mp analysis on the bridge, well-known uniform-point earthquake analysis (Up) is also performed and comparative study is carried out. Moreover, the effects of the earthquake level and hanger arrangement on the performance prediction of the bridge are investigated with a number of comparative studies. Using simplified approach,

structural response of the bridge to the multi-point earthquakes is also identified with the deck and tower natural vibration modes.

Finally, Chapter 8 presents the conclusions and recommendation along with the brief summary of the dissertation. The consequences from St-Id process of the Bosphorus Bridge indicate that the developed FE models can reliably be utilized for advanced analysis and investigations of the bridge. Moreover, the Bosphorus Bridge is determined to show elastic performance under the extreme wind load based on the experimental comparative results. Visual inspection of the PSD of the dynamic response also demonstrates an increase in the damping capacity of the lateral mode under the extreme wind load. From the multi-point and uniform-point earthquake analyses under the scenario earthquakes for Istanbul, the bridge with both inclined and vertical hangers is not likely to be damaged and no repair and strengthening intervention can be required for the bridge. Under the DD-1 spectrum compatible earthquakes, damage is estimated for the tower base-section and approach viaduct box-section of the bridge with both inclined and vertical hangers. For retrofit strategy, sectional capacity is recommended to be increased with additional longitudinal stiffener of doubly symmetric W100x499 I-beam. The comprative results also yields to necessity of the consideration of the multi-point earthquake analysis rather than the uniform-point earthquake analysis for the bridge. Some recommendations are also obtained depending on the outcomes of the dissertation. With the increase in the long-span bridges in Turkey, especially in Istanbul, there is need for command center where the all SHM systems are integrated for rapid decision making. Due to high seismicity of Istanbul, the connection of the earthquake warning system with the SHM systems of the bridges and other important infrastructures should also be integrated. Along with the preliminary attempt to operational performance criteria of the Bosphorus Bridge in this dissertation, developing extended SHM-based operational performance criteria is also necessary to take preventive measures for operational and extreme load events.

2. THE BOSPHORUS BRIDGE

The history of bridge project on the Bosphorus Straits goes back to 522 BC - 485 AC. The first decision to build a long-span bridge over the Bosphorus River was in 1957. The bridge was designed by the British firm Freeman Fox & Partners in 1968. After its construction started in 1970, the bridge was commissioned in 1973 corresponding to the 50th anniversary of the Republic of Turkey. General current views from the bridge are depicted in Figure 2.1.

Figure 2.1 : Genearal current views from the Bosphorus Bridge.

2.1 General Outline and Specifications

With its main span shown in Figure 2.2, the bridge was the longest suspension bridge in Europe until the completion of the Humber Bridge in 1981. It was also the 4th longest bridge in the world upon completed in 1973. The Bosphorus Bridge with aerodynamic deck box-section given in Figure 2.3 is a modern steel suspension bridge.

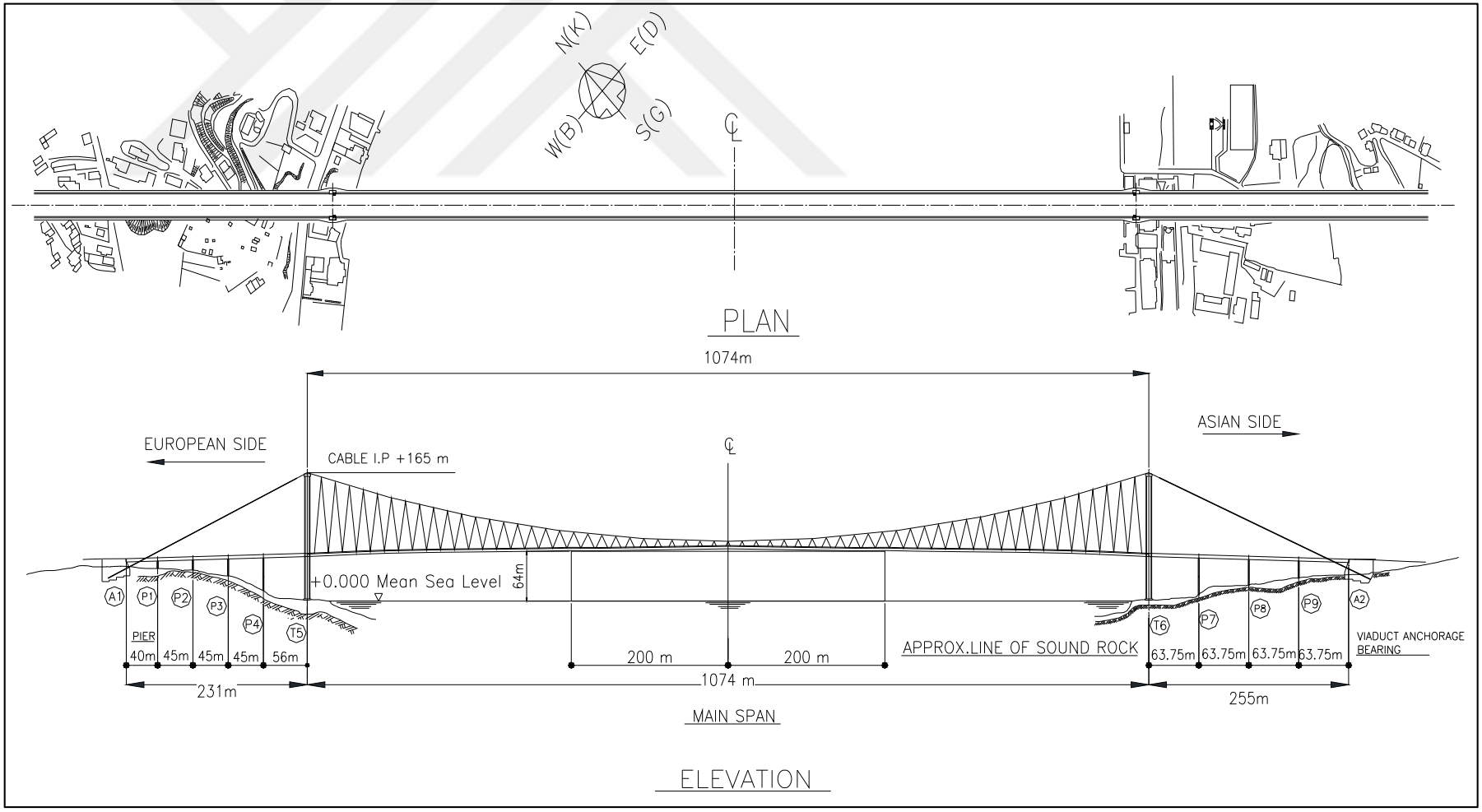

Figure 2.2 : General layout of the Bosphorus Bridge (Freeman-Fox-Partners, 1968a, 1968b and KGM, 1973).

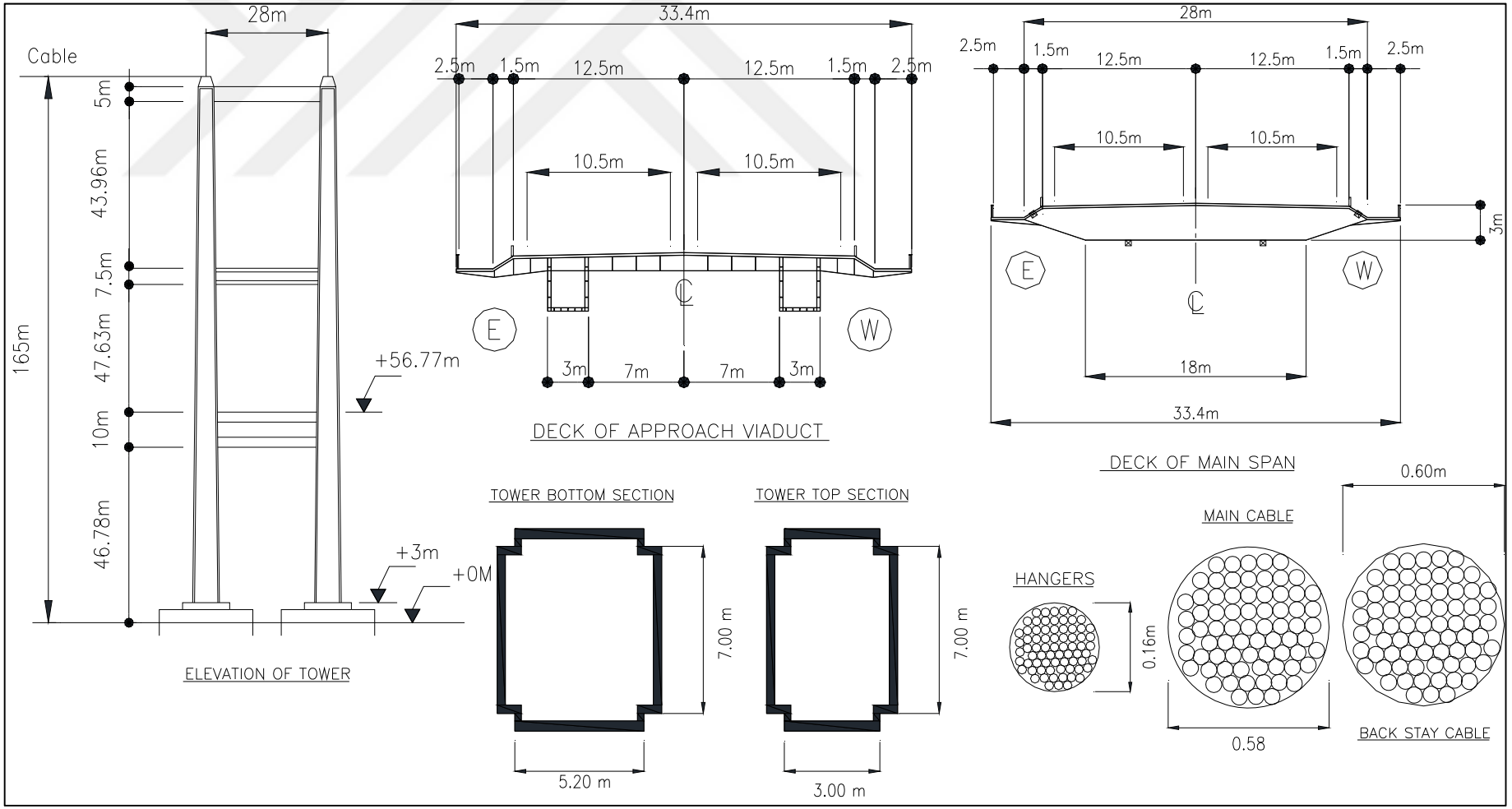

Figure 2.3 : Sectional properties of the components of the bridge (Freeman-Fox-Partners, 1968a, 1968b; KGM, 1973).

The First Bosphorus Bridge is the key transportation infrastructure in transportation networks of Istanbul, which in turn the Motorway-1 (O-1), one of the beltway between the two continents, was decided to be designed after the construction of the bridge. Therefore, the bridge currently serves as significant link for the city of Istanbul. The First Bosphorus Bridge is a gravity-anchored type of long-span steel suspension bridge. The aerodynamic deck box-section and the towers with tapered box-section are the key indicators to be a modern bridge. The bridge has the main span length of 1074 m and two approach-spans with the length of 231 m at the European side and 255 m at the Asian side, respectively. Only the main span is suspended with the suspenders; nevertheless, the approach spans are supported at the base instead of the suspender elements.

2.2 Physical and Sectional Properties

As shown in Figure 2.3, the width of the deck is 33.40 m and its height is approximately 3.00 m. The elevation view of the towers has a total height of 165 m from sea level to saddle**.** After the compacting, the equivalent diameter for the hanger rope with inclined form is 0.06 m, and for the main and backstay cables the diameter is approximately is 0.58 m and 0.60 m, respectively. Besides, the approach span of the bridge consists of a rigid superstructure including continuous rectangular box section and cross beams, and the circular box columns. All structural components of the towers, the main deck, the portal beams and the approach span were also strengthened with the bracing plates and diaphragms. Although it has experienced certain retrofit interventions, the First Bosphorus Bridge continues its critical function to annually carry more than five billion vehicles. Since trucks are detoured to the Fatih Sultan Mehmet Bridge, the First Bosphorus Bridge is in service only for cars and buses.

The detailed sectional properties of the main deck, towers, portal beams and approach viaduct box-beam of the bridge are also given in Figures 2.4-7, respectively. For this aim, the project specifications are originally considered and no idealization is made for the section analysis of the components. These detailed specifications are also helpful for the FE modelling of the bridge, which corresponds to the first step of St-Id approach.

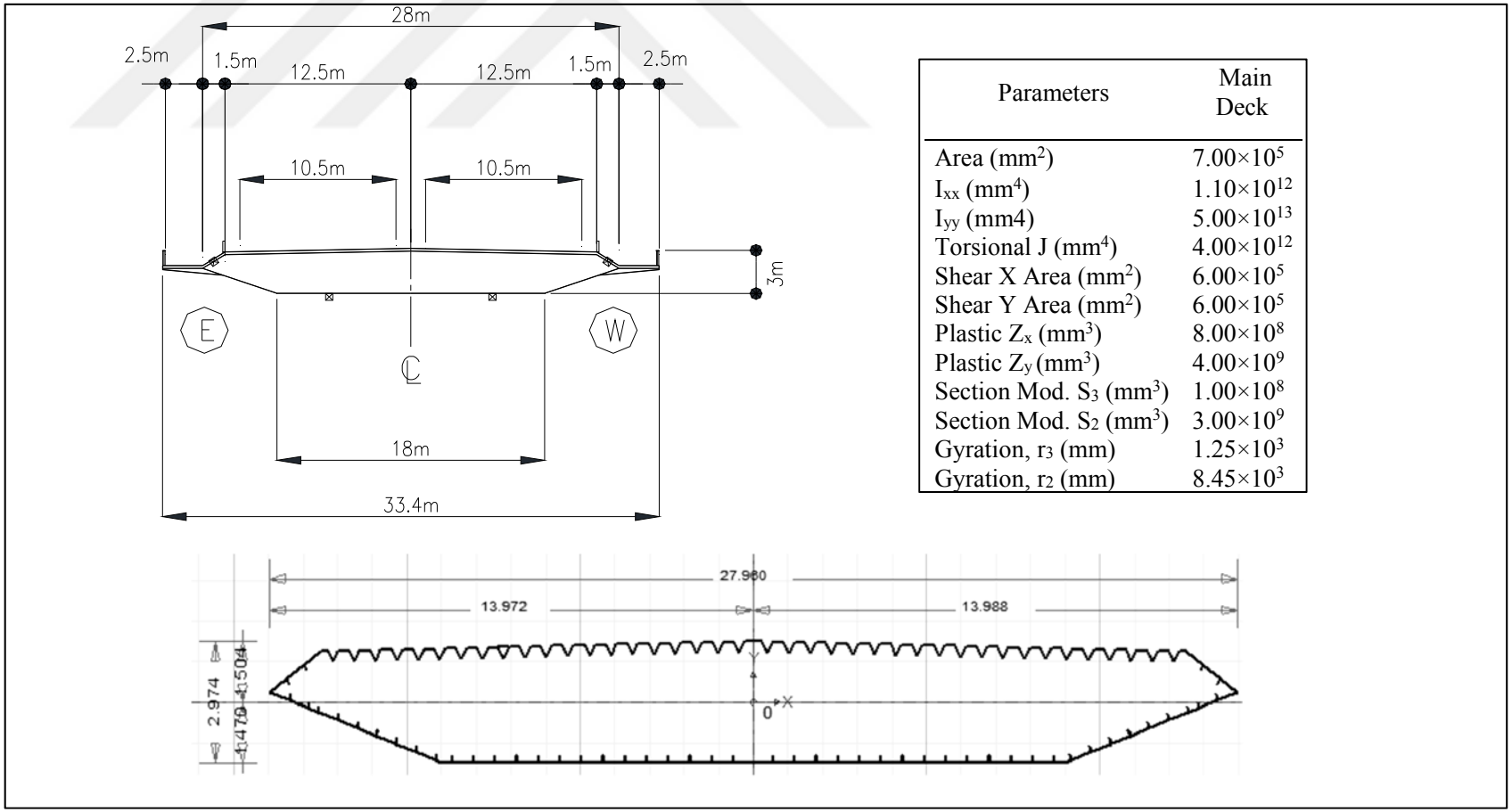

Parameters	Main Deck
Area (mm^2)	7.00×10^5
I_{xx} (mm^4)	1.10×10^{12}
I_{yy} (mm4)	5.00×10^{13}
Torsional J (mm^4)	4.00×10^{12}
Shear X Area (mm^2)	6.00×10^5
Shear Y Area (mm^2)	6.00×10^5
Plastic Z_x (mm^3)	8.00×10^8
Plastic Z_y (mm^3)	4.00×10^9
Section Mod. S_3 (mm^3)	1.00×10^8
Section Mod. S_2 (mm^3)	3.00×10^9
Gyration, r_3 (mm)	1.25×10^3
Gyration, r_2 (mm)	8.45×10^3

Figure 2.4 : Properties of the main deck section.

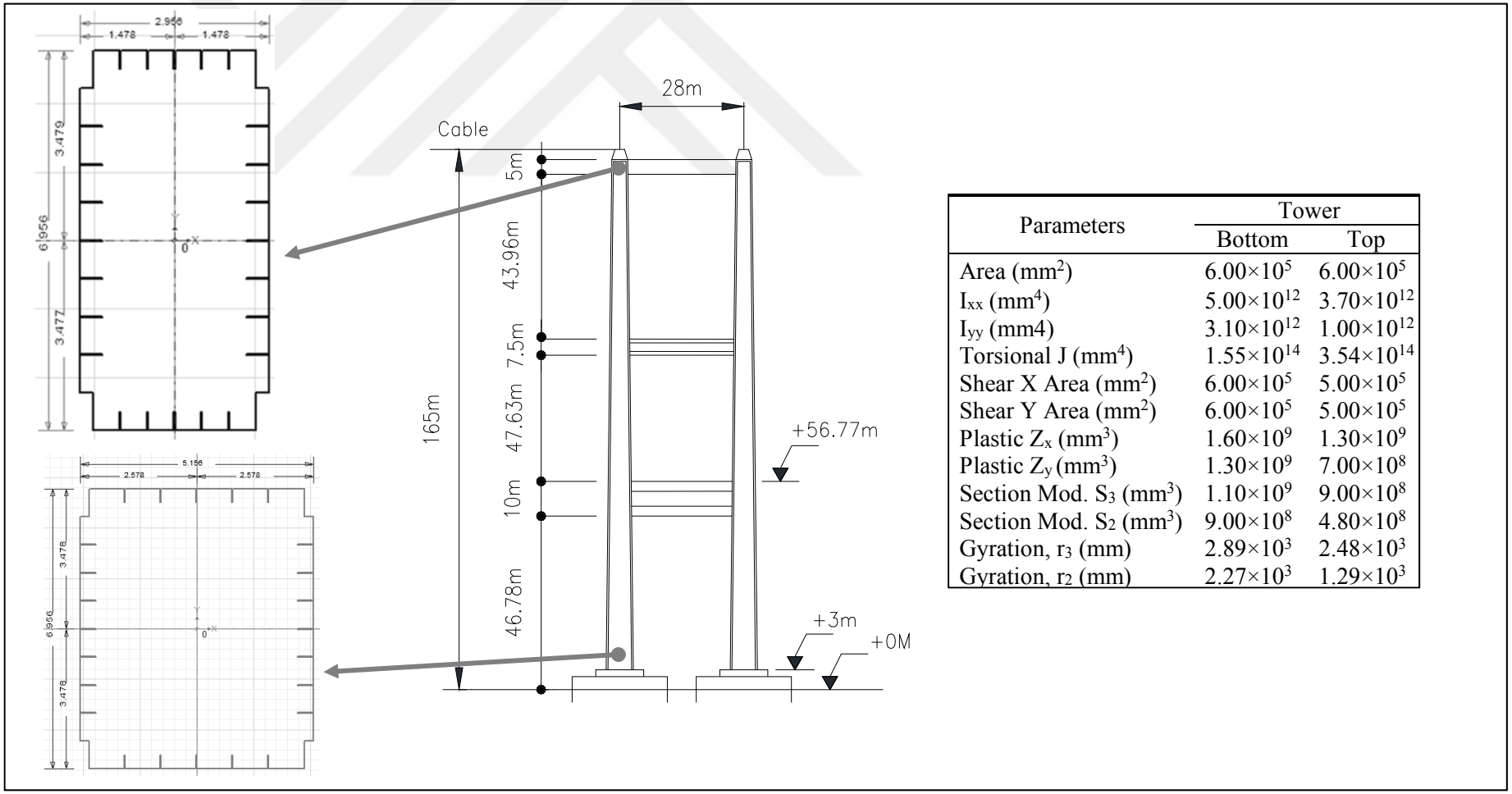

Parameters	Tower	
	Bottom	Top
Area (mm^2)	6.00×10^5	6.00×10^5
I_{xx} (mm^4)	5.00×10^{12}	3.70×10^{12}
I_{yy} (mm4)	3.10×10^{12}	1.00×10^{12}
Torsional J (mm^4)	1.55×10^{14}	3.54×10^{14}
Shear X Area (mm^2)	6.00×10^5	5.00×10^5
Shear Y Area (mm^2)	6.00×10^5	5.00×10^5
Plastic Z_x (mm^3)	1.60×10^9	1.30×10^9
Plastic Z_y (mm^3)	1.30×10^9	7.00×10^8
Section Mod. S_3 (mm^3)	1.10×10^9	9.00×10^8
Section Mod. S_2 (mm^3)	9.00×10^8	4.80×10^8
Gyration, r_3 (mm)	2.89×10^3	2.48×10^3
Gyration, r_2 (mm)	2.27×10^3	1.29×10^3

Figure 2.5 : Properties of the tower base and top-section.

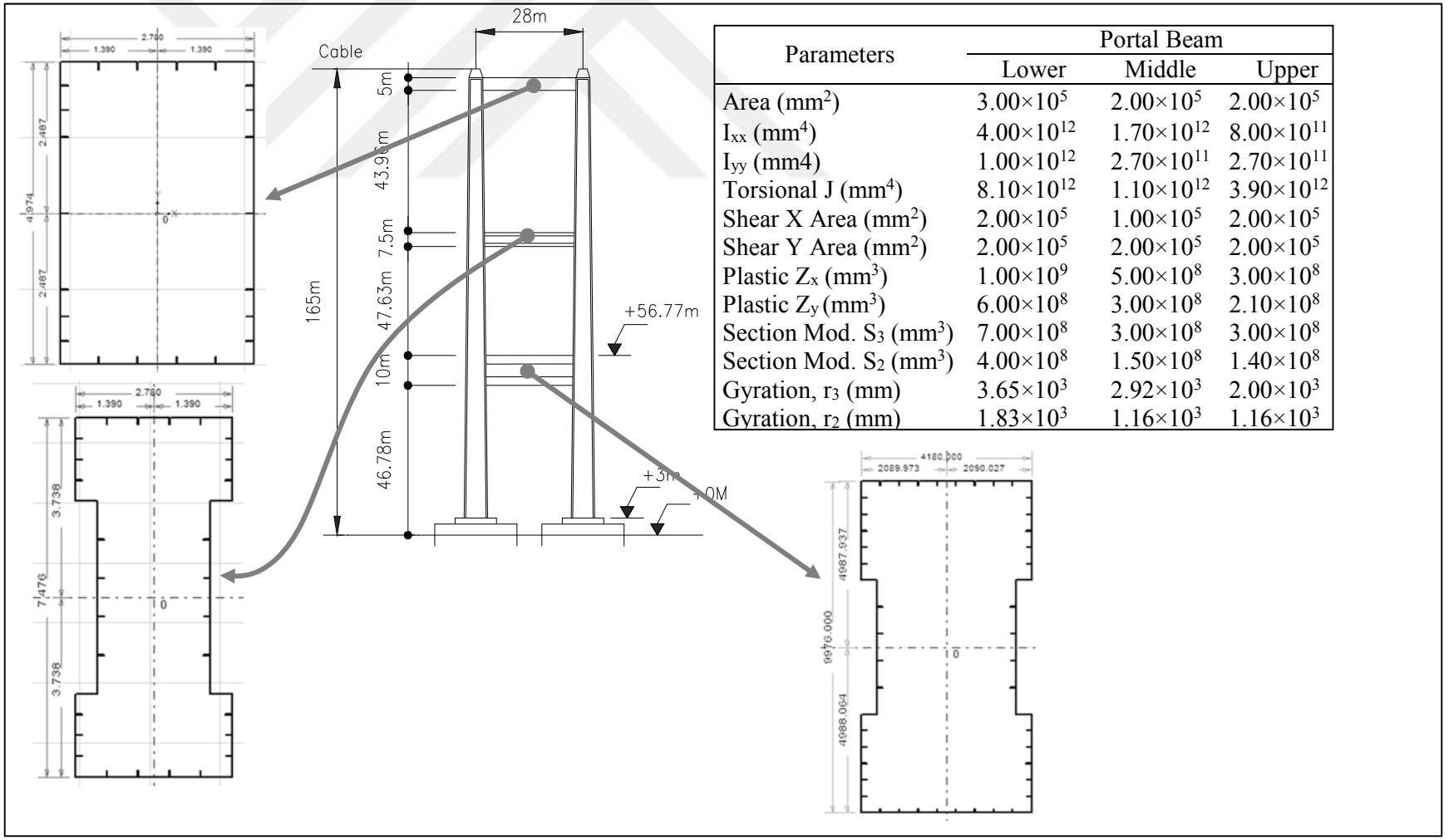

Parameters	Portal Beam		
	Lower	Middle	Upper
Area (mm^2)	3.00×10^5	2.00×10^5	2.00×10^5
I_{xx} (mm^4)	4.00×10^{12}	1.70×10^{12}	8.00×10^{11}
I_{yy} (mm4)	1.00×10^{12}	2.70×10^{11}	2.70×10^{11}
Torsional J (mm^4)	8.10×10^{12}	1.10×10^{12}	3.90×10^{12}
Shear X Area (mm^2)	2.00×10^5	1.00×10^5	2.00×10^5
Shear Y Area (mm^2)	2.00×10^5	2.00×10^5	2.00×10^5
Plastic Z_x (mm^3)	1.00×10^9	5.00×10^8	3.00×10^8
Plastic Z_y (mm^3)	6.00×10^8	3.00×10^8	2.10×10^8
Section Mod. S_3 (mm^3)	7.00×10^8	3.00×10^8	3.00×10^8
Section Mod. S_2 (mm^3)	4.00×10^8	1.50×10^8	1.40×10^8
Gyration, r_3 (mm)	3.65×10^3	2.92×10^3	2.00×10^3
Gyration, r_2 (mm)	1.83×10^3	1.16×10^3	1.16×10^3

Figure 2.6 : Properties of the portal beams.

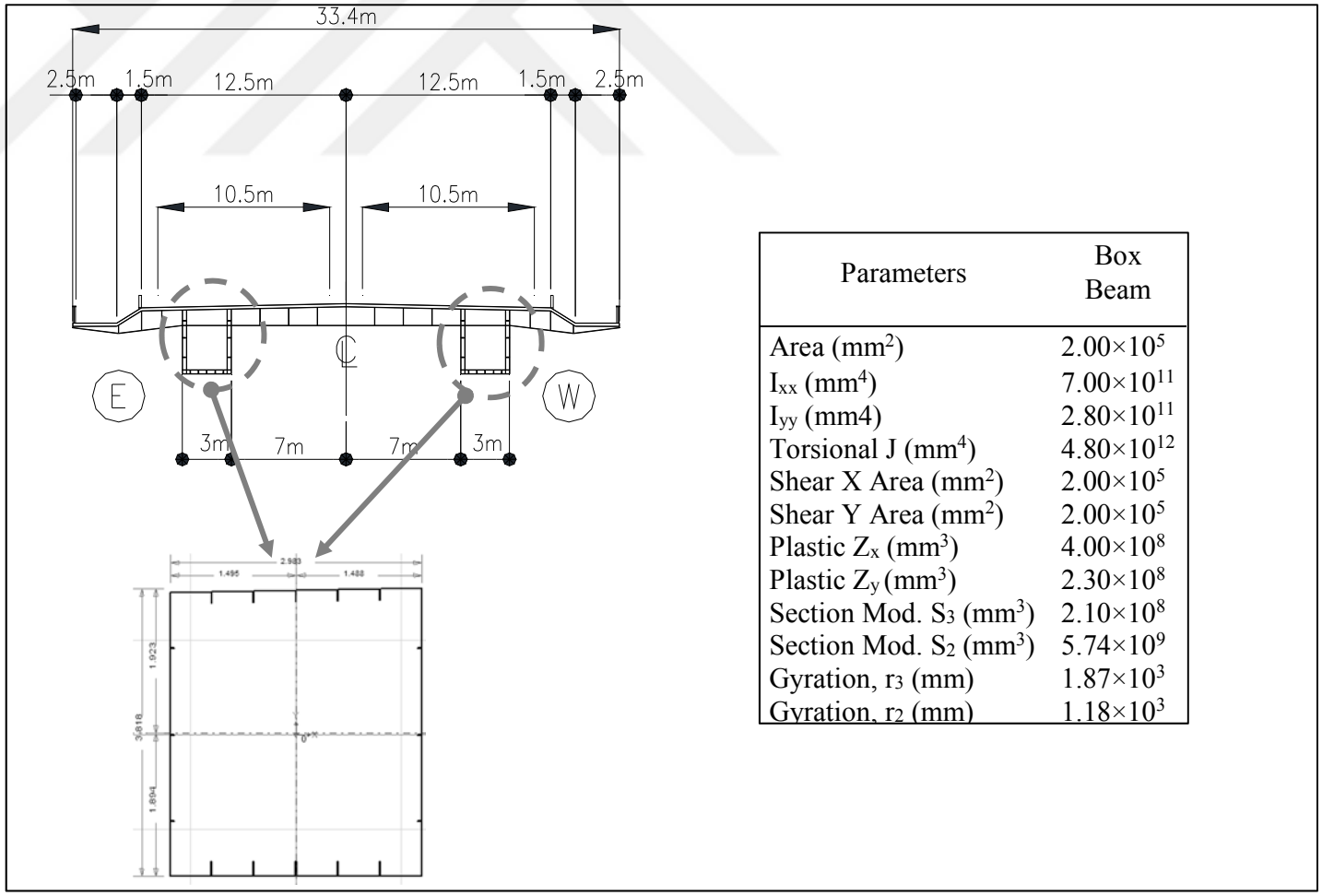

Parameters	Box Beam
Area (mm^2)	2.00×10^5
I_{xx} (mm^4)	7.00×10^{11}
I_{yy} (mm4)	2.80×10^{11}
Torsional J (mm^4)	4.80×10^{12}
Shear X Area (mm^2)	2.00×10^5
Shear Y Area (mm^2)	2.00×10^5
Plastic Z_x (mm^3)	4.00×10^8
Plastic Z_y (mm^3)	2.30×10^8
Section Mod. S_3 (mm^3)	2.10×10^8
Section Mod. S_2 (mm^3)	5.74×10^9
Gyration, r_3 (mm)	1.87×10^3
Gyration, r_2 (mm)	1.18×10^3

Figure 2.7 : Properties of the approach viaduct box-beam.

2.3 Hanger Replacement Project Specifications

The suspender elements, hangers, backstay and main cables, are the key structural components for long-span cable-supported bridges, especially for suspension bridges. As shown in Figure 1.1, the form of the main and backstay cables are generally identical for suspension bridges; however, hanger ropes are likely to be designed differently as the form of inclined or vertical. Therefore, elaborate investigation needs to be carried out so as to better understand the changes in the structural and dynamic behavior of suspension bridges under extreme events, such as seismic, strong wind etc.

2.3.1 New rocker bearings and wind tongues (shear key)

The new arrangement in the hanger elements is accompanied with the other engineering works including wind tongue, viscous damper devices, new rocker bearings and reinforcement of tower base section. As shown in Figure 2.8, new link elements of the rocker bearings and wind tongue are placed on the expansion joints.

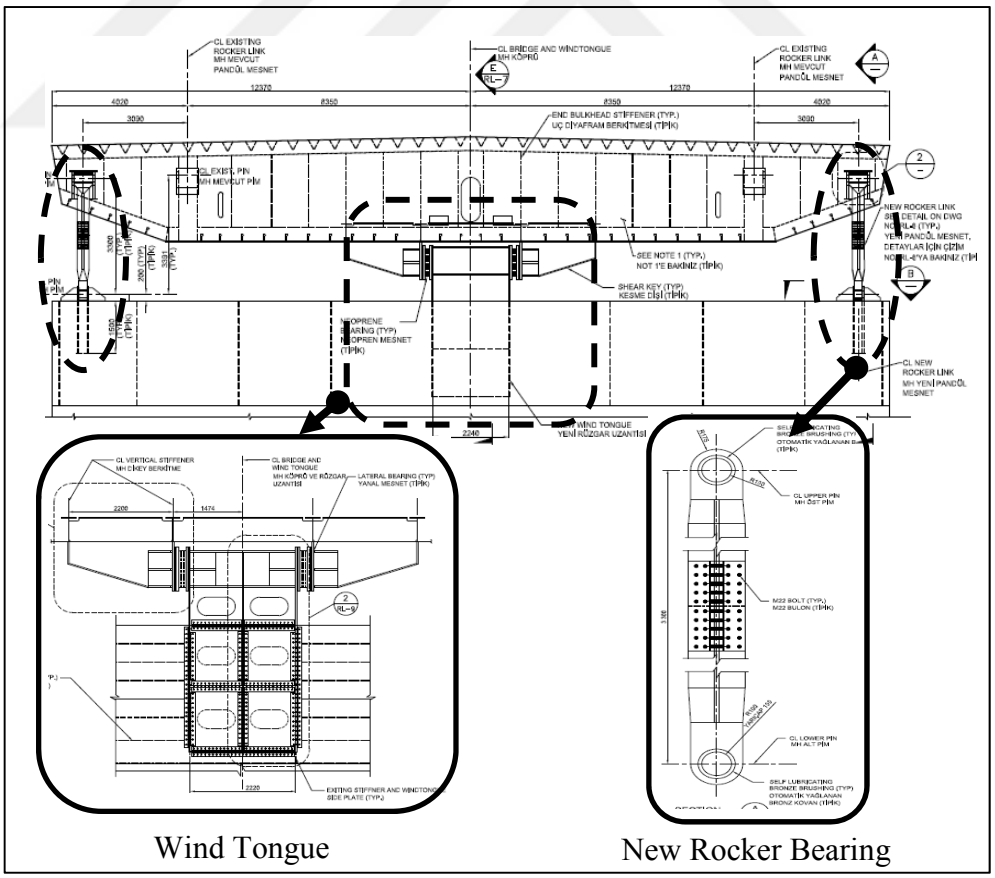

Figure 2.8 : Replacement of rocker bearings and placement of wind tongue (KGM, 2015).

2.3.2 Hanger replacement

One of the distinguished specifications of the Bopshorus Bridge is to be designed by the inclined hangers instead of widely adopted vertical hanger form in long-span suspension bridges. Within the scope of general maintenance, repair, structural reinforcement, engineering works and consultancy services of the Bosphorus Bridge, the inclined hangers were replaced with the vertical hangers. Due to replacement of 236 inclined hanger elements, this work package has longer duration than other works. As indicated in Figure 2.9, two hanger ropes are designed to be a group and aligned as parallel along the bridge. Besides, new stool plates on the deck and cable bands on the main cable are used due to the change in its connection points to the deck and main span.

2.3.3 Viscous dampers

With the new design of the expansion joints, viscous damper are considered in the project as depicted in Figure 2.10. Due to high vulnerability of the expansion joint to operational and extreme events, damage resulting from the exceedance of displacement capacity in longitudinal direction is aimed to be prevented with the viscous dampers located on two sides of the bridge. The viscous dampers are working a connection between the main deck and the tower legs as shown in Figure 2.10. A total number of four dampers are considered in the project. Besides, detailed technical specifications for the viscous dampers that include rated force, damping coefficient (c) and constant (α) are given in Figure 2.10.

2.3.4 Tower base retrofit

The project also contains the sectional retrofitting efforts for the tower base-section. For this aim, additional longitudinal stiffeners are considered and thus, doubly symmetric W530x123 I-beam are located on the section. As presented in Figure 2.11, the wide-flange I-beams are extended along a certain part of the towers. The longitudinal stiffeners are connected to the inner plates of the towers with bolts. Diaphragm plates between I-beams are also used to provide integrated response of the section. Based on these specifications, the sectional capacity of the tower base-section is estimated to be high compared to the original project section with relatively small existing longitudinal stiffeners.

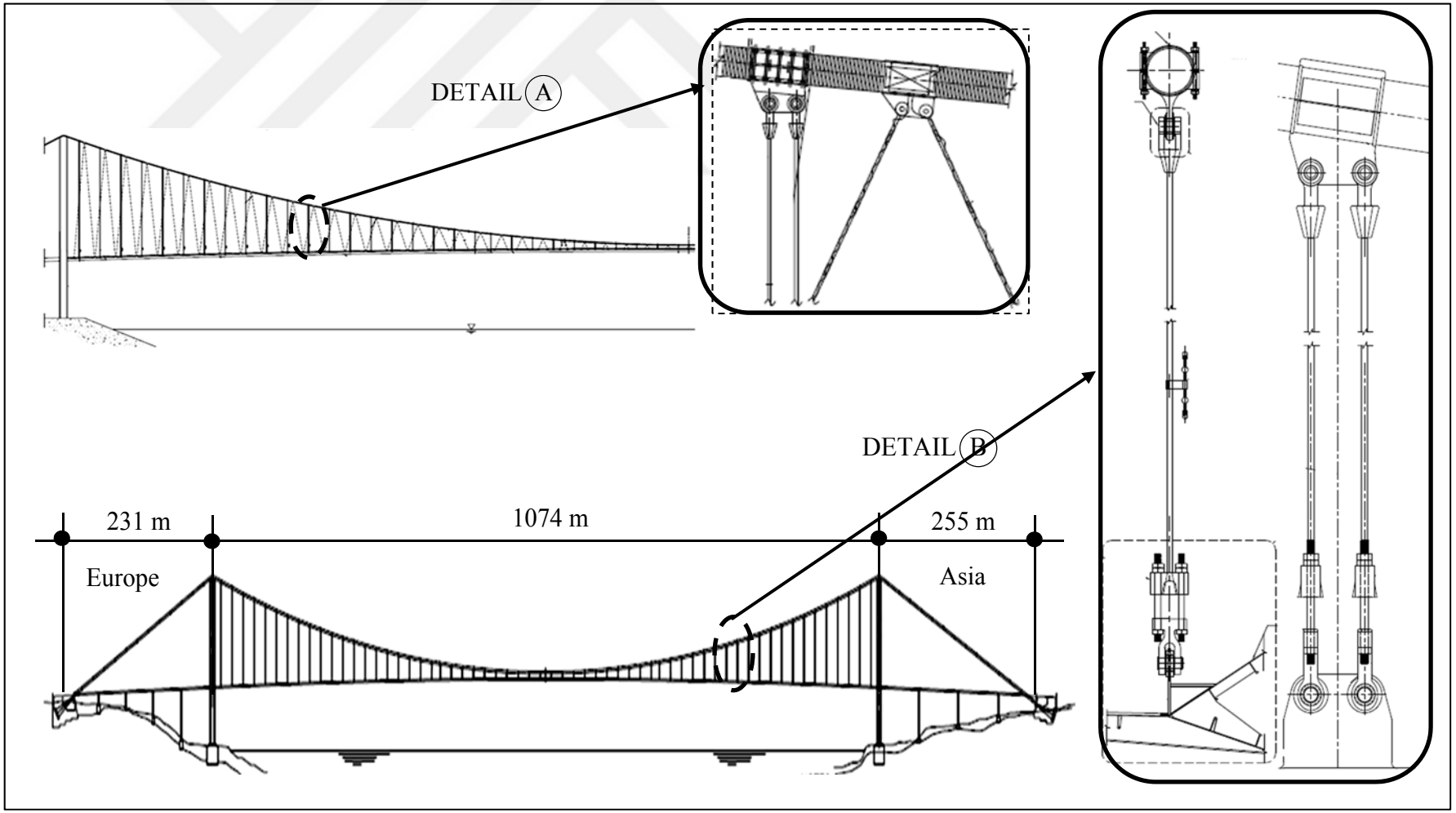

Figure 2.9 : Specifications of hanger replacement project and as-built drawings (KGM, 2015).

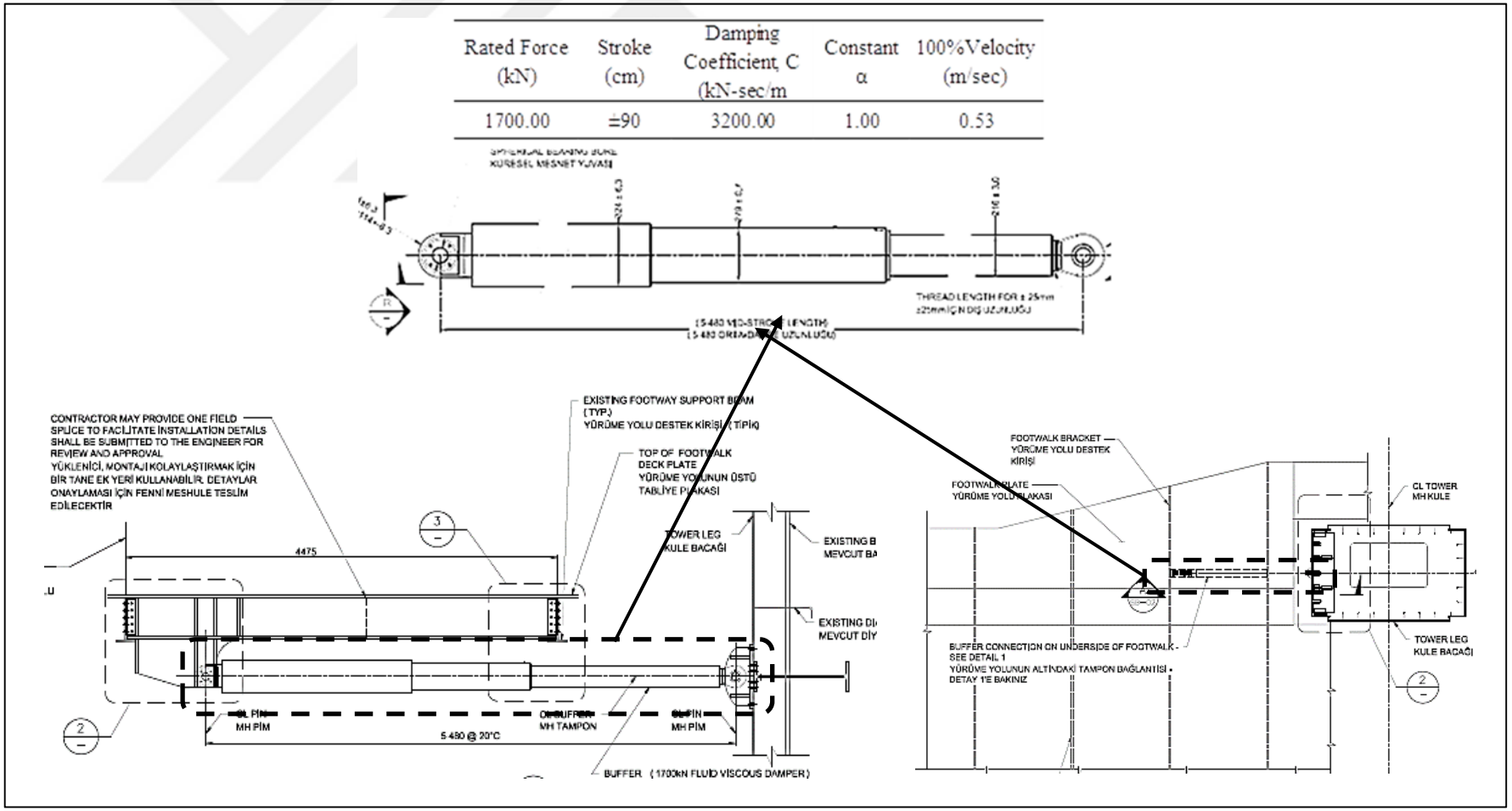

Figure 2.10 : Placement of viscous damper and damper specifications (KGM, 2015).

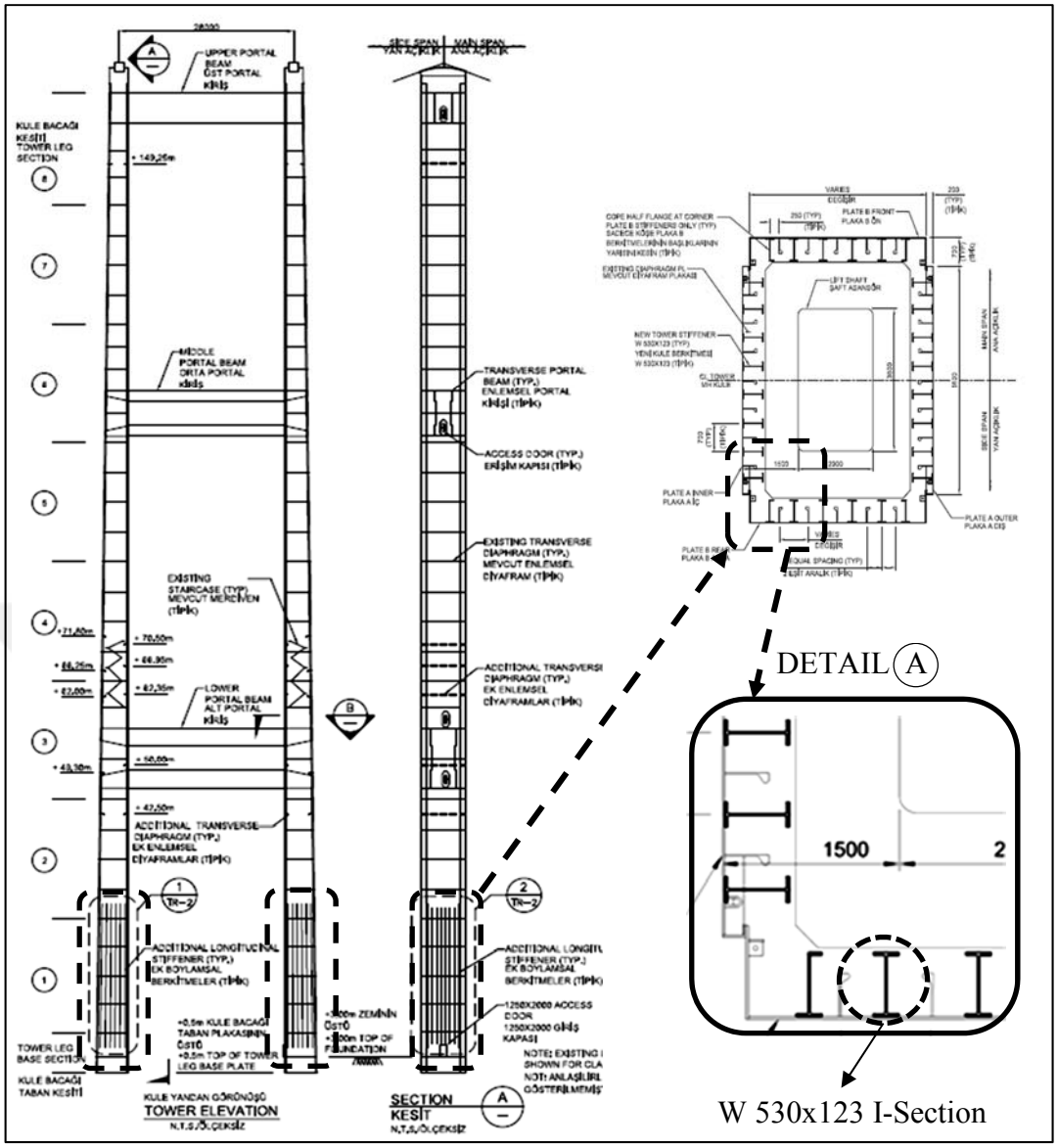

Figure 2.11 : Tower base-section retrofit specifications as-built drawings (KGM, 2015).

3. FINITE ELEMENT MODEL (FEM) OF THE BRIDGE

3.1 Background

Most of long-span cable-supported bridges are subjected to different loads, such as wind, earthquake and heavy traffic loads. Although this type of bridges has been analyzed under the loads by experimental methods to identify their real behavior, this is not possible many times since large-scale structures require comprehensive tools and techniques. Therefore, combination of experimental study with numerical study is considerably important to make an effective analysis. As in many disciplines, the application of a detailed accurate finite element model in bridge engineering has been relatively significant tool to properly assess structural performance of bridges. Hence, the finite element method has been considered as widely-accepted tool in numerical analysis. The major leaps in computation technology enable to make advanced FE modeling and analysis. Due to the complexity of long-span cable-supported bridges, these structures are modeled based on certain assumptions: (a) simplified spine-beam model, (b) multi-scale (hybrid) FE model. The spine-beam model that enables to reduce DOF of bridge structures presents their global behavior. Using the spine-beam model, modal analysis can be readily conducted to obtain the dominant modes and associated mode shapes. In addition, preliminary FE model that is developed based on project drawings can be validated using this modeling technique. Therefore, the spine-beam modeling technique helps to check the considered equivalent sectional properties of structural components. On the other hand, multi-scale modeling becomes very significant upon making analysis for local structural component. This modeling technique also provides that different element types, beam, solid, shell, and truss, are used together to establish 3D full-scale bridge model. Accordingly, both modeling techniques are utilized for different goals, and generally, they have been used together for structural analysis.

In literature of FE model of long-span bridges, the spine-beam modeling technique, which have an idealization of equivalent sectional features to the current structural components, helps to determine the dynamic characteristics and global behavior of the

bridges. However, local behavior and damage assessment at critical points, such as stress-strain variation of a component of the bridges cannot be captured directly by the spine-beam model. Instead of this method, the multi-scale modeling technique is required to make local behavior analysis. As shown in Figure 3.1, Zhang et al. (2001) developed 3-D FE model of the Kap Shui Mun Bridge in Hong Kong based on its as-built drawings including certain idealizations to calibrate dynamic characteristics of the model with the measured data. For this purpose, the spine beam FE modeling method was used utilizing elastic beam elements for the towers and deck, and truss elements for the cables, and elastic or rigid links for the connections and the boundary constraints.

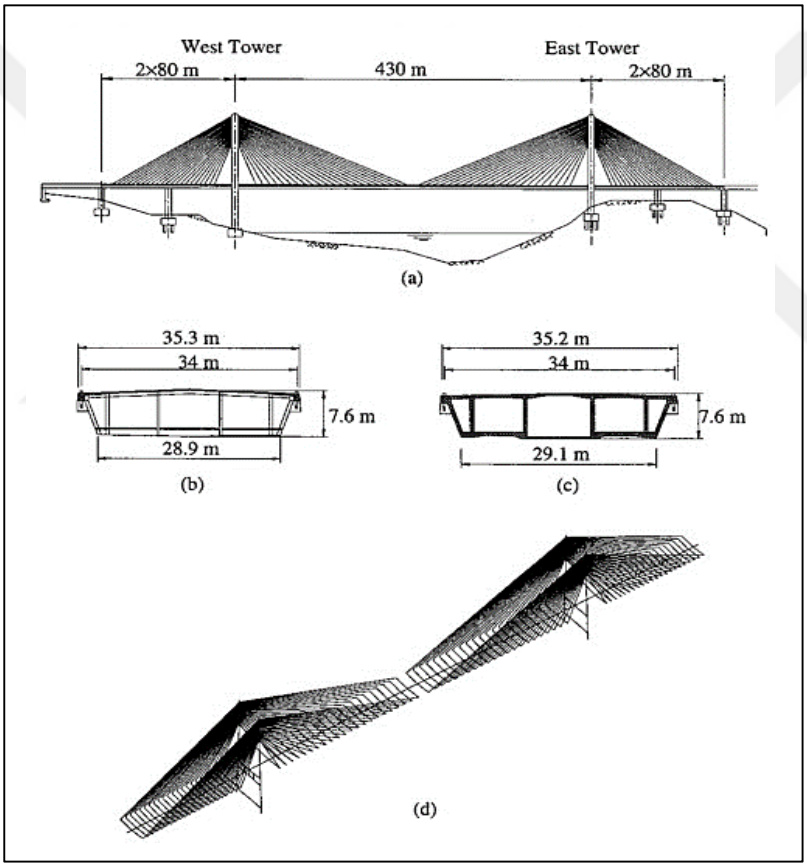

Figure 3.1 : Schematic representation of the Kap Shui Mun Bridge: (a) Elevation, (b) Typical cross section of the composite deck; (c) Typical cross section of the prestressed box girder, (d) 3-D finite element model (Zhang et al, 2001).

Upon establishing FE model of the bridge, actual sectional properties of the bridge were considered as equivalent beam and truss elements. The developed model was then calibrated on the basis of its dynamic characteristics so as to reduce discrepancies between FE model predictions and free vibration measurements (Ambient Vibration). Accordingly, more reliable modal properties can be determined by the updated FE

model. This study showed that equivalent FE element model of the Kap Shui Mun Bridge is much more helpful to determine its dynamic response properties. However, the study cannot include investigations on analysis of local structural components of the bridge. Therefore, the contribution of the study to full response of the bridge is only in global scale. Chan et al. (2003) built spine-beam finite element model of the Tsing Ma Bridge for fatigue analysis shown in Figure 3.2. The first attempt was to develop initial full-scale FE model based on the project drawings in order to make effective fatigue stress analysis. Dynamic characteristics of the developed FE model were compared with online data measured by structural health monitoring system installed on the bridge to verify the proposed FE model. The results indicated that the verified FE model relatively was suitable for fatigue analysis. Since the established FE model just provided limited results for stress analysis at critical locations of the local components, such as, welded joints where stress distribution concentrated, deck element and welded region were modeled separately from the entire bridge model as shown in Figure 3.3. The FE model of global bridge and its local element was achieved utilizing ABAQUS.

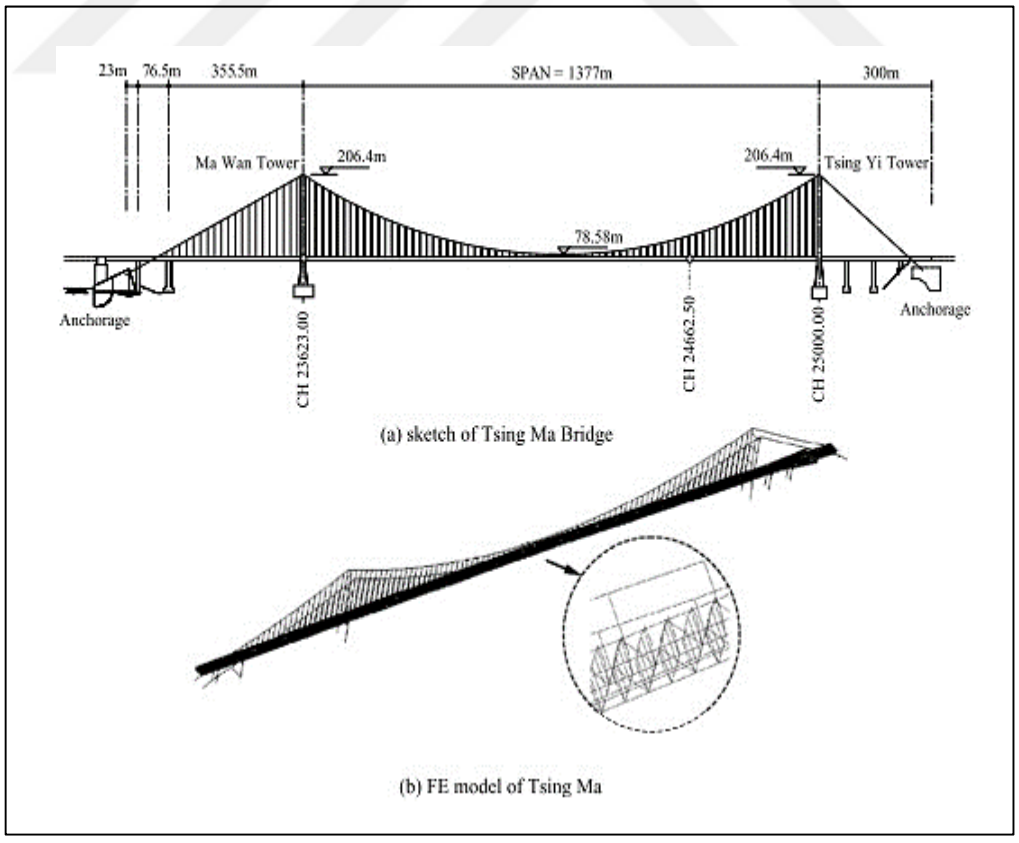

Figure 3.2 : FE model of the Tsing Ma Bridge (Chan et al, 2003).

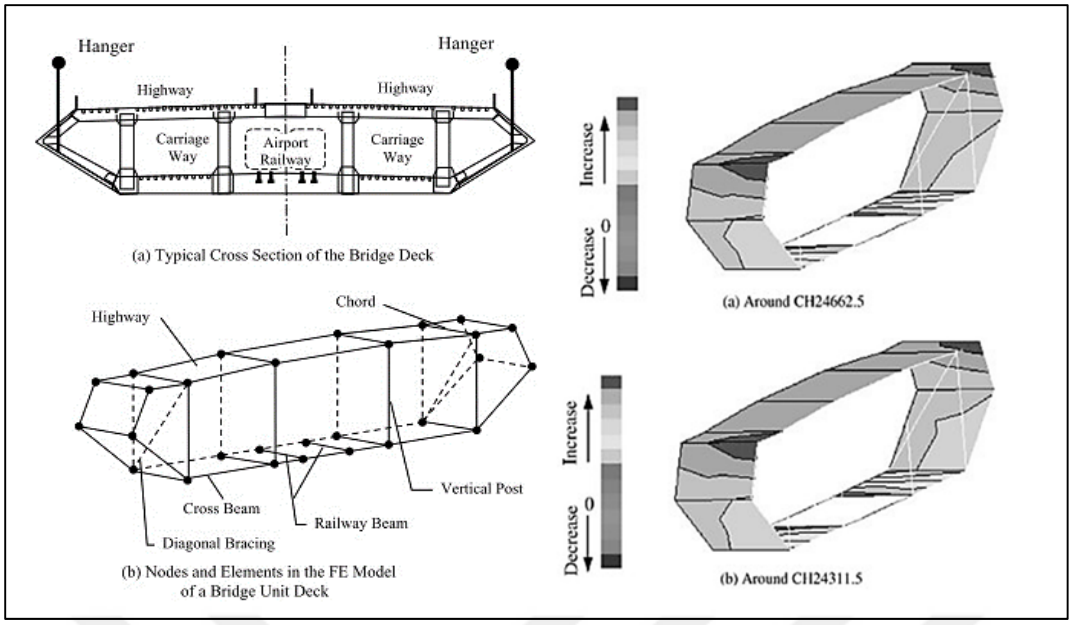

Figure 3.3 : The bridge deck element and stress distribution (Chan et al, 2003).

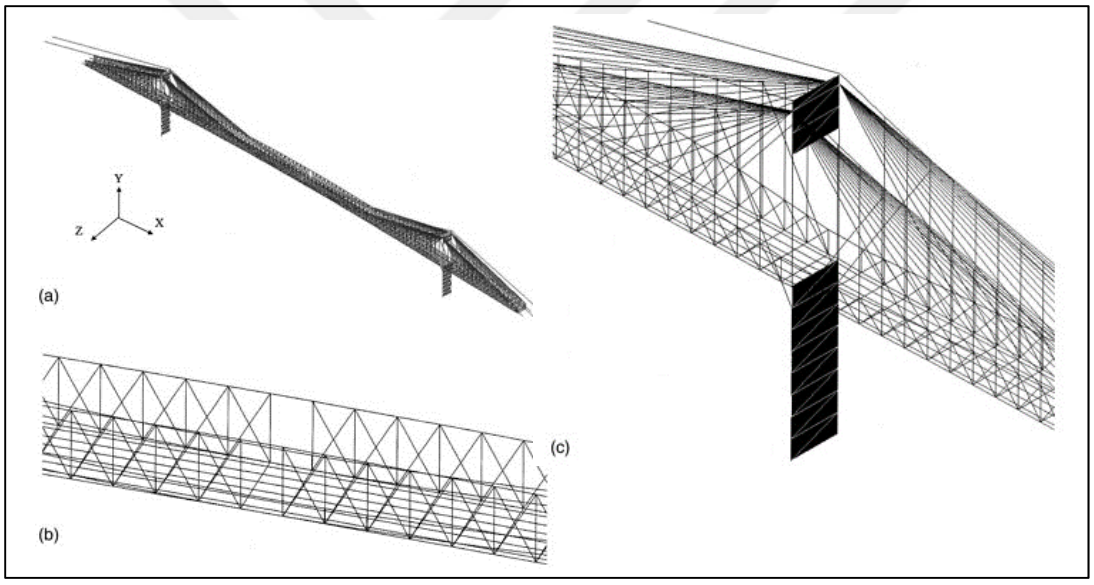

Figure 3.4 : 3-D Finite element model of Roebling Bridge: (a) 3-D elevation, (b) part elevation (span center and stiffness truss), (c) part elevation (tower and cables) (Ren et al, 2004).

The study provided insight into the use of the local structural FE model. The conclusions of the study showed that the multi-scale modeling (hybrid) including different type of elements such as shell, solid and beam elements is required for local analysis while simplified spine modeling is generally suitable and used for global behavior analysis. Ren et al. (2004) made efforts to conduct static and dynamic analysis developing FE element model of the Roebling Suspension Bridge (1867) across the Ohio River. Upon developing 3-D FE model utilizing ANSYS (2009) commercial program, all cable members were designed to bear tension force only and

modeled as truss element. Stiffening deck was also considered truss element, whereas tower was modeled elastic elements. Since the web walls of the towers undertook bending action, they were established 3-D membrane shell elements. Therefore, the hybrid modelling was taken into account for FE model of the bridge shown in Figure 3.4.

The study, which presented the results from dead-load static analysis, the prestressed modal analysis and parametric studies, indicated that the bridge had geometrically non-linear response due to cable sag effect, that dead-load has to be considered initial task to perform dynamic analysis, and that mass, cable-elastic modulus, stiffening truss stiffness, transverse-bending stiffness were the key parameter having considerable effect on dynamic characteristics of the bridge. This study provides certain contributions to how to use the hybrid modeling technique that requires different type of FE elements for the actual elements of the bridge by predicting their real behavior. Using ANSYS software, Jaishi and Ren (2005) established three-dimensional linear elastic finite element model of Beichuan River concrete-filled steel tubular arch bridge shown in Figure 3.5 so as to conduct on-site dynamic testing for model updating. This was achieved by the method of ambient vibration.

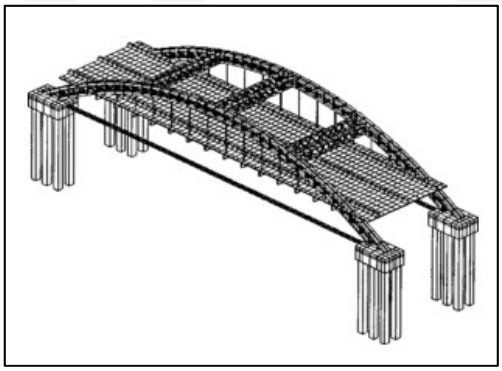

Figure 3.5 : 3-D model of the bridge (Jaishi and Ren, 2005).

In 3-D FE model, two-node beam element was considered for the arch members, cross girders, and bracing members, while all suspenders were modeled as truss elements. However, for the deck of the bridge shell element was used. As seen from these considerations, the bridge was developed using the multi-scale modeling technique. Since the study focused on dynamic properties for model updating, the bridge was developed entirely. The results obtained from the study indicated that the proposed FE model of the bridge was suitable for model updating. This study shows that similar considerations in FE modeling can be implemented on bridge structures to carry out

modal updating study. Ren et al. (2005) conducted experimental and analytical studies on the Qingzhou cable-stayed bridge in Fuzhou, Fujian Province, China to validate developed initial 3D FE model of the bridge with ambient vibration test results. With the help of the ANSYS software, the bridge was modeled by different types of finite elements: the steel girders, stringers, floor beams and concrete towers were developed by elastic beam elements. Considering the effect of cable sag, all cable elements were modeled by 3-D tension-only truss elements. The concrete slab was considered as shell elements, and solid elements were used for the piers and platforms. In addition to these elements, two different type of boundary conditions were used: fixed constraint was used to provide link between pier and deck, and expansion constraint was used for the rest of piers. Complete FE model of the bridge is shown in Figure 3.6.

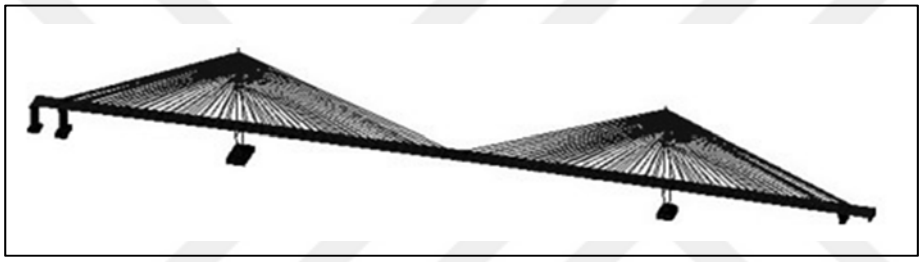

Figure 3.6 : 3-D FE model of the bridge (Ren et al, 2005).

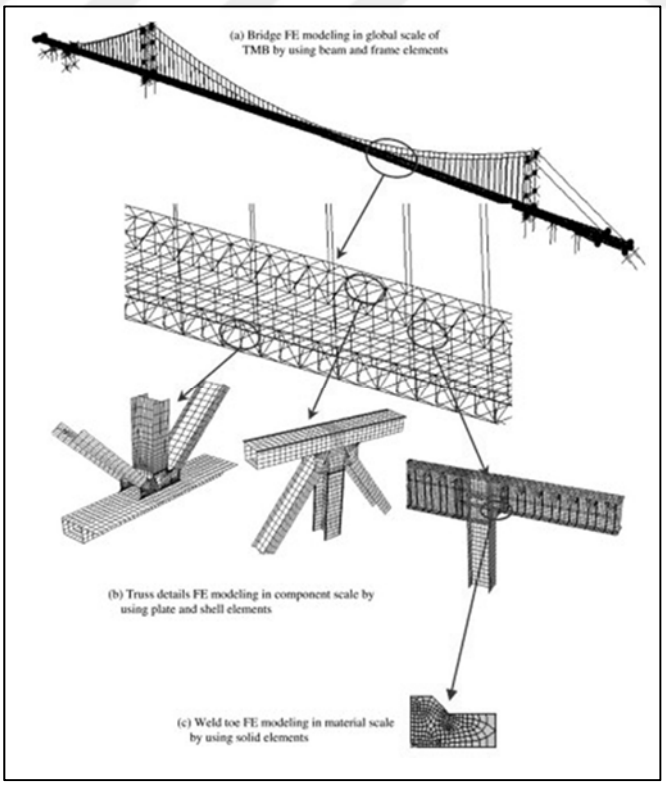

Figure 3.7 : Multi-scale modeling of the bridge (Li et al, 2007).

The study showed that even if the drawing-based idealized FE model of the bridge was realistically modeled, it must have been validated by experimental test results to make precise analysis in further study. However, initial FE model provided detailed source of information for physical and modal properties of the bridge. The contribution of the study to modeling large span bridges is that model updating is necessary, no matter how it is modeled in detail based on the design project specifications. Li et al. (2007) proposed a multi-sale numerical analysis approach for dynamic response analysis and local damage of the Tsing Ma Bridge (TMB). For this purpose, three different scale levels, global, component and material scale, were defined in the study. Global scale model was developed to predict critical components with higher internal actions by making linear analysis under service loads. Local scale model of these critical components was established to make stress-strain and damage detection analysis of their critical details, such as connection details. Material scale model of these critical details was developed to determine response of their material. As shown in Figure 3.7, the bridge was modeled in global scale using beam and truss elements, deck chord elements with welded connections were simulated in component scale considering plate and shell elements, and in material scale, weld details at these chord elements were modeled using solid elements. All works on FE modeling were achieved by the ABAQUS and ANSYS software. This study showed that the proposed multi-scale numerical procedure predicted accurately fatigue response of long-span bridges, and multi-scale modeling technique (hybrid) could be simply implemented for multi-scale numerical analysis. The concluded remarks of the study provide that specific numerical analysis procedure can be developed using the multi-scale (hybrid) modeling technique. Wang et al. (2010) presented a two-phase model updating approach to establish a baseline model for the Runyang Suspension Bridge in China. Considering the construction stage of the bridge, the initial phase was tower phase, and the other was complete bridge phase. For this purpose, towers were modeled by separating from the bridge, and the full-scale bridge model was developed shown in Figure 3.8. These models were established by the ANSYS software. In the modeling, the deck, the central buckle and the towers were modeled by beam elements while the main cables and the suspenders were simulated by truss elements. The study showed that the proposed updating process was achieved simply more than traditional approaches through the ambient vibration data. It was also stressed in the study that the updated and validated FE model of the bridge could a powerful tool for wind-

induced vibration analysis, anti-seismic assessment, long-term structural health monitoring, damage detection and more precise dynamic response analysis.

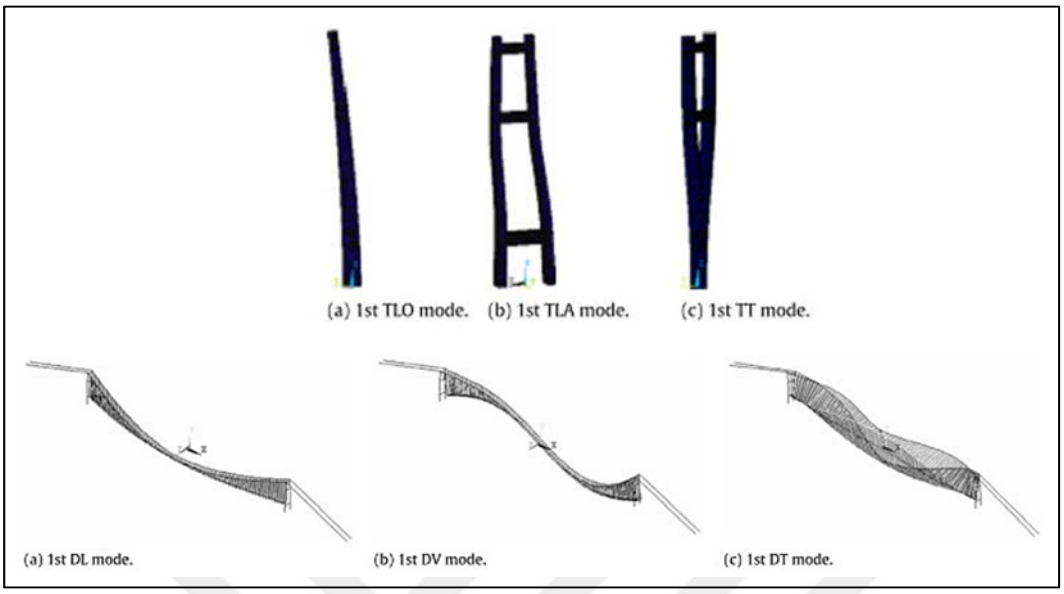

Figure 3.8 : Dynamic analysis results of towers and full-scale model of the bridge (Wang et al, 2010).

A much more comprehensive study on Structural Health Monitoring-oriented 3-D finite element model of the Tsing Ma Bridge in Hong Kong was carried out by (Duan et al. (2011) For this aim, all structural elements of the bridge including bridge deck, tower, main cables and suspenders, saddles, pier and anchorage were modeled in detail to perform structural performance analyses at local and global scales. Four parts were considered to establish FE model of the bridge: (1) modeling of the bridge deck (2) modeling of the towers and piers (3) modeling of the cable system and the fixture components and (4) modeling of the full-scale bridge. The deck plate was modeled as shell elements to make detailed stress or strain data analysis to be compared with measured results. The beam element was used for all frames and trusses. Figure 3.9 shows the developed bridge deck model. The reinforced concrete in tower legs, foundations and portal beam were modelled as solid element, and truss-bracing elements in portal beams were considered beam element. The main cables and suspenders were modeled as beam element, and cable bands were modeled as pipe element. Besides, as shown in Figure 3.9, the tower saddles were modeled partially using solid and shell element. The full-scale bridge structure was modeled by assembling these developed structural components of the bridge as indicated in Figure

3.10. For boundary conditions, fixed supports for the ends of main cables and for the bottom of the bridge as indicated in Figure 3.10.

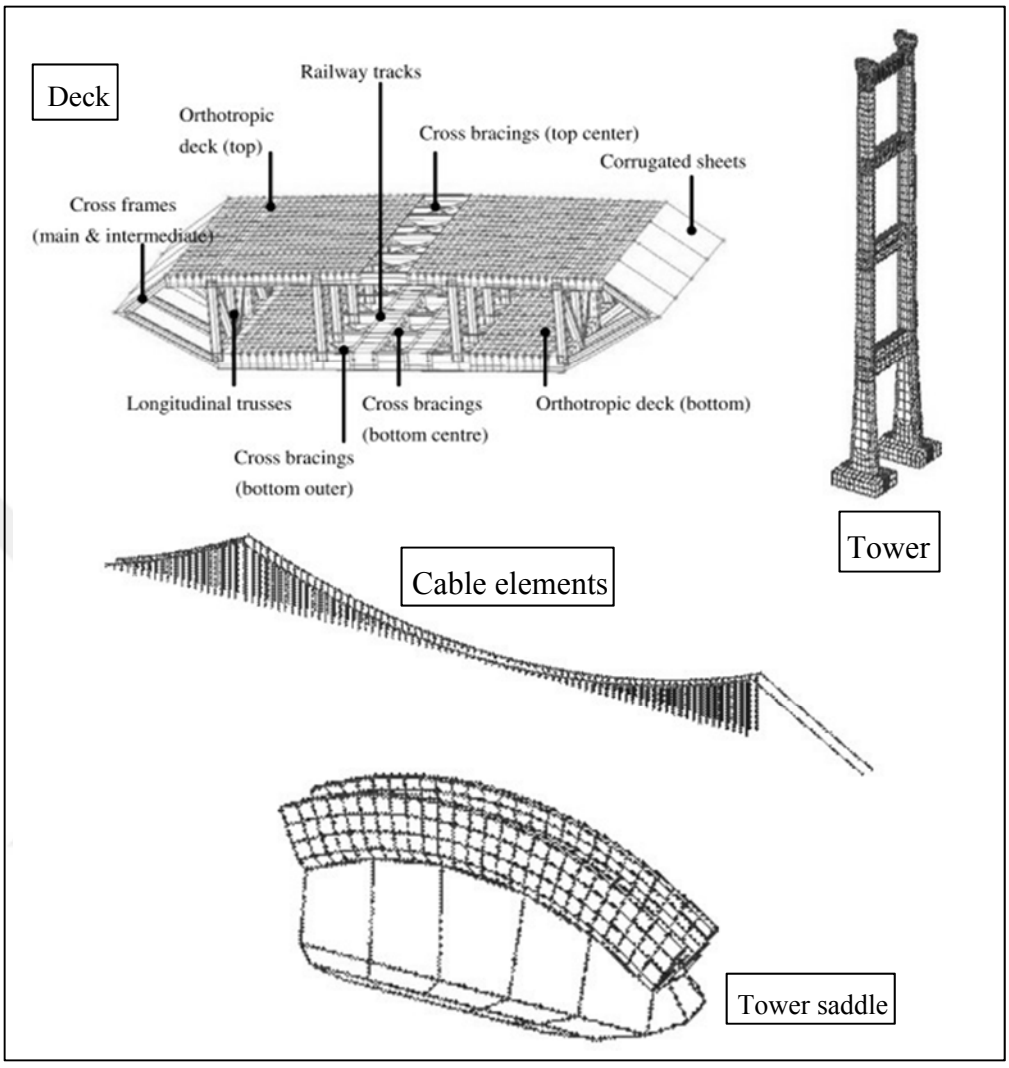

Figure 3.9 : Full-scale FE model of the Tsing Ma Bridge (Duan et al, 2011).

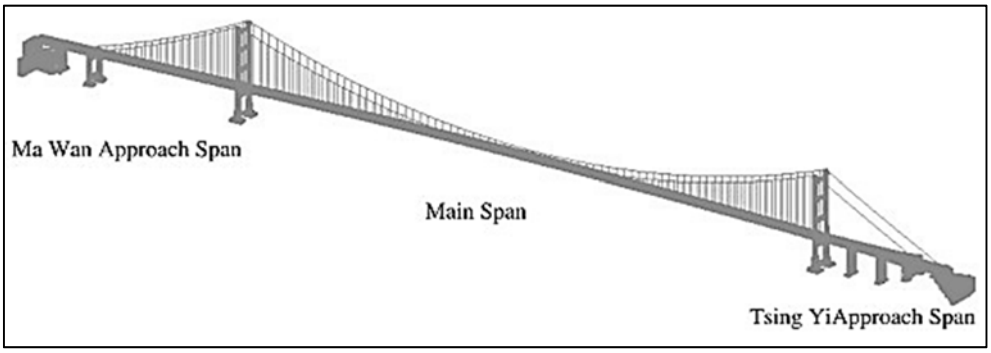

Figure 3.10 : Full-scale 3-D finite element model of the Tsing Ma Bridge (Duan et al, 2011).

For boundary conditions, fixed supports for the ends of main cables and for the bottom of all piers, and hinge and sliding supports for the deck ends of the bridge were taken

into account. In addition, Multi-point-connection (MPC) were used for deck-tower connections and deck-pier connections. All works on developing the FE model of the bridge were conducted by MSC/Patran as model builder and MSC/Nastran as finite element solver.

This study is the best example of advanced FE model of long-span bridge in literature since all elements are modeled to reflect the real structural components of the bridge. Therefore, this FE model meets approximately all requirements of SHM-oriented bridge modeling. A newly built suspension bridge in California, the New Carquinez Bridge (NCB) were modeled by Hong et al. (2011) to establish a framework for numerically predicting the wind-induced behavior of the bridge using output-only system identification. Based on the geometric and physical features of the NCB, the bridge structure was modeled by using the simplified spine-beam modeling technique: the orthotropic deck was simulated by elastic two-node beam element while two-node beam element with large displacement and strain was used for the main cables and suspenders. Rigid rocker links in any direction of interest and equivalent three degree of freedom elastic springs were utilized for boundary conditions of the bridge. All efforts to develop FE model of the NCB were achieved by program ANSYS. This study proved that dynamic characteristics-based updated FE element model of the bridge predicted its wind-excited response accurately when comparing with the measured data. Thus, this FE model also enabled to make the monitoring system installed on the bridge more effective under wind action. Asgari et al. (2013) conducted a study on developing updated FE model of Tatara Bridge in Japan. Making a comparison of modal analysis results of initial FE model with field vibration test results, the updated FE model of the bridge shown in Figure 3.11 was developed, and the verification study was also conducted.

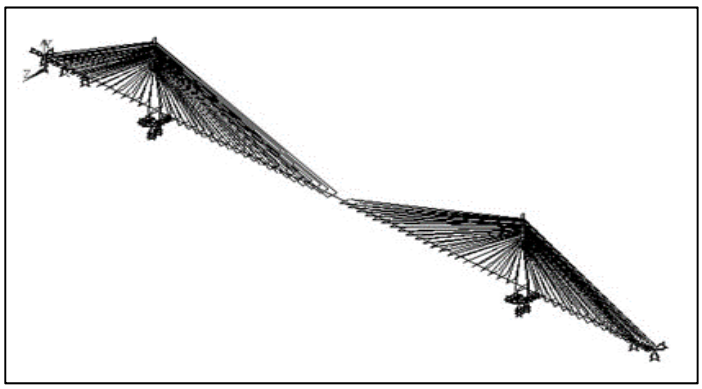

Figure 3.11 : 3-D FE model of the Tatara Bridge (Asgari et al, 2013).

Since the bridge deck has high torsional stiffness, it can be simulated by single-spine-beam element. Thus, the deck was modeled as elastic beam element using ANSYS. Similarly, the bridge towers were considered as elastic beam element, and tension only truss element was used for the stay cables of the bridge. Fix constraints for tower base, tension-link mechanism for deck ends at the abutment and the pier were considered. This study showed that single-spine girder proposed for the bridge deck and truss elements proposed for the stay cables simulated the real bridge performance of the bridge. The necessity of accurately modeling the boundary conditions for dynamic response of the bridge was also stressed in the study. Zhu et al. (2014) established FE model of the Stonecutters Bridge in Hong Kong using the multi-scale modeling technique to conduct model updating study. Since all components of a bridge were not directly monitored due to limitation in the number of sensor in SHM system, the multi-scale modeling technique was helpful for effective performance assessment. Therefore, this study presented the details of how the method could be implemented on the Stonecutters Bridge. In the modeling, the bridge deck was modeled by shell elements to directly gain stress/strain responses of the bridge. Other structural components of the bridge: the towers and the piers were modeled by equivalent beam element, and the cables were simulated by tension-only truss element. The developed 3-D FE model of the bridge is shown in Figure 3.12.

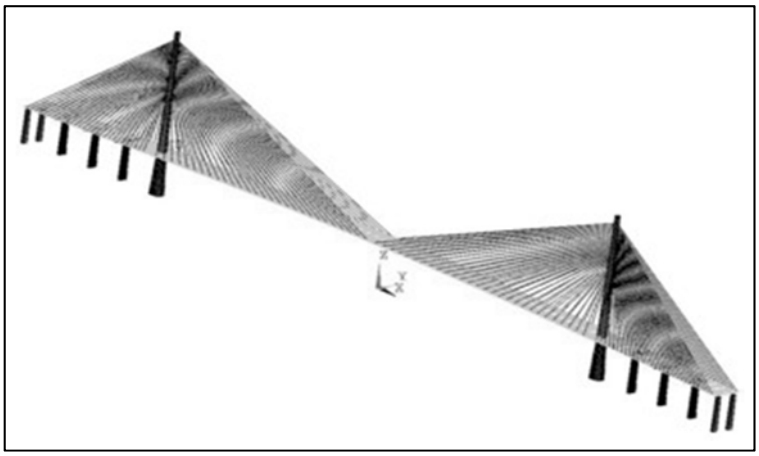

Figure 3.12 : Finite element model of the Stonecutters Bridge (Zhu et at, 2014).

ANSYS program was used for this aim. This study demonstrated that local and global behavior of the bridge were accurately estimated through the developed multi-scale model of the bridge. On the basis of dynamic modal properties of the bridge, the

validation study conducted with measured data showed that the developed FE model reflected the response of the real bridge very well.

As to the Bosphorus Bridge, restricted studies on FE modeling in literature were conducted for different aims of the bridge. Although there are certain works for the bridge, many of them are not pertinent to model updating or system identification. Therefore, they cannot focused on detailed establishment of FE model of the bridge. It is aimed in the dissertation to present newest studies especially performed for FE modeling of the bridge. As shown in Figure 3.13, Apaydin (2010) developed spine-finite element model of the bridge to make earthquake and retrofit investigation. Since the study was based on dynamic analysis and earthquake mitigation of the bridge in global scale, FE model of the bridge was established using the simplified spine-beam modeling method. Taking into the detailed physical and geometric properties account, the main span and the side span deck, the towers and the piers were modeled by equivalent elastic beam element while the cables and suspenders were simulated by cable element. All works are for connection and boundary conditions, the rocker bearing for tower-deck connections relatively affecting dynamic characteristics of the bridge, fix support for tower and pin support for anchorage were considered. The study showed that the developed FE model reflected the behavior of real bridge well when compared with the experimental studies. Since the expansion joints exceeded its longitudinal displacement capacity of 1.07 m with 1.078 m under multi-support earthquake load, the model was refined by replacing the hysteretic dampers at tower-deck connection points as shown in Figure 3.13.

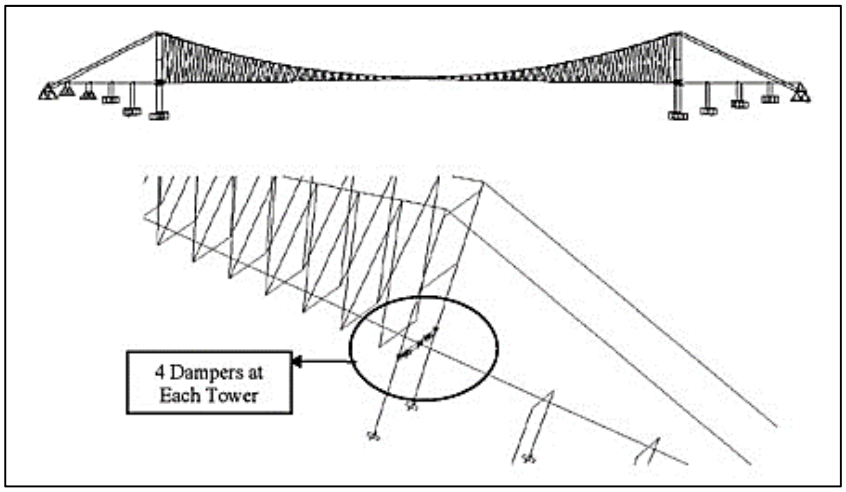

Figure 3.13 : 3-D FE model of the Bosphorus Bridge and damper replacement (Apaydın, 2010).

Other studies in literature performed by Beyen et al. (1994), Kosar (2003), Uckan and Erdik (1994) were concentrated on the dynamic analysis of the bridge. However, the proposed FE model was simpler than that of Apaydın (2010). Therefore, these studies are not detailed in this study.

Based on the studies for long-span bridges in literature and for the Bosphorus Bridge, FE modeling of this kind of bridge is a key to make further analysis without much effort. In these studies, various commercial programs are used to develop FE model of the bridge. Deciding modeling technique to be used for numerical modeling of the bridge is important issue. Considering results from conducted studies, PATRAN/NASTRAN, ABAQUS, ANSYS and SAP2000 are generally utilized due to their ability to make SHM-oriented numerical analysis.

In order to more accurately establish FE model of the Bosphorus Bridge, following questions are asked and have to be answered clearly in accordance with the aims of this dissertation,

- ? Which type of analysis will be conducted (dynamic analysis, stress/strain analysis, local bridge component analysis)?
- ✓ Within the scope of the dissertation, general steps of St-Id concept will be performed for the Bosphorus Bridge. Structural identification of the bridge requires not only global level analysis (modal, wind or earthquake analyses) but also component level analysis (stress/strain analysis). Therefore, FE program to be used should have capability of making these structural analyses. This type of analysis also requires to use various element types together (beam, shell, solid and truss). Taking into account these conclusions, FE modeling program has to be determined, and its FE model has to be developed.
- ? Which FE modeling methods (spine beam or multi-scale) will be considered depending on the aims of analysis?
- ✓ The bridge can be modeled by the spine-beam modeling technique for global level analyses, such as dynamic analysis, static and live load analysis, performance-based analysis and mode updating, and by the multi-scale technique for local component analysis, such as stress-strain history for fatigue analysis. From the aims of the disseration, both spine-beam model and multi-scale (hybrid) model of the bridge are essential to conduct these works stated

above. In addition, another solution to this issue is to consider spine-beam model for global bridge analysis and multi-scale model for local component analysis. For this purpose, local components to be considered can be modeled separately from the full-scale bridge. This means that detailed FE model is developed only for the bridge components to be analyzed instead of full-scale detailed FE model. Thus, no much more effort will be needed to deal with FE model of the bridge.

? Which FE software or programs will be used (SAP200, Patran-Nastran, Abaqus, ANSYS, etc.)

✓ From the conducted study summarized above, many sophisticated FE programs were used for various objectives. However, general tendency is on PATRAN/NASTRAN, ANSYS, ABAQUS and SAP2000, which are the most robust ones in the literature. PATRAN-NASTRAN presents two stages: building model in PATRAN and solving developed model in NASTRAN. Instead of PATRAN-NASTRAN, ABAQUS, ANSYS and SAP2000 have used the combined technique. The Bosphorus Bridge was already modeled as equivalent spine-beam model using the SAP2000 programme to carry out dynamic modal analysis and time-history analysis. Due the fact that no detailed study on system/structural identification as well as further data analysis of the bridge is conducted, multi-scale FE model of the bridge has not been established so far in literature for the Bosphorus Bridge. In this dissertation, it is intended to make comprehensive identification study; therefore, multi-scale FE model of either full-scale bridge or its local components can be built by one of the programs above. Hence, two FE modeling approaches can be used for different level of analysis of the Bosphorus Bridge.

Depending on these conclusions, the step of the St-Id, “FEM simulation”, is decided to be achieved by the SAP2000 software due to its widely-implementations and verification with many studies in the literature.

3.2 Spine-Beam FE Element Model of the Bosphorus Bridge

3.2.1 FE model of the bridge with inclined hangers

Based on the project specifications and general properties of the bridge in the previous section, the improved FE model of the bridge is developed utilizing the spine-beam modeling approach as summarized in Figure 3.14. The bridge's structural components of the tower, the main deck, the portal beams, and approach span are modeled as equivalent frame element corresponding their mechanical and sectional properties. For elaborate sectional properties, all points of the components as indicated in Figure 3.14 are precisely determined depending on the project drawings, and thus much more realistic dimensions of them are adopted. Considering these realistic dimensions, sectional parameters of the structural components of the bridge given Table 3.1 are obtained.

Table 3.1 : Cross-sectional properties of the components of the bridge**.**

Parameters	Tower		Main	Portal Beam			Box
	Bottom	Top	Deck	Lower	Middle	Upper	Beam
Area (mm^2)	6.00×10^5	6.00×10^5	7.00×10^5	3.00×10^5	2.00×10^5	2.00×10^5	2.00×10^5
I_{xx} (mm^4)	5.00×10^{12}	3.70×10^{12}	1.10×10^{12}	4.00×10^{12}	1.70×10^{12}	8.00×10^{11}	7.00×10^{11}
I_{yy} (mm4)	3.10×10^{12}	1.00×10^{12}	5.00×10^{13}	1.00×10^{12}	2.70×10^{11}	2.70×10^{11}	2.80×10^{11}
Torsional J (mm^4)	1.55×10^{14}	3.54×10^{14}	4.00×10^{12}	8.10×10^{12}	1.10×10^{12}	3.90×10^{12}	4.80×10^{12}
Shear X Area (mm^2)	6.00×10^5	5.00×10^5	6.00×10^5	2.00×10^5	1.00×10^5	2.00×10^5	2.00×10^5
Shear Y Area (mm^2)	6.00×10^5	5.00×10^5	6.00×10^5	2.00×10^5	2.00×10^5	2.00×10^5	2.00×10^5
Plastic Z_x (mm^3)	1.60×10^9	1.30×10^9	8.00×10^8	1.00×10^9	5.00×10^8	3.00×10^8	4.00×10^8
Plastic Z_y (mm^3)	1.30×10^9	7.00×10^8	4.00×10^9	6.00×10^8	3.00×10^8	2.10×10^8	2.30×10^8
Section Mod. S_3 (mm^3)	1.10×10^9	9.00×10^8	1.00×10^8	7.00×10^8	3.00×10^8	3.00×10^8	2.10×10^8
Section Mod. S_2 (mm^3)	9.00×10^8	4.80×10^8	3.00×10^9	4.00×10^8	1.50×10^8	1.40×10^8	5.74×10^9
Gyration, r_3 (mm)	2.89×10^3	2.48×10^3	1.25×10^3	3.65×10^3	2.92×10^3	2.00×10^3	1.87×10^3
Gyration, r_2 (mm)	2.27×10^3	1.29×10^3	8.45×10^3	1.83×10^3	1.16×10^3	1.16×10^3	1.18×10^3

As to the FE model considerations for the bridge, 3-D frame element is utilized for the deck, the tower, the portal beams, the approach span box-beam and the circular box-columns. In order to take the cable sag effects significant for the P-Δ analysis into account, the main cable, the back-stay cable and the hangers are modeled cable element. Besides, link elements with no mass are also utilized for the tower-deck and approach span-tower connections. For the rocker bearings, gap elements are also considered. In Figure 3.15, these considerations are represented in detail. So as to provide the connection between the hanger elements and the main deck element, rigid link elements with higher rigidity for all degree-of-freedom are used. As shown in Figure 3.15, the boundary conditions of the towers, the circular box columns and the approach span box-column at anchorage points are also defined. For the asphalt

pavement on the approach span deck, and concrete and asphalt pavements on the main span deck, shell element specifications are assigned.

Based on the sectional specifications and the FE modeling considerations, 3-D finite element model of the bridge is developed. The general views from the model are given in Figure 3.16. As shown in Figure 3.16, the camber at the mid-span of the deck is also provided in the model. The established model is considered for the modal analysis and the multi-point earthquake analysis of the Bosphorus Bridge. The accuracy of the FE model is verified by the comparison with the numerical and experimental studies in literature.

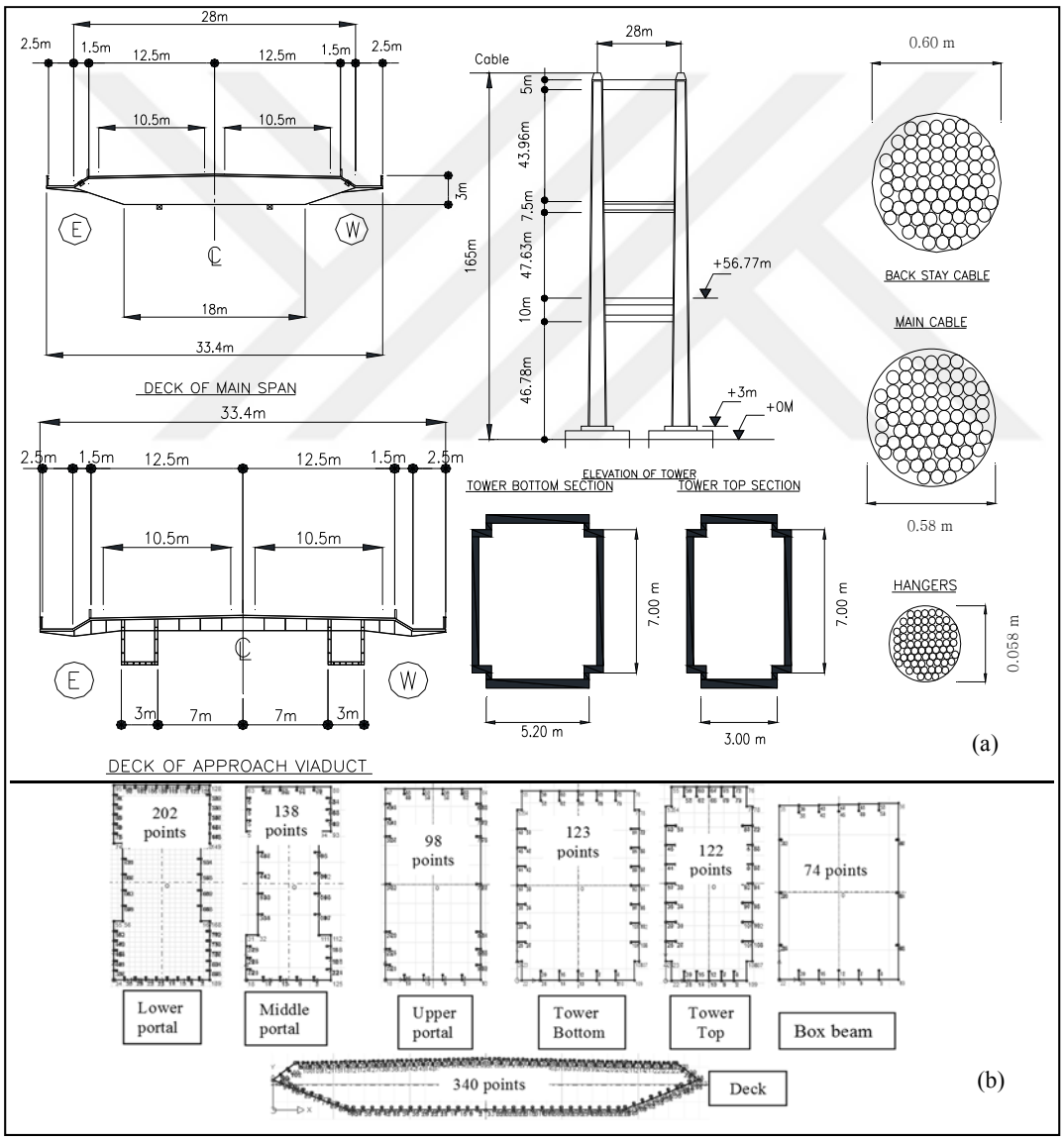

Figure 3.14 : (a) sectional properties of the bridge and (b) considered sectional points of the components for the section analysis

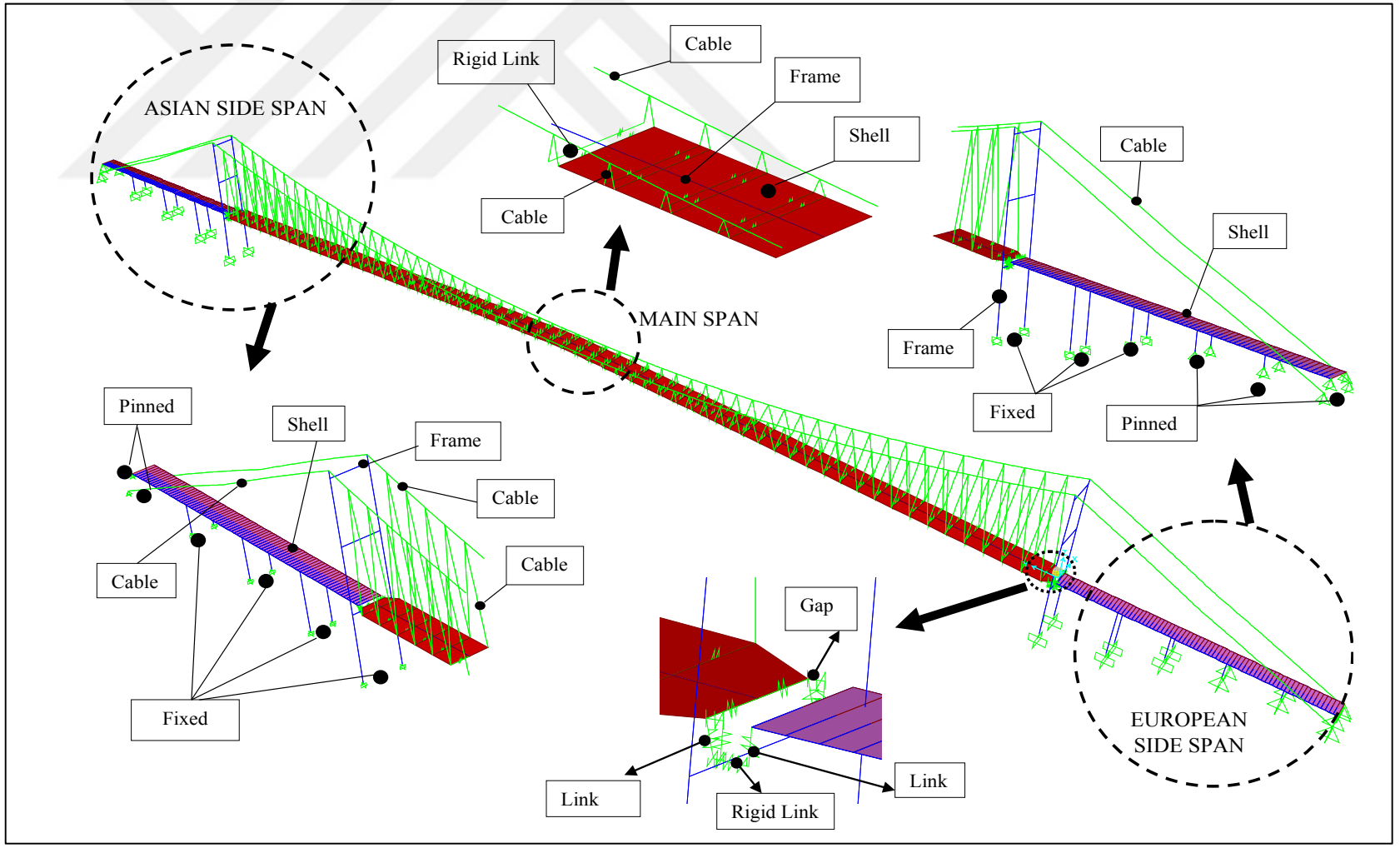

Figure 3.15 : The spine-beam FE modelling considerations of the bridge.

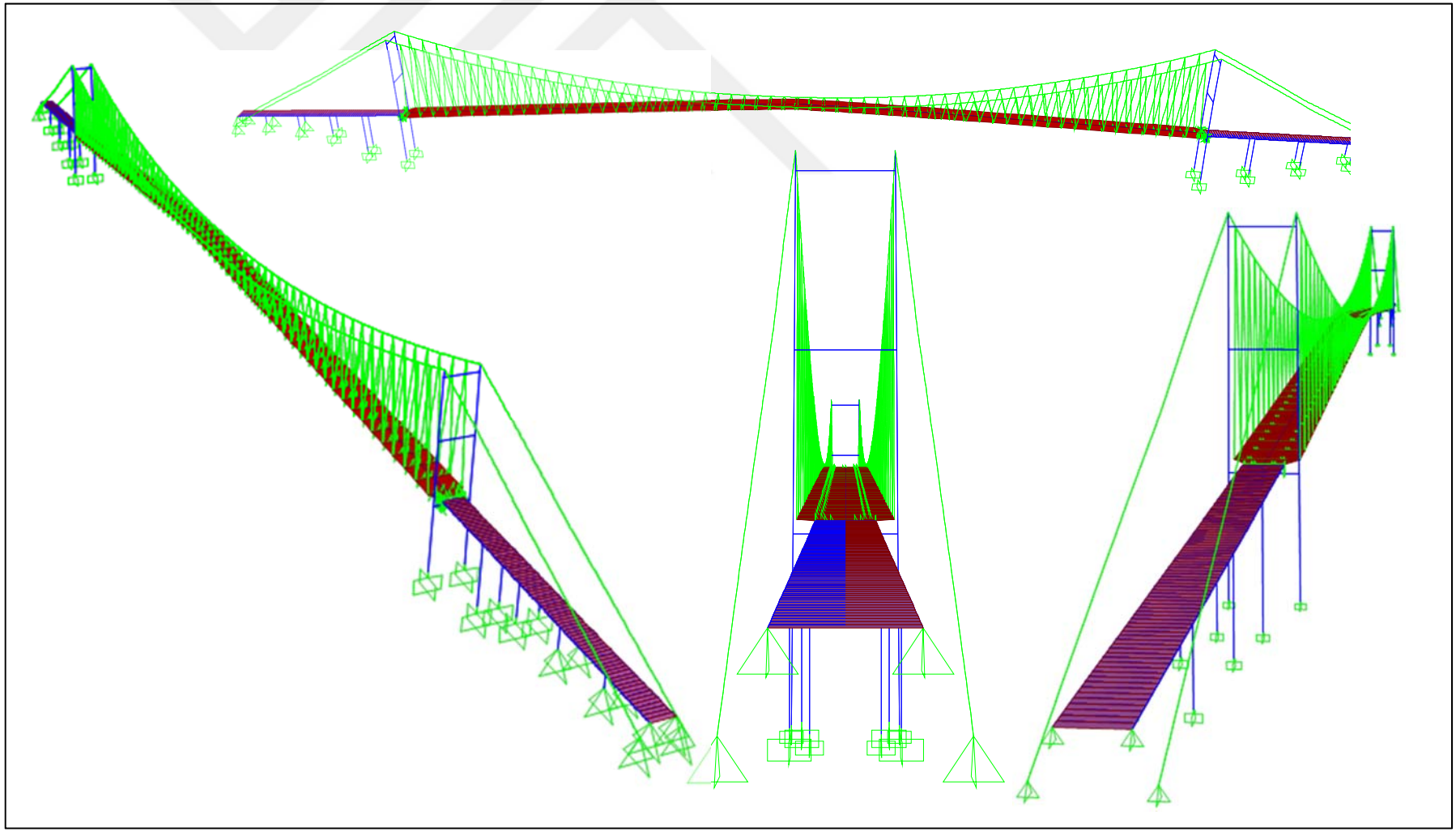

Figure 3.16 : General views from the improved spine-beam model with inclined hangers.

3.2.2 FE model of the bridge with vertical hangers

With the decision on hanger replacement project of the bridge, a retrofitted project is also prepared for the tower base-section, changing the expansion joints with new ones, placing the viscous damper and the wind tongue at the both deck-ends. Therefore, not only vertical hanger but also these structural retrofit and safety requirements are taken into account for FE modelling of the Bosphorus Bridge.

Along with sectional strengthening of the tower base-section with the additional stiffener element of doubly symmetric steel W530x123 I-beam shown in Figure 3.17, new rocker bearing and wind tongue are also considered for FE modelling of the bridge. The specifications of viscous damper devices mounted to reduce the effect of large movement of the deck in the longitudinal direction are presented in Figure 3.18. Using these specifications, the parameters of the damping coefficient (C) and the exponential value (α) to be utilized for the corresponding link element calculation are also specified as indicated in Figure 3.18. Damper is adopted as a nonlinear link characterized by the exponential formulation of $F=CV^{\alpha}$. Similar conception is taken into account for the wind tongue with elastomeric neoprene pads and laminated steel plates as shown in Figure 3.19. In FE model of the bridge, the linear link element is used for simulation of the wind tongue.

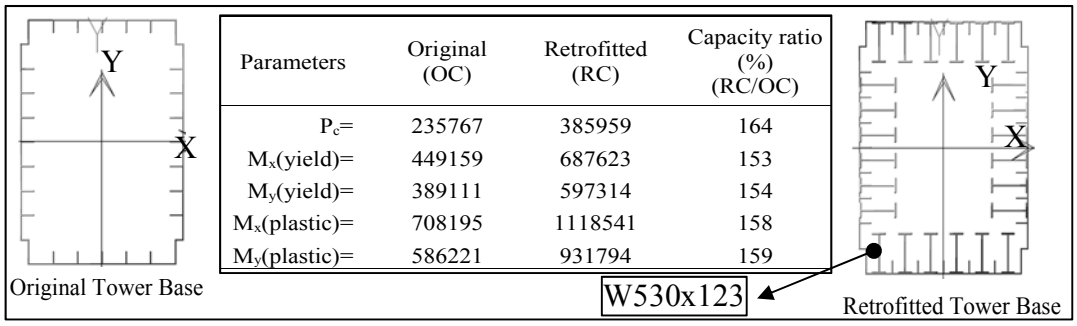

Figure 3.17 : Retrofitting of the towers.

As revealed in Figure 3.19, horizontal (K_H) and vertical (K_V) spring constant are calculated according to AASTHO-LRFD requirements. All these considerations are used in FE modeling of the bridge with vertical hangers. Figure 3.20 summarized the implementation of the considerations to the FE model. Consequently, the established 3-D FE model of the Bosphorus Bridge with vertical hangers is shown in Figure 3.21 by a detailed view from the retrofitted base-section. Besides, general views for FE model of the bridge with vertical hanger are depicted in Figure 3.22.

Rated Force (kN)	Stroke (cm)	Damping Coefficient, C (kN-sec/m	Constant α	100%Velocity (m/sec)
1700.00	±90	3200.00	1.00	0.53

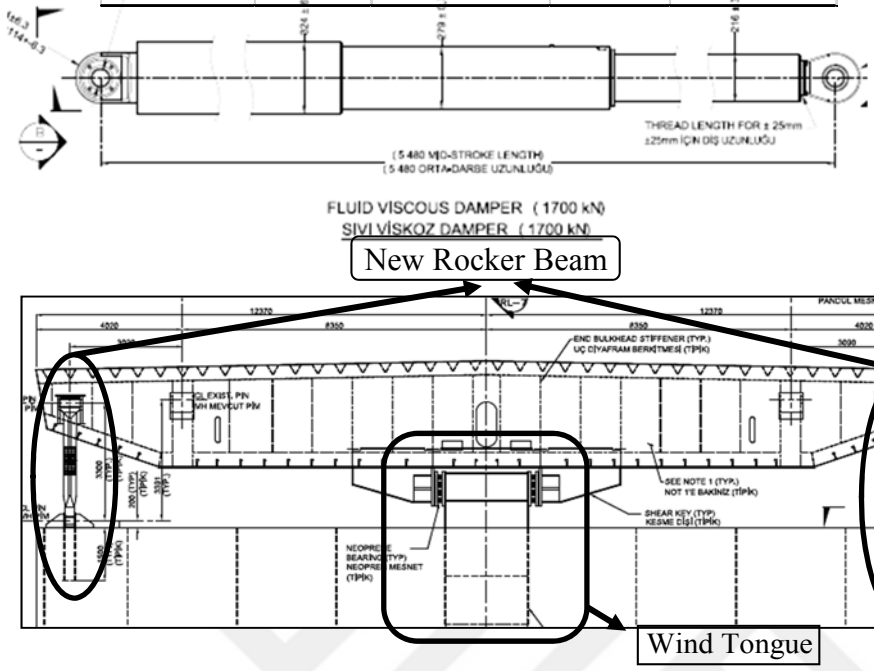

Figure 3.18 : Specifications of viscous damper, new rocker bearing and wind tongue.

Hardness (Shore A)	Young's Modulus Eo	Shear Modulus G	k Factor
50	312 psi (2.2 MPa)	100 psi (0.68 MPa)	0.73
60	635 psi (4.4 MPa)	150 psi (1.04 MPa)	0.57
70	1040 psi (7.2 MPa)	245 psi (1.69 MPa)	0.53

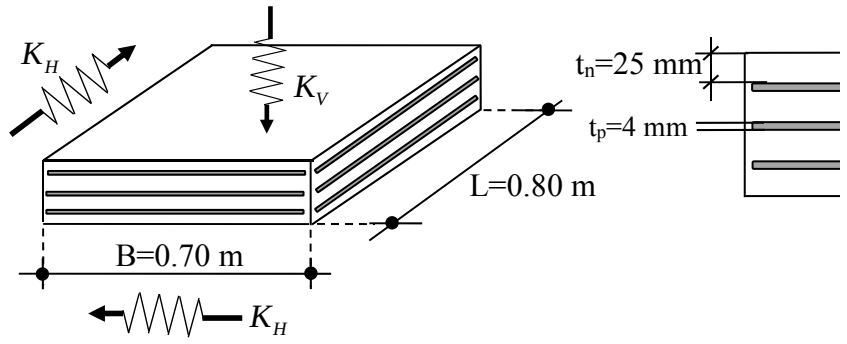

$$K_H = \frac{E_c \cdot A}{t \cdot n} = \frac{284048\ (\text{kN/m}^2) \cdot 0.56(m^2)}{0.025(m) \cdot 4} = 1420238\ \text{kN/m}$$

$$K_V = \frac{G \cdot A}{t \cdot n} = \frac{1040(\text{kN/m}^2) \cdot 0.56(m^2)}{0.025(m) \cdot 4} = 93184\ \text{kN/m}$$

Figure 3.19 : Equivalent spring calculation for the wind tongue.

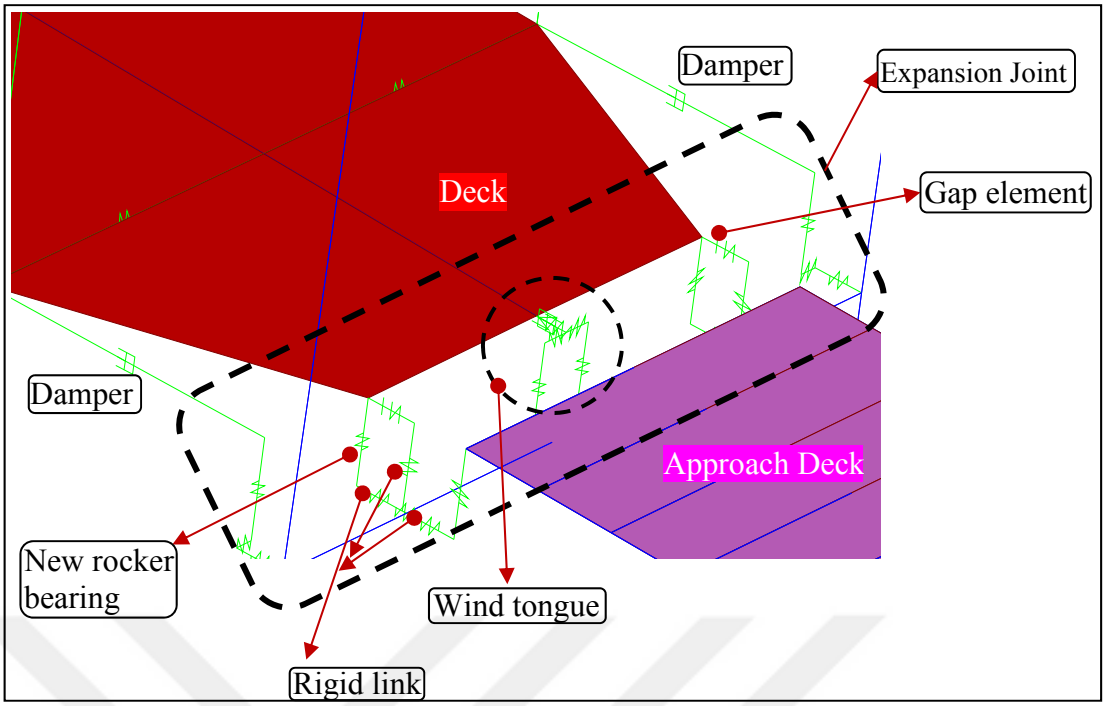

Figure 3.20 : Mechanical modeling of the expansion joint of the bridge.

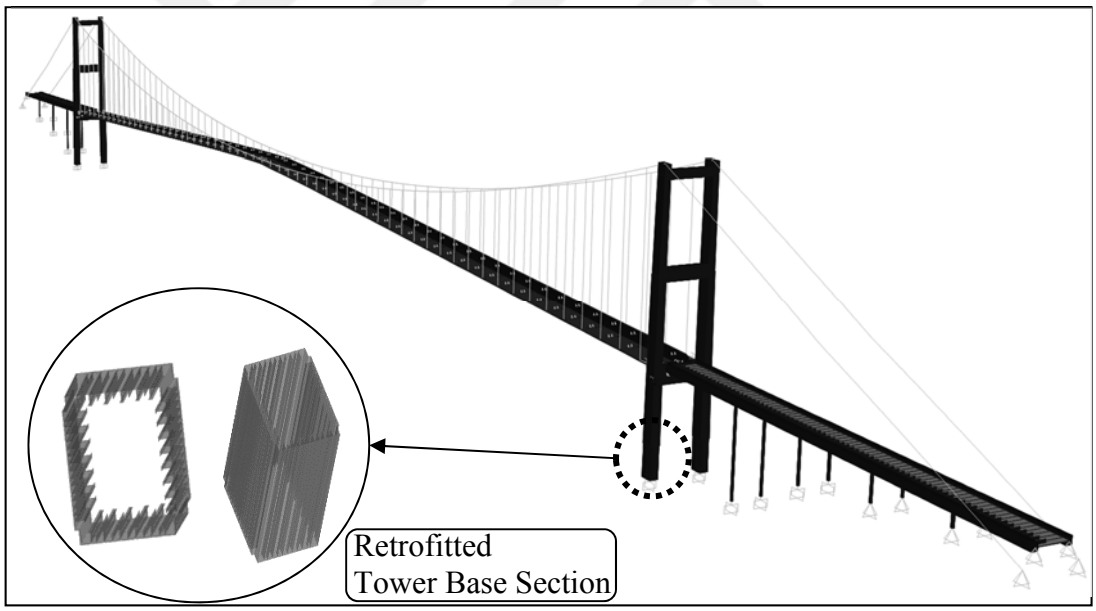

Figure 3.21 : 3D view of the bridge with vertical hanger and retrofitted base section.

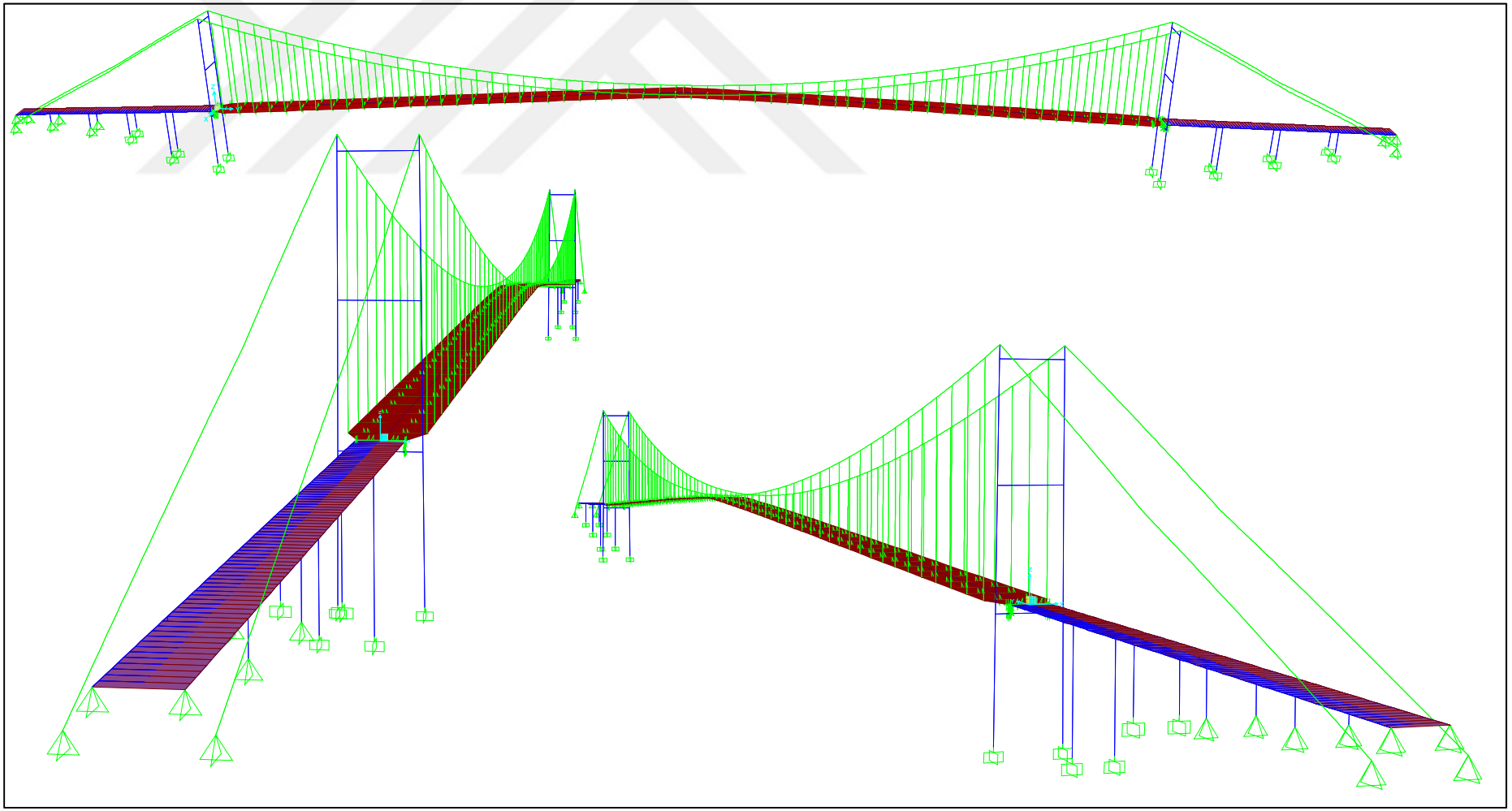

Figure 3.22 : The spine-beam FE model of the bridge with vertical hangers.

3.3 3D Full-Scale Shell FE Model and Considerations

The spine-beam FE model of the bridge enables to determine the global behavior of the bridge. Further investigations, such as stress-strain history-based studies can be carried out limitedly by this FE model of the bridge. Therefore, the bridge needs to be modeled elaborately using multi-scale modeling technique that considers advanced FE elements, such as solid, shell for FE modeling. For this aim, 3-D full-scale shell model of the Bosphorus Bridge is developed and the considerations for this modeling are given in this section.

3.3.1 3D full-scale shell FE model of the bridge with inclined hangers

The bridge was made of constructional steel thin plate. As stated in the former sections, deck, tower, portal beams and approach viaduct beam have box-section and these sections are braced with the stiffener plates and diaphragms along their length. Based on the model specifications of the spine-beam modeling of the bridge given in the previous section, 3D full-scale FE model of the bridge is established taking shell element into account. In addition, the geometry and assignment of element specifications are mostly achieved with the help of the project drawings of the bridge.

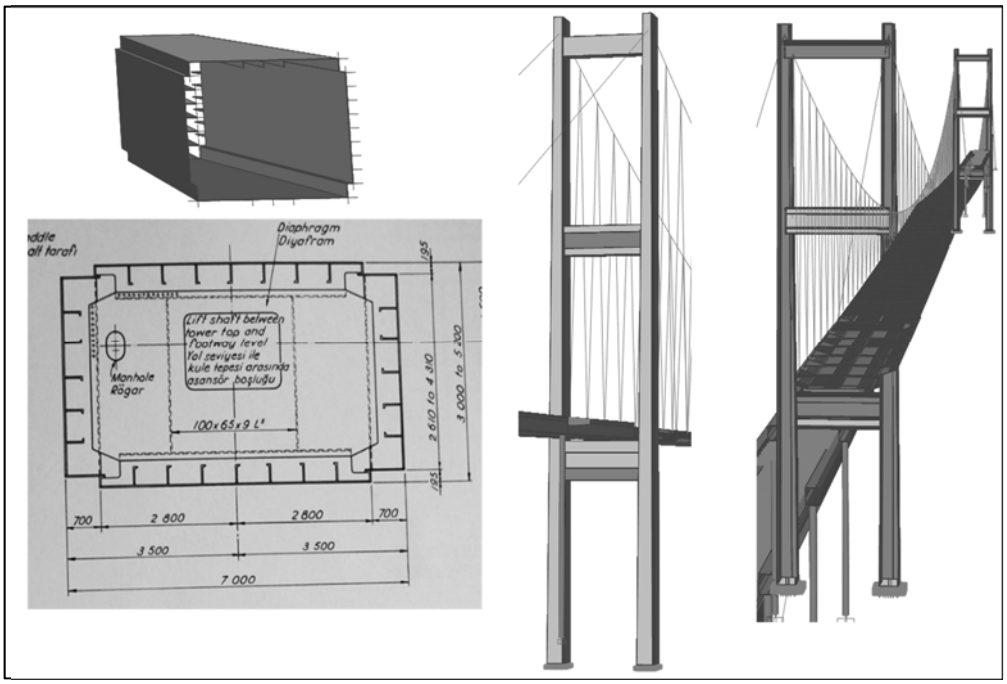

Figure 3.23 : 3D full–scale modeling of the tower of the bridge.

In Figure 3.23, the tower section with bracing ribs is modeled according to the project drawings and 3D full-scale model of the towers are developed using shell elements. Similarly, the main deck in Figure 3.24, the approach-viaduct deck consisting of steel box girder and hand-built steel cross-beam in Figure 3.25, the portal beams in Figure 3.26 and the approach-viaduct with the pipe columns in Figure 3.27 are modeled thorugh shell element depending on their project properties. The cable elements, hanger, backstay and main cables, are also developed featuring the cable properties including sag effect. Moreover, rigid link is defined for the portal beam-tower joints, circular column-box beam joints. For the expansion joint providing deck-tower and side span-tower connections, gap link elements are also used. The rocker bearings are modeled with link elements. All modeling considerations are presented in Figure 3.28. Accordingly, 3-D full-scale FE shell model of the bridge is developed as shown in Figure 3.29. After from the spine-beam model developed for global behavior of the bridge, the much more detail model helps to make local and global analyses of the bridge. All these efforts are performed with the SAP2000 software due to its friendly graphical user interface-GUI and easily defining the structural features of the bridge.

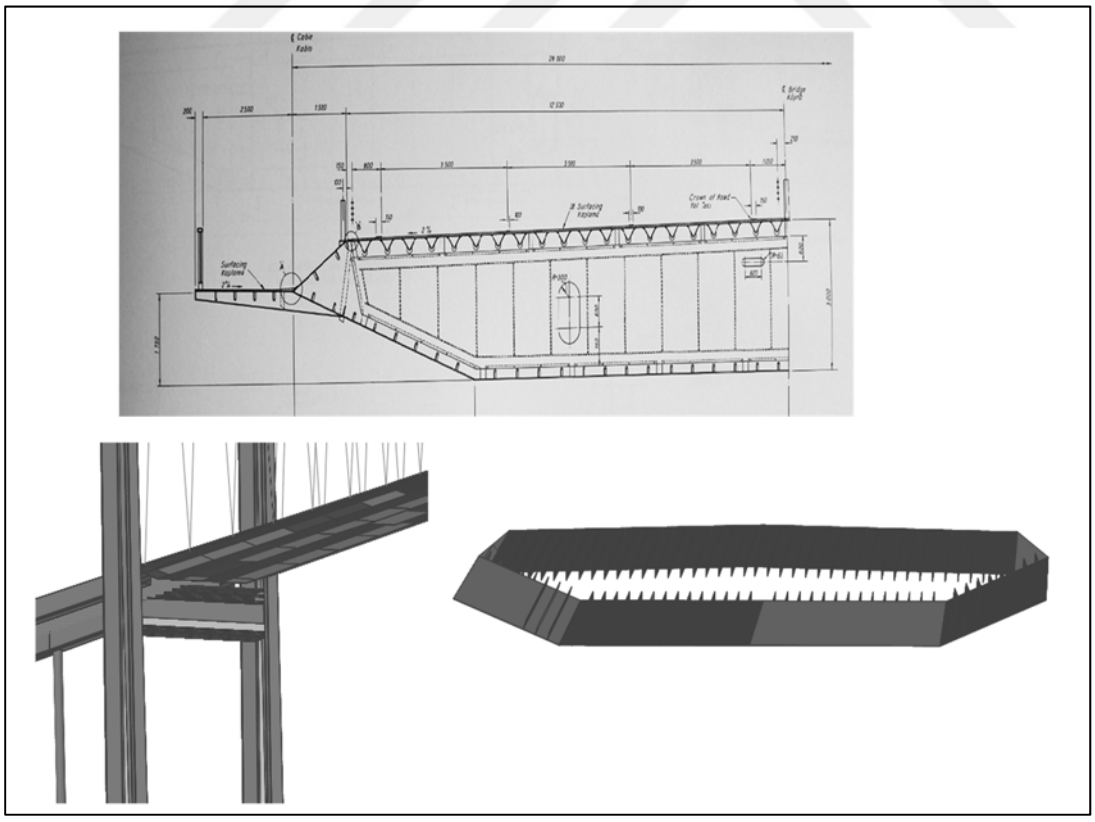

Figure 3.24 : 3D full–scale modeling of the main deck of the bridge.

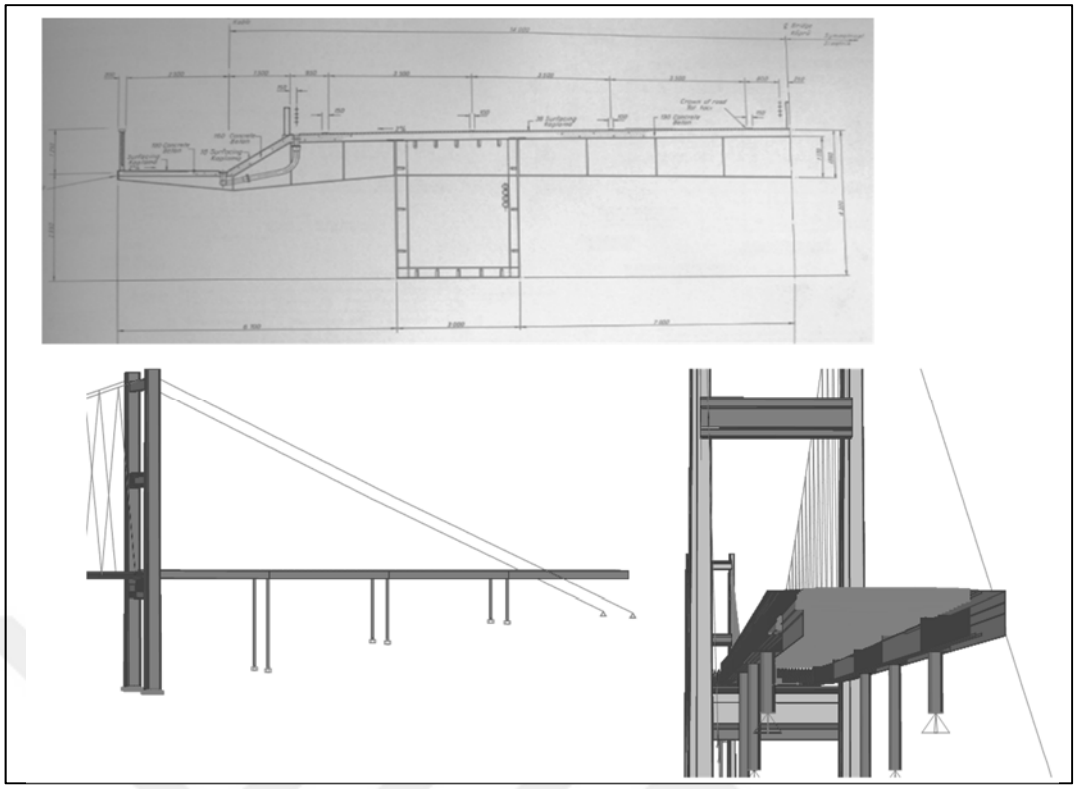

Figure 3.25 : 3D full–scale modeling of the approach viaduct deck.

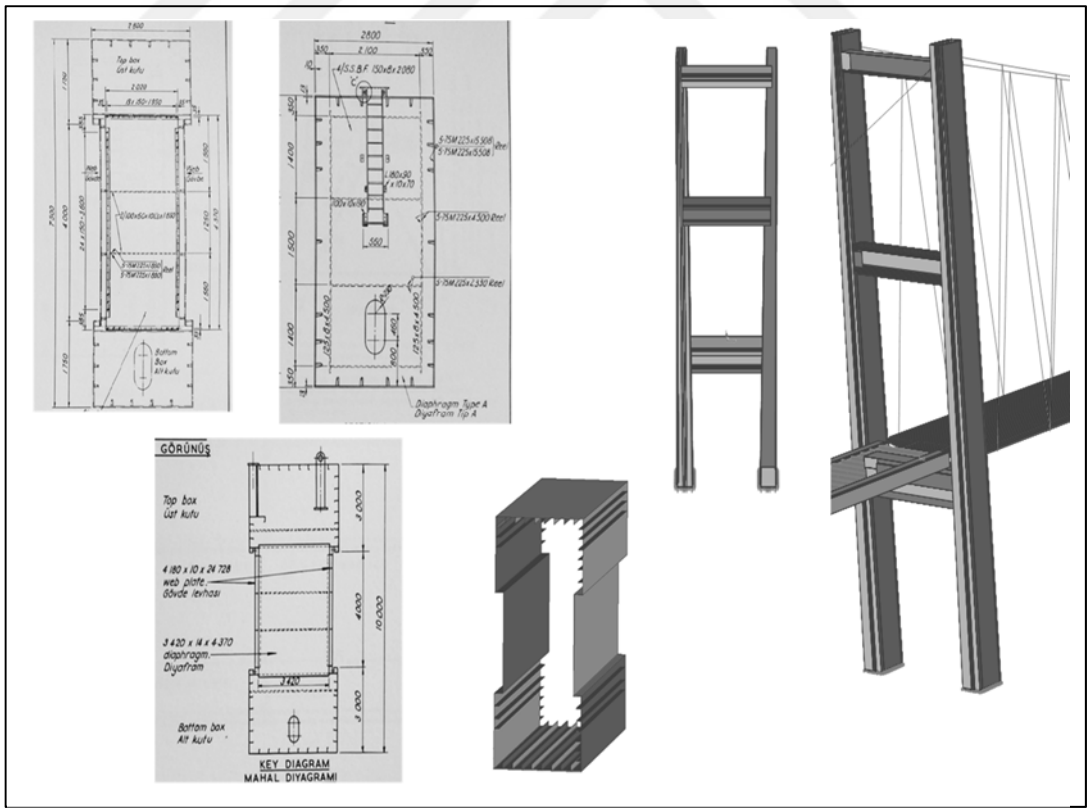

Figure 3.26 : 3D full–scale modeling of the portal beams.

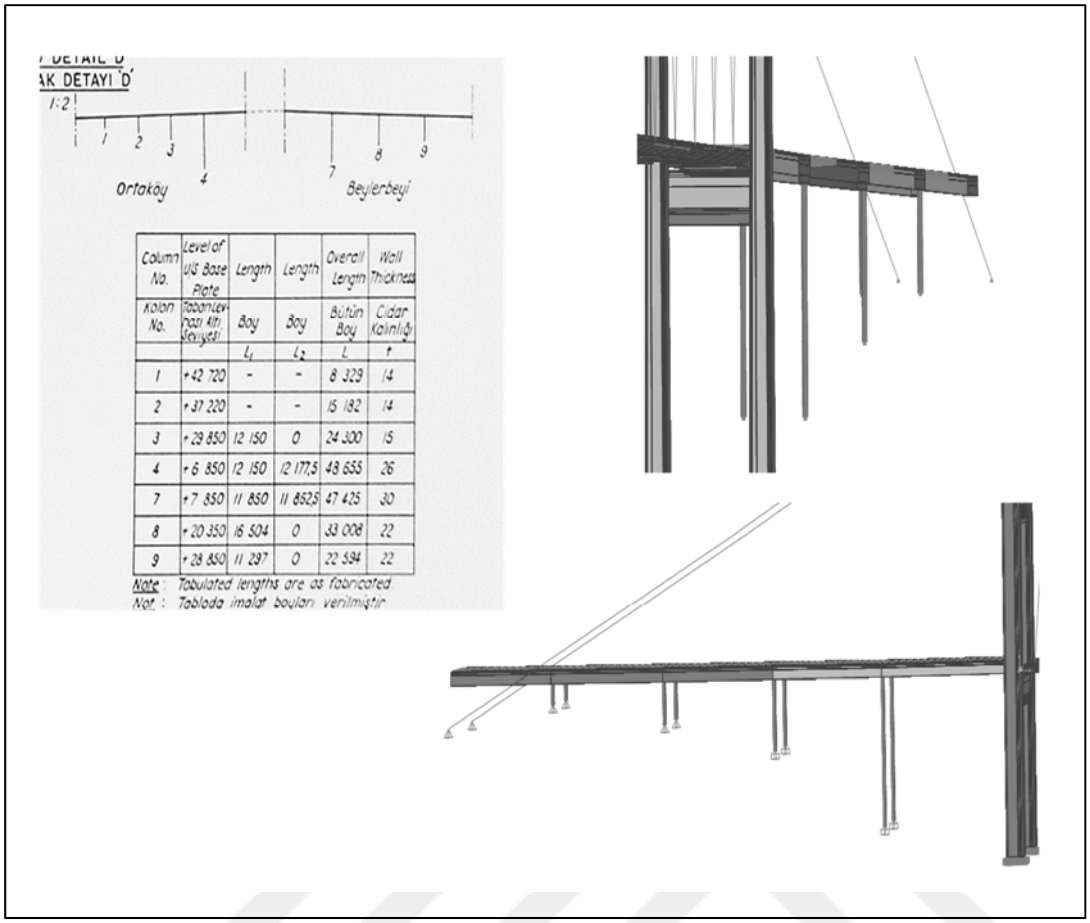

Figure 3.27 : 3D full–scale modeling of the approach viaduct columns.

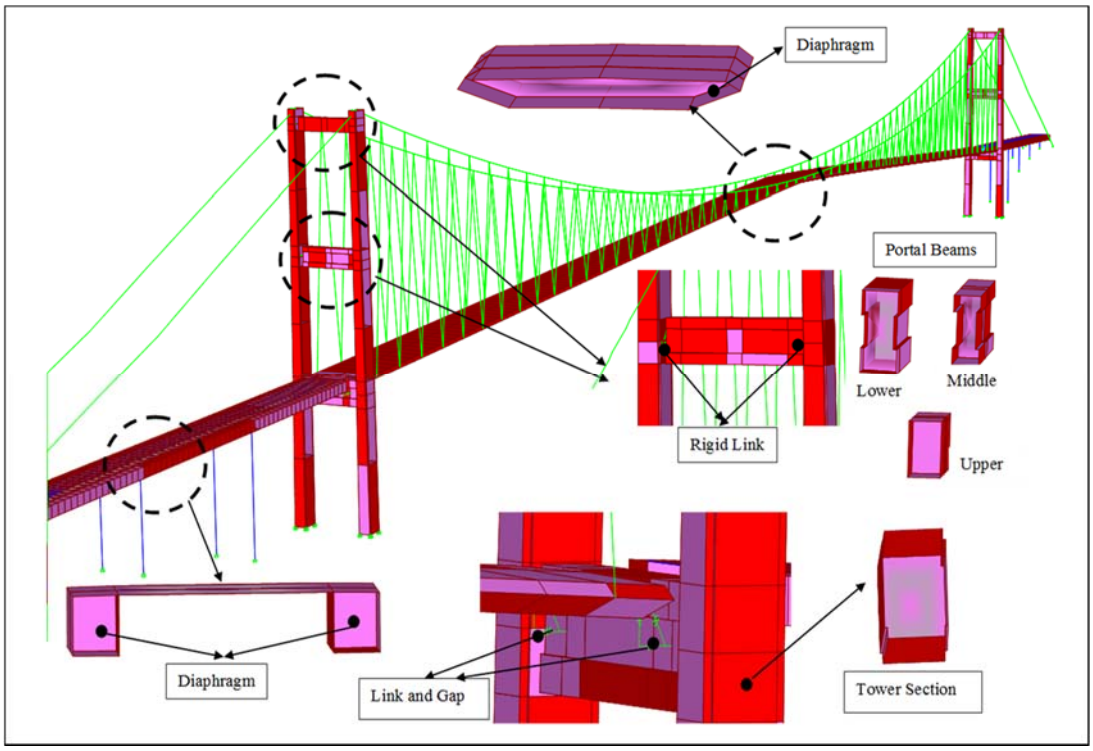

Figure 3.28 : General considerations for 3-D full-scale FE model of the bridge.

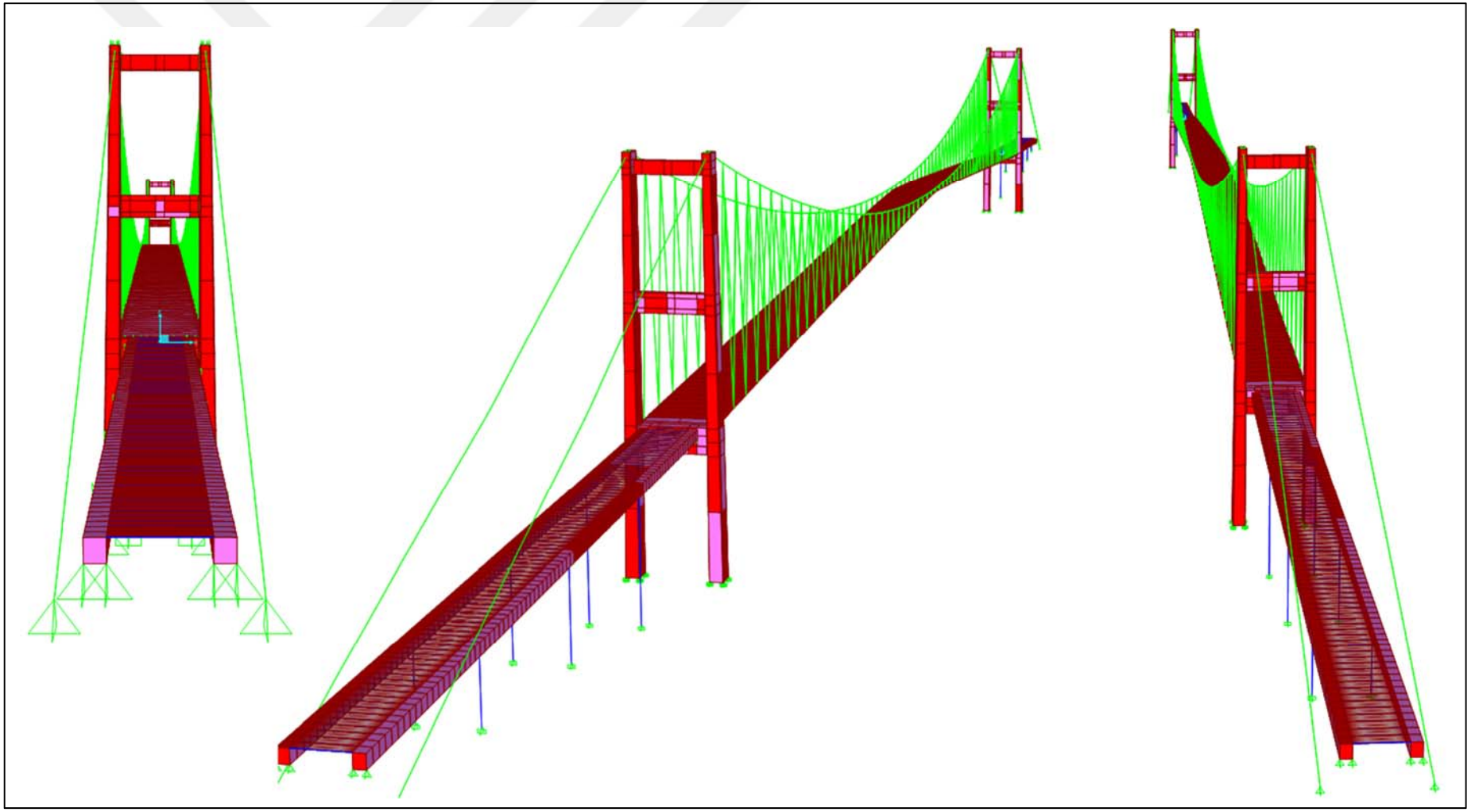

Figure 3.29 : General views from 3-D full-scale shell model of the bridge with inclined hangers.

3.3.2 3D full-scale shell FE model of the bridge with vertical hangers

Due to recently conducted hanger replacement project on the Bosphorus Bridge, inclined hangers are changed with vertical hangers. Thus, the location and geometry of the new hangers on the deck and main cable becomes different from the previous inclined hangers. In order to investigate the influence of the vertical hangers on modal and structural behavior of the bridge, 3-D full-scale shell FE model of the bridge is developed. For this objective, the project drawings given in Figures 2.8-11, the considerations and specifications presented in the section 3.2.2 are directly taken into account. Apart from the change in hanger arrangement from inclined to vertical, the other works demonstrated in Figure 3.30 are also adopted in 3D full-scale FE model of the bridge with vertical hangers which is completed as shown in Figure 3.31.

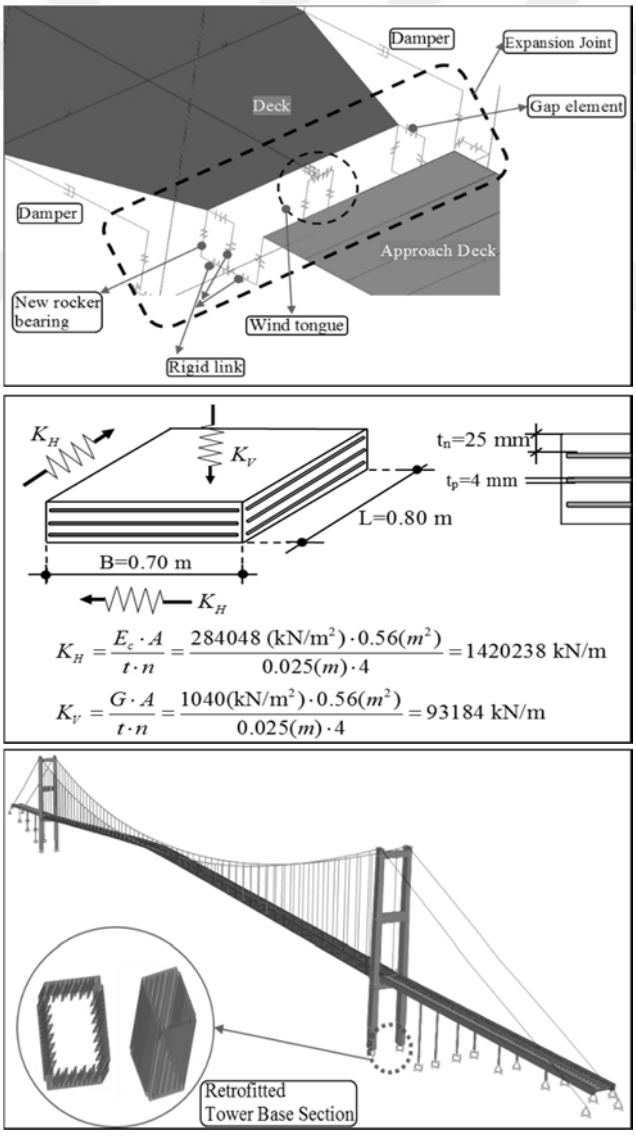

Figure 3.30 : Other structural works in the new hanger project.

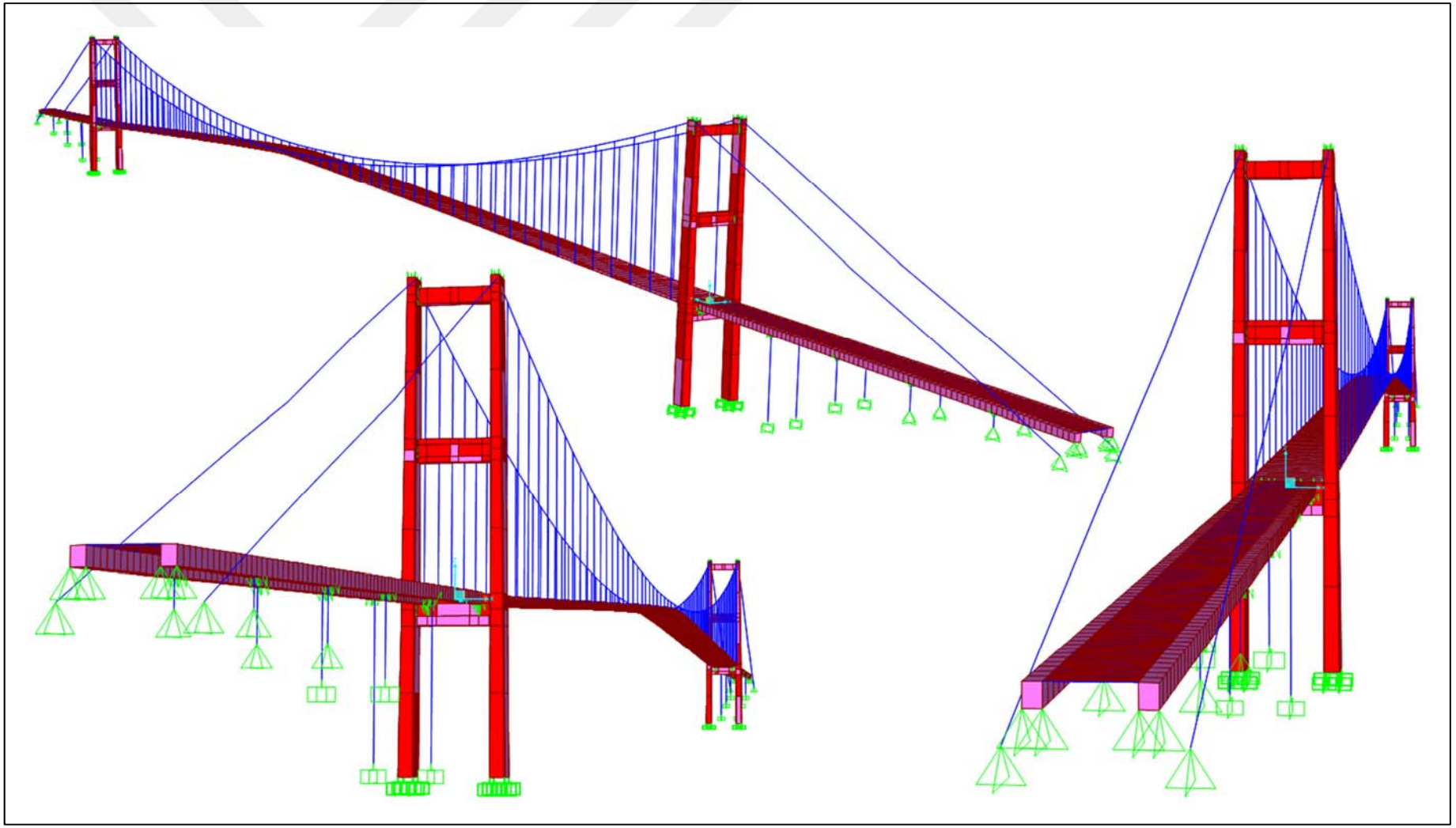

Figure 3.31 : General views from 3-D full-scale shell model of the bridge with inclined hangers.

4. MODAL ANALYSIS OF THE BRIDGE

The modal analysis of structures is a powerful tool for earthquake excitation analysis of structures. Through this analysis, the response of structures to dynamic input can be estimated and certain outcomes related to dynamic inputs can be explained (Chopra, 2012). For large-scale bridge structures with different size of structural component, such as main deck, tower etc., the mode shapes may show which component dominated the dynamic response of long-span bridges (Apaydin et al, 2016). In order to verify the developed FE model, the modal analysis is first employed.

The bridge was made up of BS-968 (1962) high yield structural steel. However, no detailed specifications of this code are available in literature; therefore, ASTM/A709-Gr50 steel model that corresponds to almost all provisions of the BS-968 is considered as structural steel for FE modelling of the bridge dynamic and earthquake analysis of the bridge. More details are given in Figure 4.1.

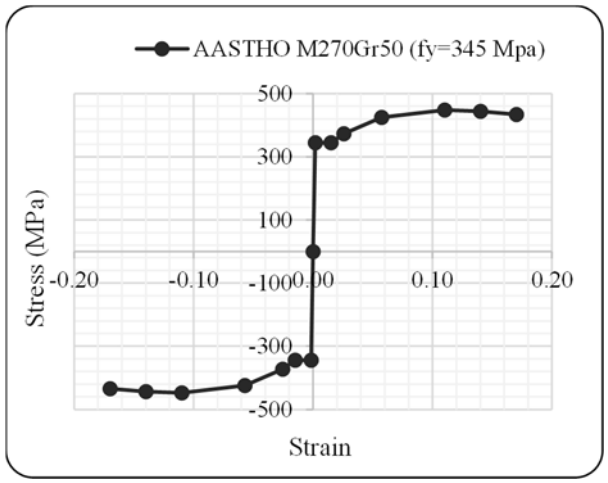

Stress (Mpa)	Strain
-434	-0.1700
-444	-0.1400
-448	-0.1100
-425	-0.0572
-373	-0.0256
-345	-0.0150
-345	-0.0017
0	0.0000
345	0.0017
345	0.0150
373	0.0256
425	0.0572
448	0.1100
444	0.1400
434	0.1700

Figure 4.1 : Structural steel specfications of ASTM/A709-Gr50.

The Bosphorus Bridge has a camber of 8.0 m height at the middle of the main deck under dead load. In an attempt to provide the camber and dead load as initial condition,

the finite-element-based practice-oriented approach is proposed for the FE model. For this objective, general steps of the procedure are summarized for the Bosphorus Bridge. Prior to the modal analysis of the bridge, this approach is considered in Figure 4.2. In the procedure, the geometry of the bridge was firstly determined depending on the project drawings. This geometry without dead-load is called “Geometry 1” as shown in Figure 4.2. Non-linear geometric analysis (NNLGEO) was then performed considering “Geometry 1”. Thus, the deformed shape of the bridge after from the analysis, “Deformed 1” and “Geometry 1” are used for the next step, “New Geometry 1”. After from three steps, the camber of 8.0 m height is determined under NNLGEO dead load, which means that all coordinates of the nodal points from the analysis of “New Geometry 3” are provided to be same as those of “Geometry 1”. Accordingly, “New Geometry 3” is considered both for the modal analysis and for the earthquake analysis of the bridge.

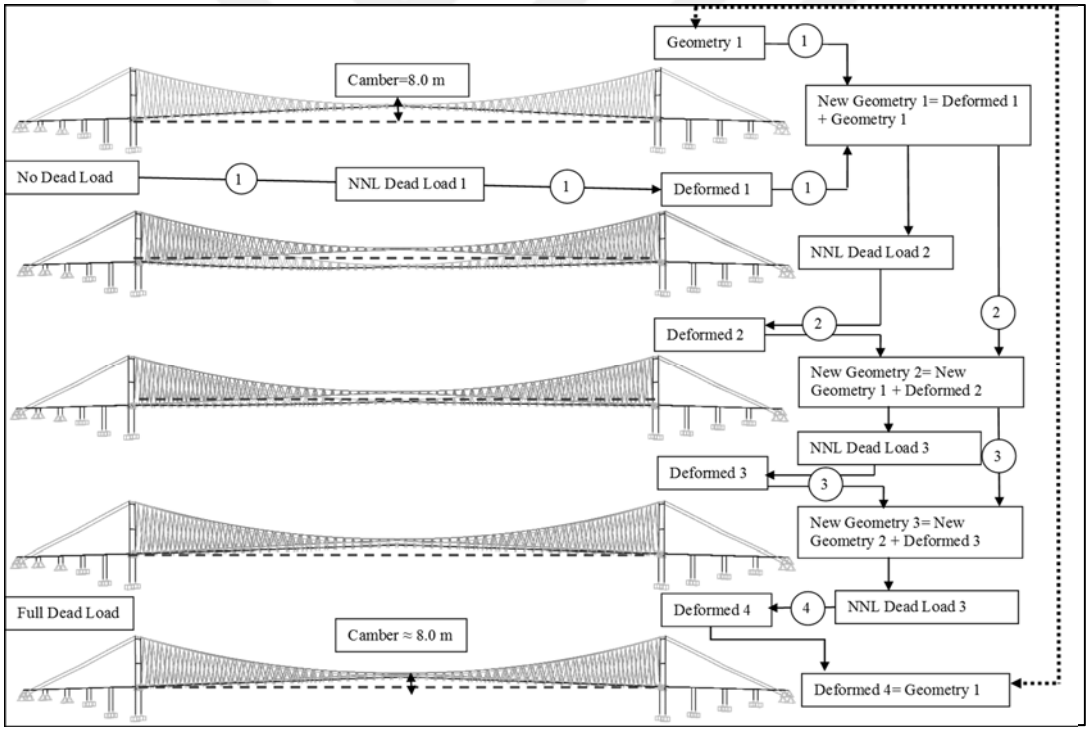

Figure 4.2 : General steps for dead load initial condition consideration.

4.1 Modal Analysis of the 3-D Spine-Beam FE Element Model of the Bosphorus Bridge

4.1.1 Results from the 3-D spine-beam FE model of the bridge with inclined hangers

Considering the specifications stated previous section for the modal analysis, the first 50 natural frequencies and associated mode shapes are obtained, and the first five modes are given in Table 4.1 with a comparison to the other investigations in literature. Corresponding mode shapes of the bridge are also depicted in Figures 4.3-.7, respectively.

Table 4.1 : Comparison of the 3-D spine-beam FE model of the bridge with inclined hangers with the other studies.

Mode Number	Mode Shape	Frequency/Period [Hz]/[s]					
		Brownjohn et al. (1989)	Erdik and Uckan (1989)	Kosar (2003)	Apaydin (2010)	Current 3-D spine-beam FE (Inclined)	
						Period [s]	Freq. [Hz]
Mode-1	1st L_{sym}	0.073	0.072	0.069	0.074	12.984	0.077
Mode-2	1st V_{asym}	0.126	0.144	0.125	0.120	7.217	0.139
Mode-3	1st V_{sym}	0.165	0.202	0.190	0.158	6.453	0.155
Mode-4	1st L_{asym}	0.180	0.225	0.223	0.210	4.926	0.203
Mode-5	2nd V_{sym}	0.218	0.323	0.273	0.262	4.561	0.219

L_{sym}: Lateral symmetric; L_{asym}: Lateral asymmetric;V_{sym}:Vertical symmetric; V_{asym}:Vertical asymmetric; DL: Dead-load; LL: Live-load

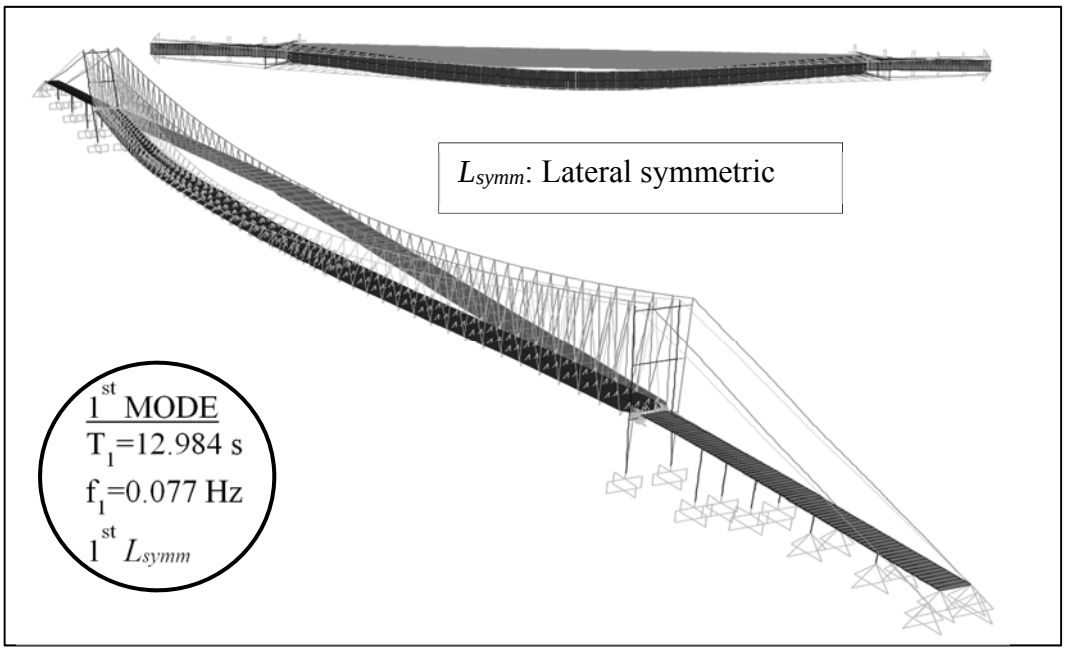

Figure 4.3 : 1st Mode of the 3-D spine-beam FE bridge model with inclined hangers.

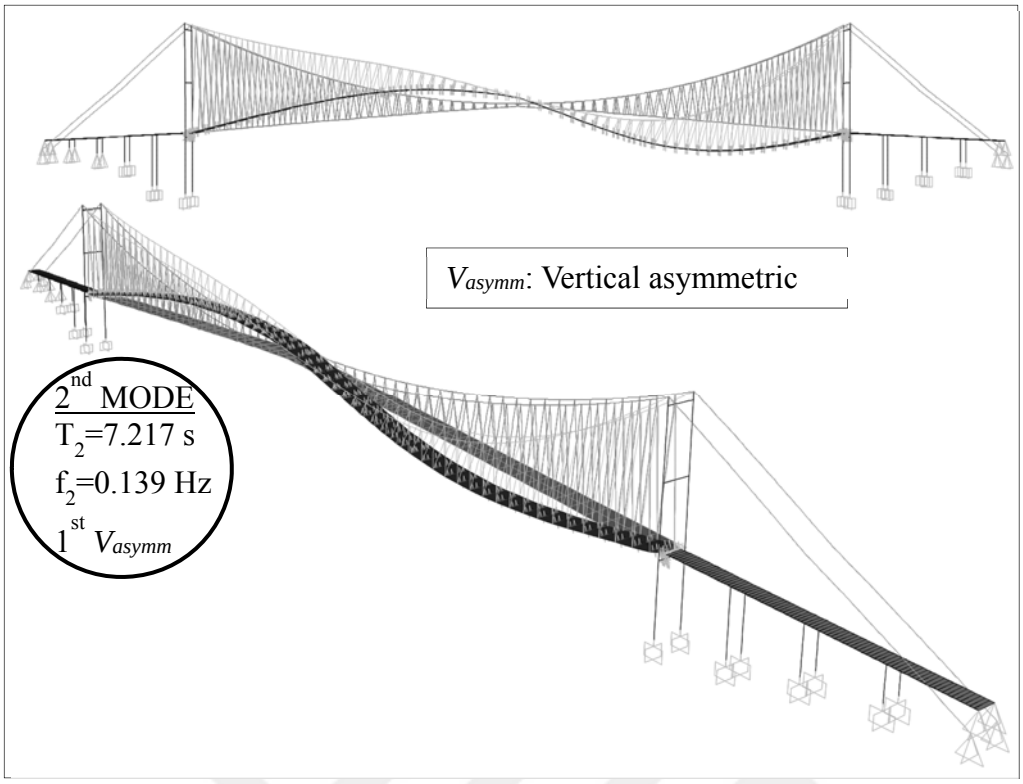

Figure 4.4 : 2nd Mode of the 3-D spine-beam FE bridge model with inclined hangers.

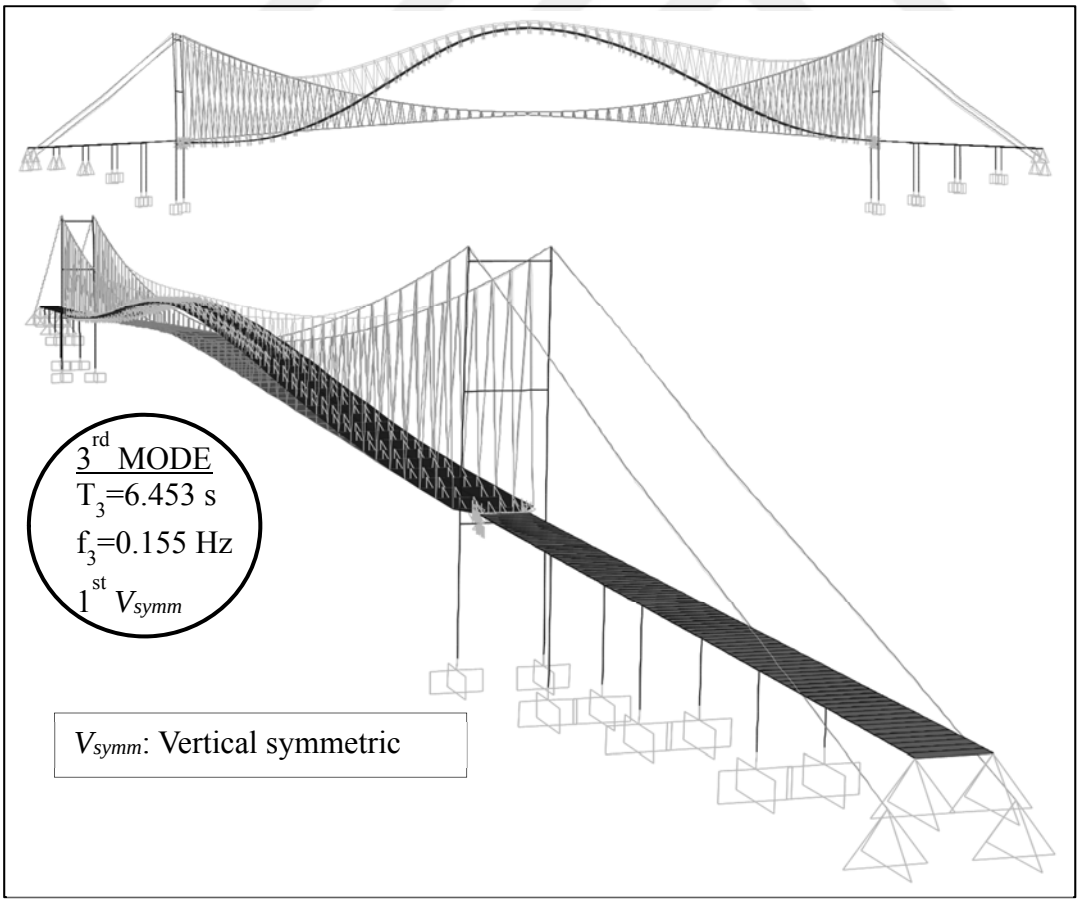

Figure 4.5 : 3rd Mode of the 3-D spine-beam FE bridge model with inclined hangers.

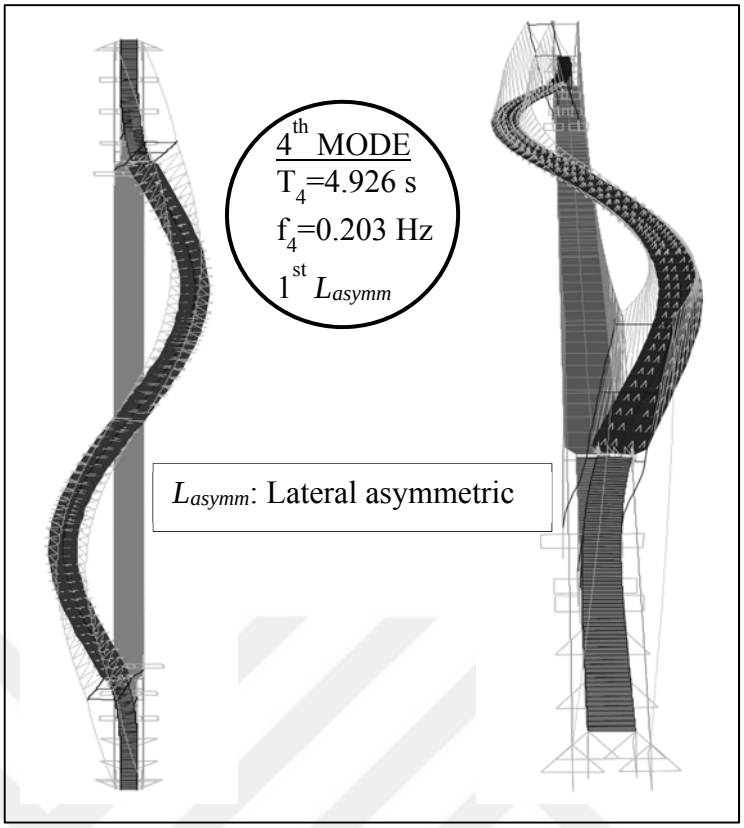

Figure 4.6 : 4th Mode of the 3-D spine-beam FE bridge model with inclined hangers.

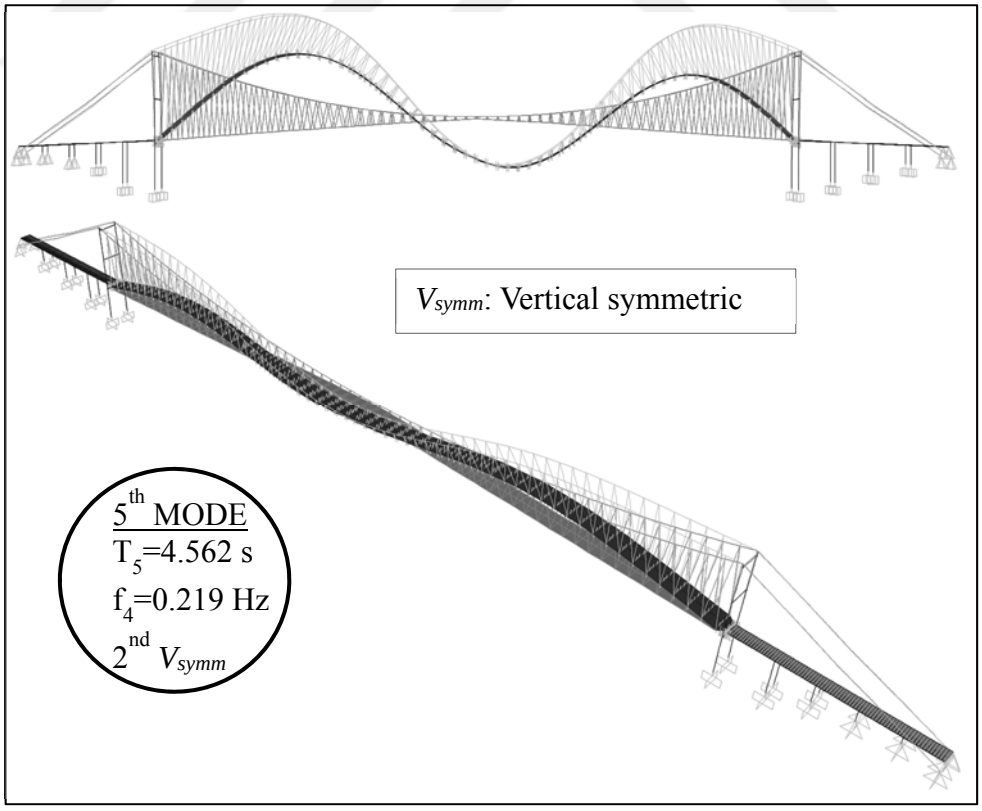

Figure 4.7 : 5th Mode of the 3-D spine-beam FE bridge model with inclined hangers.

Moreover, the change in the modal frequencies of the bridge shown in Figure 4.8 indicated that the results from the FE model showed a good agreement with those from the other studies of Brownjohn et al. (1989), Erdik and Uckan (1989), Kosar (2003) and Apaydin (2010) although Mode-3 and Mode-5 were less compatible than the other modes. Based on the comparison, the developed FE model can be reliably utilized for further analysis of the bridge such as, earthquake, wind etc.

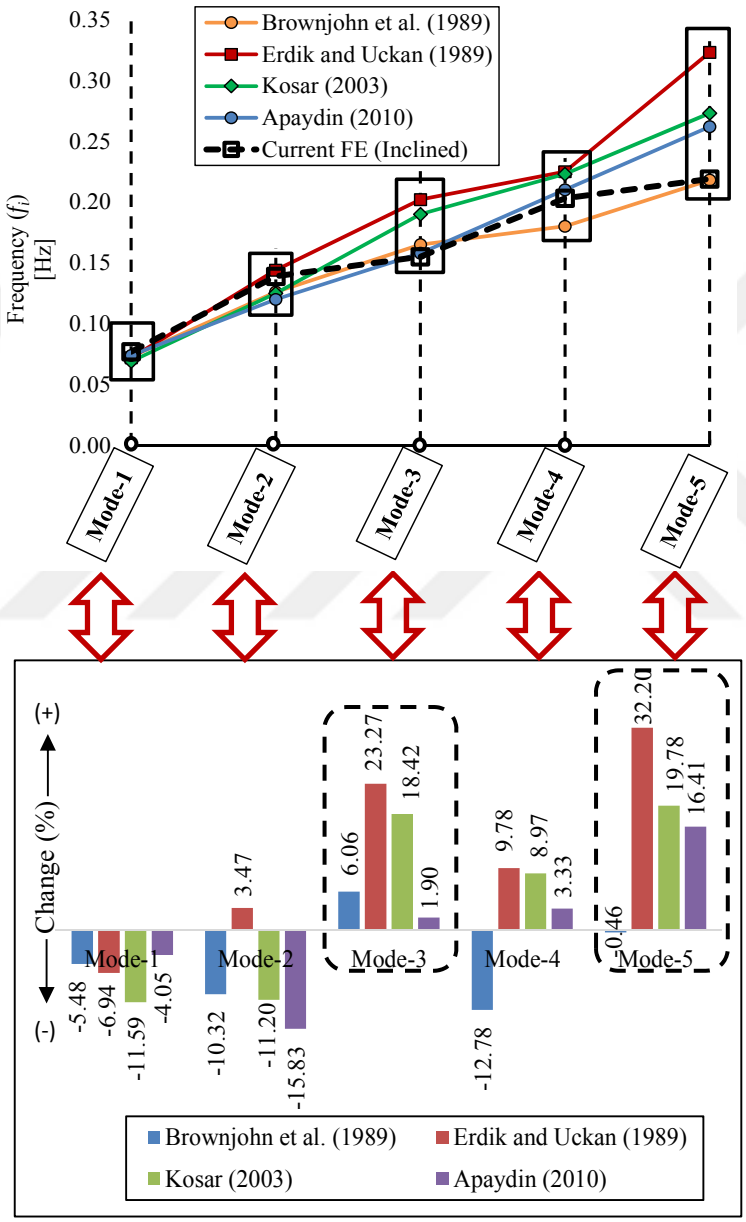

Figure 4.8 : Modal frequency change (%) of the 3-D spine-beam FE model of the bridge with the other studies.

It is also worthy to note that the FE model should be verified or updated through newly detected experimental data (for instance SHM data) since the compared experimental results given in the studies of Brownjohn et al. (1989), Erdik and Uckan (1989), Kosar

(2003) and Apaydin (2010) might not feature the current status of the bridge. From the analysis, the main deck of the bridge is obtained to be effective for lateral and vertical response of the bridge to a dynamic input. Particularly, modal participating total mass ratio for transvers direction of the main deck is determined as 67 % at the end of the first ten modes directly pertinent to the main deck mode shapes as given in Table 4.2. Compared to modal participating total mass ratio of 96 % at the end of 50 modes, this value indicated the efficiency of the main deck mode shapes on the dynamic response of the bridge. Similar single mode shapes are also determined for the tower and cable after the main deck mode shapes. All these single mode shapes of the main deck, the tower and the cables are seen in the first ten mode shapes. The other mode shapes are obtained as the combination of these single mode shapes. Based on these consequences, the main deck and the tower dynamic response are estimated to dominate the behavior of the Bosphorus Bridge under extreme loading events such as earthquake, strong wind, heavy traffic or human induced load etc.

Table 4.2 : Modal mass participation ratios of the 3-D spine-beam FE model with inclined hangers.

Mode	Period [s]	Frequency [Hz]	Mass Participation Ratio [%]					
			X-Direction (Horizontal)		Y-Direction (Longitudinal)		Z-Direction (Vertical)	
			Mx	Rx	My	Ry	Mz	Rz
1	12.984	0.077	**0.566**	0.000	0.000	0.027	0.000	0.000
2	7.217	0.139	0.000	**0.162**	0.001	0.000	0.001	0.000
3	6.453	0.155	0.000	0.003	0.002	0.000	**0.286**	0.000
4	4.926	0.203	0.000	0.000	0.000	0.000	0.000	**0.303**
5	4.561	0.219	0.000	0.008	0.000	0.000	**0.155**	0.000
6	3.806	0.263	0.017	0.000	0.000	0.025	0.000	0.000
7	3.759	0.266	0.000	0.083	0.000	0.000	0.015	0.000
8	3.308	0.302	0.081	0.000	0.000	0.386	0.000	0.000
9	3.222	0.310	0.001	0.000	0.000	0.002	0.000	0.062
10	3.061	0.327	0.000	0.000	0.000	0.000	0.000	0.000
		Total [%]=	**0.666**	**0.256**	**0.004**	**0.440**	**0.457**	**0.365**

4.1.2 Results from the 3-D spine-beam FE model of the bridge with vertical hangers

Similar considerations and outcomes are taken into consideration for the bridge with vertical hangers. The modal analysis results are given in Table 4.3. Since no detailed experimental investigations on the bridge have been conducted so far, the presentation of the mode shapes are not given in a comparative form with the other studies in

literature. The mode shapes are indicated in Figure 4.9 and all results from corresponding mode frequency/period to modal mass participation ratios are given in Table 4.3.

Table 4.3 : Modal mass participation ratios of the 3-D spine-beam FE model with vertical hangers.

Mode	Period [s]	Frequency [Hz]	Mass Participation Ratio [%]					
			X-Direction (Horizontal)		Y-Direction (Longitudinal)		Z-Direction (Vertical)	
			Mx	Rx	My	Ry	Mz	Rz
1	13.030	0.077	**0.535**	0.000	0.000	0.028	0.000	0.000
2	6.383	0.157	0.000	**0.244**	0.002	0.000	0.000	0.000
3	5.436	0.184	0.000	0.000	0.000	0.000	**0.335**	0.000
4	4.886	0.205	0.000	0.000	0.000	0.000	0.000	**0.261**
5	4.082	0.245	0.000	0.000	0.000	0.000	**0.282**	0.000
6	3.974	0.252	0.012	0.000	0.000	0.022	0.000	0.000
7	3.290	0.304	0.062	0.000	0.000	0.350	0.000	0.002
8	3.245	0.308	0.000	0.059	0.000	0.000	0.000	0.000
9	3.210	0.311	0.001	0.000	0.000	0.010	0.000	0.056
10	3.083	0.324	0.000	0.000	0.000	0.000	0.000	0.000
		Total [%]=	**0.611**	**0.303**	**0.002**	**0.411**	**0.617**	**0.320**

These consequences demonstrates that the deck and tower mode shapes will dominate the dynamic response of the bridge to a dynamic input. As shown in Table 4.3, the first effective ten modes are obtained as single modes of the deck, towers and cables, respectively, but the rest of them are observed to be combination of these modes. Compared to total mass participation ratio of 95 % for the first 50 mode, the ratio of 61-62 % in horizontal direction for the first ten mode can also be a key indicator for the effectiveness of the deck and tower modes. Therefore, these single modes are predicted to be effective on the dynamic behavior of the bridge. Apart from, comparative study between the vertical and the inclined hanger are presented in detail in the further section, thus no further explanations are given here. Modal Analysis of 3-D Full-Scale Shell FE Model of the Bridge

4.1.3 Results from 3-D full-scale shell FE model of the bridge with inclined hangers

The considerations given in the section “4. Modal Analysis of the Bridge” are also adopted for the modal analysis of the 3-D full-scale shell FE model. The results obtained are given in a comparison with the other studies in literature.

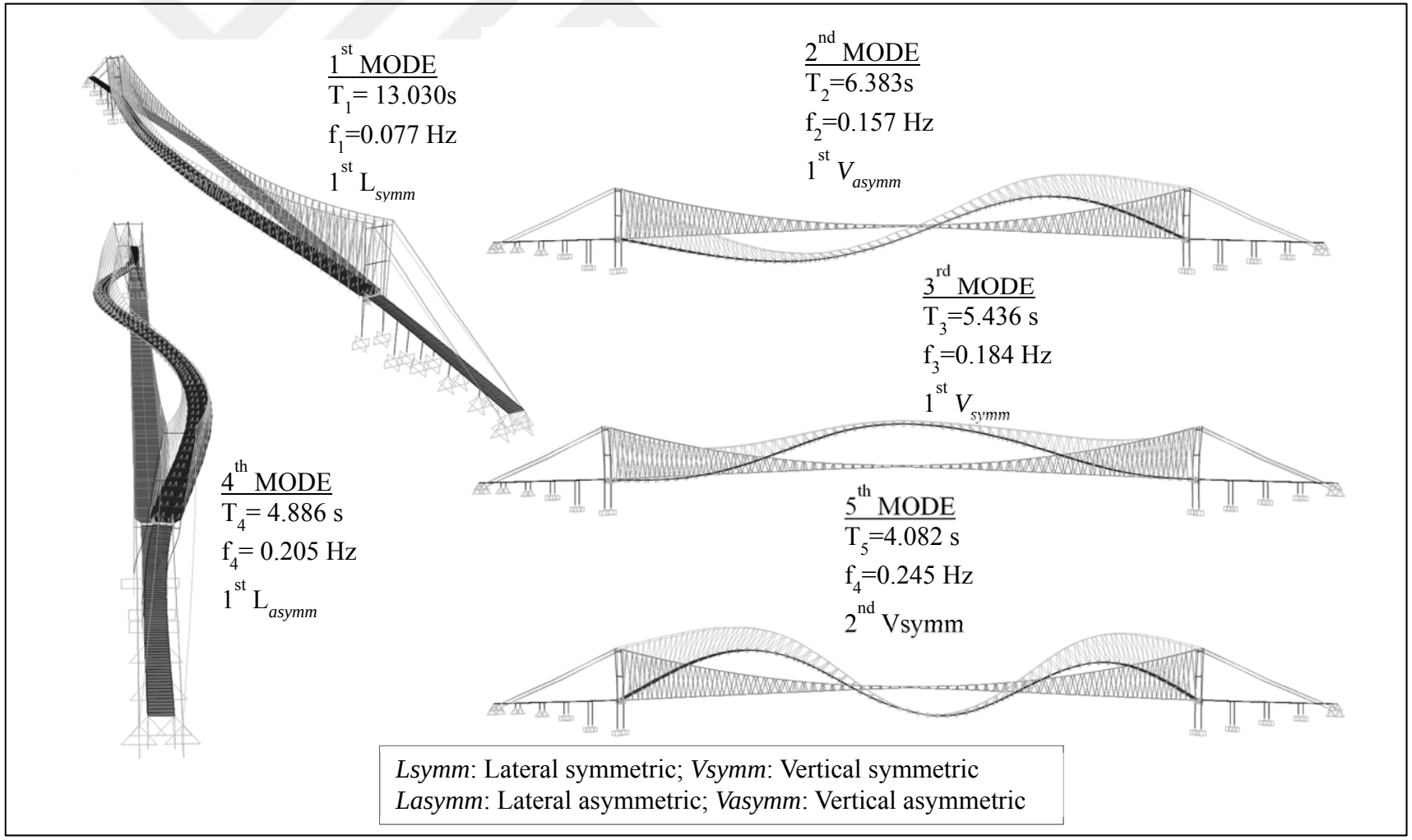

Figure 4.9 : The first five mode shapes of the spine-beam FE bridge model with vertical hangers.

According to Table 4.4, a good agreement between the results from the studies in literature and those obtained from the developed 3-D full-scale FE model of the bridge. In addition, Table 4.5 indicates the distribution of mass in the modes.

Table 4.4 : Comparison of the 3-D full-scale shell FE model with inclined hangers with the other studies.

Mode Number	Mode Shape	Frequency/Period [Hz]/[s]					
		Brownjohn et al. (1989)	Erdik and Uckan (1989)	Kosar (2003)	Apaydin (2010)	Current 3-D Shell FE (Inclined)	
						Period [s]	Freq. [Hz]
Mode-1	1st L_{sym}	0.073	0.072	0.069	0.074	13.090	0.076
Mode-2	1st V_{asym}	0.126	0.144	0.125	0.120	7.220	0.139
Mode-3	1st V_{sym}	0.165	0.202	0.190	0.158	6.481	0.154
Mode-4	1st L_{asym}	0.180	0.225	0.223	0.210	5.020	0.199
Mode-5	2nd V_{sym}	0.218	0.323	0.273	0.262	4.620	0.216

L_{sym}: Lateral symmetric; L_{asym}: Lateral asymmetric;V_{sym}:Vertical symmetric; V_{asym}:Vertical asymmetric; DL: Dead-load; LL: Live-load

Table 4.5 : Modal mass participation ratios of the 3-D full-scale shell FE model with inclined hangers.

Mode	Period [s]	Frequency [Hz]	Mass Participation Ratio [%]					
			X-Direction (Horizontal)		Y-Direction (Longitudinal)		Z-Direction (Vertical)	
			Mx	Rx	My	Ry	Mz	Rz
1	13.090	0.076	**0.526**	0.000	0.000	0.020	0.000	0.001
2	7.220	0.139	0.000	**0.135**	0.003	0.000	0.018	0.000
3	6.481	0.154	0.000	0.008	0.001	0.000	**0.265**	0.000
4	5.020	0.199	0.000	0.000	0.000	0.000	0.002	**0.252**
5	4.620	0.216	0.000	0.001	0.000	0.000	**0.234**	0.002
6	3.834	0.261	0.000	0.040	0.001	0.000	0.000	0.000
7	3.588	0.279	0.044	0.000	0.000	0.277	0.000	0.002
8	3.453	0.290	0.000	0.000	0.000	0.000	0.000	0.000
9	2.920	0.342	0.007	0.000	0.000	0.027	0.000	0.021
10	2.490	0.402	0.000	0.000	0.000	0.000	0.000	0.000
		Total [%]=	**0.578**	**0.184**	**0.005**	**0.324**	**0.518**	**0.277**

As in the spine-beam model of the bridge, the first ten modes of the bridge are single modes of the deck, towers and cables, respectively. Upon compared to the total mass participation percentage of 94 % corresponding to 50 modes, total modal mass participation (58 %) of the first ten modes in horizontal direction proves the efficiency of the deck and tower modes. Hence, the deck and tower mode shapes are estimated to dominate the dynamic behavior of the bridge under dynamic load.

The modal frequency variation of the FE model with the other investigations is also presented in Figure 4.10. The results are obtained to be compatible with the other studies. Similar to the spine-beam FE model of the bridge, Mode-3 and Mode-5 are

different from the others particularly compared to the results from the study of Erdik and Uckan (1989). The first five mode shapes are given in Figures 4.11-15.

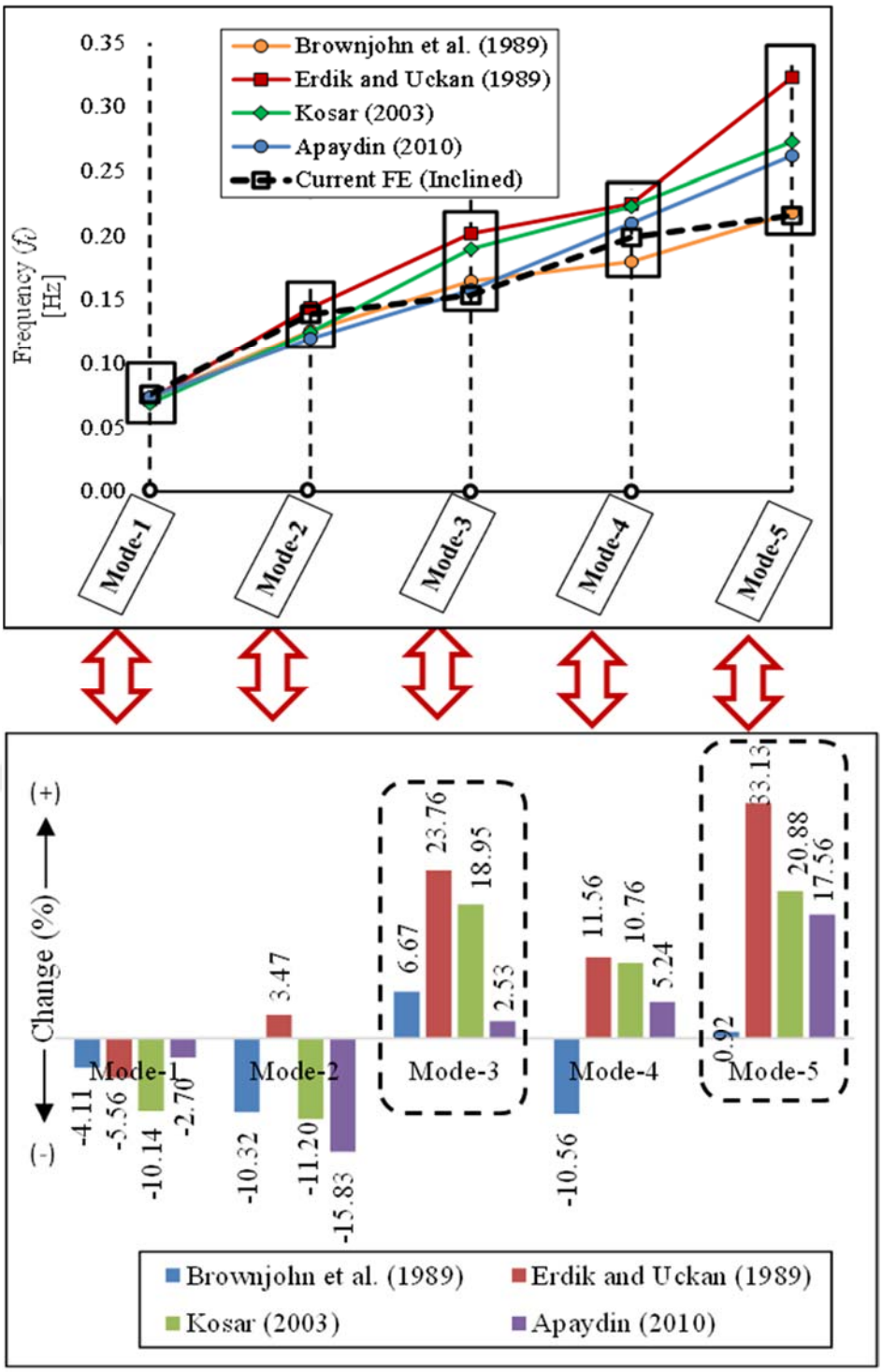

Figure 4.10 : Modal frequency change (%) of the 3-D full-scale shell FE model of the bridge with the other studies.

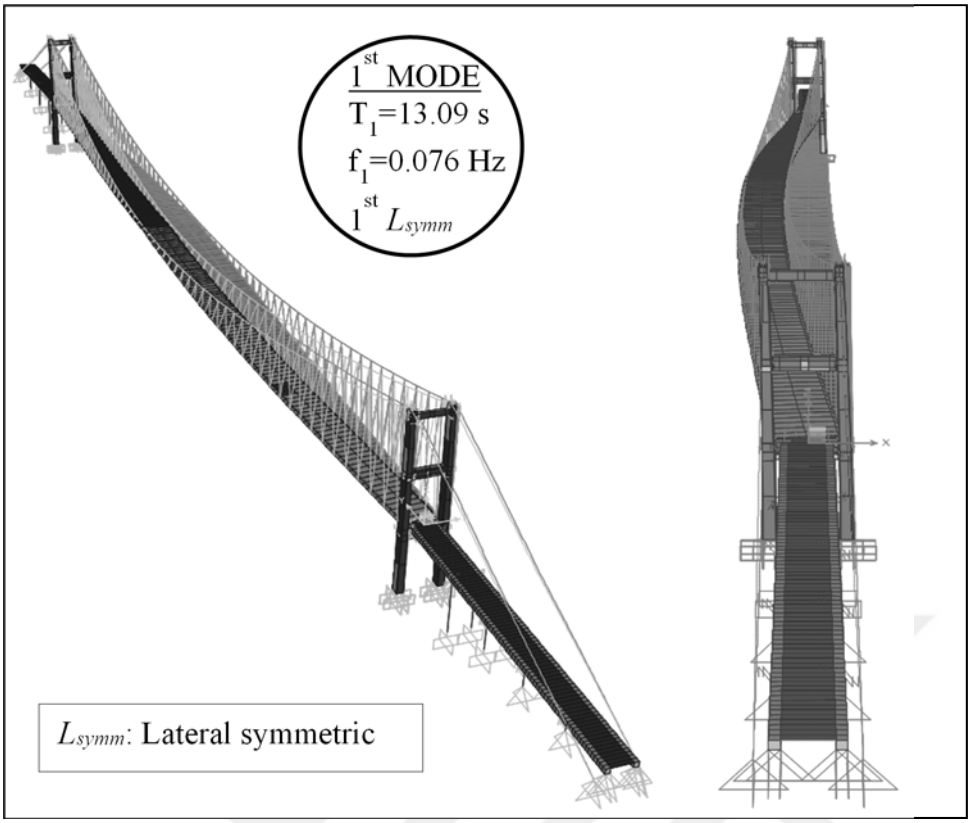

Figure 4.11 : 1st Mode shape of 3-D full-scale FE model of the bridge with inclined hangers.

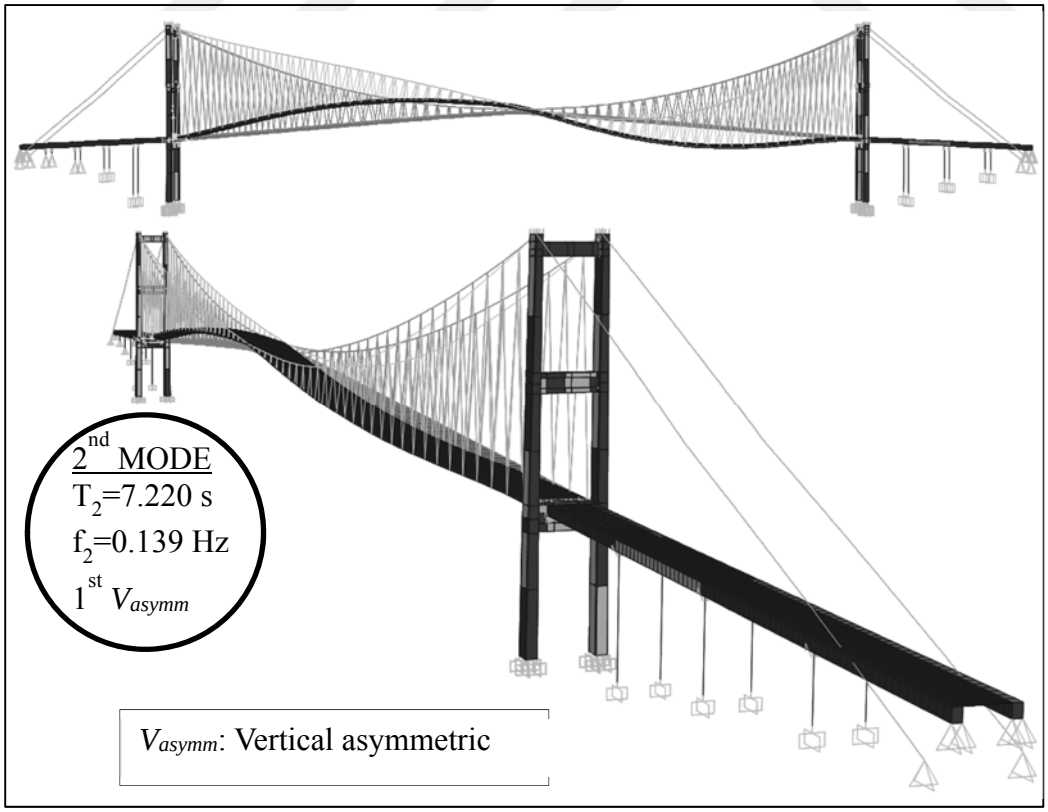

Figure 4.12 : 2nd Mode shape of 3-D full-scale FE model of the bridge with inclined hangers.

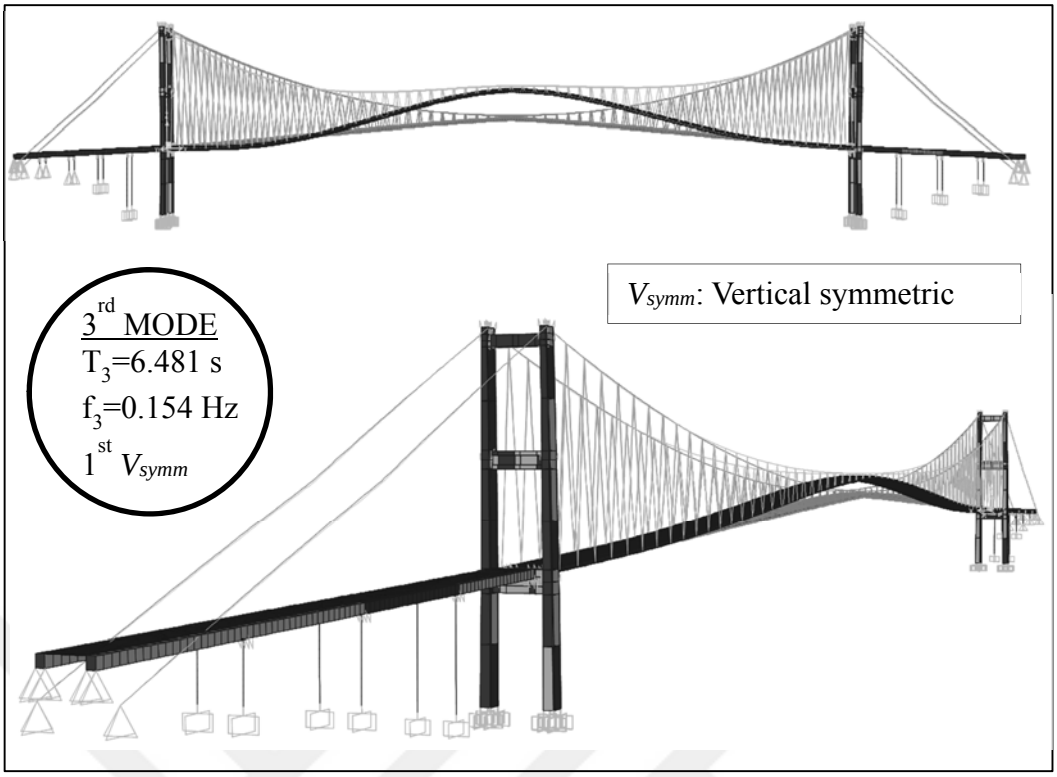

Figure 4.13 : 3rd Mode shape of 3-D full-scale FE model of the bridge with inclined hangers.

Figure 4.14 : 4th Mode shape of 3-D full-scale FE model of the bridge with inclined hangers.

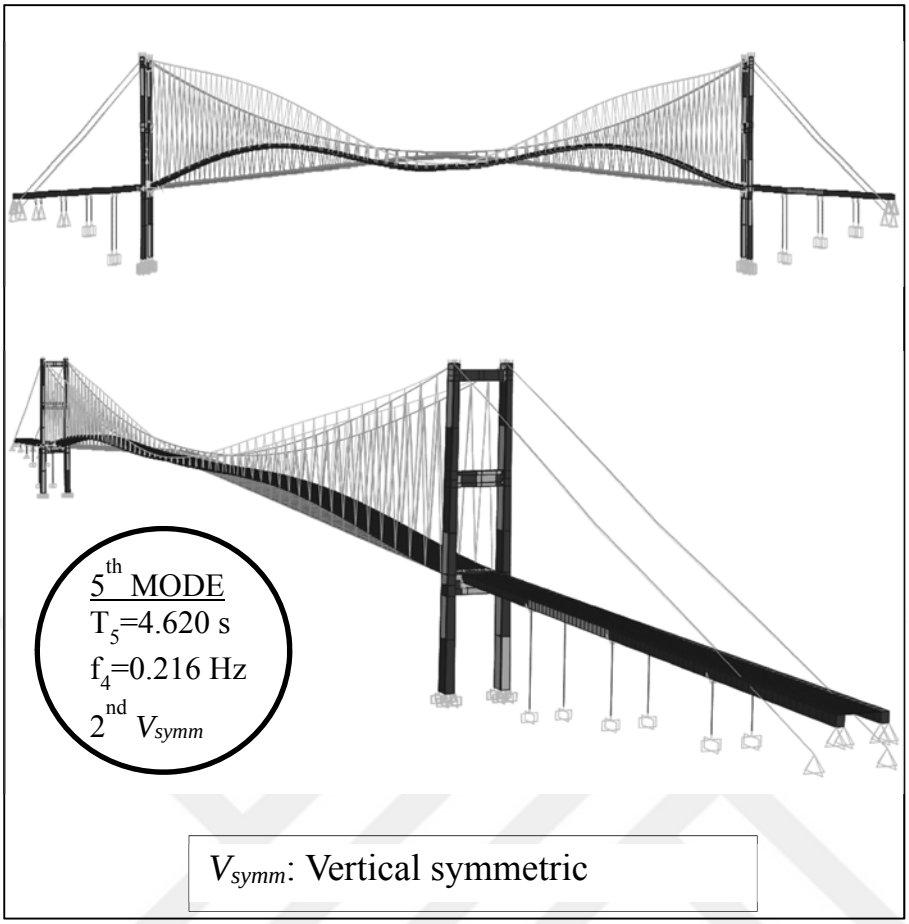

Figure 4.15 : 5th Mode shape of 3-D full-scale FE model of the bridge with inclined hangers.

4.1.4 Results from 3-D full-scale shell FE model of the bridge with vertical hangers

Similar considerations obtained in the previous sections on FE modelling of the bridge are utilized for 3-D full-scale shell FE bridge model with vertical hanger. Due to the new hanger replacement project that is recently implemented on the bridge, experimental data to identify the natural vibration properties of the bridge are not recorded enough. Therefore, the outcomes from the FE model of the bridge with vertical hangers are presented in Table 4.6. The associated mode shapes are also depicted in Figures 4.16-20. The modal analysis results demonstrate that the first 10 modes are effective single modes of the deck, tower and cables. The other mode shapes are not identifiable to determine which structural component dominates the dynamic vibration of the bridge, which means that they are combined mode shapes of three effective components of the deck, tower and cables.

Table 4.6 : Modal mass participation ratios of the 3-D full-scale shell FE model with vertical hangers.

Mode	Period [s]	Frequency [Hz]	Mass Participation Ratio [%]					
			X-Direction (Horizontal)		Y-Direction (Longitudinal)		Z-Direction (Vertical)	
			Mx	Rx	My	Ry	Mz	Rz
1	13.120	0.076	**0.497**	0.000	0.000	0.021	0.000	0.000
2	6.435	0.155	0.000	**0.203**	0.004	0.000	0.000	0.000
3	5.228	0.191	0.000	0.001	0.000	0.000	**0.310**	0.000
4	4.911	0.204	0.001	0.000	0.000	0.000	0.000	**0.217**
5	4.183	0.239	0.005	0.000	0.000	0.000	**0.425**	0.000
6	3.725	0.268	0.048	0.000	0.000	0.011	0.000	0.000
7	3.145	0.318	0.000	0.000	0.000	0.310	0.000	0.002
8	3.101	0.322	0.000	0.033	0.000	0.000	0.000	0.000
9	3.050	0.328	0.007	0.000	0.000	0.116	0.000	0.019
10	2.988	0.335	0.000	0.000	0.000	0.045	0.000	0.000
		Total [%]=	**0.558**	**0.237**	**0.004**	**0.504**	**0.735**	**0.237**

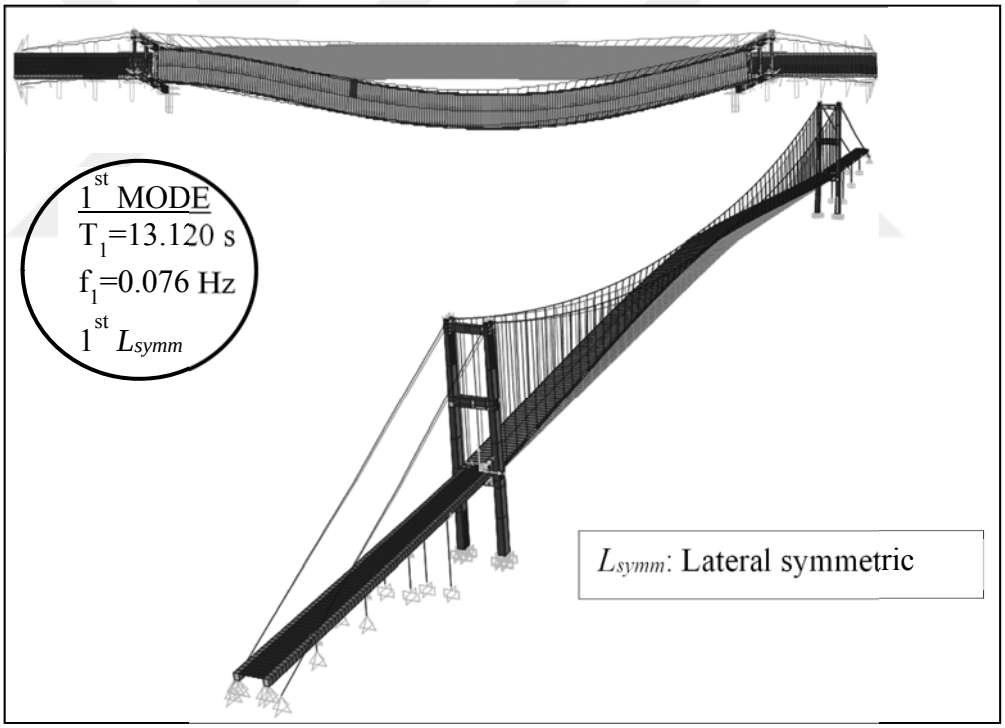

Figure 4.16 : 1st Mode shape of 3-D full-scale FE model of the bridge with vertical hangers.

It is also clear to conduct elaborate experimental testing on the bridge for the verification/updating of the developed FE models with vertical hangers. Owing to new hanger replacement project recently implemented, SHM data have not been recorded enough. Therefore, this aim will be achieved as future work of this thesis. The

comparison of vertical hanger with inclined hanger also presents a significant opportunity to identify the effects of the vertical hanger arrangement.

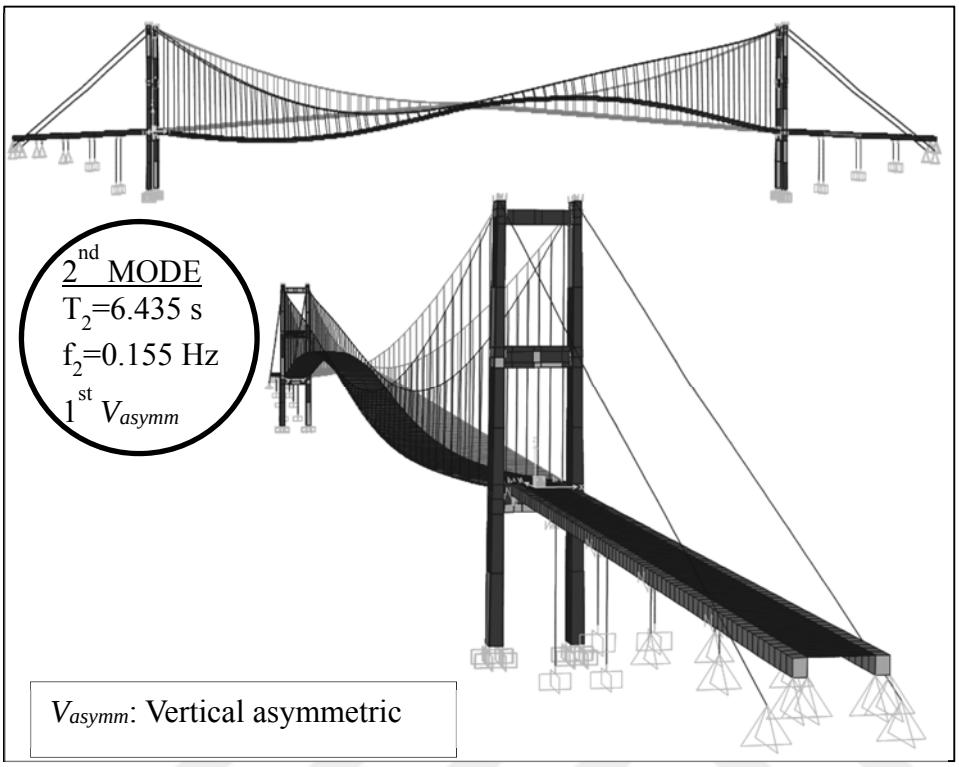

Figure 4.17 : 2nd Mode shape of 3-D full-scale FE model of the bridge with vertical hangers.

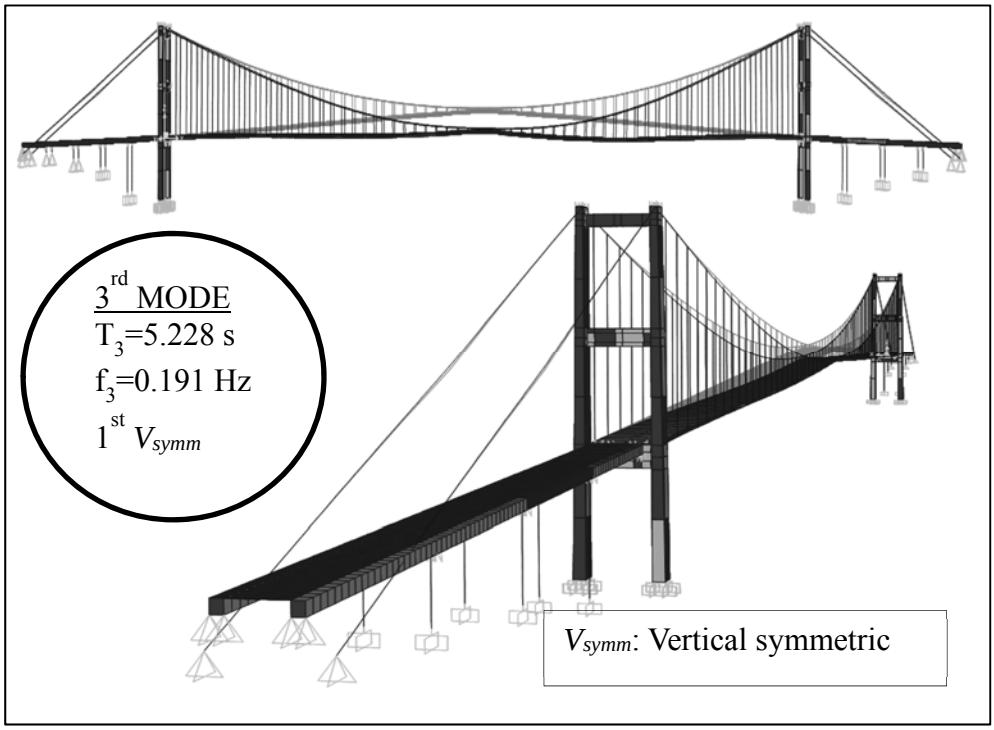

Figure 4.18 : 3rd Mode shape of 3-D full-scale FE model of the bridge with vertical hangers.

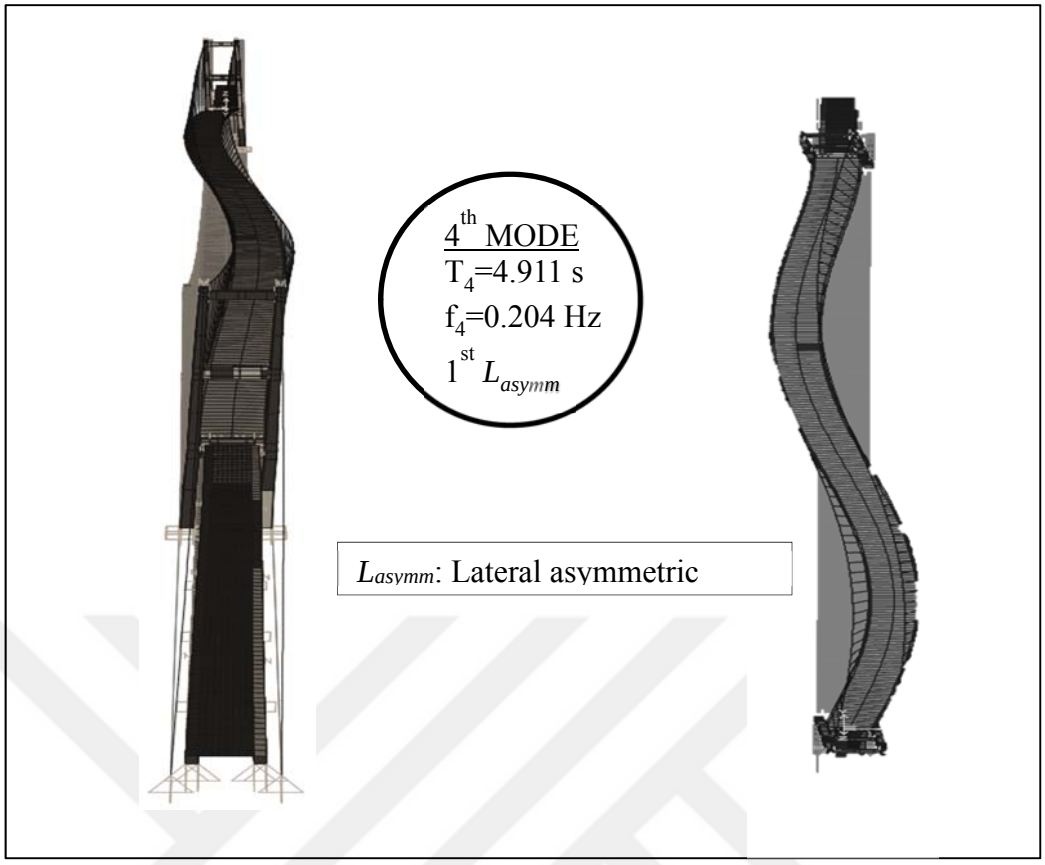

Figure 4.19 : 4th Mode shape of 3-D full-scale FE model of the bridge with vertical hangers.

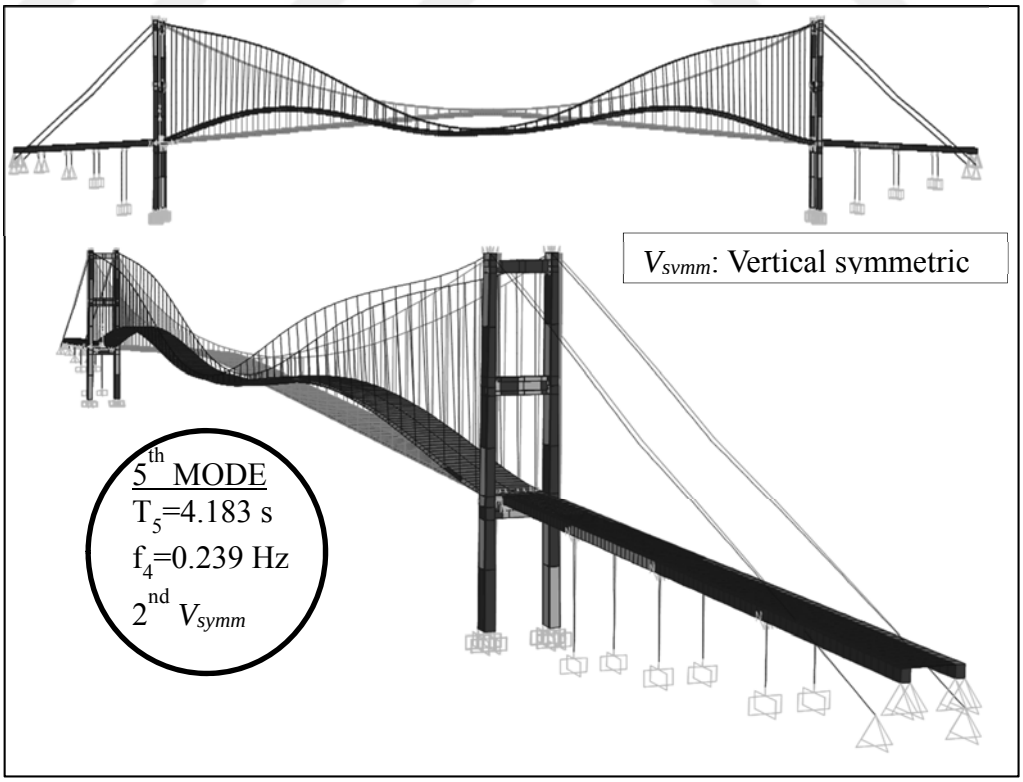

Figure 4.20 : 5th Mode shape of 3-D full-scale FE model of the bridge with vertical hangers.

4.2 Comparison of the Modal Analysis Results from the FE Models

Based on the modal analysis results, comparison between two different FE modeling approaches and two different hanger arrangements is a significant indicator for the following aims;

- to decide whether there is a compatibility between the developed FE models or not.
- to identify the effects of the hanger replacement from inclined to vertical on dynamic response of the bridge.

For the first aim, the developed FE models with inclined hanger (IH) using the spine-beam (F) and multi-scale (S) approaches are compared. As given in Table 4.7, the spine-beam model with inclined hangers (F-IH) and multi-scale model with inclined hangers (S-IH) shows a good performance with maximum error percent of 2%.

Table 4.7 : Comparison between the spine-beam (F-IH) amd shell (S-IH) models with inclined hangers.

Mode Number	Mode Shape	Inclined Hanger (IH)						Graphical Presentation
		Frame (F-IH)		Shell (S-IH)		Change (%)		
		Period [s]	Freq. [Hz]	Period [s]	Freq. [Hz]	Period [s]	Freq. [Hz]	
Mode-1	1st L_{sym}	12.984	0.077	13.090	0.076	0.817	**-1.322**	
Mode-2	1st V_{asym}	7.217	0.139	7.220	0.139	0.037	**0.321**	
Mode-3	1st V_{sym}	6.453	0.155	6.481	0.154	0.431	**-0.621**	
Mode-4	1st L_{asym}	4.926	0.203	5.020	0.199	1.903	**-1.968**	
Mode-5	2nd V_{sym}	4.561	0.219	4.620	0.216	1.282	**-1.472**	

L_{sym}: Lateral symmetric; L_{asym}: Lateral asymmetric;V_{sym}:Vertical symmetric; V_{asym}:Vertical asymmetric

Table 4.8 : Comparison between the spine-beam (F-IH) amd shell (S-IH) models with vertical hangers.

Mode Number	Mode Shape	Vertical Hanger (VH)						Graphical Presentation
		Frame (F-VH)		Shell (S-VH)		Change (%)		
		Period [s]	Freq. [Hz]	Period [s]	Freq. [Hz]	Period [s]	Freq. [Hz]	
Mode-1	1st L_{sym}	13.030	0.077	13.120	0.076	0.690	**-0.971**	
Mode-2	1st V_{asym}	6.383	0.157	6.435	0.155	0.810	**-1.059**	
Mode-3	1st V_{sym}	5.436	0.184	5.228	0.191	-3.821	**3.822**	
Mode-4	1st L_{asym}	4.886	0.205	4.911	0.204	0.517	**-0.331**	
Mode-5	2nd V_{sym}	4.082	0.245	4.183	0.239	2.468	**-2.434**	

L_{sym}: Lateral symmetric; L_{asym}: Lateral asymmetric;V_{sym}:Vertical symmetric; V_{asym}:Vertical asymmetric

Similar decent agreement is obtained for the models with vertical hangers as presented in Table 4.8. Accordingly, the percentage change in the modal properties of the bridge with inclined and vertical hangers reveals high compatibility in the modeling techniques. In addition, another sign for accuracy of the FE models and modeling approaches is to compare the modal analysis results from the FE models with the other experimental/numerical studies in literature. In Figure 4.21, the developed FE models of the bridge with inclined hangers are compared with the studies in literature. According to Figure 4.21, relatively reliable FE models are obtained to be established, and these models can be easily utilized for further analysis/investigation of the bridge.

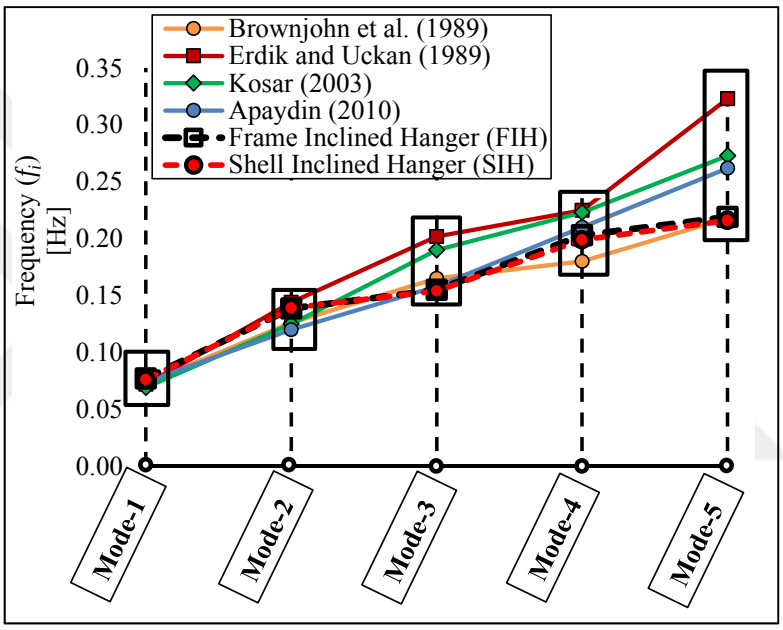

Figure 4.21 : Comaprison of the spine-beam and shell FE models with inclined hangers with the other studies in literature.

Table 4.9 : Comparison of inclined hanger (IH) with vertical hanger (VH) for spine-beam FE modeling technique.

Mode Number	Mode Shape	3-D Spine-beam FE model						Graphical Presentation
		Inclined Hanger (IH)		Vertical Hanger (VH)		Change (%)		
		Period [s]	Freq. [Hz]	Period [s]	Freq. [Hz]	Period [s]	Freq. [Hz]	
Mode-1	1st L_{sym}	12.984	0.077	13.030	0.077	0.356	**-0.355**	
Mode-2	1st V_{asym}	7.217	0.139	6.383	0.157	-11.556	**13.066**	
Mode-3	1st V_{sym}	6.453	0.155	5.436	0.184	-15.767	**18.718**	
Mode-4	1st L_{asym}	4.926	0.203	4.886	0.205	-0.822	**0.829**	
Mode-5	2nd V_{sym}	4.561	0.219	4.082	0.245	-10.506	**11.740**	

L_{sym}: Lateral symmetric; L_{asym}: Lateral asymmetric;V_{sym}:Vertical symmetric; V_{asym}:Vertical asymmetric

For the second aim of the comparison, influence of the hanger arrangement on modal characteristics of the bridge is investigated for two FE modeling approaches: spine-beam and multi-scale modeling. In Table 4.9, the results from the spine-beam models of the bridge are given. As expected, considerable increase in the vertical modes of Mode-2: 1st vertical asymmetric (1st V_{asymm}), Mode-3:1st vertical symmetric (1st V_{symm}) and Mode-5: 2nd vertical symmetric (2nd V_{symm}) is obtained. The increase reaching to 20 % indicates that vertical hangers leads to increase in the rigidity of the bridge in vertical direction compared to inclined hangers. Similar outcomes are obtained for multi-scale modeling technique as presented in Table 4.10.

Table 4.10 : Comparison of inclined hanger (IH) with vertical hanger (VH) for multi-scale FE modeling technique.

Mode Number	Mode Shape	3-D Full-scale shell FE model						Graphical Presentation
		Inclined Hanger (IH)		Vertical Hanger (VH)		Change (%)		
		Period [s]	Freq. [Hz]	Period [s]	Freq. [Hz]	Period [s]	Freq. [Hz]	
Mode-1	1st L_{sym}	13.090	0.076	13.120	0.076	0.229	**0.000**	
Mode-2	1st V_{asym}	7.220	0.139	6.435	0.155	-10.873	**11.511**	
Mode-3	1st V_{sym}	6.481	0.154	5.228	0.191	-19.333	**24.026**	
Mode-4	1st L_{asym}	5.020	0.199	4.911	0.204	-2.171	**2.513**	
Mode-5	2nd V_{sym}	4.620	0.216	4.183	0.239	-9.459	**10.648**	

L_{sym}: Lateral symmetric; L_{asym}: Lateral asymmetric;V_{sym}:Vertical symmetric; V_{asym}:Vertical asymmetric

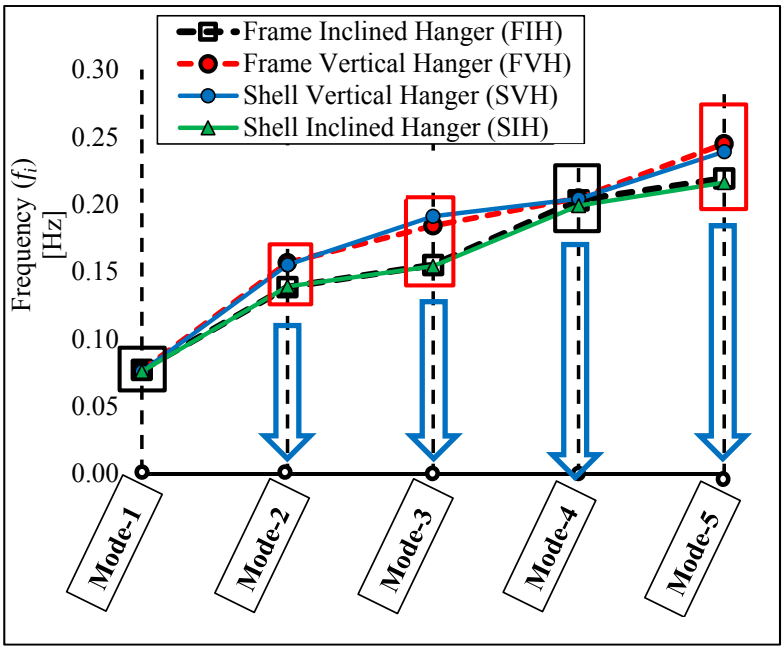

Figure 4.22 : Comparison of the modeling techniques and hanger arrangement.

Moreover, the variation of the modeling techniques and hanger arrangement parameters is depicted in Figure 4.22. From this figure, high compatibility between the established FE models of the bridge and vertical hanger replacement effects on dynamic behavior of the bridge are clearly observed. The conclusions obtained from Tables 4.9-10 are also obtained schematically with red-box in Figure 4.22.

Comparative results from the modal analyses enable,

- to verify the developed FE models for reliable further analysis of the bridge, such as earthquake, strong wind, heavy-truck, human-induced etc.
- to identify the effects of vertical hanger replacement on the dynamic response of the bridge.

5. STRUCTURAL HEALTH MONITORING SYSTEM OF THE BRIDGE

The first studies related to the installation of a monitoring system on the Bosphorus Bridge were conducted by Brownjohn et al. (1989), Erdik and Uckan (1989), Petrovski et al. (1974) and Tezcan et al. (1975). Nevertheless, these initial studies including a temporal SHM system with portable sensors showed the need for a permanent SHM system. Therefore, a well-designed SHM system with three subsystems of sensor, data acquisition and recordings was installed on the bridge in 1993. After critical wind effect in 2004 leading to damage in stool plate of hanger element at south tower of Ortakoy side, the need to SHM system for the bridge became inevitable. Therefore, the bridge authority KGM decided to design a comprehensive SHM system and alert system not to interrupt operational service of the bridge. This system is aimed to determine response of the bridge under daily and unusual events, such as, heavy traffic, wind and earthquake loads. Accordingly, it helps to previously take appropriate measure against possible structural anomalies and to determine the best maintenance method at the right time.

Several studies, which are necessary to be able to establish a SHM system for the bridges, were conducted to determine dynamic characteristics under critical loading and environmental conditions by using certain experimental techniques and to calibrate analytical model by using the measured dynamic parameters. The first attempts to make experimental investigations for the First Bosphorus Bridge were made just before it was opened to service in 1973. In those studies of (Brownjohn et al, 1989; Erdik and Uckan, 1989; Petrovski et al, 1974; Tezcan et al, 1975), modal vibration characteristics were determined by ambient and forced vibration tests. For this aim, three different types of accelerometers were utilized and deployed on the bridge under wind loading. The force vibration test was achieved through two shakers welded on the deck mid-span and on quarter span of the bridge. Consequently, the results from the studies showed a good compatibility with those from the studies of Brownjohn et al. (1989) and Erdik and Uckan (1988). After the first system identification studies with the limited number of sensors, the next comprehensive

experimental investigations for the First Bosphorus Bridge were done by Brownjohn et al. (1989) and Erdik and Uckan (1989). Under wind and traffic loading events, the obtained experimental results from spectral density and transfer function were compared with theoretical results from finite element model of the bridge. A relatively good agreement was obtained between two methods. Depending on these prominent studies, a SHM system for the First Bosphorus Bridge was established in 1993. The initial SHM system was designed to include three subsystems: (i) sensor system (ii) data acquisition system and (iii) data recording/monitoring system. A sensor system with 28 channels consists of accelerometers, seismometers, and wind speed and direction meters. Utilizing the installed SHM system, Beyen et al. (1994) also conducted ambient vibration survey of the Bosphorus Bridge to compare experimentally obtained results with those of FE model and the previous experimental and theoretical studies. The comparative study revealed a decent agreement between the results. Recent documents for the structural monitoring of the First Bosphorus Bridge were prepared by Apaydin et al. (2015), Apaydin et al. (1999), Bas et al. (2016) and Erdik and Apaydın (2007). A number of implementations for the monitoring of the bridge were presented in these studies. Except for those conducted before the critical wind effect in 2004 leading to damage in the stool plate of hanger element at the south tower of European side, portable or temporary sensor deployment on the bridge was utilized. After the critical event, the KGM decided to urgently improve the previous SHM system of the bridge. Thus, the newly designed SHM system was installed on the bridge. Therefore, a limited number of studies on the recent SHM system of the bridge in literature were carried out by Apaydin et al. (2015) and Bas et al. (2016).

5.1 General Design Considerations, Monitoring Objectives and Parameters of the SHM System

In order to design a SHM system, the first attempt is to define the monitoring objectives and requirements of bridge. It is also relatively significant to have information for special features of bridge. Therefore, clearly determining the special characteristics of bridge is also of crucial stage. This aim is achieved together with the common work of SHM and bridge designers. In spite of many studies on SHM system for long-span bridges in literature, Aktan et al. (2002), Jan-Ming and Ni (2005), Mufti

(2001), Wenzel (2009), Wong (2007) and Xu and Xia (2011) are mostly referenced ones. In the studies, all considerations and knowledge for design a SHM system for long-span bridges are given. Therefore, the SHM system considerations of the long-span bridges in Turkey are presented in compliance with those given in these studies.

Before effectively installing a SHM system, special characteristics of the bridge need to be identified. Particularly, the in-service bridge, the Bosphorus Bridge, has experienced different loading experiences. Therefore, the main elements and phenomena of the bridges to be closely monitored are similar and given below:

- Hanger load variation
- Expansion joint movement
- Deck fatigue
- Tower displacement at the saddle

General monitoring strategy of the SHM system of the Bosphorus Bridge is presented in the following. It is well known that each bridge has special characteristics for SHM system. Upon designing SHM systems for the bridge, the following main monitoring objectives are obtained based on the recommendations of the bridge authority, General Directorate of Turkish State Highways (KGM):

- Rapid reporting the bridge operation condition just after extreme events such as earthquake, wind, marathon and heavy truck loads.
- Tracking certain structural parameters (fatigue, geometrical change and stress variation) indicating structural condition of the bridge.
- Confirming the geometry and performance of the bridge during extreme events that has been possible in the future.

In these objectives, the extreme loading events of (i) Seismic loading (ii) Extreme wind loading (iii) Extreme traffic loading and (iv) Extreme thermal loading are considered in the design of the SHM systems. After specifying the monitoring objectives, the second issue is which monitoring parameters will be utilized to achieve the objectives of the SHM system. The monitoring parameters are directly pertinent to the bridge's own characteristics. In general, the SHM system of the bridge has the following monitoring parameters:

- Hanger load variation
- Deck expansion
- Response monitoring (Tower, deck and cable response)
- Deck fatigue/traffic effect monitoring
- Wind and hanger monitoring
- Thermal monitoring
- GPS system

In order to quantitate these monitoring parameters, the Sensory System (SS), one of the main component of the SHM system, needs to be better identified. Type of sensors, the number of sensor, sensitivity range of sensor etc. are the main issues of the Sensory System. Table 5.1 generally summarizes the monitoring parameters and corresponding sensor types of the SHM system of the bridge.

Table 5.1 : Monitoring parameters and corresponding sensor types.

Monitoring Parameters	Sensor type							
	Acceleration	Strain gage	Weather	Thermocouple	GPS	Force Transducer	Pin	Laser
Hanger load variation		x				x	x	
Deck expansion								x
Bridge response	x							
Deck fatigue and traffic effect monitoring		x						
Wind and hanger monitoring	x	x	x					
Thermal monitoring				x				
GPS system					x			

The following step is to identify the main components of the SHM system. In Figure 5.1, general components of the SHM system of the bridge are depicted. In this figure, the design requirements of the SHM system of the bridge are also shown to be closely related to the components of the monitoring system. The SHM system of the bridge is consisted of six components as shown in Figure 5.1. Data acquisition system (DAS) is consisted of (i) Site Supervisor (ii) Backup Computer (iii) on-structure acquisitions (ACQ1, ACQ 2, and ACQn). Site supervisor is located on the KGM building. These systems contains data acquisition hardware and National Instruments Lab-VIEW Real-

Time operating system. The measurements acquired are sent via a traditional network to a PC based on the bridge for storage. The number of data acquisition systems are determined depending on the quantity of channels. For example, the ACQ2 is divided into separate acquisition systems. As shown in Figure 5.2, the sensors are directly connected with the junction boxes distributed along the bridge. Measured data come to the three data acquisition systems from the junction boxes. The Data Transmission System (DTS) are designed according to the local and global cabling networks. The connection between the sensors and the junction boxes are provided with the local cabling networks. The global cabling networks are utilized for connection between the data acquisition (DAS) and the Data Processing System (DPS), and between the other components.

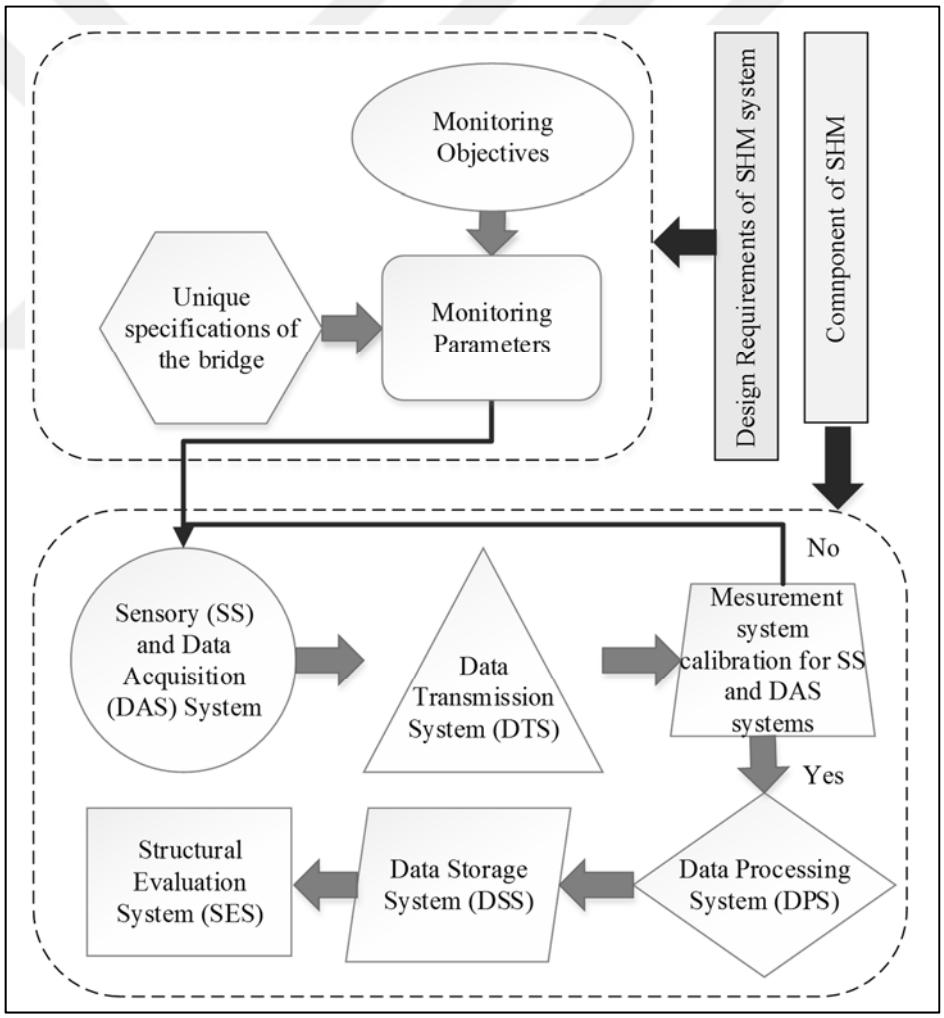

Figure 5.1 : General components of the SHM systems.

After configuration of the hardware systems of the SHM system, Data Processing System includes sensor scaling, signal filtering, rain-flow calculation and spectrum

analysis. The sensor scaling process is applied to convert the raw signals coming outfrom the signal conditioning of the sensors into engineering units. The signal filtering process provides functions for filtering the unwanted signals. Typically, unwanted signals are generated either by uninteresting phenomena, or by pollution of the raw electric signals of the sensors. An aliasing of the signal can also occur if a parasitic signal appears at a higher frequency than the sampling rate of the system. If it is a harmonic signal, it can generate unreal signals on the records of the acquisition unit. The rain-flow process is used in order to reduce a varying stress signal into a set of simple stress reversals. It allows an assessment of fatigue usage.

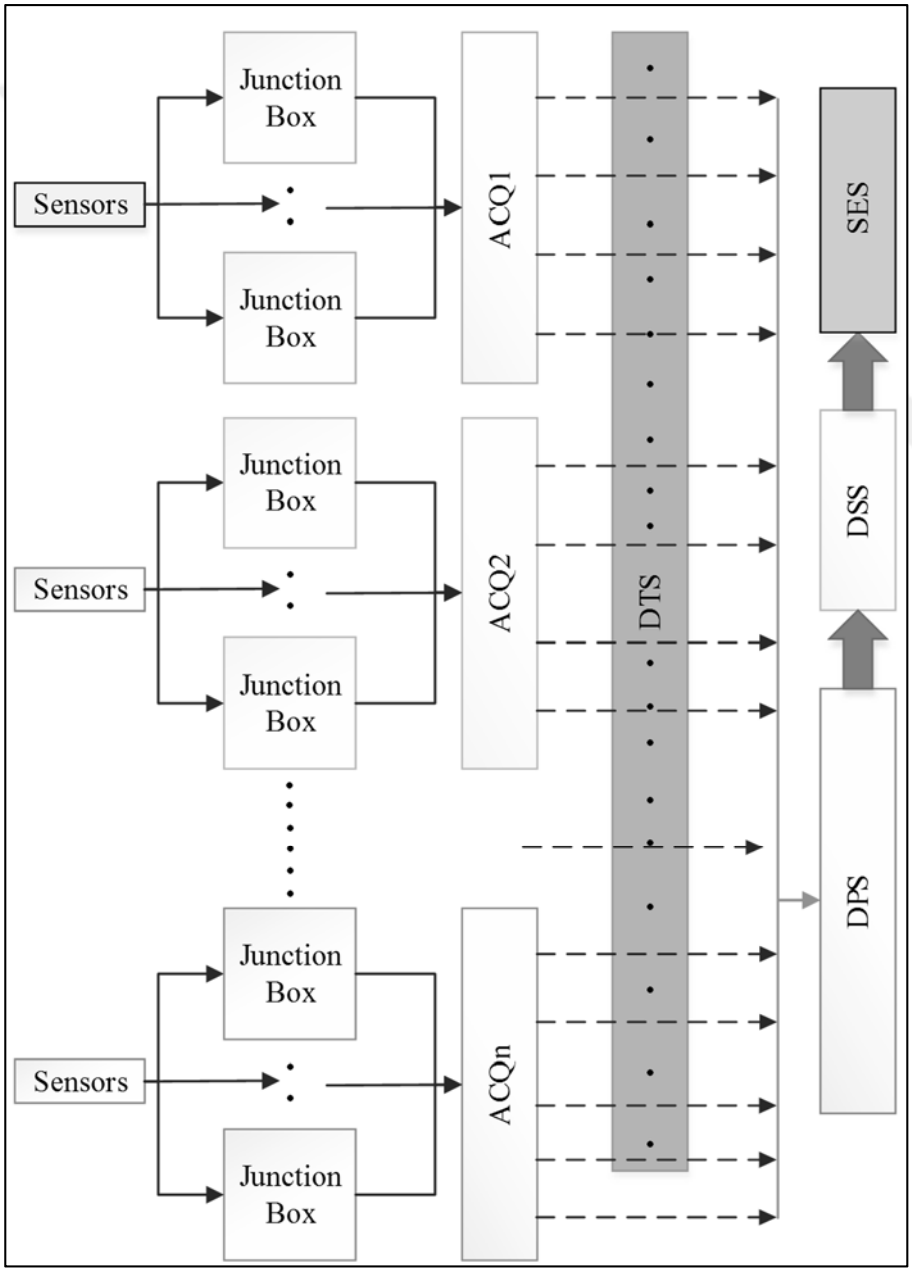

Figure 5.2 : Flow chart for data recording in the SHM system of the bridge.

The spectrum analysis process, called Duhamel Spectrum Analysis, is aimed to analyze earthquake effects. The spectrum is directly calculated from the channel signals specifically defined in the SHM system. The Structural Evaluation System (SES) is designed according to threshold approach. Besides, the frequency domain analysis, Fast Fourier and Inverse Fourier Analyses, is performed for data from the accelerometer channels. The threshold-based alert system can be defined with different colors of sensors as given below:

- Green, when the channels of the sensor type group are within their thresholds
- Orange, when one of the channels of the sensor type group has over passed its warning threshold
- Red, when one of the channels of the sensor type group has over-passed its alert threshold.

Table 5.2 : Maintenance strategy of the SHM systems of the bridge.

Maintenance Strategy of SHM System	
Preventive maintenance	▪ Checking system operation at different locations ▪ Sensor testing ▪ Cleaning of the system ▪ Checking of the systems component fixings ▪ Replacement of filters ▪ Maintenance of connections when required
Curative maintenance	▪ Remote technical assistance to identify the problem ▪ Postage of the equipment if replacement is easily performed remotely
Technical assistance	▪ Daily remote connection to the system to check its operation, and notification of any malfunction ▪ Technical support for the use of the software ▪ Follow up of updated software versions

The general maintenance strategy to deal with durability issues of the SHM systems of the bridges is also identified. The maintenance strategy with three stages is generally covered with fair wear and tear and the considerations are given in Table 5.2. The SHM system has also different monitoring types of (i) Verification Monitoring (ii) Operational Monitoring and (iii) Condition Monitoring. For this aim, the sensors can

be grouped. Based on the aims of the SHM systems of the bridges, the first active strategy of the SHM systems is to control whether or not they exceed their design limits. For this aim, a threshold value is defined for each characteristics of the bridge. OA system/structural identification strategy is also planned to be designed by adding a module to the current SHM system. In addition, it is aimed to extend the monitoring systems with damage detection process. However, these additional strategies will probably be conducted in the future.

5.2 Sensor Specifications, Configuration and Layout of the SHM System

Depending on the general structural characteristics of the bridge, the SHM system is developed to track critical responses using sensors and real-time data acquisition components. The sensors include accelerometers, tilt meters, force transducers, strain gauges, laser displacement, GPS, thermocouples and weather stations. In total, there are 168 sensors, using 258 channels, located at strategic positions on the bridge. The quantity and location of the sensors are determined after certain temporal installation tests on its SHM system. In Table 5.3, the number and type of sensors installed on the bridge are listed. In the same table, their essential specifications are also given.

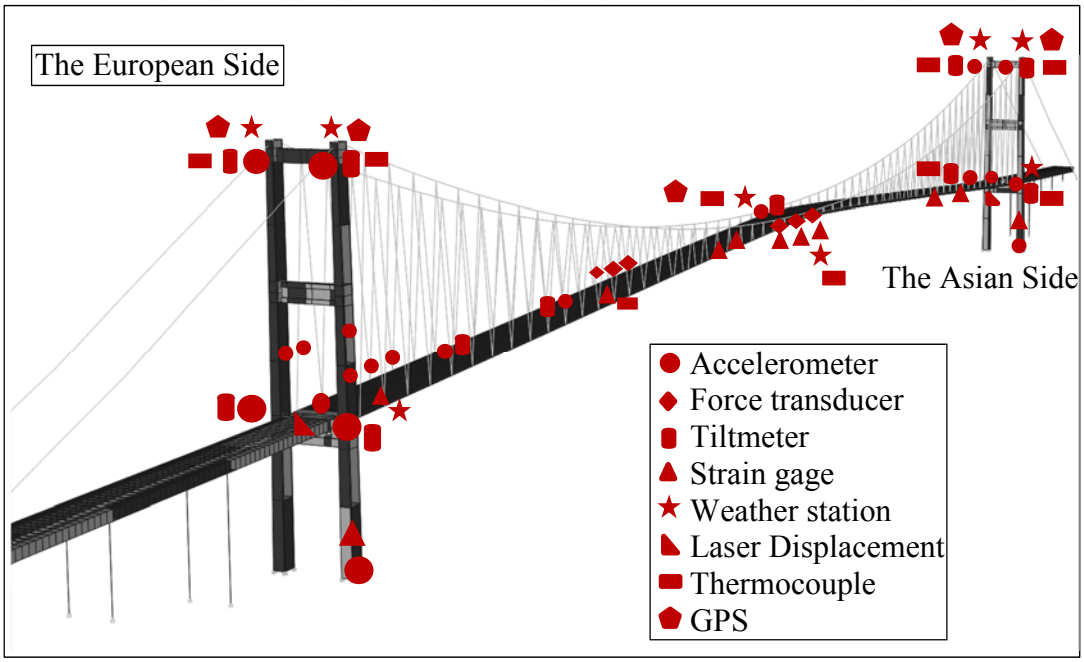

Figure 5.3 : Sensor arrangement of the SHM system of the First Bosphorus Bridge.

Further, the locations of the sensors are schematically presented with the general arrangement in Figure 5.3. As shown in Figure 2.2, the Bosphorus Bridge has inclined

hanger elements instead of a typical vertical hanger arrangement. Due to this feature, hangers and stool plates are instrumented with 14 strain gages and 12 force transducers as well as 6 accelerometers for vibration monitoring. Further, technical specifications of each sensor are given in more detail below (KGM 2008a, 2008b). In addition, elaborate layouts for the location of the sensors are given in Figures 5.4-6.

Table 5.3 : Types, specifications and quantity of the sensors of SHM system of the Bosphorus Bridge.

Sensor type and specifications			**Quantity**
Force transducer		• Measuring range(mm) : +/-1.50 mm • Repeatability(mm/m): 0.30 x 10^{-3} • Linearity (mm/m): 0.30 x 10^{-3} • Operating temperature : - 10 to 80 °C	12
Accelerometer	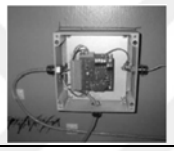	• Measuring range (g) : +/-2.00 • Sensitivity (mV/g) : 2000 • -3 dB frequency cutoff (Hz): 300 • Shock survival (0. 1 ms, ½ sine) (g) : 2000	19
Tiltmeter		• Measuring range (°) : +/-14.50 • Resolution (Arc second) : 1.00 • -3 dB frequency cutoff (Hz): 5.00 • Shock survival (0.5 ms, ½ sine) (g) : 1000	15
Strain gage and		• Resistance tolerance (%) : +/-0.30 • Gage factor : approx. 2.00 • Operation temperature (°C) ▪ For static : -70 t 200 ▪ For dynamic : -200 to 200	70
Weather station		• Wind speed range (mph) : 0 to 130 • Threshold sensitivity (mph): 2.40 • Pitch (cm): 29.4 cm air passage/revolution • Operation temperature (°C) : -50 to +50	6
Laser displacement		• Measuring range (mm) : 200 to 2000 • Resolution (mm) : 1 to 3 • Max. measuring freq. (Hz) : 10 • Operation temperature (°C) : -20 to +70	8
Thermocouple		• J type thermocouple • Accuracy (%) : +/-0.10 • Fixed on copper or steel collar	33
GPS		• Precision (mm) : 0.2 • Humidity (%) : up to 95 • Sampling rate (Hz) : 1.0 Hz • Operation temperature (°C) : -40 to +65	5
		Total	168

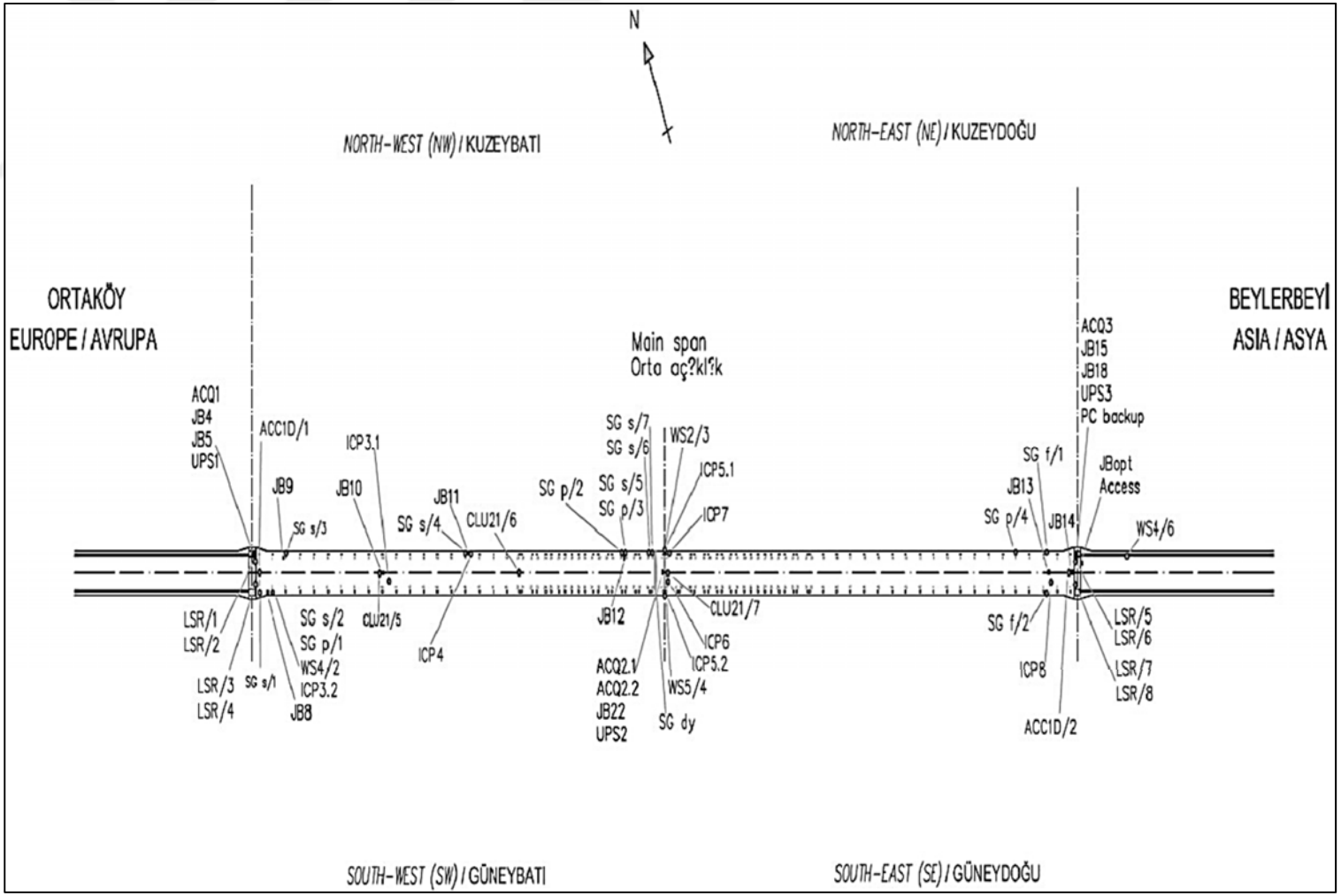

Figure 5.4 : SHM project layout of the bridge in plan (KGM, 2008a, 2008b).

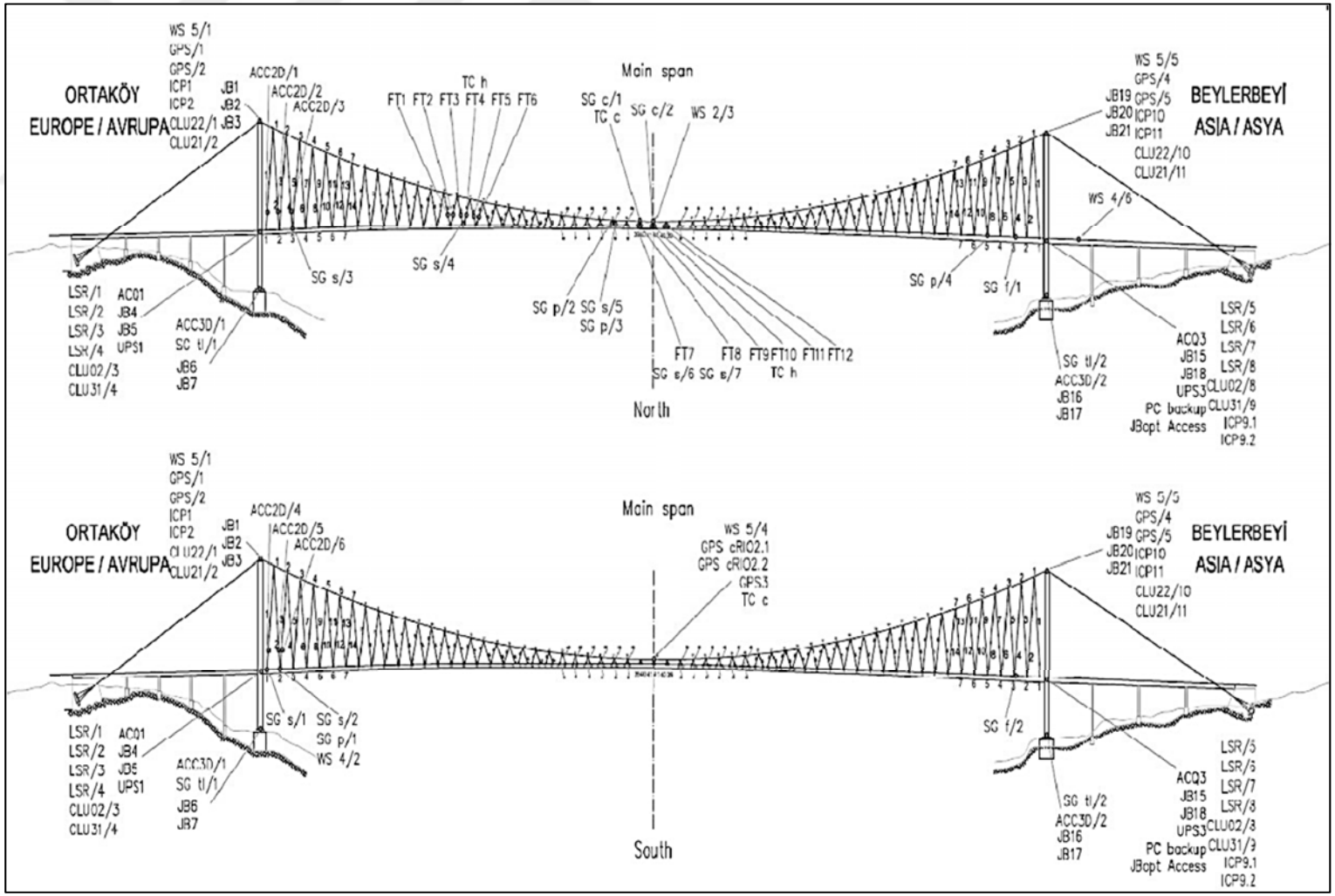

Figure 5.5 : SHM project layout of the bridge in elevation KGM, 2008a, 2008b

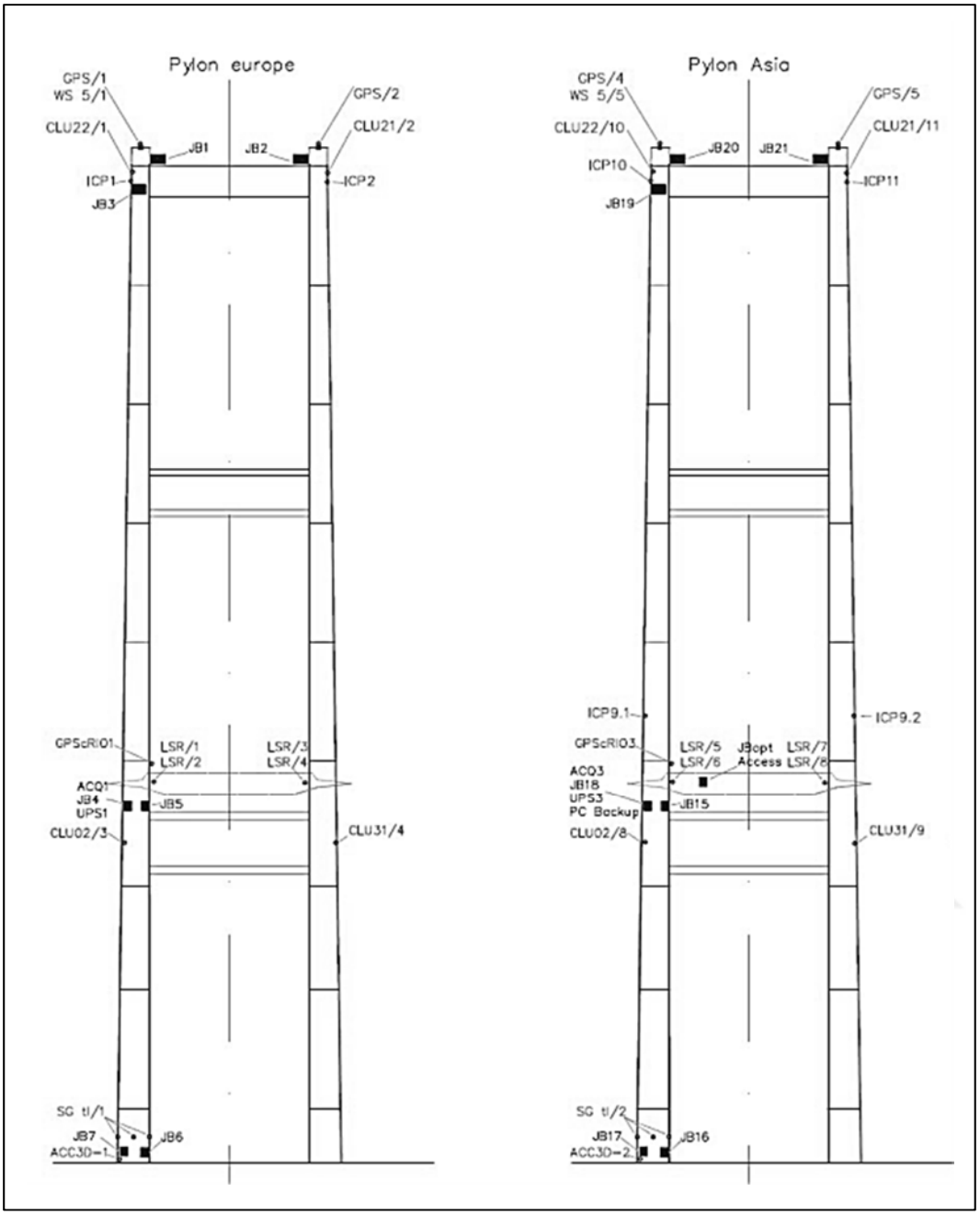

Figure 5.6 : SHM project layout of the tower of the bridge (KGM, 2008a, 2008b).

- Force Transducer (FT): The main objective of the force transducers is to monitor load variation in the hangers and instrumented pins. The force transducer is based on an Invar steel bar extensometer. The LVDT transducer measures longitudinal displacements of the Invar bar when the rope is tensioned. Displacements observed on the basis of measurement give strain in the rope. The distance between fixings of the bar and the sensor determines the basis of measurement. Technical properties of FT is presented in Table 5.4.

General view of force transducer located on hanger element of the bridge is shown in Figure 5.7.

Table 5.4 : Technical specifications of force transducer.

Measuring range (mm)	+/- 1.5 mm
Repeatability (mm/m)	0.3×10^{-3}
Linearity (mm/m)	0.3×10^{-3}
Operating temperature	-10 to +80

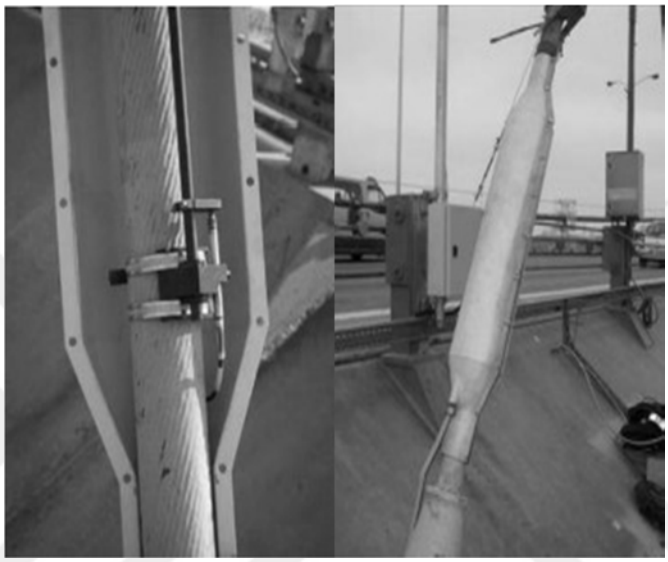

Figure 5.7 : General view of force transducer on hanger elements.

- Accelerometer (ACC): These instruments are installed for bridge response identification, and wind and hanger monitoring. Accelerometers on hanger elements have 2D capability of measuring, but those on tower leg have 3D capability of measuring. Technical properties of installed accelerometer are summarized in Table 5.5. General pictures of the accelerometer installed on the bridge are given Figure 5.8.

Table 5.5 : Technical specifications of accelerometer.

Measuring range (g)	+/- 2
Full Range Output (V)	4
-3dB Frequency Cutoff (Hz)	300
Sensitivity (mV/g)	2000
Output Noise ($\mu g/Hz^{1/2}$)	13
Cross Axis Sensitivity – TYPICALLY (%)	2
Non Linearity – TYPICALLY (% full scale)	0.5
Output impedance (ohms)	1
Operating Voltage (V)	9 to 32
Shock Survival (0.1 ms, ½ sine) (g)	2000

Figure 5.8 : 2D accelerometer on hanger.

- Tiltmeters (TILT): Tiltmeters are required to obtain bridge response. The LSI Series are a precision gravity referenced tilt sensor with High-level DC output signal proportional to sine of the angle of tilt. Some of the tiltmeters are deployed in the cluster providing the best platform for accelerometers and tiltmeters to record data precisely. Technical specifications of tiltmeters are given in Table 5.6. Tiltmeter picture from the bridge is given in Figure 5.9.

Table 5.6 : Technical specifications of tiltmeter.

Measuring Range (°)	+/- 14.5
Full Range Output (V)	+/- 5
Output Noise (μV/Hz$^{1/2}$)	20
Resolution (Arc second)	1
Non Linearity (%Full Range Output) MAX	0.02
Non Repeatability (%Full Range Output) MAX	0.004
-3dB cutoff Frequency (Hz)	5
Thermal Zero Shift (%FRO/°C) MAX	0.003
Operating Temperature Range (°C)	-20 to +80
Survival Temperature Range (°C)	-40 to +90
Shock Survival	1000g, 0.5msec, ½ sin
Sealing	IP64
Excitation Voltage (V)	+9 to +36
Power Consumption (W) MAX	1.5
Output Impedance (Ohms)	<10

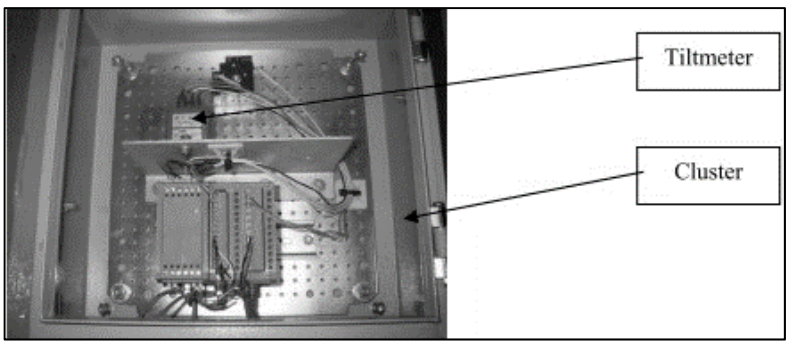

Figure 5.9 : Tiltmeter in cluster.

- Strain Gages (SG)**:** A total of 70 strain gages are installed on various members of the bridge. Four of them are selected as instrumented hanger pin. These sensors are necessary for hanger load variation, deck fatigue and traffic effect, and wind and hanger monitoring. These pins are replaced on stool plate of hanger element. Stress value on hanger pins can be measured directly, and thus stress value of hanger is easily determined. Figure 5.10 shows location of some strain gages on the bridge.

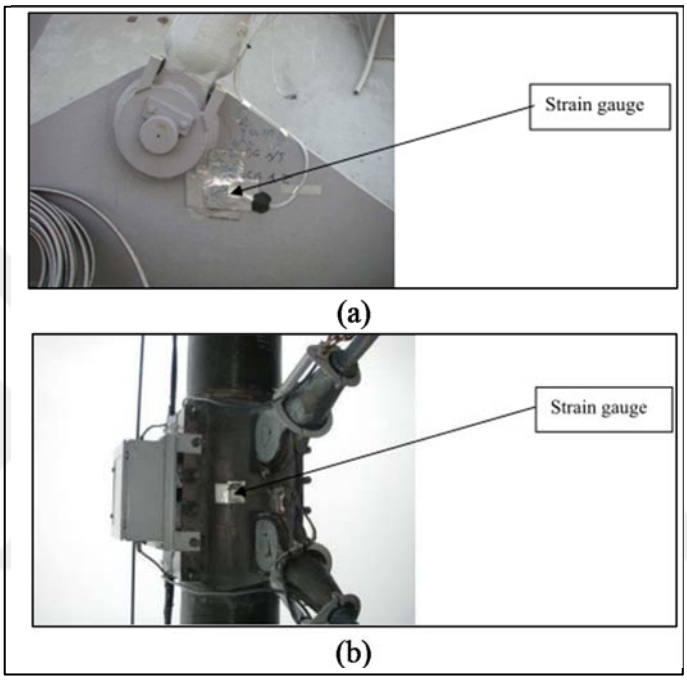

Figure 5.10 : (a) Strain gages on stool plate (b) Strain gages on cable clamp.

- Weather station (WS): The bridge is instrumented by both 2D and 3D weather stations. Table 5.7 gives general specifications of these sensors, respectively. General view from the weather station is presented in Figure 5.11.

Table 5.7 : Technical specifications of the weather station.

Range	0 to 60 m/s (130 mph), gust survival 100 m/s (220 mph)
Sensor	18 cm diameter 4-blade helicoid propeller molded of polypropylene
Pitch	29.4 cm air passage per revolution
Distance Constant	2.7 m (8.9 ft.) for 63% recovery
Threshold Sensitivity	1.1 m/s (2.4 mph)
Transducer	Centrally mounted stationary coil, 2K 0hm nominal DC resistance
Transducer Output	AC sine wave signal induced by rotating magnet on propeller shaft. 125 mV p-p at 100 rpm. 12.5 V p-p at 10,000 rpm.
Output Frequency	3 cycles per propeller revolution (0.098 m/s per Hz)

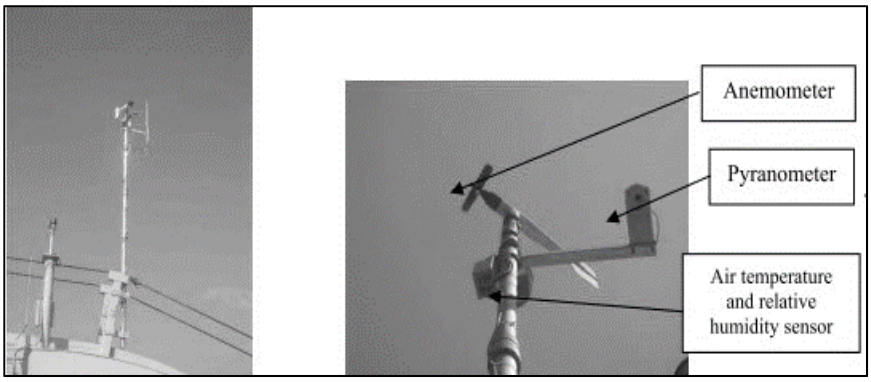

Figure 5.11 : Weather station on its mast.

- Laser displacements (LSR): Technical specifications of laser displacements are summarized in Table 5.8, and general view of laser displacements are presented in Figure 5.12. Laser displacements are utilized for monitoring deck expansion and movement of expansion joints.

Table 5.8 : Technical specifications of laser displacements.

Measuring range (mm)	200 – 2000
Output Range (mA)	4-20
Resolution (mm)	1 to 3
Maximum Measuring Frequency (Hz)	10 Hz
Power Supply (VDC)	18 – 30
Operating Temperature (°C)	-20 to +70

Figure 5.12 : Laser displacements on the bridge.

- Thermocouples (TC): The thermocouples are J type thermocouple. They measure thermal variation in hangers, leading to stress change in hanger. The sensitive part of the sensor is fixed on copper plate or stainless steel collar (for hangers). Figure 5.13 shows thermocouple at top of the tower.
- GPS (GPS): The primary aim of these sensors is to monitor displacement variation of the towers and deck. The GPS monitoring system is constituted by GMX 901 & GMX902. While GMX 901 are sampling at 1Hz and are mono frequency (only GPS mode), GMX902 are at 10 Hz with dual frequency GPS/GNSS. Current location of these sensors are shown in Figure 5.14

Figure 5.13 : Thermocouple at the top of tower.

Figure 5.14 : GPS on its mast.

The data acquisition components consist of site supervisor software, backup computers, and the data acquisition hardware. The site supervisor is located in the KGM monitoring building and includes server tower, optical junction box, power supply, power-switch, ADSL router, UPS etc. The supervisor software has the following functions:

- Collect the live data from the backup computer on the bridge.
- Analyze data to check if thresholds are exceeded.
- Analyze data to track a possible seismic activity.
- Store continuous statistical data.
- Store dynamic files in case of exceedance of a threshold.
- Generate automatic seismic reports.
- Perform rain-flow counting on selected channels.
- Allow creation of virtual channels defined as being a combination of real physical channels on data acquisition unit.

- ❖ Provide data analysis functionalities on recorded data.

The backup computer is located in the Asian-side tower. It has the following functions:

- ➢ Collect measured data of all of the acquisition system of the installation.
- ➢ Apply anti-aliasing filtering.
- ➢ Re-sample signals to their burst record frequency.
- ➢ Store of the processed data.
- ➢ Provide storage capacities in case of failure of communication with supervisor.
- ➢ Allow for autonomy of acquisition in case of a power failure.
- ➢ Prove information on status of the acquisition components.
- ➢ Provide possibility to manually reboot the acquisition units.

The data from each sensor is acquired and stored on the backup PC. The supervisor PC then retrieves, processes, and displays this data. The monitoring system interface on the supervisor PC is also shown in Figure 5.15. It shows measurements and alerts, modifies threshold and storage parameters, detects earthquakes and creates automatic reports (KGM 2008a, 2008b).

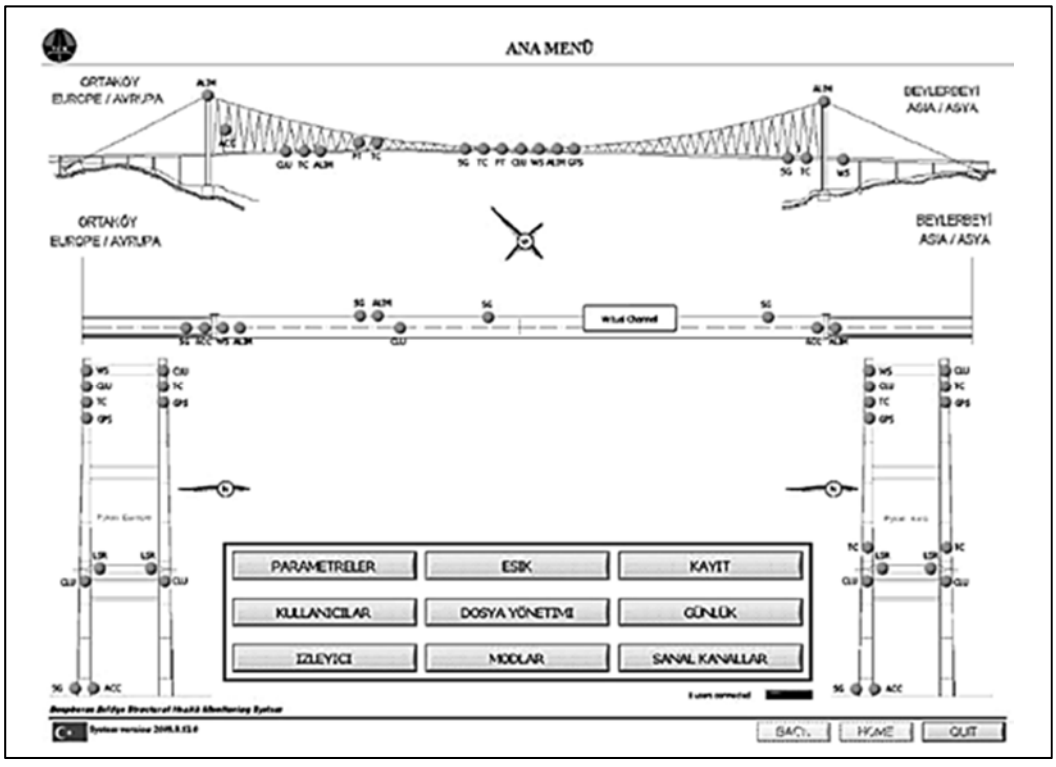

Figure 5.15 : The main screen of the SHM software interface at the First Bosphorus Bridge.

The monitoring system also has threshold levels for each sensor. Once a channel exceeds the threshold level, the desired number of measurements needs to be registered above that threshold before an alert is declared. In Figure 5.16, a sample presentation of threshold tracking is given. When an alert is declared, an alert file is created, and the defined pre-trigger duration of data is added to the file (the blue line in Figure 5.16). In this example, the pre-trigger duration is 2.0 seconds. When the signal goes below the threshold, the channel will continue to record data for the duration or until the channel overpasses the threshold once again, as shown in Figure 5.16 by the green line, thus requiring five more values above threshold to reset the record duration progression. If an alert file is being recorded when another alert is registered, data is added to the existing alert file.

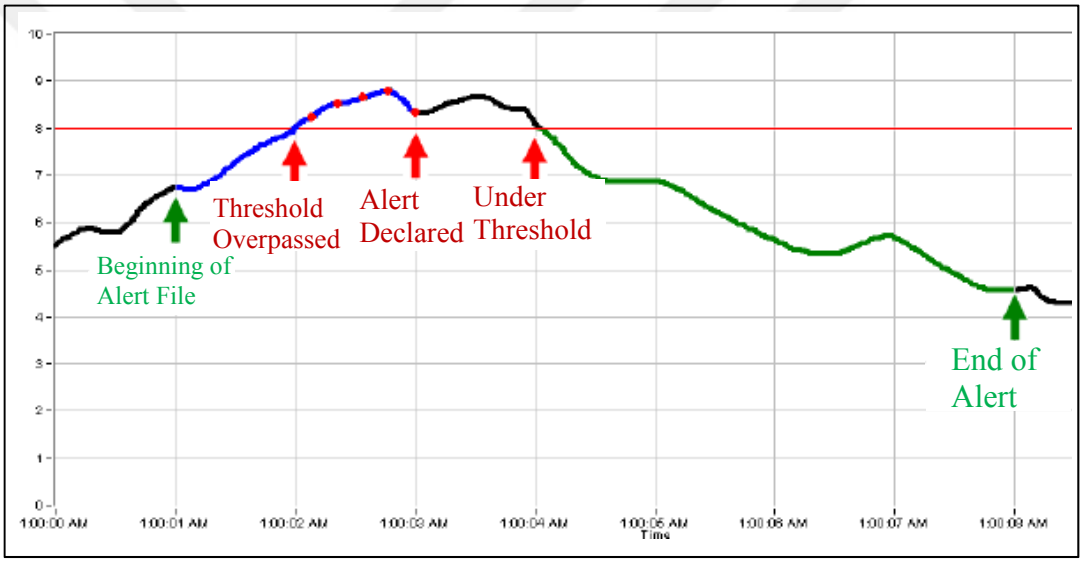

Figure 5.16 : The illustration for the data recorded following an alert on a channel.

5.3 Operational and Extreme Events for the SHM System

As stated in the previous sections related to SHM system specifications, a SHM system has to be designed in compliance with a specific mesearument capacity. Before the design of a SHM system, therefore, critical loading events should be predicted and environmental conditions of the located regions of long-span bridges should be identified. For the Bosphorus Bridge, the following critical loading events were considered depending on its operational properties, and environmental conditions and seismicity of its located region (the Bosphorus Straits);

- Earthquake (site-specific simulated motions)

- Wind (strong wind on April 18 2012)
- Traffic (live-load)
- Human-induced (marathon)

The bridge has experienced several extreme loading events such as earthquake, wind, marathon etc. However, the monitoring system tracked some of these events. For example, the bridges experienced the destructive 1999 Kocaeli EQ, but no SHM data for this event is available due to the absence of the permanent SHM system on the bridges. Therefore, the bridges have limited experiences on the extreme events. The most important one is the marathon loading. Istanbul Marathon Organization is held every year in Istanbul. The SHM data obtained during the event were processed by the bridge authority (KGM). The results of the report for the marathon loading showed that the bridge was excited in the vertical direction. Due to the dynamic loading of the runners, the expansion joints reached the movement capacity of 1.07 m. This displacement resulted in increased movement of the tower top-saddle in longitudinal direction. Based on these experiences during the marathon, the bridge authority decided to further improve the tracking and alerting system. This system depends on the threshold values that warn the bridge authority while enabling admissible traffic on the bridge. The lessons from the extreme events are to develop operational performance criteria for this type of extreme events. Besides, this event led to the utilization of certain damping devices (viscous damper etc.) in order to reduce the vibration effects. The second important extreme event for the Bosphorus Bridge is the strong wind. The SHM data from this event is presented for the first time in this dissertation. Although no experimental data were obtained from the bridge under during strong earthquakes, earthquake response analysis of the bridge is also aimed to be numerically performed in the present study. For this purpose, multi-point earthquake records were simulated considering the geographic coordinates and site-specific properties of each support of the bridge, and the multi-point earthquake analysis was carried out using the simulated earthquake records.

5.4 Monitoring points, Critical Components and Operational Performance Criteria for the Bridge

In order to conduct a preliminary study on proposing the main considerations of SHM data-based operational performance criteria for the Bosphorus Bridge, critical monitoring points and structural elements of the bridge and corresponding sensor requirements should be determined. For this purpose, monitoring objectives and requirements of the SHM system are first identified well with a collaboration with experiences of the bridge authority (KGM) and theoretical investigations as well as recommendations of practitioners in the field of bridge engineering.

- Monitoring objectives of the SHM system
  - To report rapidly the bridge operation conditions just after a strong earthquake and wind loads.
  - To determine the various structural parameters indicating structural condition of the bridge (fatigue, geometrical change and stress variation).
  - To confirm geometry and performance of the bridge during possible extreme events in the service life of the bridge.

In order to perform the monitoring objectives of the SHM system of the Bosphorus Bridge, the monitoring parameters and their requirements are also to be identified well considering the bridge own structural characteristics given in previous section. These are followed below.

- Hanger load variation: the variation in hanger load is very important to control the safety working limits of them and to check fatigue problems over long-term periods. For these aims, force transducer and strain gage are deployed at the quarter and middle points of the bridge. The hangers at the quarter points are the most affected by thermal variation, but the hangers at the mid-span are vulnerable to traffic and seismic loads. Totally, six hangers are equipped with these sensors.
- Deck expansion: the movement of the decks at the expansion joints is necessary to monitor the travel of the expansion joints and to assess potential damage to bridge before, during and after wind and seismic events. Four laser displacement transducers are located at each tower to measure the

movement of the deck ends. Two of them at each tower are installed on the rocker bearing of the main span and the approach viaduct, respectively.

- Bridge response: Response monitoring includes various instruments best suited to monitoring seismic effects. Most of these sensors (accelerometers and titltmeters) are deployed on the tower and deck since bridge response is based on the response of deck and tower. The primary aims of bridge response are,
  - ✓ To enable KGM to have a rapid means of measuring the response of the bridge to an extreme event.
  - ✓ To confirm within minutes of the event that the bridge has remained in its operational envelope.
- Deck fatigue and traffic effect monitoring: the bridge deck is likely to remain considerable fatigue effect. This problem is verified by visual inspection on the bridge. Stress variation in the trough-to-decks welds become very important to indicate whether a critical problem remains, and how to deal with the problem. For this aim, strain gauges are deployed on the upper steel plate of the deck. Thus, stress variation resulting from the effect of different loading condition such as traffic load, crack and thermal changes is recorded.
- Wind and Hanger Monitoring: it is aimed to monitor the hanger vibration and to determine its effects. This problem faced in the hanger elements close to the tower. In order to monitor vibration of the hangers, strain gauges and accelerometers are deployed on the longest hangers close to Ortakoy tower. Besides, weather stations including wind speed, wind directions, air temperature, humidity and solar radiation sensors are installed on the bridge to evaluate the recorded data reliably.

The third step to develop operational performance criteria for the Bosphorus Bridge is to specify corresponding sensor types and quantities to the determined monitoring parameters. For this aim, Table 5.9 is prepared.

In general, one of the primary aims of a SHM system is to monitor bridges throughout their life cycle to control the performance of them. Therefore, conceptualizing the health of a bridge starts with determining its performance requirements. For the first

time, the LRFD Bridge Design Specifications AASHTO-LRFD (2004) proposed the limit-states concepts including performance criteria for various design limit states. On the other hand, the health monitoring system with a plenty of data offers a more comprehensive and quantitative description of performance and a large spectrum of limit states.

Table 5.9 : Monitoring parameters and corresponding sensors.

Monitoring Parameters	Type and Quantity of Sensor							
	Acc	Strain gage	Weather station	GPS	Force transducer	Pin	Laser	Total
Hanger load variation		14			12	4		30
Deck expansion							8	8
Bridge response	26							26
Deck fatigue and traffic effect monitoring		16						16
Wind and hanger monitoring	6	11	26					43

Based on various data recorded by SHM system, performance considerations can be renewed. In order to deal with these comprehensive requirements, performance assessment concept should be divided to certain section. Detailed study related to this issue was conducted by Aktan et al. (2002) considering some modifications of the provisions of Eurocode (1994). They presented a table for better understanding the performance evaluation based on SHM system. As shown in Table 5.10, (i) Utility and Functionality, (ii) Serviceability and Durability, (iii) Safety and stability of Failure, and (iv) Safety at Conditional Limit States are considered by the corresponding limit events that should be considered in design and evaluation. Return period of associated loading events including heavy traffic, critical wind load and strong earthquake loads is of very important issue required to be identified. In Table 5.10, return period and performance goal are indicated for each event.

After definition of limit-states, limit-events, return periods and performance goal, another crucial issue is to determine the quantitative limits for each limit-events in order to find corresponding performance limit state and performance goal of the bridge. This consideration is required to know whether desired performance limits exceed that of each events. To overcome this issue, a formulation for the quantitative

limits for each limit-event can be developed or can be expected utilizing SHM system providing numerous data.

Table 5.10 : Performance limit-states and performance (Aktan et al, 2002).

	Utility and Functionality	Serviceability and Durability	Safety and Stability of Failure	Safety at Conditional Limit States
Limit events	▪ Environmental, social impact ▪ Initial cost ▪ Life-cycle cost ▪ Operational capacity and safety ▪ Feasibility of: ▫ Construction ▫ Inspection ▫ Maintenance ▪ Aesthetics	▪ Vibrations ▪ Deformations ▪ Deterioration ▪ Damage ▪ Durability	▪ Excessive movements ▪ Settlements ▪ Material failure ▪ Stability failure ▪ Incomplete (premature) collapse mechanism(s) ▪ Undesirable failure mode(s), eg, progressive collapse	▪ Natural hazards associated with very long return periods (eg, New Madrit EQ) ▪ Catastrophic accidents, fire ▪ Cascading of accidents ▪ Terrorism ▪ War
Return	Events with 0–25 year Return Period (RP)	Conditional events with 25–100 yr RP	250–500 year RP such as Major CA quakes)	Events with 2500–5000 yr RP
Goal	▪ No service disruption	▪ Momentary service disruption	▪ Minimization of casualties ▪ Quick recovery	▪ Protection of escape routes ▪ Minimization of casualties

Considering the preparatory efforts to develop SHM-based operational performance evaluation concept for the Bosphorus Bridge, the followings are selected as key components in accordance with KGM's recommendation and experiences.

- ❖ Towers
- ❖ Deck
- ❖ Expansion joints

As conducted in Akashi Kaikyo Bridge, the SHM system of the Bosphorus Bridge has three monitoring systems (i) Design verification monitoring (ii) Operational monitoring and (iii) Condition monitoring. Utilizing these monitoring systems and the recommendations proposed by Aktan et al. (2003) as in Table 5.10, the limit-states and limit-events for the key elements of the deck, tower and expansion joints are defined as given below in detail.

- Expansion joints: Movement in the bridge axis or longitudinal direction is considered. Corresponding limit-events for the expansion joints are selected as "Operational Capacity and Safety" and "Excessive Movements". These limit-events require the limit-states of "Utility and Functionality" and "Safety and Stability of Failure".
- Deck: Fatigue and traffic effect, and bridge response are considered. Corresponding limit-events are selected as "Damage" and "Material Failure" for fatigue and traffic effect, and as "Vibration" and "Operational Capacity and Safety" for bridge response. These limit-events require "Serviceability and Durability" and "Safety and Stability of Failure" limit-states for fatigue and traffic effect, and "Serviceability and Durability" and "Utility and Functionality" limit-states for bridge response.
- Towers: Bridge response is considered. Corresponding limit-events are selected as "Vibration" and "Excessive movements". These limit-events require the limit-states of "Serviceability and Durability" and "Safety and Stability of Failure".

In addition to the limit-states and limit-events, performance goals are determined using Table 5.10. However, associated return period has not yet been determined since it depends on recorded data. All assignments except for return period are given in Table 5.11. As shown in Table 5.11, five different limit-events including "Operational Capacity and Safety", "Excessive Movements", "Damage", "Material Failure" and "Vibration" are considered for determining the quantitative limits of them. These limit events can be extended for possibility of future evaluation of condition of the bridge through use of SHM. The simplest way to determine quantitative limits is to use particular threshold value (Karbhari and Ansari, 2009). In this procedure, a SHM system is programmed to issue alert in case that the value of the measurement data exceeds the predefined threshold value. This approach was proposed for the bridges in Hong Kong. Threshold values are considered as a certain percentage of design value of the components of the bridges. For this aim, the ratio of measurement value to design value is determined as 75 %, which is the reference ratio proposed by the United States' Federation Highway Administration's Bridge Ratings for Operation. In consideration of these items, certain operation levels are also defined for the bridges.

Table 5.11 : Operational performance specifications of the Bosphorus Bridge.

Key Element	Physical Parameter	Limit-events	Limit-states	Performance Goal
Expansion joints	Movements in bridge direction	Operational capacity and safety	Utility and functionality	>No Service disruption
		Excessive movements	Safety and stability of failure	>Minimization of casualties >Quick recovery
Deck	Fatigue and traffic effect	Damage	Serviceability and durability	>Momentary service Disruption
		Material failure	Safety and stability of failure	>Minimization of casualties >Quick recovery
	Bridge response	Vibration	Serviceability and durability	>Momentary service disruption
		Operational capacity and safety	Utility and functionality	>No service disruption
Tower	Bridge response	Vibration	Serviceability and durability	>Momentary service disruption
		Excessive movements	Safety and stability of failure	>Minimization of casualties >Quick recovery

Table 5.12 : Design values of key elements of the Bosphorus Bridge (JBSI, 2004).

Key Elements	Design Value
Tensile Strength of Main Cable [kN]	133674
Tensile Strength of Side Span Cable [kN]	142268
Axial Force of Main Cable at Tower Top Saddle [kN]	111100
Shear Force of Main Cable at Tower Top Saddle [kN]	4513
Movement Capacity of Expansion Joints in Bridge Axis [m]	1.07
Displacement Capacity of Deck in Vertical Direction [m]	1.15
Displacement Capacity of Deck in Transverse Direction [m]	1.5

In the light of these considerations, this concept is readily employed for the Bosphorus Bridge since its SHM system has ability to record threshold value. The most important point is to determine threshold value. Design values for the key elements of the Bosphorus Bridge are given in Table 5.12. These values are obtained from seismic retrofit project of the bridge in JBSI (2004). However, data analysis is indispensable to predict threshold value. In literature, various data analysis methods were introduced to determine this value. Generally, these methods are based on peak value estimation, since the maximum effects govern the structural capacity. Susoy et al. (2008) proposed two methods focusing on the extreme value: maxima block and threshold. Detailed information for these approaches is not given. Only their primary features are stated.

Block Maxima approach is based on Extreme Value Theory. Worden et al. (2002) and Messervey and Frangopol (2007) utilized this theory for bridge structures. In this approach, data sets are divided into some blocks, such as one-minute duration, and peak value in each block is obtained. Susoy et al. (2008) implemented this procedure to bridge structure. They concluded that the block duration should be considered relatively longer for long-span bridges. In the Threshold Approach, the maximum values are investigated. These values are determined by comparing them with certain threshold value, such as design or yield value. For two approaches, probability distribution function is defined to determine the probability distribution of daily maximum or peak value. Using this distribution, annual probability of exceedance is calculated (Karbhari and Ansari, 2009). With the help of these approaches, daily, monthly, yearly peak values can be determined by a probability distribution, which provides to handle valuable data. Considering peak value as threshold value, quantitative limits for key points can be obtained. These studies reveal that numerous data recorded from various loading events are an essential point to develop quantitative limit states for the given performance levels of the Bosphorus Bridge. For this objective, specifying more suitable data processing approach given above in agreement with the bridge and SHM system specificationsis is also another critical issue. The Bosphorus Bridge experienced a number of extreme and operational load cases; however, no more data for these events were recorded due to new installation of its SHM system. For example, no data were recorded during the most destructive earthquake of Kocaeli (1999) in Turkey. Therefore, the proposed operational performance criteria concept for the Bosphorus Bridge in this dissertation will be completed and improved with the implementation on the bridge.

6. STRUCTURAL IDENTIFICATION (ST-ID) OF THE BOSPHORUS SUSPENSION BRIDGE

The St-Id approach is a general integrated method, which offers an opportunity to unveil the properties of interest of civil infrastructures under extreme and operational loads. In order to make structural identification and FE model updating/verification of bridge, the St-Id concept requires experimental study that is one of the most essential step of the St-Id. Due to fact that SHM system provides consistent experimental data for long-span bridge under operational and unexpected loading event, structural identification is generally recommended to be made by SHM data. The SHM system of the Bosphorus Bridge, as mentioned in the previous sections, has measurement capacity for the following loading events;

- Seismic load
- Extreme wind load
- Traffic load
- Thermal load

Based on the operational documents of the KGM Bridge Department, the Bosphorus Bridge has experienced the extreme wind and traffic load loads from the loading events above. Thus, an extreme event of strong wind on April 18 2012 is considered for the St-Id in this dissertation.

6.1 Extreme Wind Event

Strong winds are not very frequent in Istanbul due to its location. However, during the daytime on April 18 2012, a strong storm occurred in Istanbul. It was the first time that the bridge experienced such a high wind. According to the measurement of Turkish Meteorology Service as shown Figure 6.1, the maximum wind-speed reached to 122 km/h. Although ultimate design wind speed of the bridge is 162 km/h, the bridge was closed to the traffic in a period of time for precautionary measures. The change of wind speed with time is also shown in Figure 6.1. This variation is obtained by weather

station sensors installed on the bridge. As seen from the figure, the average wind speed before the storm was around 20 km/h. However, it suddenly increased to 100 km/h in 10 minutes. The authority responsible for the bridge, General Directorate of Turkish State Highways (KGM), reported that this wind load excited the bridge in lateral direction. This site observation is also verified by SHM data recorded at the deck mid-span. For this objective, weather station data (wind speed-wind direction) is plotted with the bridge layout as shown in Figure 6.2. Polar plot of wind speed-wind direction is plotted for corresponding maximum wind variation range. Accordingly, it is proved that the bridge is subjected to wind load in N-S direction.

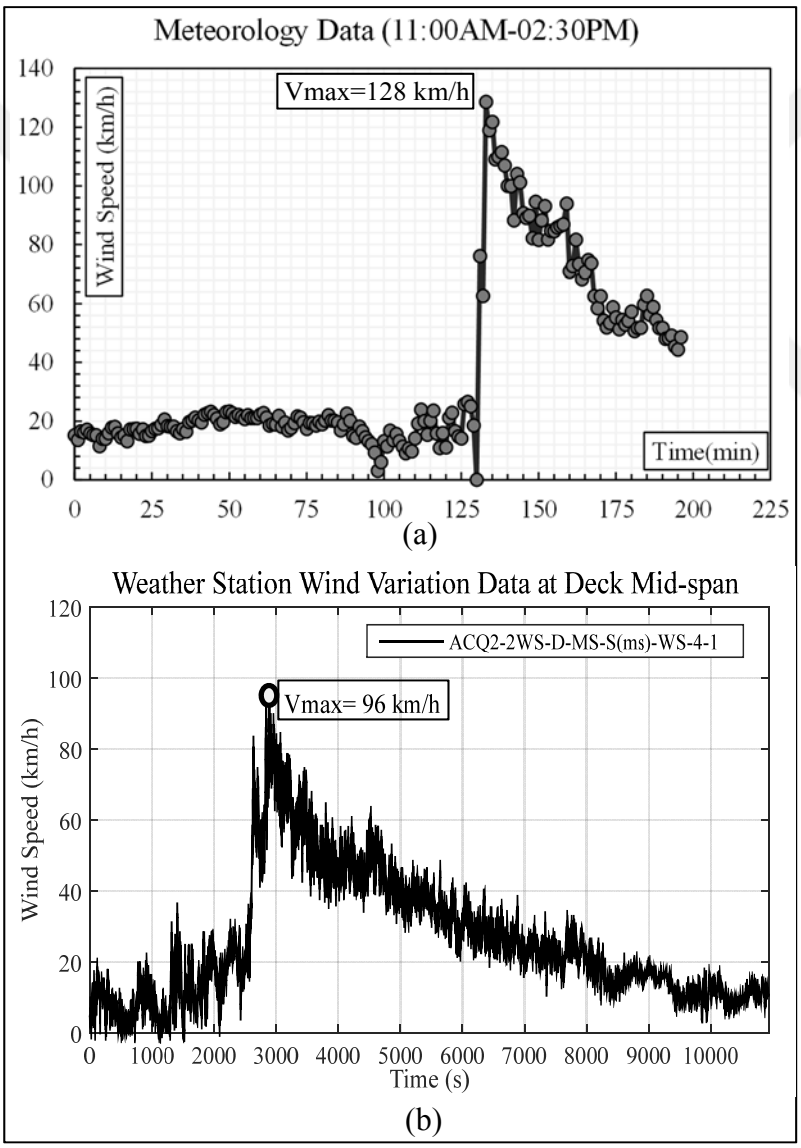

Figure 6.1 : Identifcaiton of strong wind: (a) Meteorology data (b) SHM data.

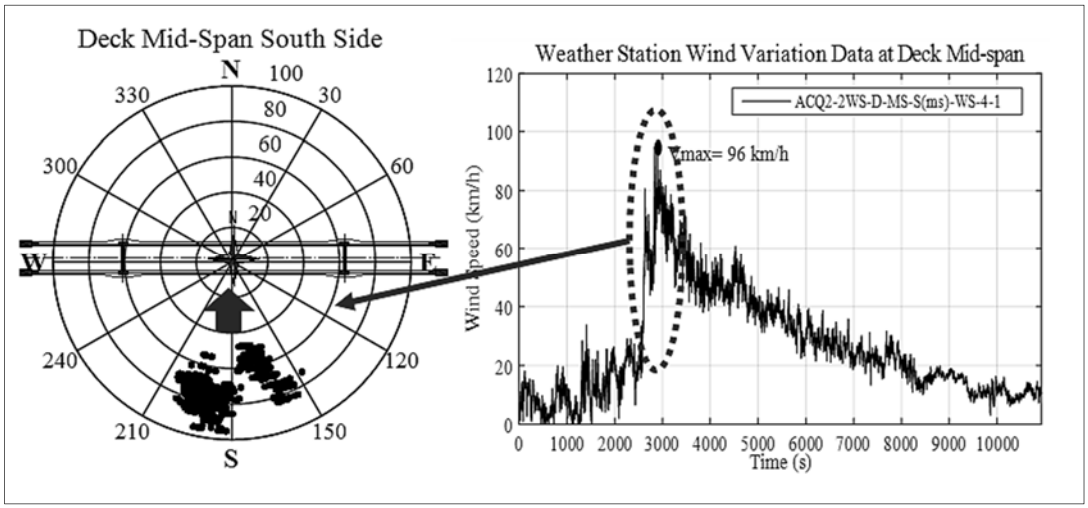

Figure 6.2 : Identification of wind direction from the deck mid-span SHM data.

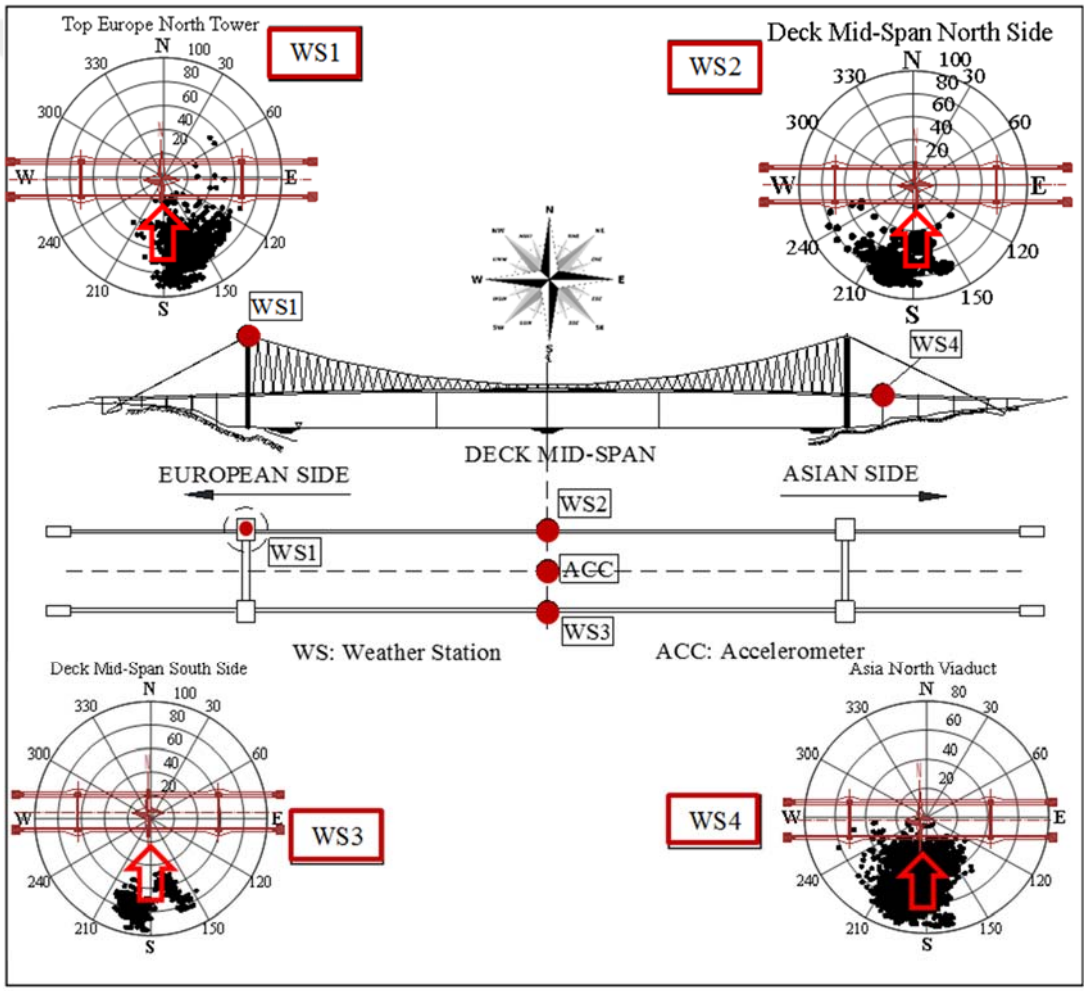

Figure 6.3 : Wind direction-wind velocity variation in polar charts obtained from the weather stations.

In addition, the excitation of the strong wind load is also corrected with the other weather station data recorded from different critical points of the bridge. As seen from Figure 6.3, the lateral wind direction is verified with all of the polar charts, and the

bridge was determined to be greatly induced in N-S direction during the critical wind event.

6.2 Data Pre-processing and Preliminary Outcomes

After accurately verifications of the wind direction with all weather station data, corresponding acceleration data measured at deck mid-span in lateral direction is used to preliminarily obtain modal characteristics under this event. Therefore, the fundamental process of standard Fast Fourier Spectrum (FFT) is adopted to obtain smooth frequency response from the acceleration data.

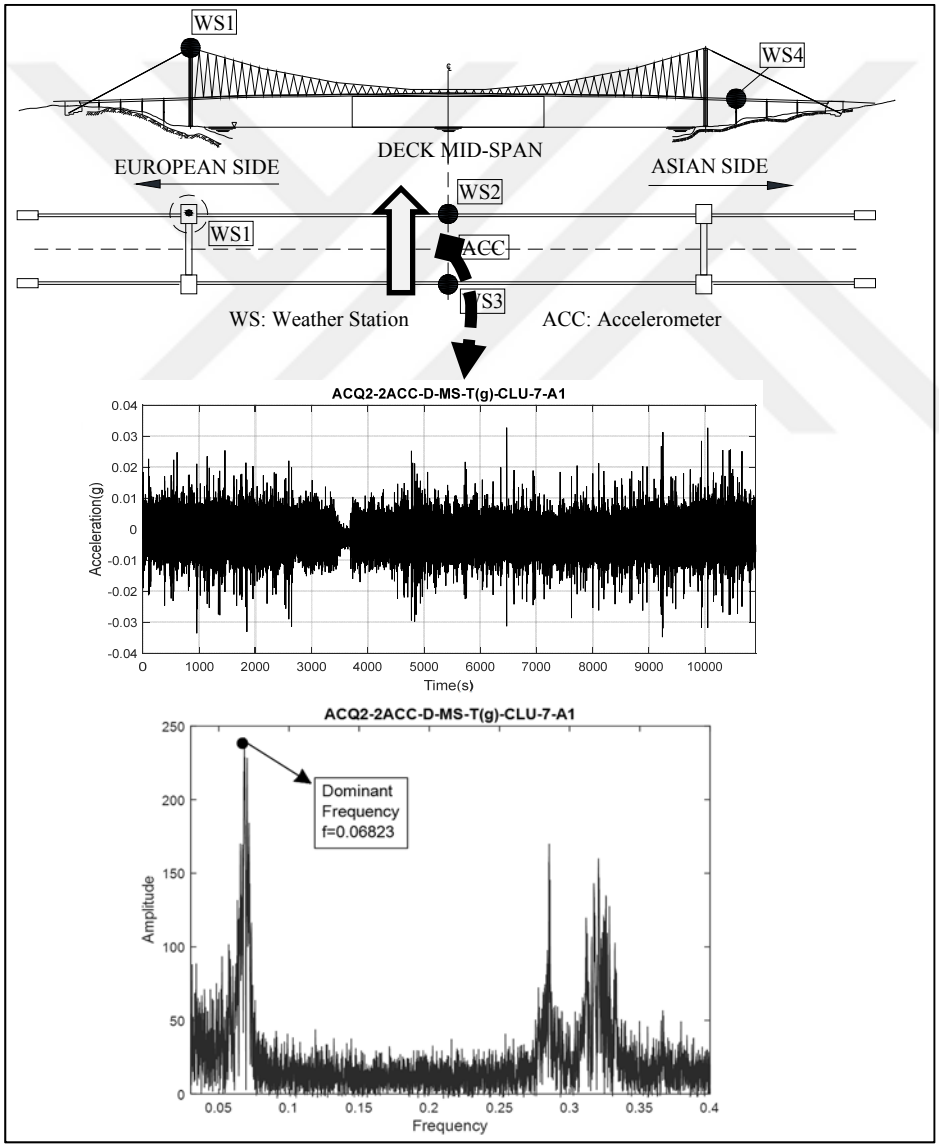

Figure 6.4 : FFT analysis of the raw acceleration data at deck mid-span.

As indicated in Figure 6.4, acceleration raw data recorded during before and after the event contains a noise band resulting from the traffic effect. This noise content is clearly observed depending on the FFT analysis of the raw data as depicted in Figure 6.4 and the noise effect was decided to be extracted from the data. For this aim, certain fundamental data pre-processing is conducted and the frequency domain content of the same data are investigated again. Firstly, Baseline Correction was performed and this process provided to subtract linear trends from the data. Linear trend shown in Figure 6.5 was eliminated from data. Besides, corrected and raw data are also indicated in Figure 6.5.

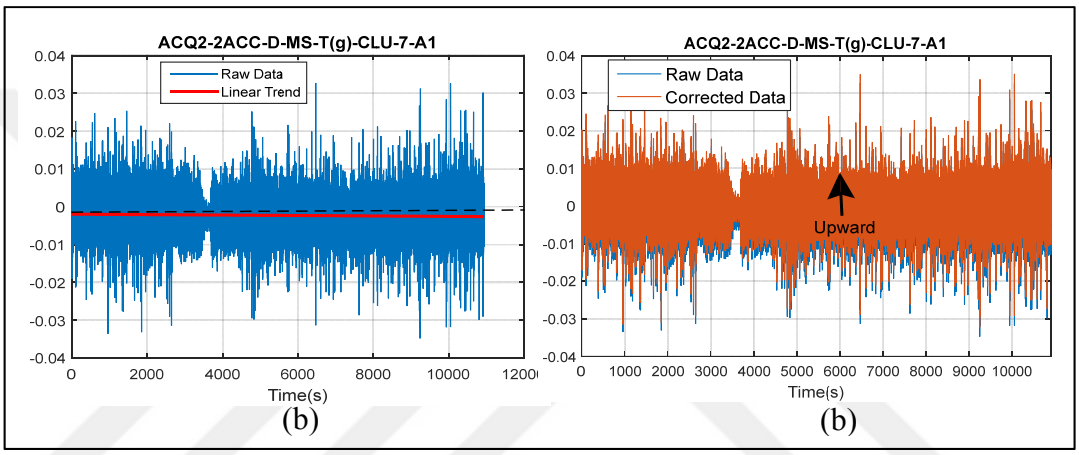

Figure 6.5 : Baseline correction: (a) Linear trend (b) Raw and corrected data.

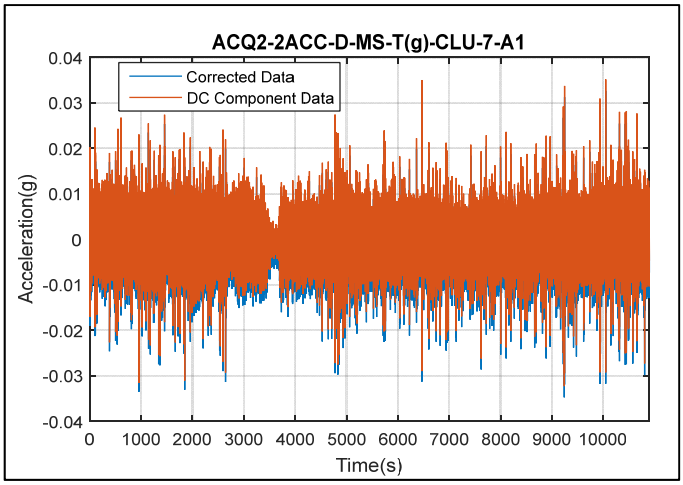

Figure 6.6 : DC Component substraction.

Considered the corrected data through Baseline Correction, DC component subtraction process was conducted. DC component leads to misunderstanding frequency content of data. Especially, the initial value of the frequency content goes to infinity due to this component. To illustrate, FFT of the data with DC component cannot give

reasonable results in frequency domain. DC component is practically eliminated from data extracting mean value of data. In the light of this consideration, DC component was removed from the corrected data, and the difference is indicated in Figure 6.6. After the two steps, the last one is filtering of the data. All measured data generally includes noise due to environmental and traffic effects. The noise-polluted data can be analyzed using electronic filtering techniques: low-pass, bandpass and highpass filtering. Band pass filtering considerations can be estimated by the modal frequency properties of structure. From the numerical analysis of the bridge, the modal frequency of the bridge varies from 0.05 Hz to 5.0 Hz; therefore, the corner frequencies are determined as these frequencies (Apaydın et al, 2012). Using these corner frequencies, fourth-order Butterworth electronic filter was created using MATLAB Signal Processing Toolbox. The bandpass filtered data is shown comparing with the DC component data in Figure 6.7.

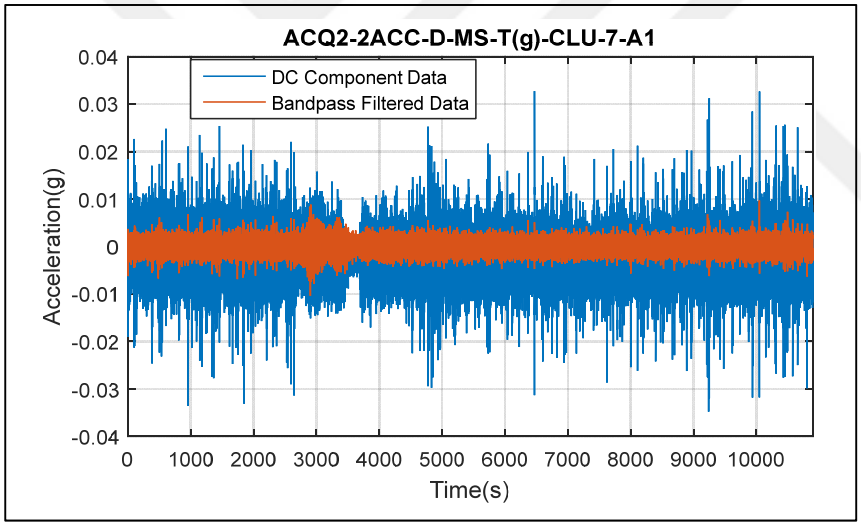

Figure 6.7 : Bandpass filtered data.

Following completion of the data preprocessing, modal properties of the bridge under the extreme wind event are preliminarily estimated using standard FFT analysis. To determine the effect of the extreme wind event on the bridge, the refined acceleration data is divided into three ranges: “Before”, “During” and “After”. Figure 6.8 presents these ranges. Moreover, three different time intervals for each range are considered as given in Figure 6.8 for the FFT analysis. Since the bridge is only loaded by service loads before and after the event, the modal properties are estimated to be close to natural vibration. Thus, these two ranges are taken into account as ambient vibration. However, the modal characteristics are estimated to be different during the extreme

wind event. Comparing the frequency content of "During" with "Before" and "After", the effect of the wind event is tried to be predicted.

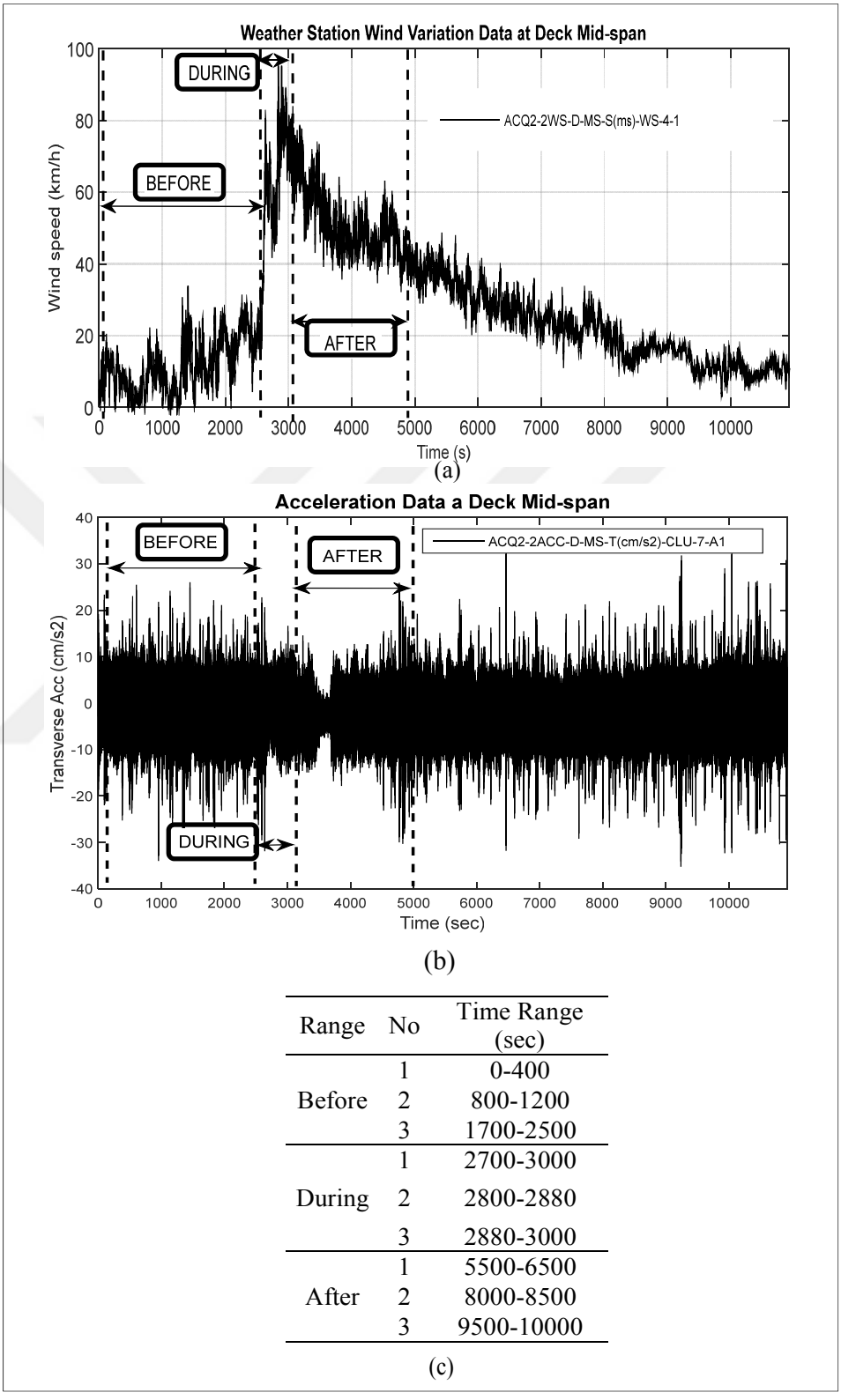

Range	No	Time Range (sec)
Before	1	0-400
	2	800-1200
	3	1700-2500
During	1	2700-3000
	2	2800-2880
	3	2880-3000
After	1	5500-6500
	2	8000-8500
	3	9500-10000

(c)

Figure 6.8 : (a) The range on wind variation data, (b) The range on acceleration data at deck mid-span (c) The time-intervals for each range.

Considering the corresponding data range, the FFT analysis is performed, and the results are shown in Figure 6.9, Figure 6.10 and Figure 6.11, respectively for "Before", "During" and "After" ranges. From Figure 6.9, modal frequencies are estimated as 0.068-0.073 for "Before" range. Similar results, as shown in Figure 6.11, are determined for "After" range with the frequency of 0.070-0.074. However, many peaks in the FFT analysis of these ranges are observed. Therefore, the estimated value of frequencies for these ranges are not clear. In contrast, the peaks in "During" range are clearly obtained as shown in Figure 6.10. Besides, the corresponding acceleration data with a harmonic form shown in Figure 6.11 can be estimated to result in smooth FFT outcomes.

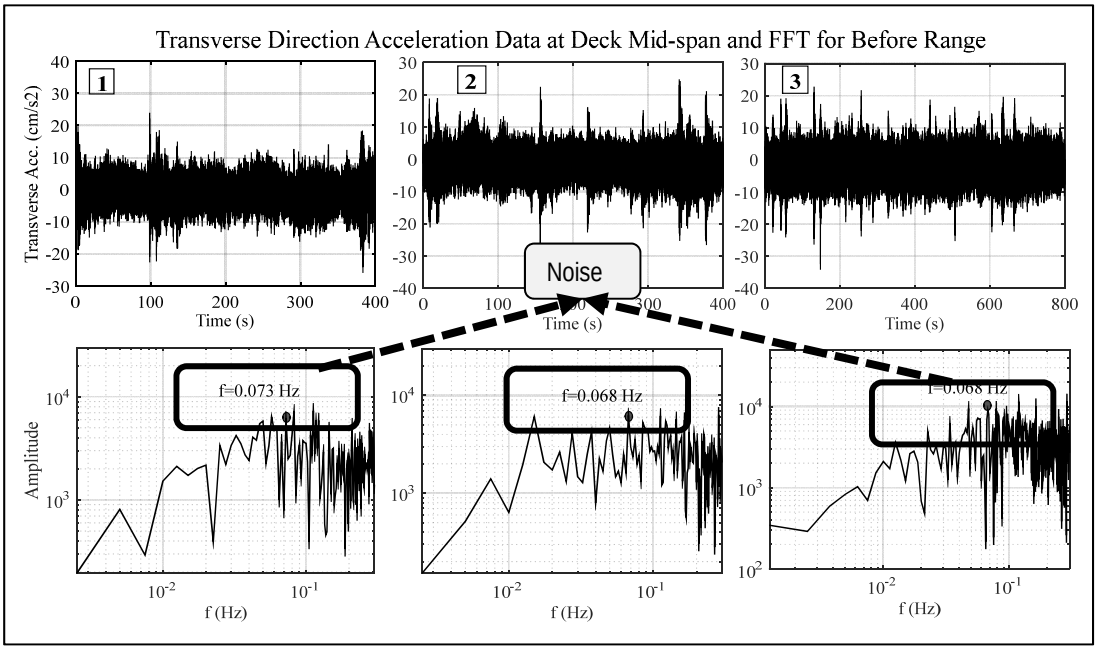

Figure 6.9 : The FFT analysis for "Before" range.

These results showed that although the raw data was refined by data preprocessing, noise component is not removed from the data. To eliminate noise or other effects, further processing need to be performed. Thus, averaging, windowing and overlapping techniques were decided to be implemented considering the bridge's own characteristics.

According to the results, fundamental period of the bridge increases approximately as 1.0 sec in "During" range. The increment of the period causes to increase in amplitude as ten folds. The bridge is estimated to provide operational performance level for "Before" and "After" ranges due to natural vibration response in these ranges.

However, for “During” range, the operational performance level is not predicted due to high amplitude that results also in high displacement of the deck in lateral direction.

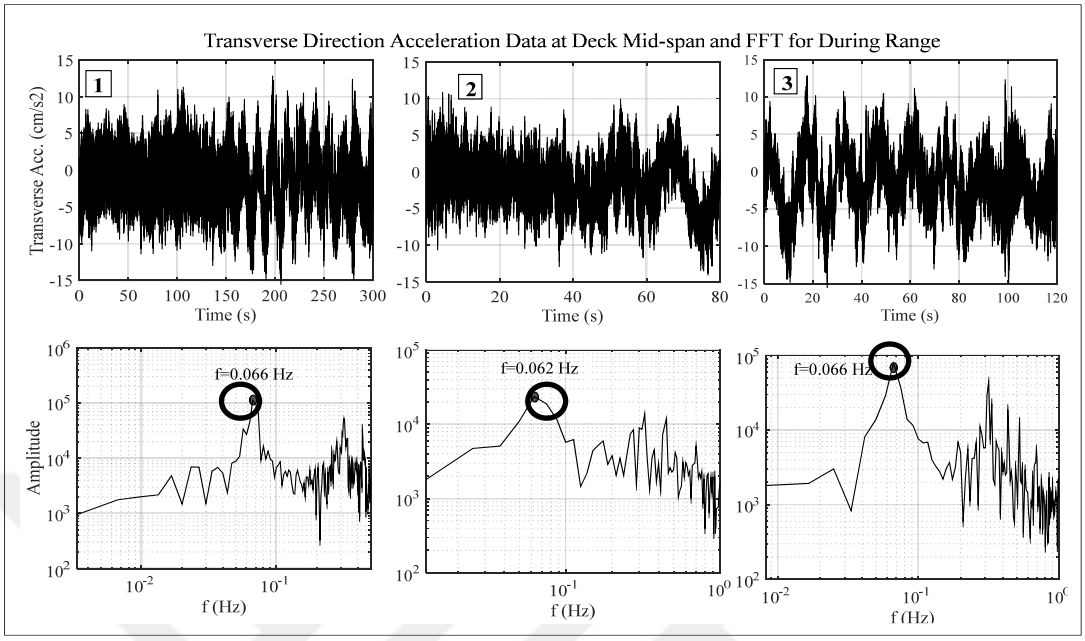

Figure 6.10 : The FFT analysis for “During” range.

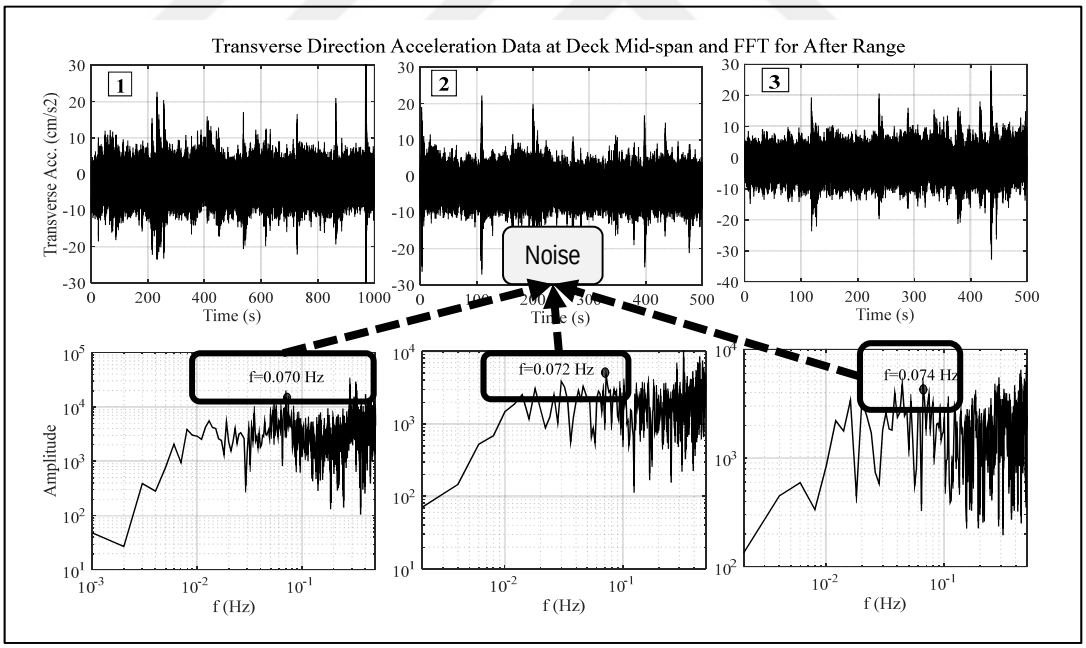

Figure 6.11 : FFT analysis for “After” range.

Mean frequency values, periods and amplitudes are given in Table 6.1 for each range. In order to obtain more smooth FFT results especially for “Before” and “After” ranges, a new MATLAB code is developed, which extracts unwanted content in the data. This code is based on the average approach reducing negative effects of noise on the analysis results. After verification of this code with the previous results obtained from

the processed data, this code is intended to be utilized for the other related data recorded from a sensor on the bridge. Before presenting the details of the code, Windowing, Overlapping and Averaging concept are briefly explained to better understand the steps of the code.

Table 6.1 : FFT analysis results.

Range	No	Time Range (sec)	f (Hz)	T (sec)	Amplitude	f, Mean (Hz)	T, (Mean) (sec)	Amplitude (Mean)
Before	1	0-400	0.0725	13.80	6.20×10^{3}	0.070	14.40	7.17×10^{3}
	2	800-1200	0.068	14.70	6.30×10^{3}			
	3	1700-2500	0.068	14.70	9.03×10^{3}			
During	1	2700-3000	0.066	15.15	1.10×10^{5}	0.064	15.50	70.86×10^{3}
	2	2800-2880	0.062	16.13	2.36×10^{4}			
	3	2880-3000	0.066	15.15	7.90×10^{4}			
After	1	5500-6500	0.070	14.30	1.50×10^{4}	0.072	13.90	7.89×10^{3}
	2	8000-8500	0.072	13.88	4.80×10^{3}			
	3	9500-10000	0.074	13.51	3.88×10^{3}			

Windowing is the processes that makes FFT results clearer and smoother. The Fast Fourier Transform algorithm (FFT) has considered that time record repeats within total record time. If data is continuous and periodic during record time, FFT computes frequency values very well as shown in Figure 6.12. However, SHM data cannot generally provide this continuity and periodic trend since SHM data is either long-term data or consists of integrated many parts consecutively as demonstrated in Figure 6.13. From Figure 6.13, FFT results of the non-periodic and non-continuous are not clear and its FFT curve is not smooth compared to the periodic data. This is also called as leakage problem in literature. This drawback misleads researchers/engineers upon estimating structural characteristics of structures. For these reasons, pre-processed data to be used for structural identification should be windowed with one of the well-known window functions (weighting function) given in the following;

- Hanning window
- Hamming window
- Flattop window

The window functions provides that both ends of data become zero and that each windowed part of data is kept to be continuous and periodic. As an example in Figure 6.13, the raw data collected during the critical wind event of the bridge is weighted with Hanning window function.

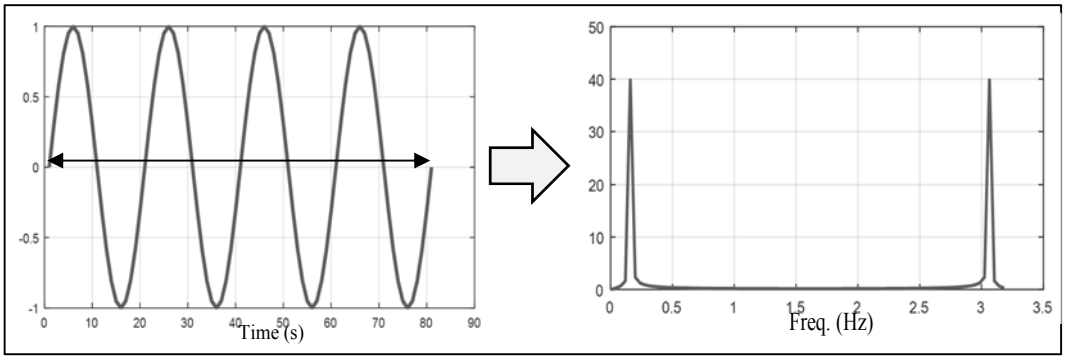

Figure 6.12 : Continuous periodic data and corresponding FFT.

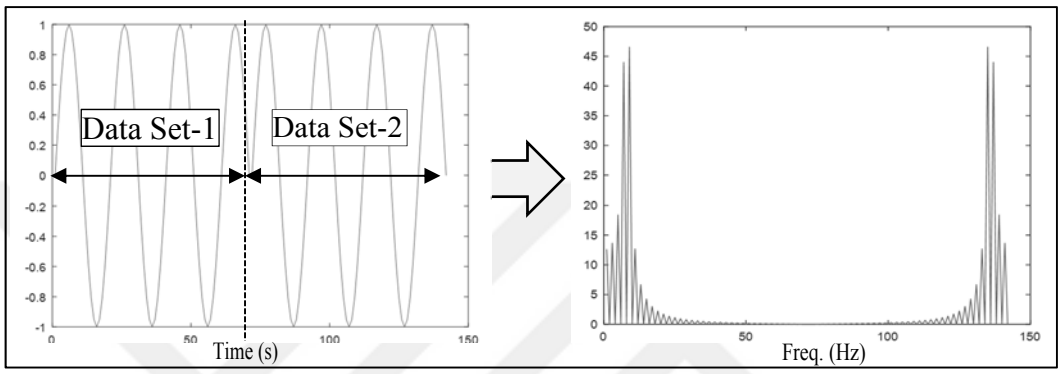

Figure 6.13 : Integrated non-periodic data and its FFT.

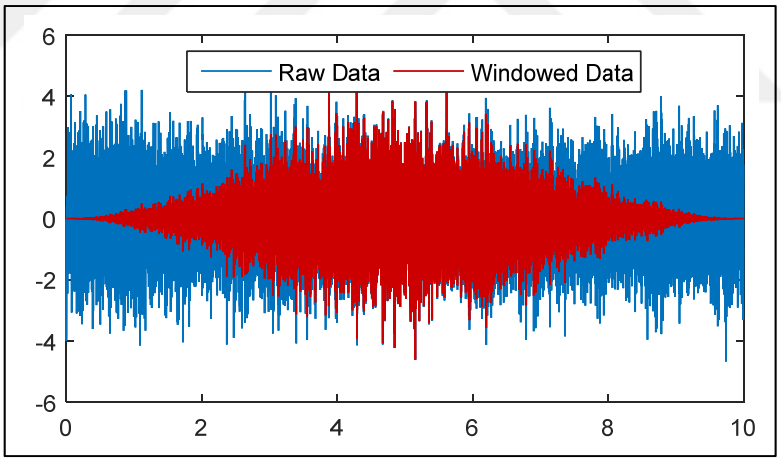

Figure 6.14 : Raw data and windowed data.

Overlapping processes that provides a combination of previous windowed data with the next windowed data considering the designated percentage (25%, 50% and 75%) is also related to averaging processes. In the windowing processes, the windowed data has the ends with zero value. Mitigating this loss of the end values can be achieved by integrating each window with the next window considering the certain overlapping percentage. The concept of this approach is schematically depicted as shown in Figure 6.15. After from brief explanations for these pre-processes, all windowed parts of the data are averaged considering the overlapping percentage of interest.

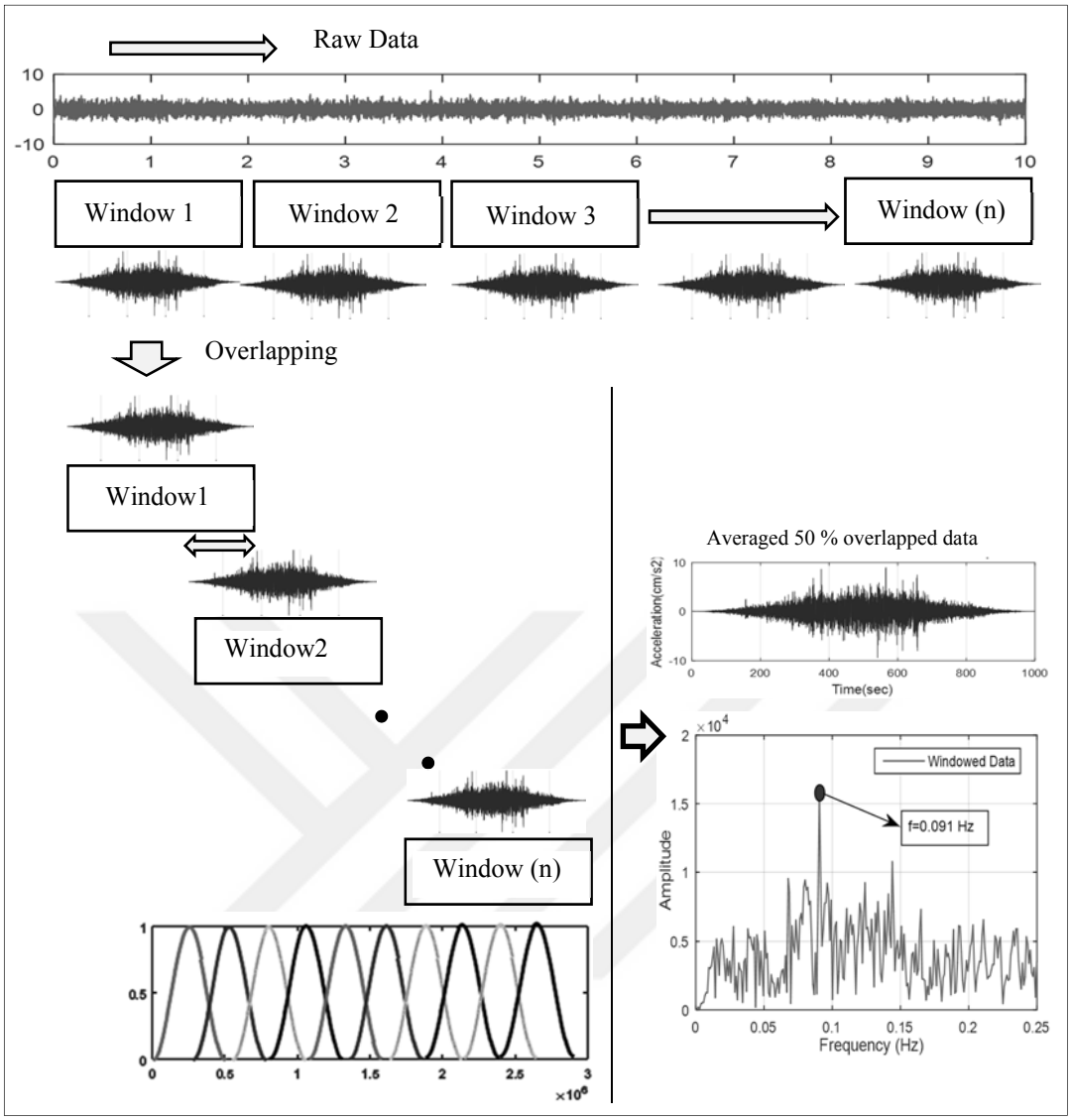

Figure 6. 15 : Identification of the overlapping and windowing process.

```
% ***************The Code for Data Average*********************
% *************Developed by Selcuk Bas/Jun 20 2016**************
%                                    First Version : Jun 20 2016
%                                    ITU Istanbul/Turkey
%-------------------------------------------------------------------------
% [Section I] Data Loading
%*************************************************************************
clc
clear all
a=9.81*(importdata('ACQ2_2ACC-D-MS-T(g)_CLU_7_A1_(acc6).dat'));% Load Data
in=input('Input the initial boundary(for instance:4e6):');
outp1=input('Input the last boundary(forainstance:5e6):');
delta=outp1-in;
d2=2^nextpow2(delta);
outp=d2;
cd1=a(in:(in+outp-1),1);
load('fd.mat');
dc1=filter(fd,cd1);% Bandpass Filter for 0.05 s - 5.0 s
%dc1=cd1;
dc=detrend(dc1)-mean(detrend(dc1)); % Detrending and extraction mean value
dt=0.002;
Fs=1/dt;
tr=0:dt:length(dc)*dt-dt;
```

Figure 6.16 : The developed Matlab code (M-File) for data averaging.

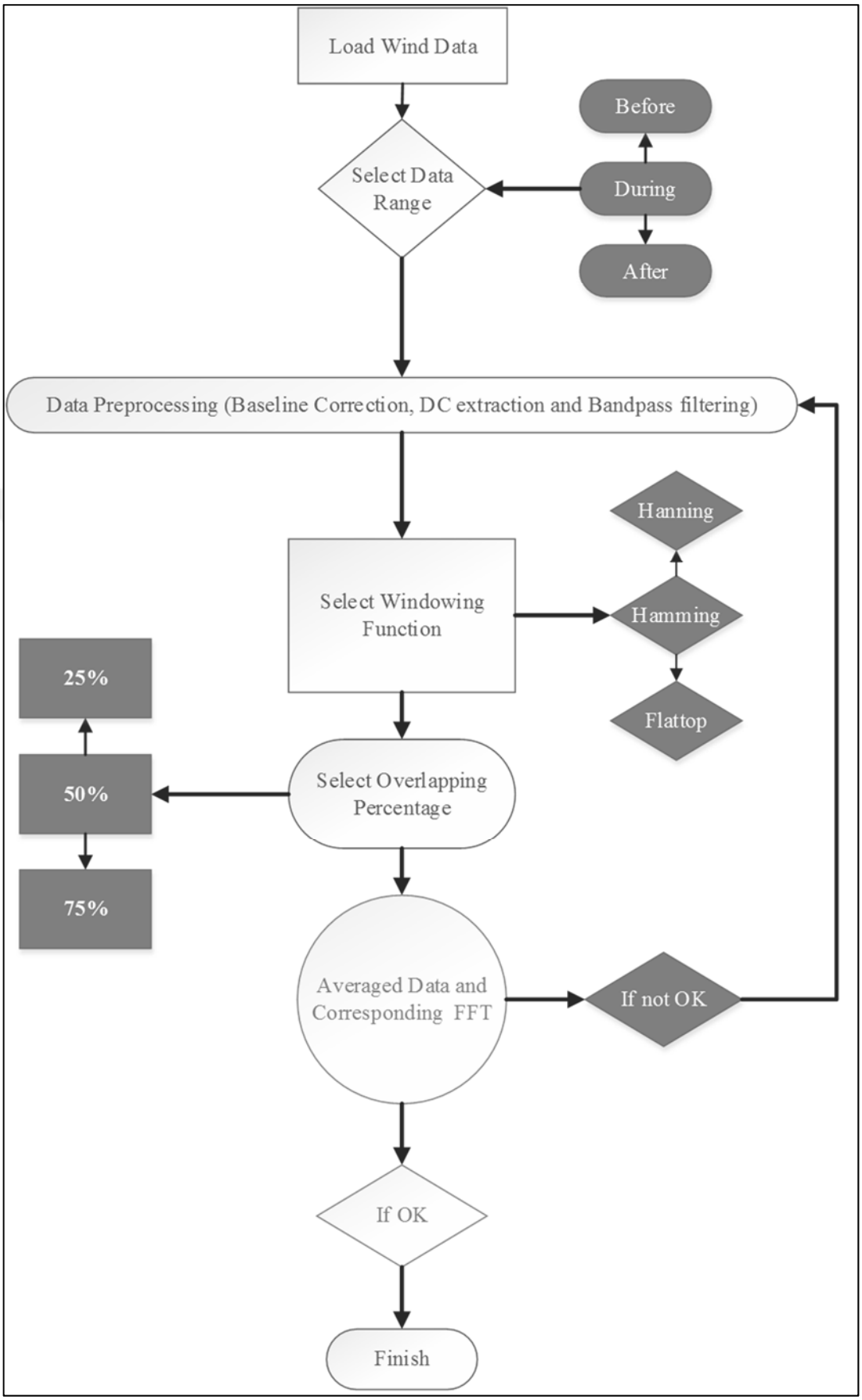

Figure 6.17 : The flowchart for the developed Matlab averaging code.

Taking these considerations required for averaging into account, a MATLAB code is developed for the critical wind data collected from the deck mid-span of the Bosphorus Bridge. In addition, a part of the code is depicted in Figure 6.16. Brief demonstration of this code is given with the flow chart as depicted in Figure 6.17. According to this flowchart, nine different data processes can be performed to indicate the effects of windowing function and the overlapping percentage on the results. These analyses are carried out for each data range. In this code, the most important point is to determine the optimum window length for averaging. For this aim, a specific method is not considered; instead, window length is determined according to frequency resolution of interest. For the Bosphorus Bridge, the frequency resolution (Δf) is taken into account as Δf =0.01 depending on the minimum frequency difference between consecutive first five mode frequencies that are determined from the developed FE models of the bridge in Chapter 4. The differences are given in Table 6.2 and minimum difference is obtained Δf=0.016 Hz, which means that the selected Δf should be equal to or lower than the minimum Δf=0.016 Hz. Thus, the selected Δf=0.01 Hz provides this condition. Besides, sampling frequency of F_{sample}=500 Hz is known from SHM system. After selection of the frequency resolution for the bridge, the window length (L_w) is determined as L_w= 5x10^4 using the equation 6.1. However, the code recalculates this window length as closest value to the power of 2^n that is necessary for FFT algorithm. Thus, the window length is determined L_w=65536 (2^{12}) for the averaging process.

Table 6.2 : Frequency difference between the mode shapes of the bridge.

Mode Number	Mode Shape	Freq. [Hz]	Δf [Hz]	
Mode-1	1st L_{sym}	0.077	|Mode 1-2|	0.062
Mode-2	1st V_{asym}	0.139	|Mode 2-3|	0.016
Mode-3	1st V_{sym}	0.155	|Mode 3-4|	0.048
Mode-4	1st L_{asym}	0.203	|Mode 4-5|	0.016
Mode-5	2nd V_{sym}	0.219	Δf_{min}=0.016 Hz	

$$\Delta f_{min} = \frac{F_{sample}}{L_w} \Rightarrow L_w = \frac{F_{sample}}{\Delta f_{min}} = \frac{500}{0.01} = 5 \times 10^4 \qquad (6.1)$$

With the help of a number of data analysis, the most compatible window function and overlapping percentage for the critical wind data are investigated. The results from the

data analyses are given in Figures 6.18-26 for “Before”, in Figures 6.27-35 for “During” and in Figures 6.36-44 for “After” ranges.

- “BEFORE” range data analysis

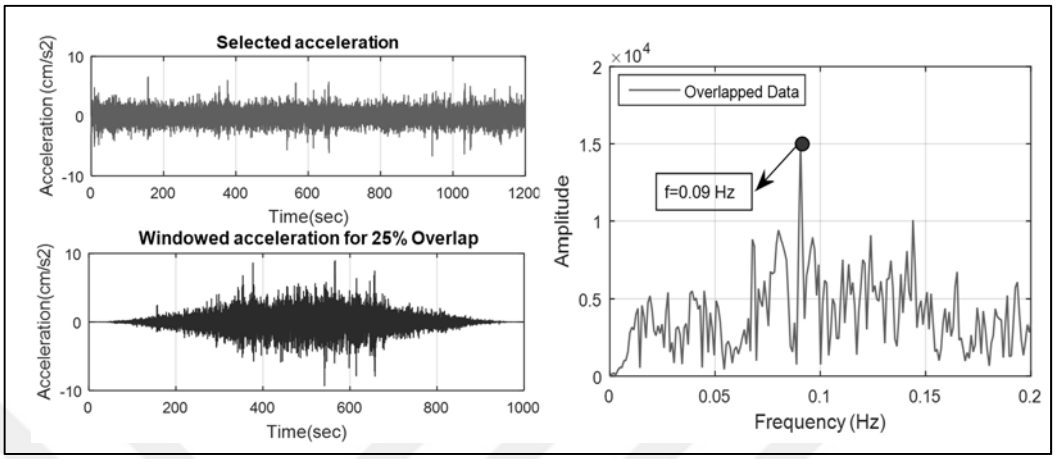

Figure 6.18 : Before Range: Hanning window 25% overlap percentage.

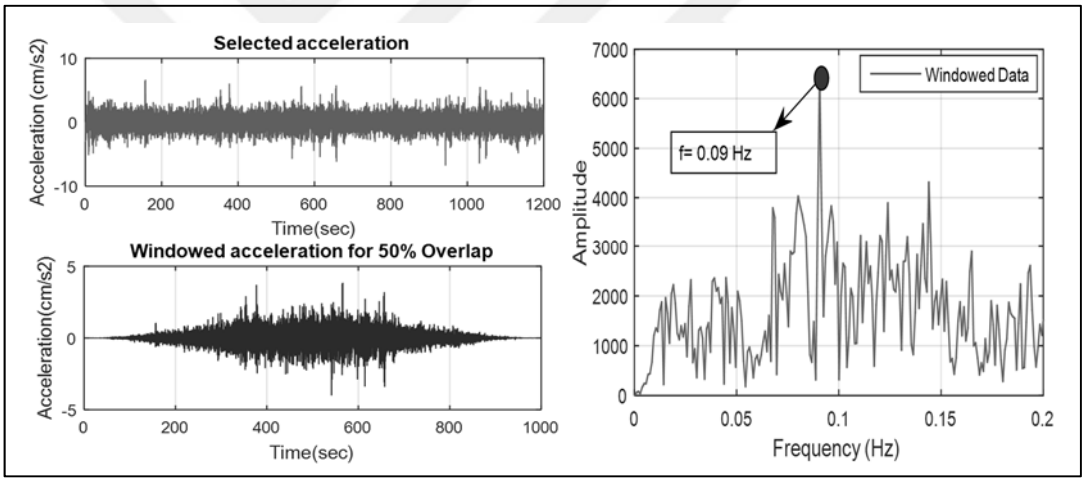

Figure 6.19 : Before Range: Hanning window 50% overlap percentage.

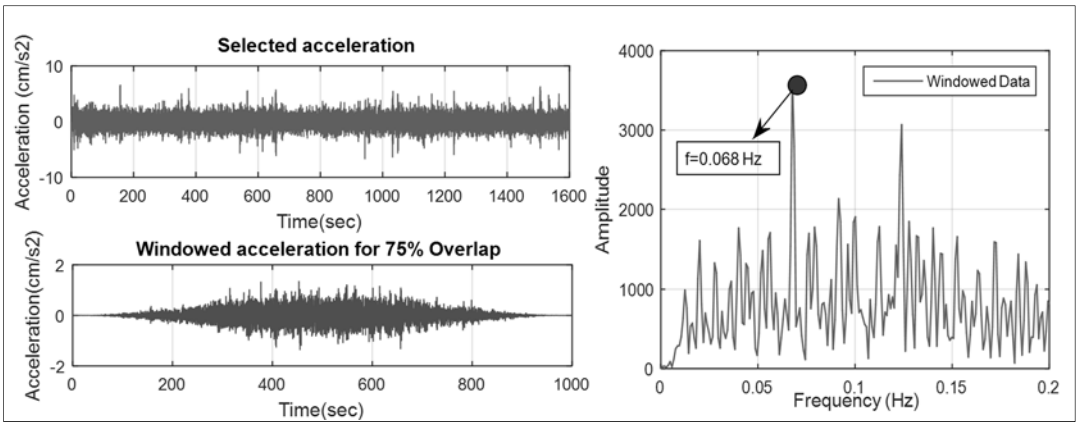

Figure 6.20 : Before Range: Hanning window 75% overlap percentage.

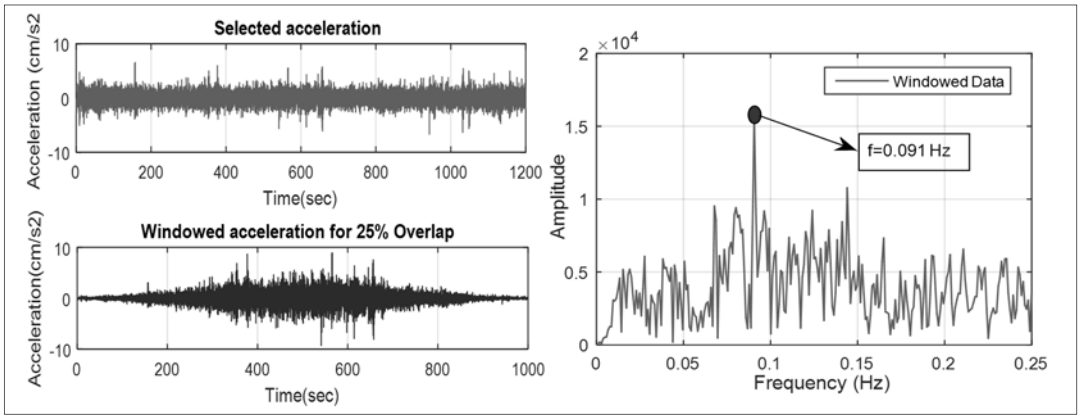

Figure 6.21 : Before Range: Hamming window 25% overlap percentage.

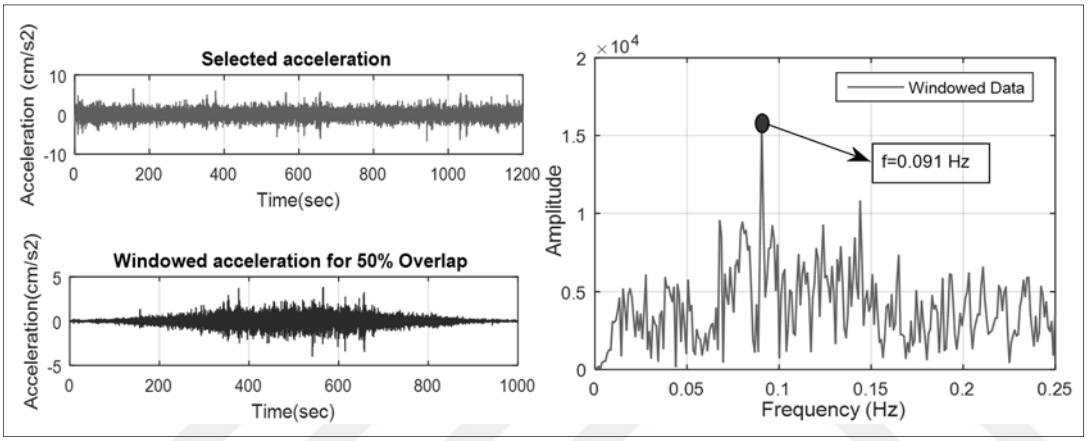

Figure 6.22 : Before Range: Hamming window 50% overlap percentage.

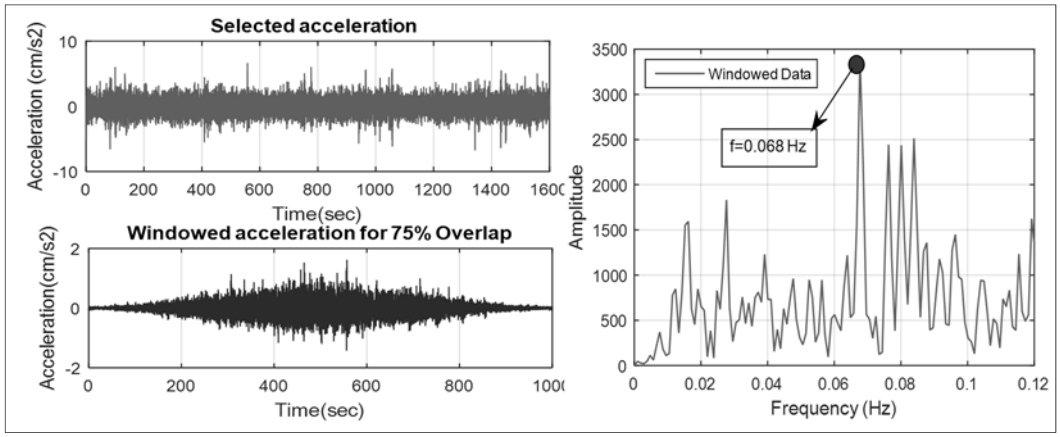

Figure 6.23 : Before Range: Hamming window 75% overlap percentage.

From the analysis for "Before" range given in Table 6.3, Flattop window function differs from the others. Besides, the results from this function vary depending on the overlapping percentage. However, hanning and hamming window functions have similar results for all overlapping percentages.

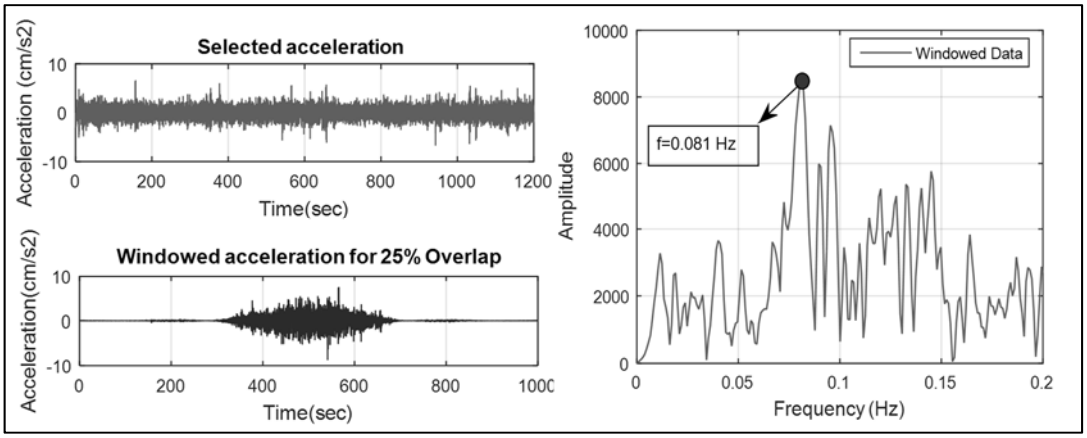

Figure 6.24 : Before Range: Flattop window 25% overlap percentage.

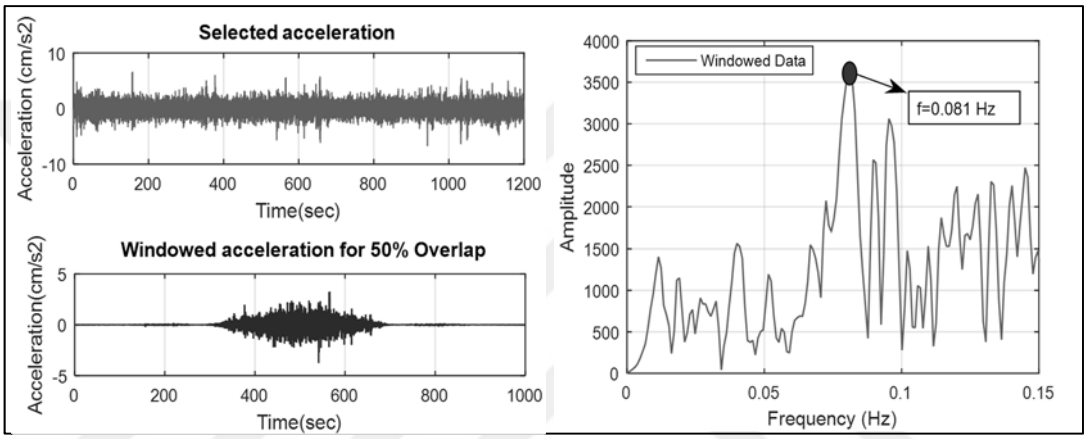

Figure 6.25 : Before Range: Flattop window 50% overlap percentage.

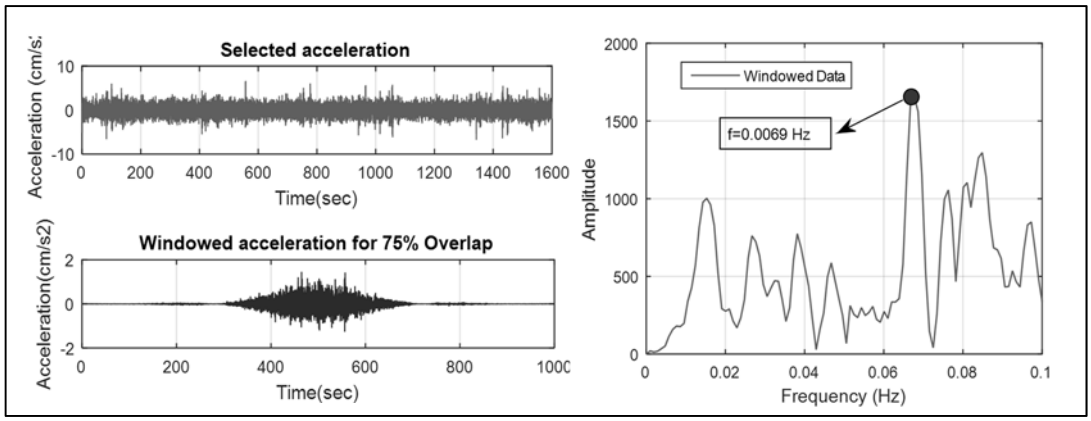

Figure 6.26 : Before Range: Flattop window 75% overlap percentage.

When compared to the FFT curves as shown in Figures 6.18-26 with those in the previous results, they are clearer and smother even though noise or other negative effects are not properly eliminated from the data.

Table 6.3 : Results for "Before" range.

BEFORE, FFT Results (Hz)			
Window Function	Overlapping percentage		
	25%	50%	75%
Hanning	0.090	0.090	0.068
Hamming	0.091	0.091	0.068
Flattop	0.081	0.081	0.069

- "DURING" range data analysis

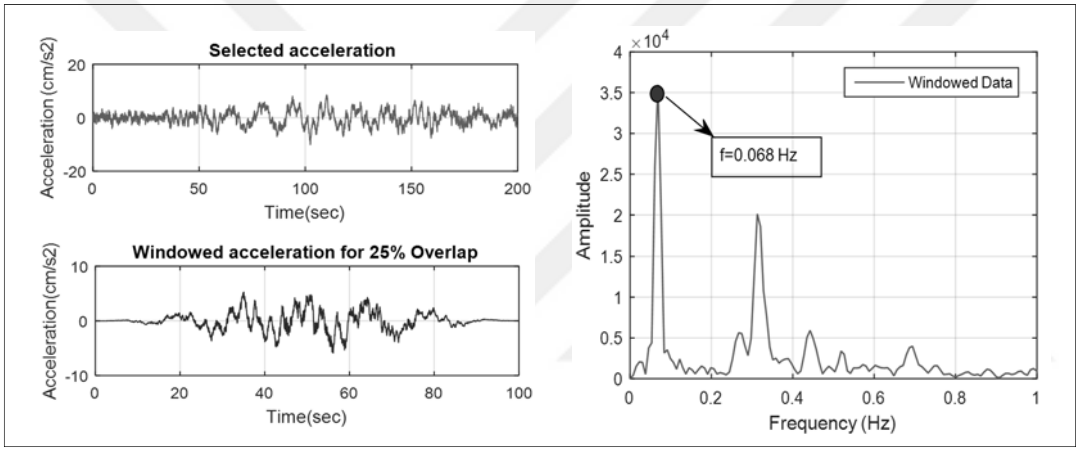

Figure 6.27 : During Range: Hanning window 25% overlap percentage.

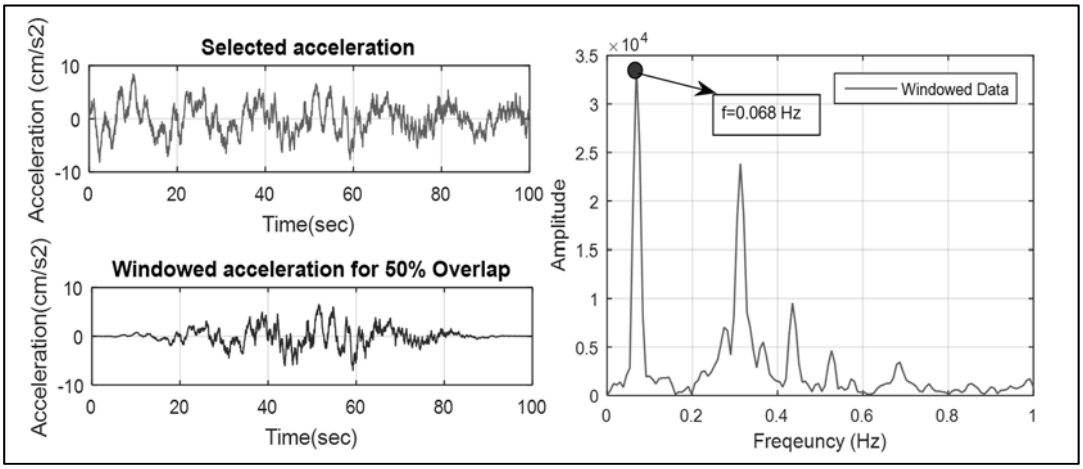

Figure 6.28 : During Range: Hanning window 50% overlap percentage**.**

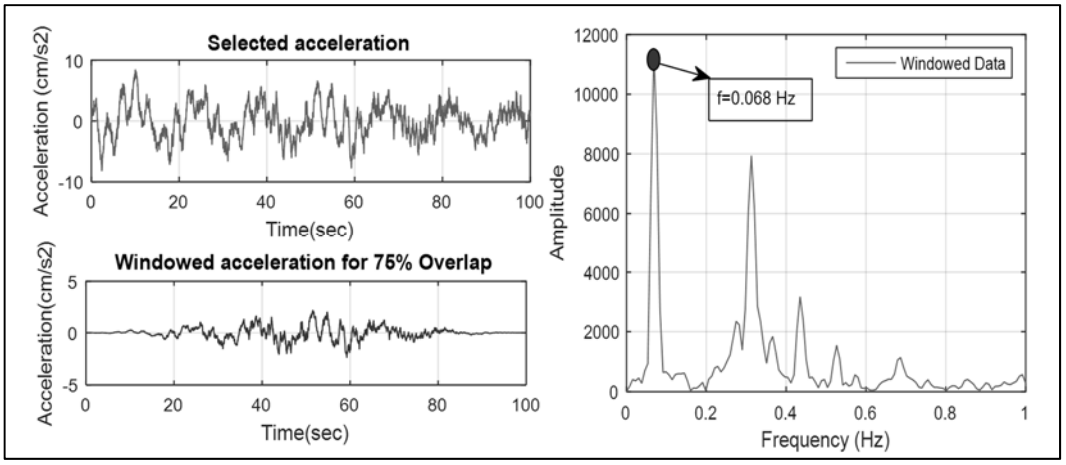

Figure 6.29 : During Range: Hanning window 75% overlap percentage.

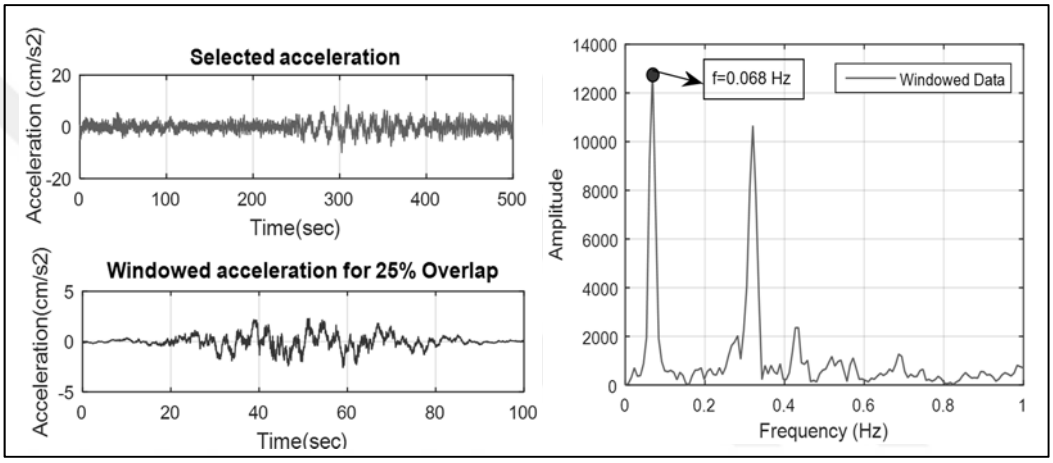

Figure 6.30 : During Range: Hamming window 25% overlap percentage.

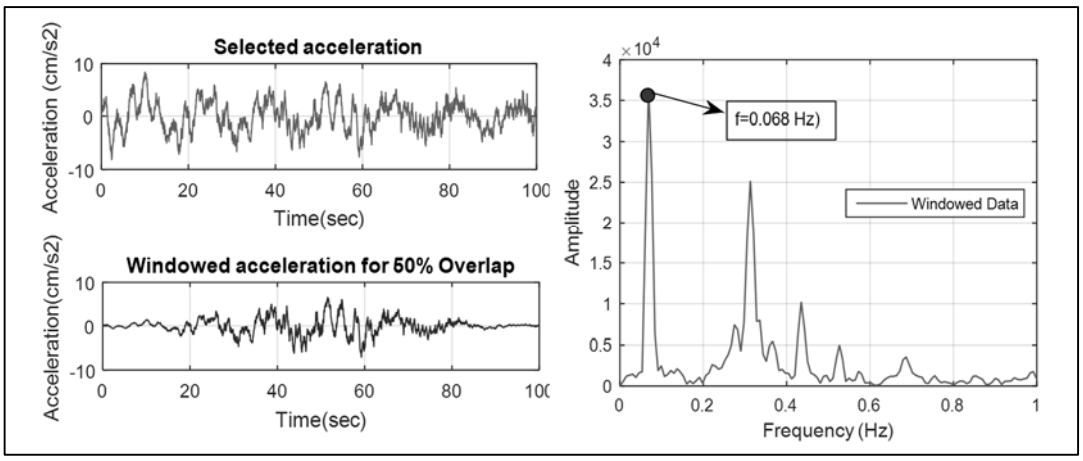

Figure 6.31 : During Range: Hamming window 50% overlap percentage**.**

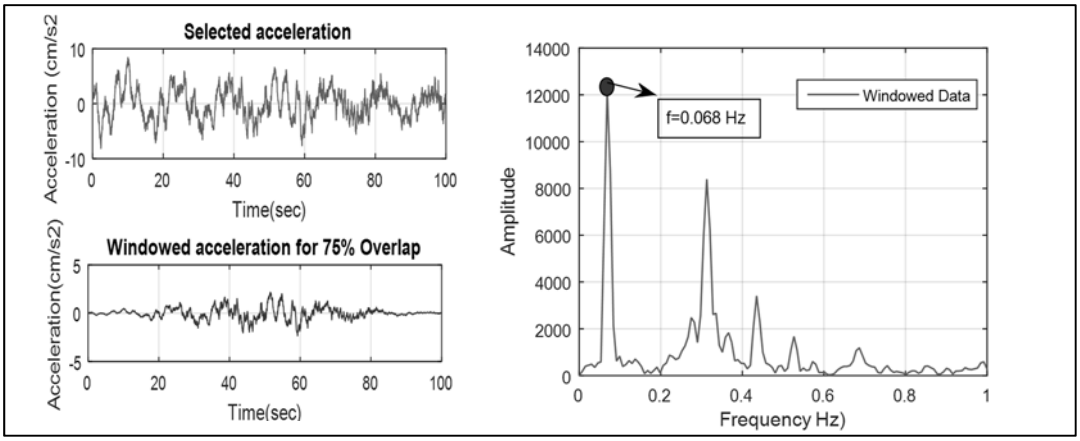

Figure 6.32 : During Range: Hamming window 75% overlap percentage.

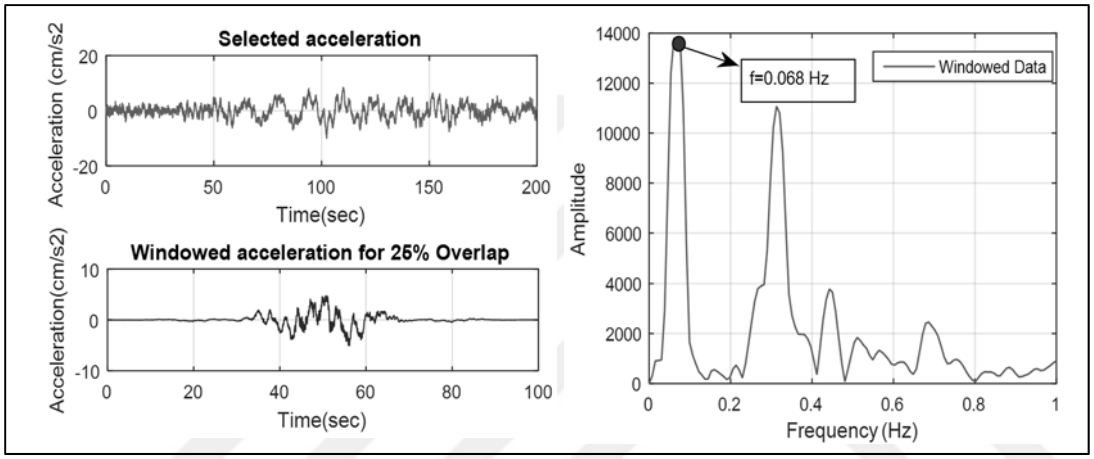

Figure 6.33 : During Range: Flattop window 25% overlap percentage.

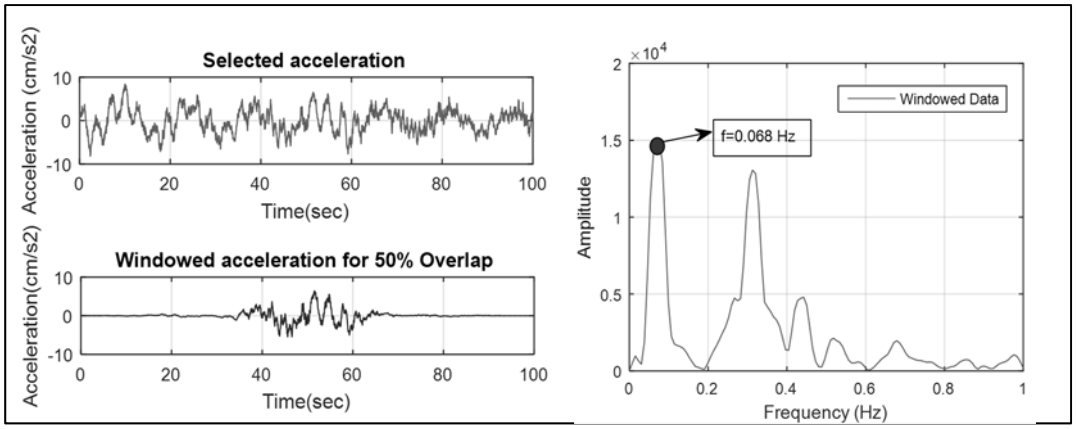

Figure 6.34 : During Range: Flattop window 50 % overlap percentage**.**

For "During" range, as shown in Figures 6.27-34, the FFT curves for all window functions and overlapping percentages are obtained as clearly smooth since the bridge is fully excited at this range. The results are given in Table 6.4. Therefore, almost no considerable effects of the window functions and the overlapping percentages on the

frequency response of the data are determined, which means that same results are obtained for all considerations.

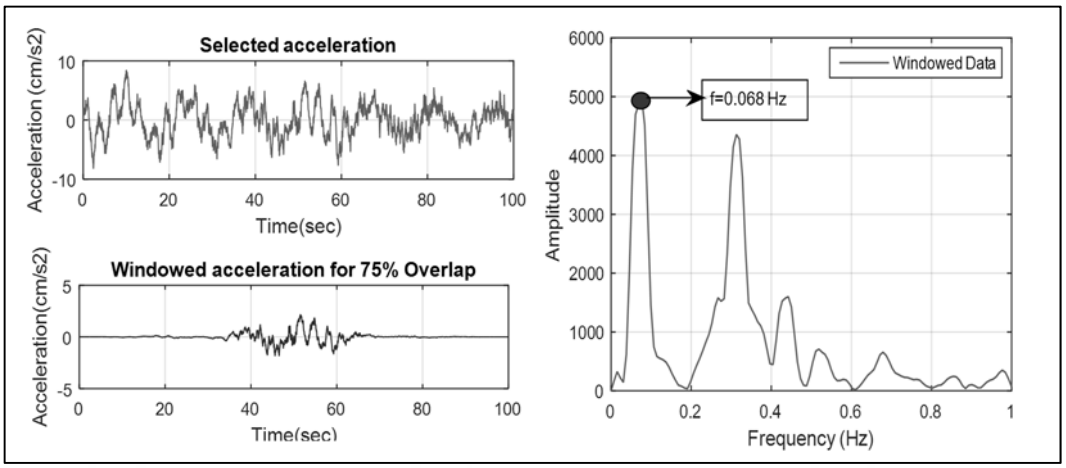

Figure 6.35 : During Range: Flattop window 75 % overlap percentage.

Table 6.4 : Results for "During" range.

DURING, FFT Results (Hz)			
Window Function	Overlapping percentage		
	25%	50%	75%
Hanning	0.068	0.068	0.068
Hamming	0.068	0.068	0.068
Flattop	0.068	0.068	0.068

- "AFTER" range data analysis

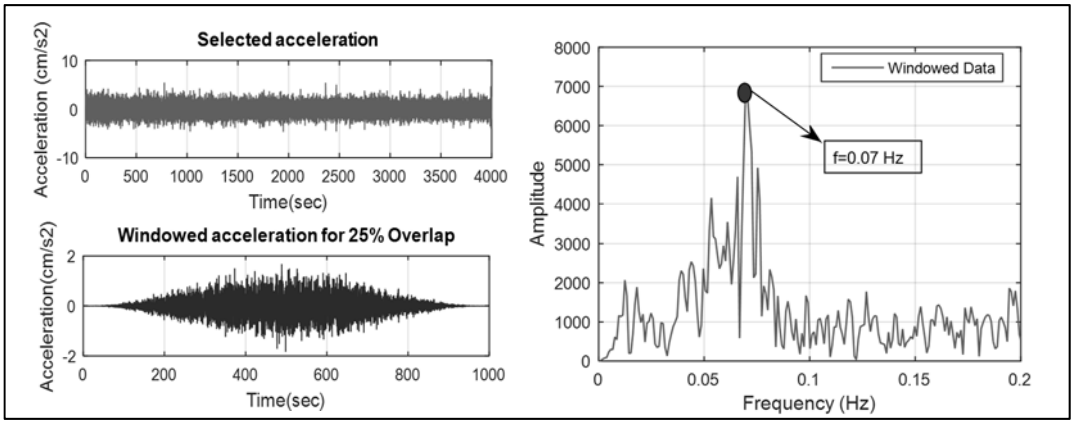

Figure 6.36 : After Range: Hanning window 25% overlap percentage**.**

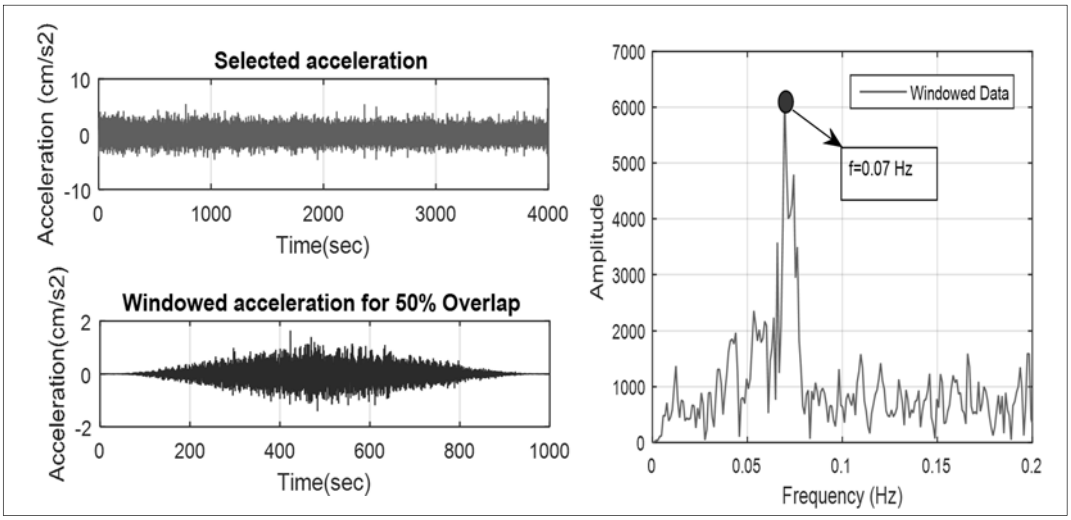

Figure 6.37 : After Range: Hanning window 50% overlap percentage**.**

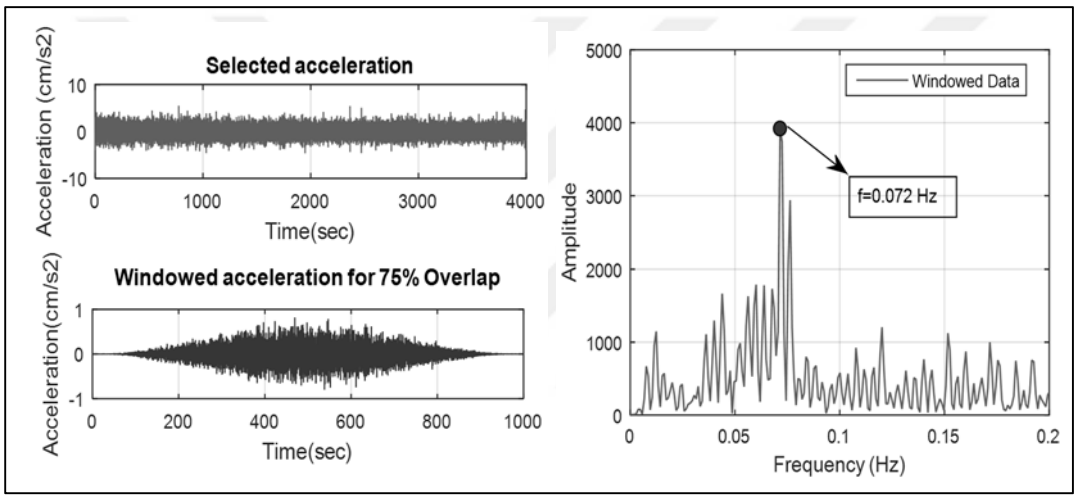

Figure 6.38 : After Range: Hanning window 75 % overlap percentage.

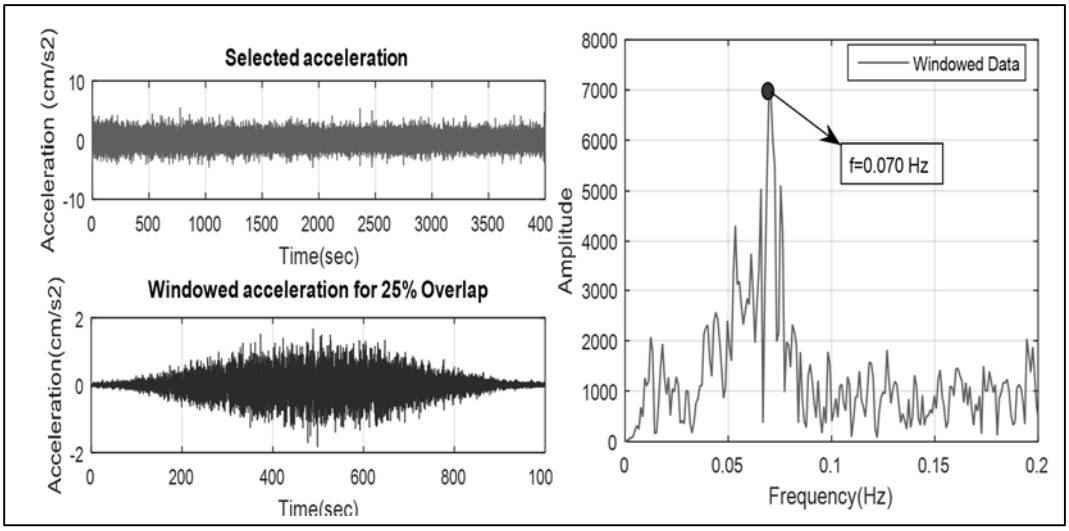

Figure 6.39 : After Range: Hamming window 25 % overlap percentage.

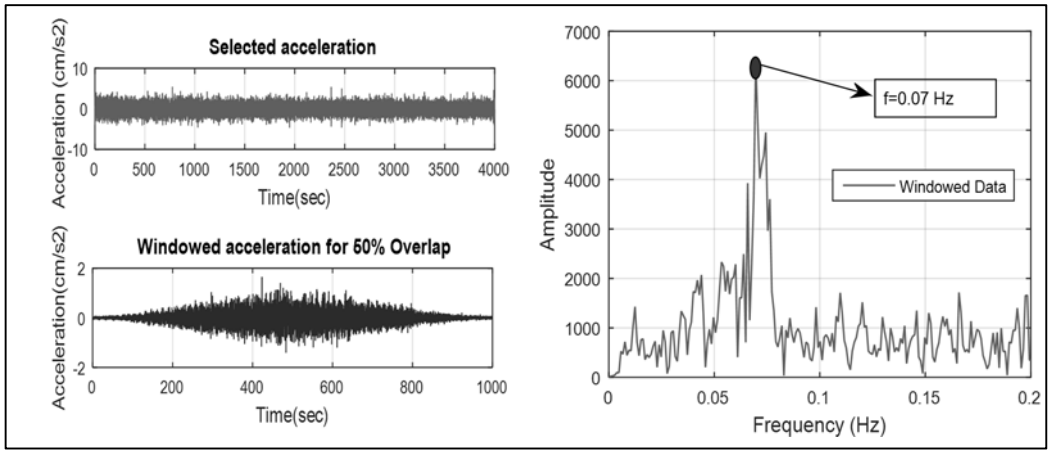

Figure 6.40 : After Range: Hamming window 50% overlap percentage**.**

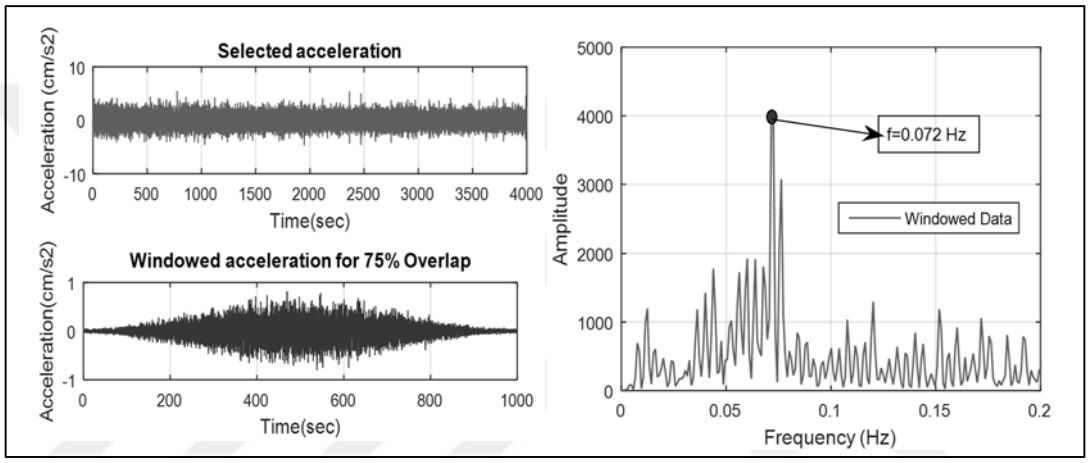

Figure 6.41 : After Range: Hamming window 75 % overlap percentage.

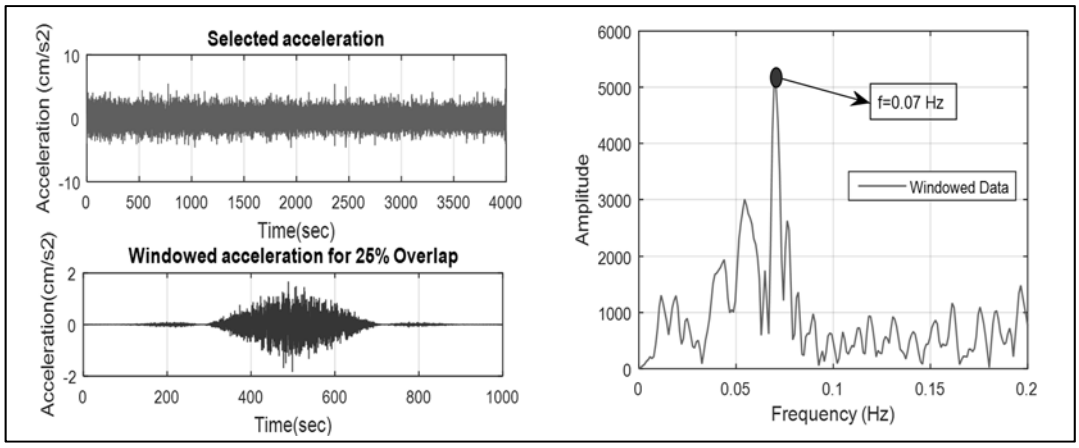

Figure 6.42 : After Range: Flattop window 25 % overlap percentage.

According to Table 6.5 for "After" range data, the frequency response of the bridge is not affected from types of the window functions and the overlapping percentages. However, the FFT curves in Figures 6.36-44 are relatively smoother than those from the preprocessed data.

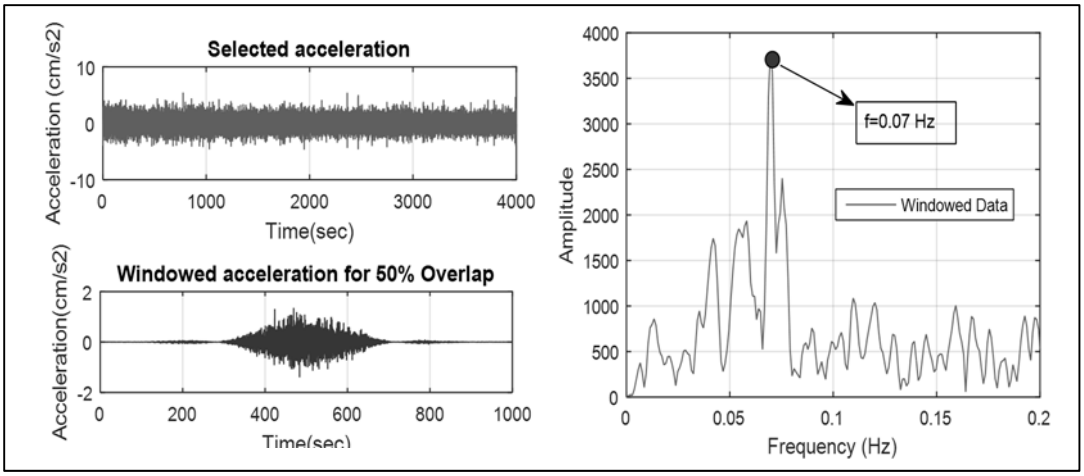

Figure 6.43 : After Range: Flattop window 50% overlap percentage.

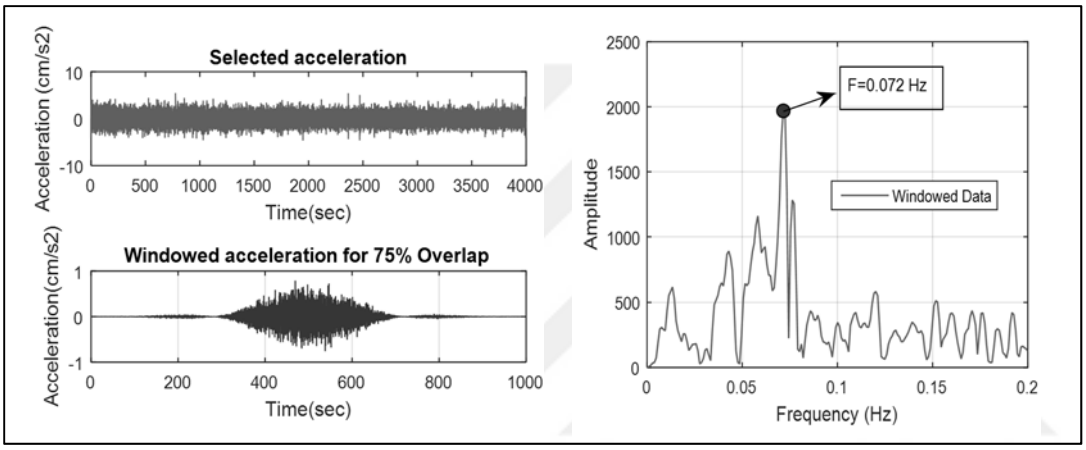

Figure 6.44 : After Range: Flattop window 75% overlap percentage.

Table 6.5 : Results for "After" range.

AFTER, FFT Results (Hz)			
Window Function	Overlapping percentage		
	25%	50%	75%
Hanning	0.070	0.070	0.072
Hamming	0.070	0.070	0.072
Flattop	0.070	0.070	0.072

The results from the overlapped data averaging process have shown that the almost all window functions and the overlapping percentages can be applied to obtain clearer and smoother FFT curves necessary for better understanding and detecting dynamic

response of the bridge. Based on a number of try&error studies conducted during the analyses, the most suitable window function and the most effective overlapping percentage for this data are determined as Hanning or Hamming window function and 50% overlapping percentage, respectively.

When compared FFT peaks from "After" range with those from "Before"range, "After" range is obtained to be clearer than "Before" range. This conclusion is based on less sensivity of the sensors to traffic noise. In addition, traffic noise was also high in this range since the bridge continues its function for a length of time during "Before"range. This also leads to increase of noise content in data. Hence, "After" range is considered as ambient vibration to obtain natural modal frequencies of the bridge. For further investigation on modal characteristics of the bridge, "After" range will be adopted and will be compared with "During" range to identify the effect of the extreme wind event on the bridge.

6.3 Structural Modal Identification of the Bridge

The verification of the developed averaging code with the preliminary frequency domain results enables to make structural modal identification of the bridge and to compare the results from the estimated FE models with the ambient vibration results. As mentioned in previous section, "Before" range including a number of peaks are relatively distorted with the noise while those obtained from the "After" range are smooth. Moreover, a certain part of "After" range data was recorded after the bridge was closed to traffic, which means that the bridge vibrates only by itself oscillations without traffic. Therefore, "After" range data is considered to obtain natural vibration characteristics of the bridge. In the modal identification, Power Spectral Density Function (PSD) curves that yield to clearer results than FFT are adopted and computed for "After" and "During" ranges. For this purpose, acceleration data recorded from the specific points of the bridge as depicted in Figure 6.45 are utilized. For these points, transverse (T), longitudinal (L) and vertical (V) directions are also taken into account. Modal identification results are obtained for both "After" and "During" range to identify the effects of the extreme wind load on the bridge. The first nine mode shape frequencies that are the single mode of the deck and the towers are obtained. Noticeable change in the modal mass participation of the modes are considered as the key indicator to find which PSD peak value belongs to mode shape.

In Figure 6.46, the acceleration data recorded at the tower-top-south-east in transverse direction is analyzed and the PSD results for "During" and "After" ranges are given. As shown in Figure 6.46, Mode-8 (1st Tower L_{sym}) and Mode-9 (1st Tower L_{asym}) are obtained according to the change in mass participation of the modes. For Mode-8 (1st Tower L_{sym}) and Mode-9 (1st Tower L_{asym}) as shown in Figure 6.47, similar outcomes are obtained from the data recorded at the tower-top-south-west in transverse direction. Consequently, only two transverse tower modes of Mode-8 and Mode-9 are identified from these sensors with the same PSD value for "During" and "After" ranges. In transverse direction, the accelerometers installed on the deck mid-span in transverse direction, the deck 2/3-span and the deck 1/3-span are also utilized to especially obtain the deck mode shapes. From Figure 6.48 Mode-1(1st Deck L_{symm}) and Mode-8 (1st Tower L_{symm}) are identified from both "After" and "During" ranges. As expected, considerable difference between "After" and "During" ranges for Mode-1 is determined with 15% increase in the period. Similarly, Mode-8 (1st Tower L_{symm}) is also obtained from the two ranges; however, Mode-9 is only identified from "After" range. In addition, the PSD values of Mode-8 and Mode-9 from the accelerometers at the towers are also verified with those from this sensor. Consequently, Mode-1, Mode-8 and Mode-9 are obtained from the PSD analysis of the accelerometers at the deck mid-span in the transverse direction.

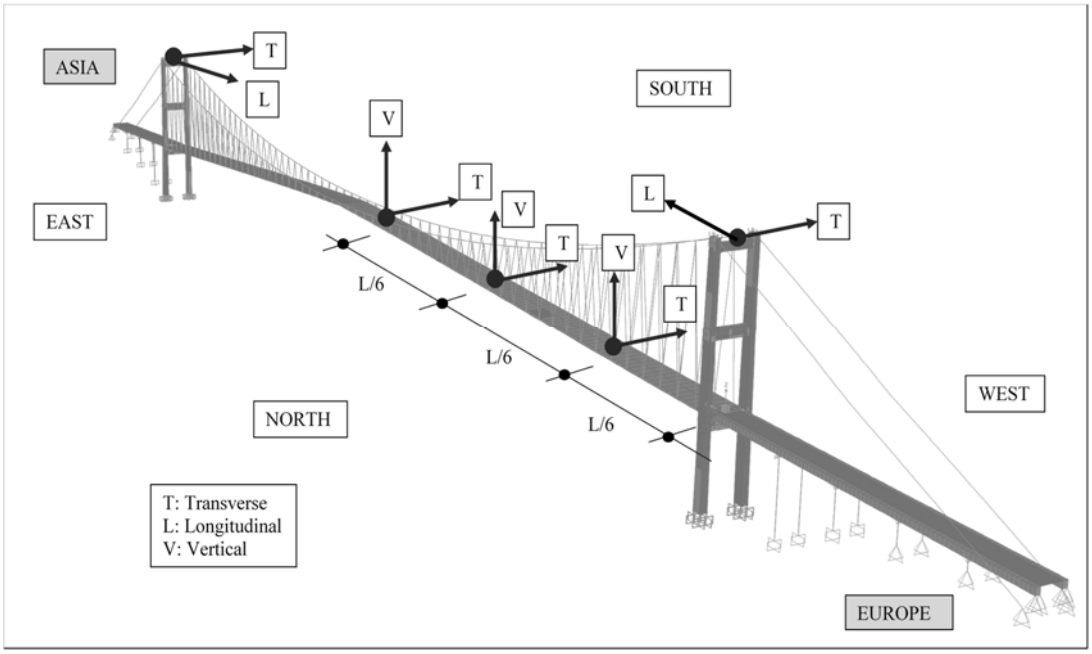

Figure 6.45 : General configuration for the accelerometers on the bridge.

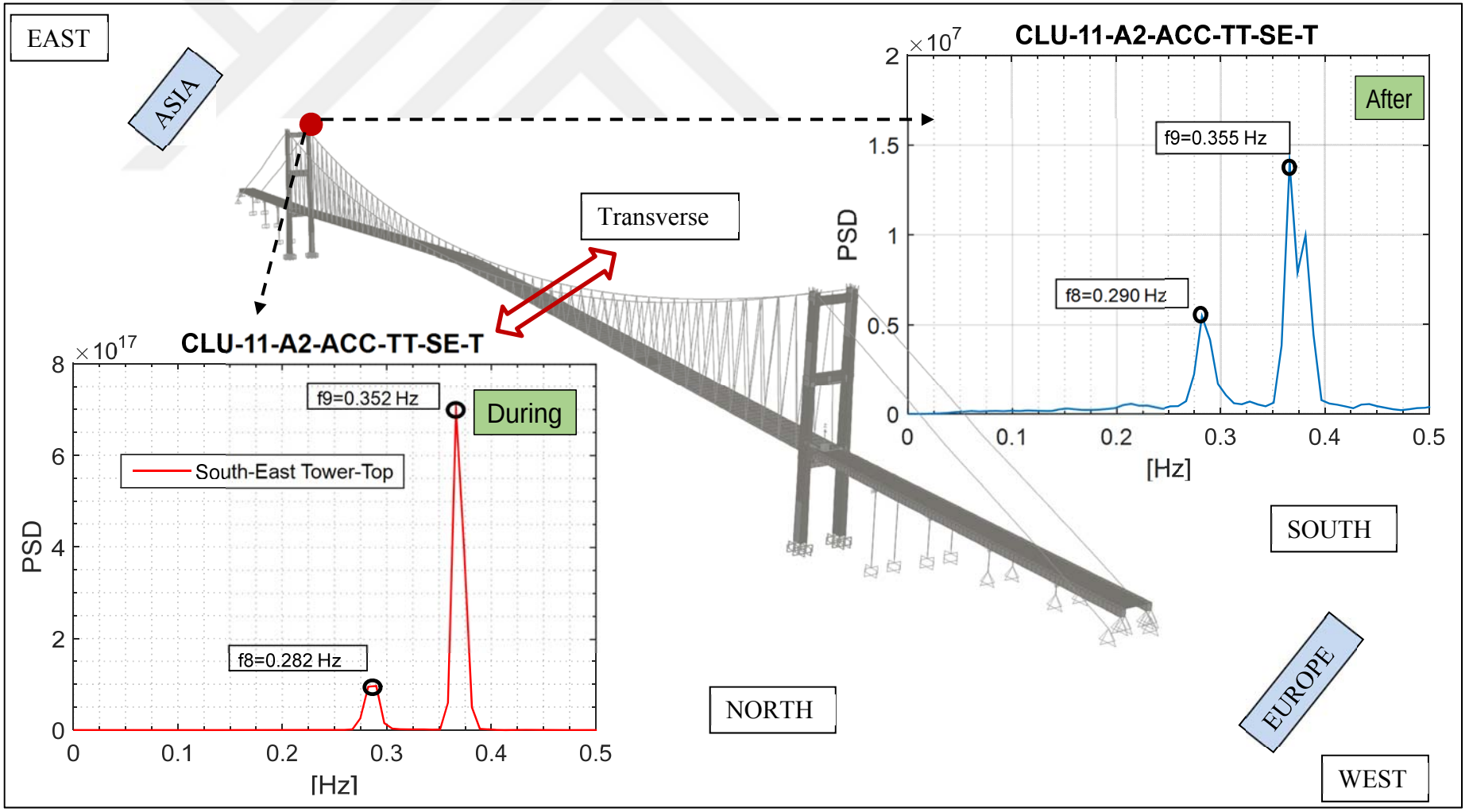

Figure 6.46 : Power Spectral Density (PSD) of the acceleration data at tower-top-south-east in transvrse direction.

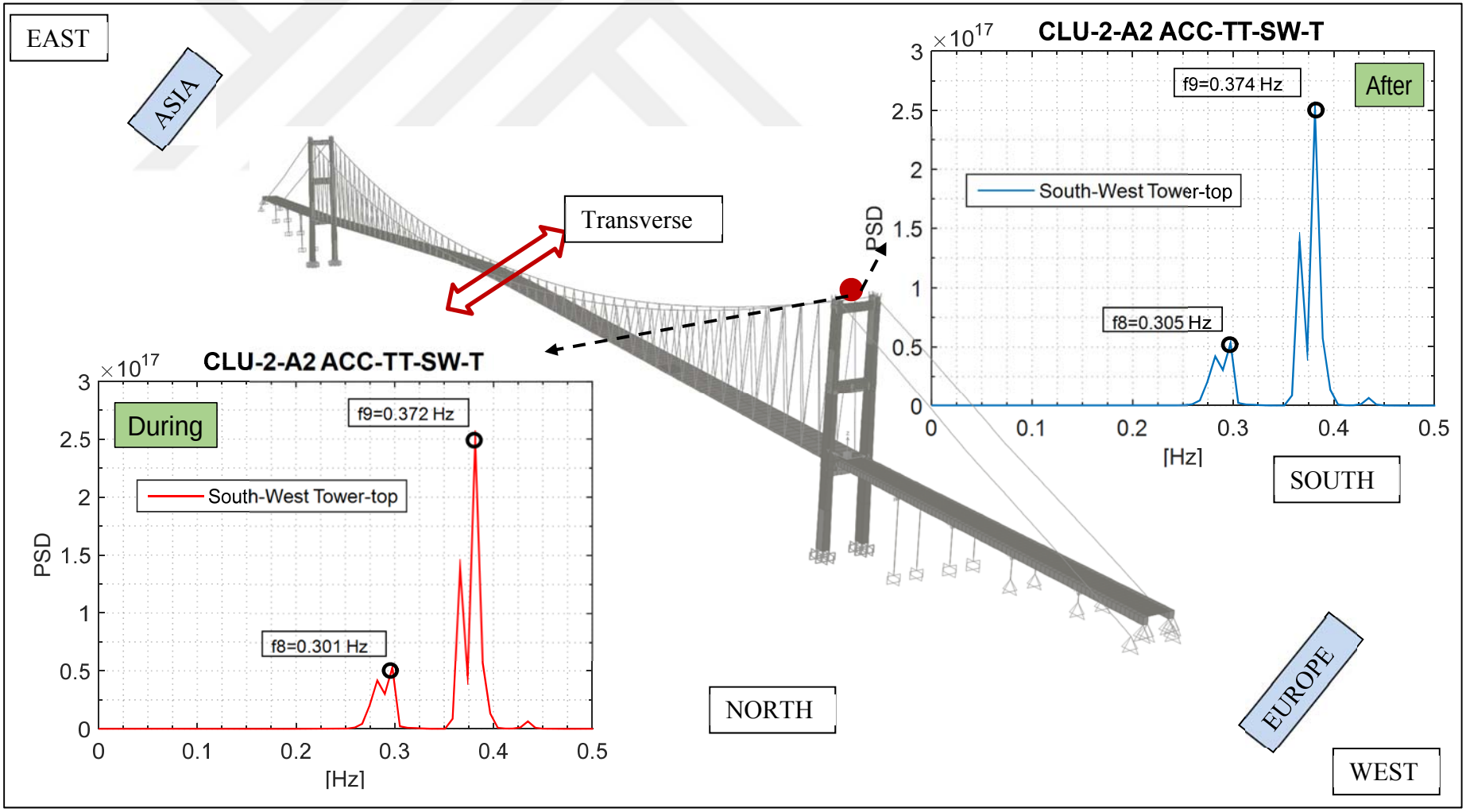

Figure 6.47 : Power Spectral Density (PSD) of the acceleration data at tower-top-south-west in tranverse direction.

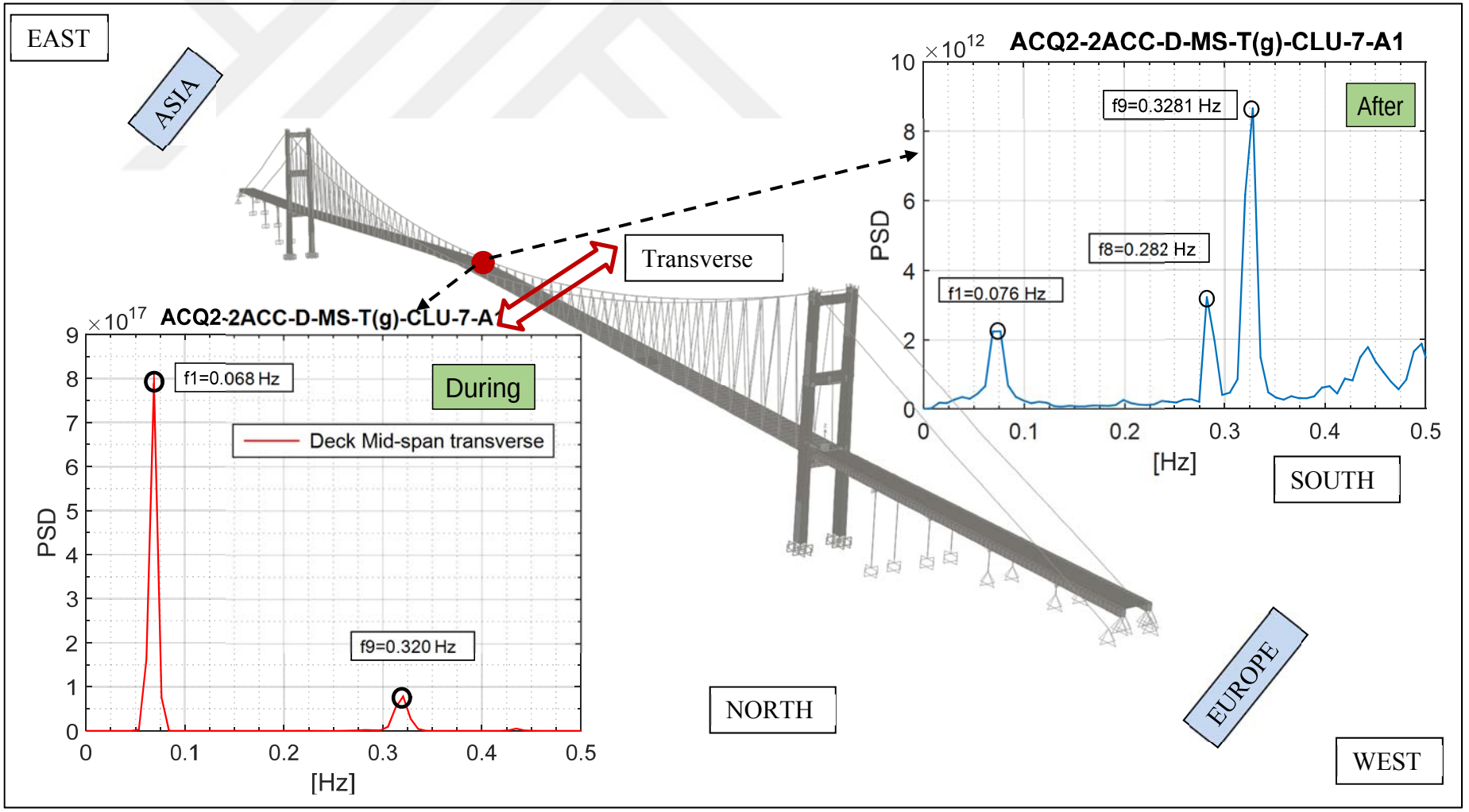

Figure 6.48 : Power Spectral Density (PSD) of the acceleration data at the deck-midspan in tranverse direction.

The acceleration data obtained from the deck 2/3-span and the deck 1/3-span in the transverse direction are estimated to identify the deck and tower modes. The results from the sensor at the deck 2/3-span as indicated in Figure 6.49 reveal that Mode-1 and Mode-8 are obtained for two ranges, but Mode-4 (1st Deck L_{asym}) and Mode-9 are identified only from "After" range. Similar consequences are expected from the acceleration data at the deck 2/3-span. In Figure 6.50, the same modes of Mode-1, Mode-4, Mode-8 and Mode-9 are identified from two ranges. Except for Mode-1, Mode-4 and Mode-8, Mode-9 is obtained only from "During" range as depicted in Figure 6.50.

Table 6.6 : Modal identification of lateral modes of the bridge.

Mode Type	Mode Number	Mode Shape	Experimental (Transvers Direction)						Graphical Presentation
			During		After		Change (%)		
			Period [s]	Freq. [Hz]	Period [s]	Freq. [Hz]	Period [s]	Freq. [Hz]	
Deck Modes	Mode-1	1st L_{sym}	14.706	0.068	12.766	0.078	15.196	**-13.191**	
	Mode-2	1st V_{asym}							
	Mode-3	1st V_{sym}							
	Mode-4	1st L_{asym}	4.854	0.206	4.967	0.201	-2.265	**2.318**	
	Mode-5	2nd V_{sym}							
	Mode-6	1st T							
	Mode-7	2nd V_{asym}							
Tower Modes	Mode-8	1st L_{sym}	3.405	0.294	3.319	0.301	2.611	**-2.544**	
	Mode-9	1st L_{asym}	2.837	0.353	2.855	0.350	-0.647	**0.615**	

L_{sym}: Lateral symmetric; L_{asym}: Lateral asymmetric;V_{sym}:Vertical symmetric; V_{asym}:Vertical asymmetric; T: Torsional

Apart from the modal identification, the effects of the extreme wind event on dynamic response of the bridge are presented in Table 6.6 in terms of % change comparing natural vibration mode frequencies obtained from "After" range data with those from "During" range data. From the table, all effective lateral modes are identified. Since certain identified modes have different PSD values from different five acceleration data, the mean value of the modes with different PSD is considered in Table 6.6 for each range. Compared to those from "After" range, modal identifications from the developed FE models are obtained to be accurately achieved. More details are presented in the section of verification of the FE models.

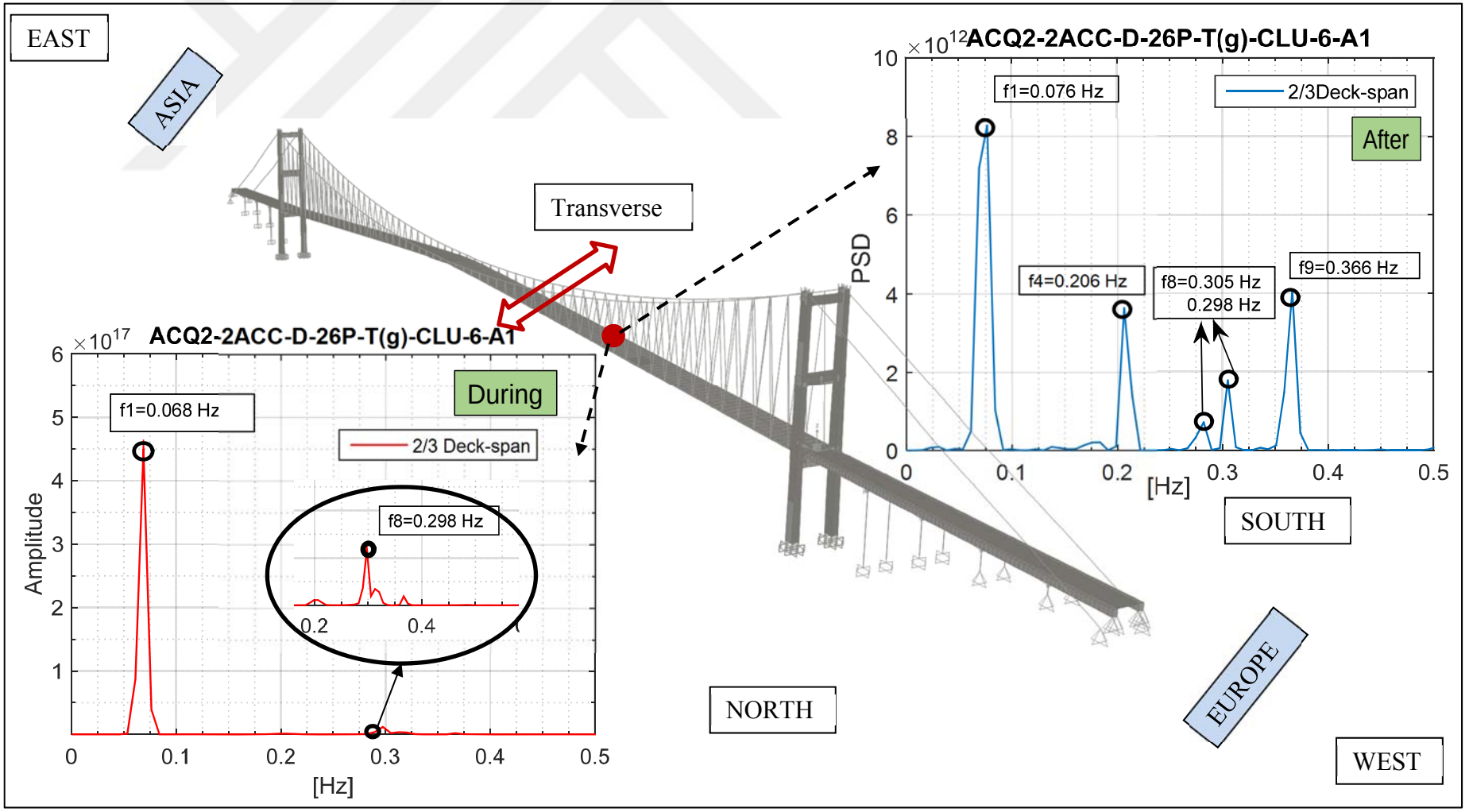

Figure 6.49 : Power Spectral Density (PSD) of the acceleration data at the deck-2/3-span in tranverse direction.

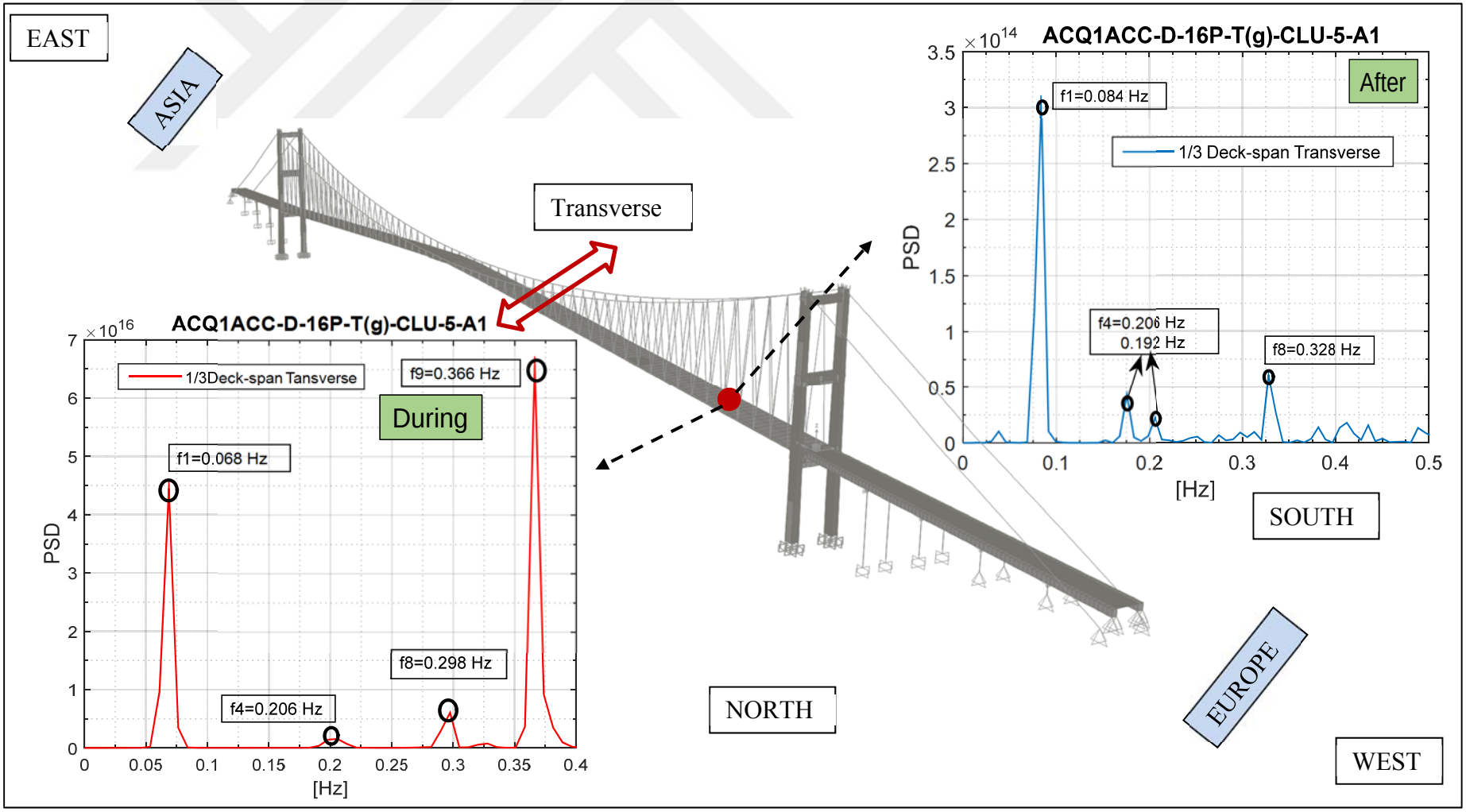

Figure 6.50 : Power Spectral Density (PSD) of the acceleration data at the deck-1/3-span in tranverse direction.

As for the comparison of "During" and "After" range, approximately no change in Mode-4 (1st Deck L_{asymm}), Mode-8 (1st Tower L_{symm}) and Mode-9 (1st Tower L_{asymm}) is determined while 15 % increase in the period of Mode-1 is obtained, which means that during extreme wind, the bridge vibrates in transverse direction with high displacement.

Table 6.7 : Modal identification of vertical modes of the bridge.

Mode Type	Mode Number	Mode Shape	Experimental (Vertical Direction)						Graphical Presentation
			During		After		Change (%)		
			Period [s]	Freq. [Hz]	Period [s]	Freq. [Hz]	Period [s]	Freq. [Hz]	
Deck Modes	Mode-1	1st L_{sym}							
	Mode-2	1st V_{asym}	8.065	0.124	8.065	0.124	-	-	
	Mode-3	1st V_{sym}	6.096	0.164	6.250	0.160	-2.469	**2.531**	
	Mode-4	1st L_{asym}							
	Mode-5	2nd V_{sym}	4.561	0.219	4.525	0.221	0.798	**-0.792**	
	Mode-6	1st T	3.591	0.279	3.542	0.282	1.376	**-1.358**	
	Mode-7	2nd V_{asym}	3.591	0.279	3.542	0.282	1.376	**-1.358**	
Tower Modes	Mode-8	1st L_{sym}							
	Mode-9	1st L_{asym}							

L_{sym}: Lateral symmetric; L_{asym}: Lateral asymmetric;V_{sym}:Vertical symmetric; V_{asym}:Vertical asymmetric; T: Torsional

In the vertical direction, total number of three accelerometer sensors mounted on the deck mid-span, the deck 1/3-span and the deck 2/3-span are considered for the PSD analyses. As shown in Figure 6.51, only Mode-3 (1st Deck V_{symm}) from "During" range data, and Mode-3 (1st Deck V_{symm}) and Mode-5 (2nd Deck V_{symm}) from "After" range are identified. In addition to Mode-3 and Mode-5, Mode-2 (1st Deck V_{asymm}) and Mode-7 (2nd Deck V_{asymm}) are obtained from the accelerometer at the deck 2/3-span indicated in Figure 6.52. As given in Figure 6.53, similar modes are also identified from the deck 1/3-span accelerometer. Mode-6 (1st Deck T) is tried to be identified from the vertical response of the bridge. In the analyses, the PSD value of Mode-6 is observed to be generally close to that of Mode-7; therefore, modal frequency of the torsional mode of the bridge is considered to be equal to that of Mode-7. Accordingly, all vertical modes of Mode-2, Mode-3, Mode-5, Mode-6 and Mode-7 are obtained from the acceleration data in the vertical direction. The mean values of the determined modes are given in Table 6.7. As seen from the table, no % change calculation for Mode-2 is made due to identification of this mode only from the "During" range. Hence, the results from "During"range is considered the same for "After" range.

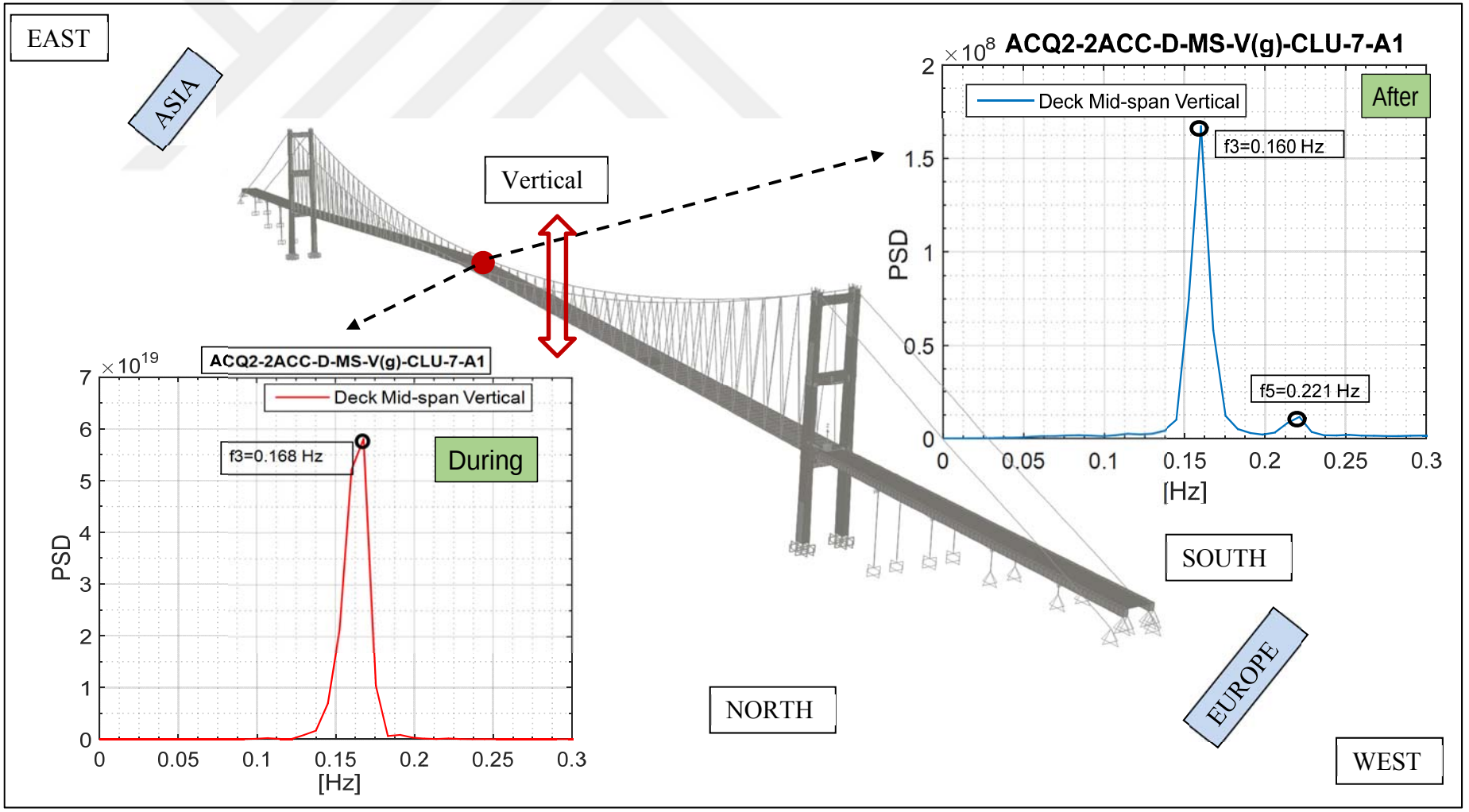

Figure 6.51 : Power Spectral Density (PSD) of the acceleration data at the deck-midspan in vertical direction.

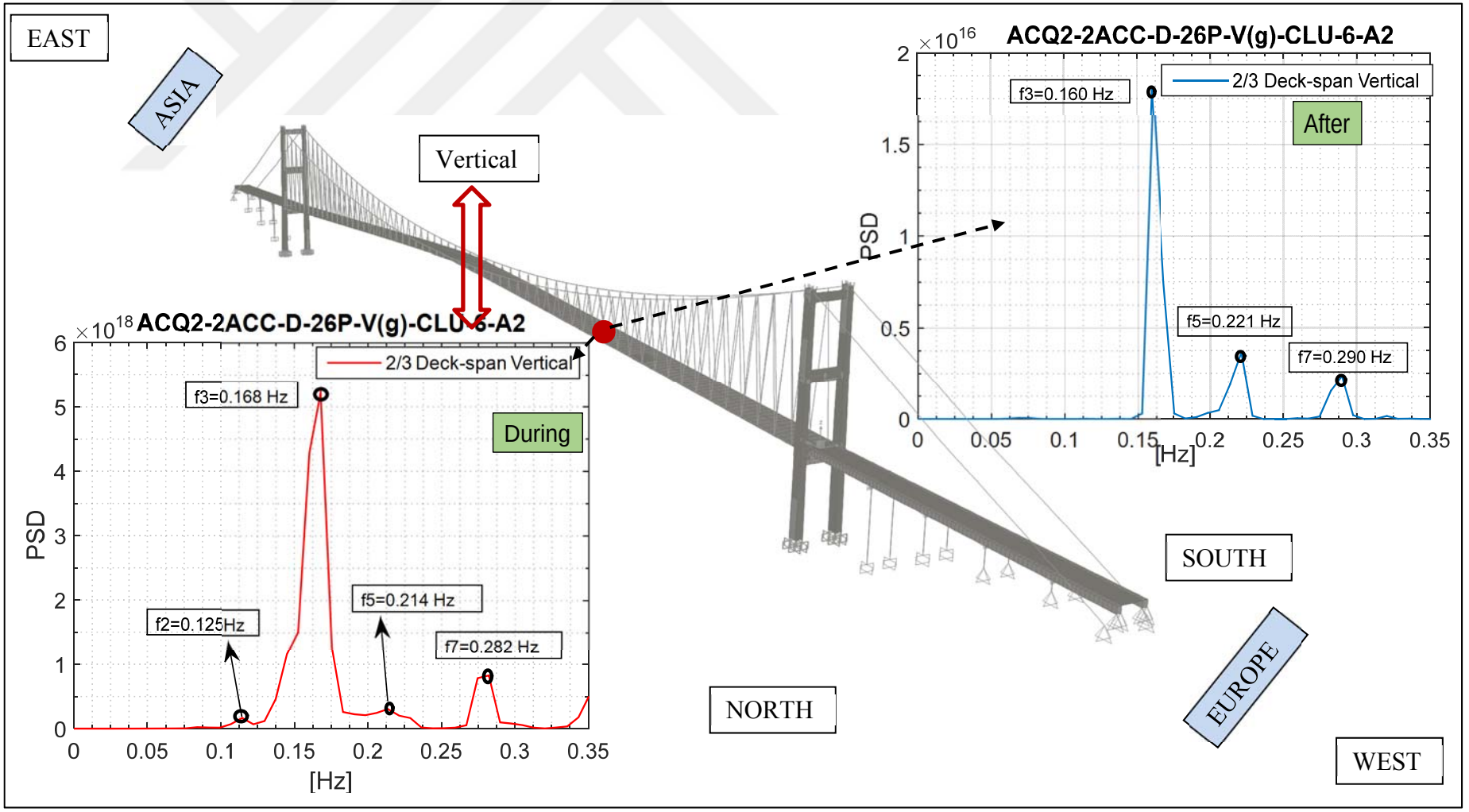

Figure 6.52 : Power Spectral Density (PSD) of the acceleration data at the deck-2/3-span in vertical direction.

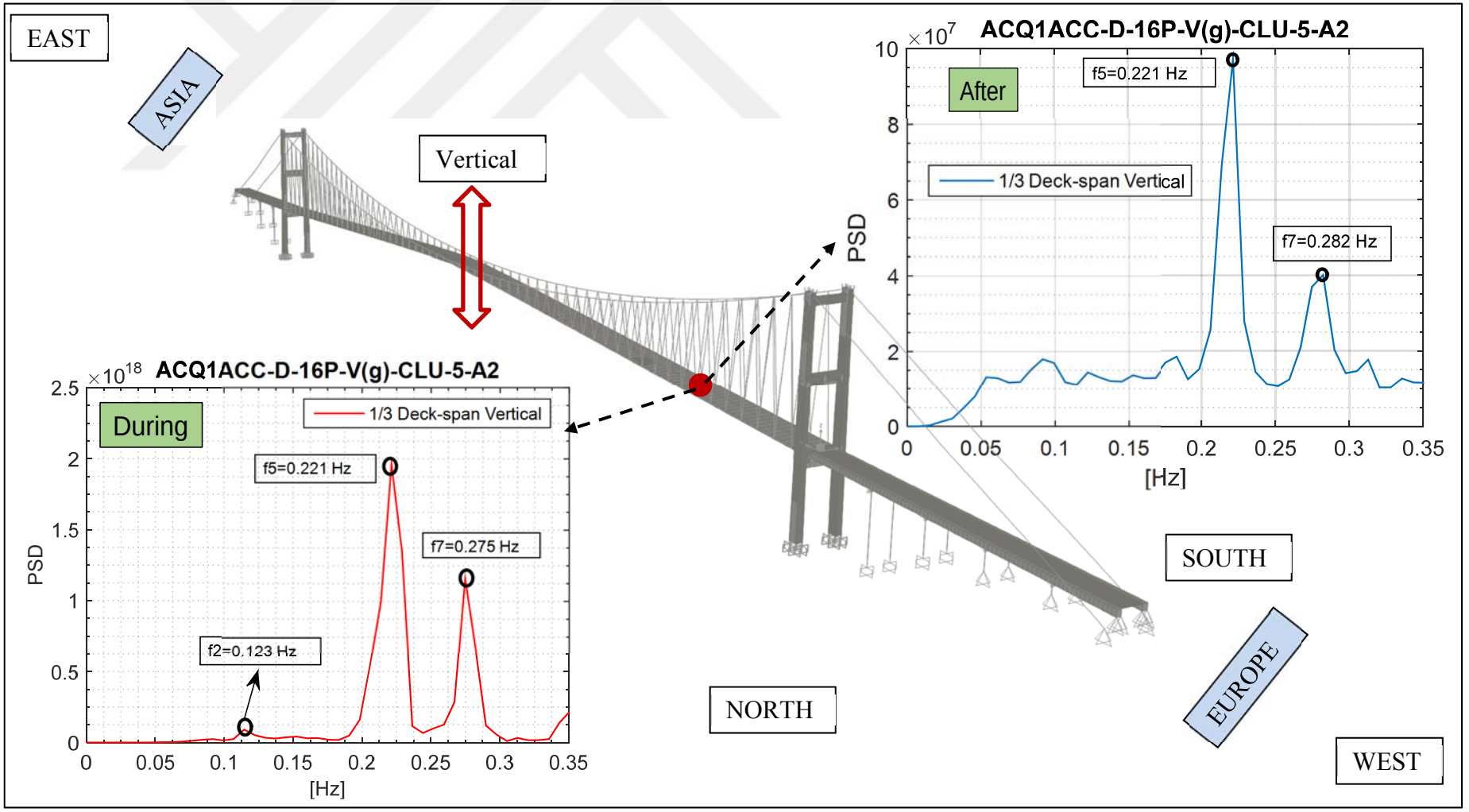

Figure 6.53 : Power Spectral Density (PSD) of the acceleration data at the deck-1/3-span in vertical direction.

Owing to the mentioned reason above for Mode-6 (1st Deck T), % change of this mode is obtained to be same as that of Mode-7. Depending on % change in the vertical modes of the bridge under the strong wind, only Mode-3 (1st Deck V_{symm}) is determined to be slightly influenced with 2.50 % increase in its period/frequency, whereas the other vertical modes with % change less than 1.0 are estimated not to be affected.

When it comes to the longitudinal direction, the acceleration data obtained from both tower top-saddles are considered for PSD analyses as indicated in Figures 6.54-55. Any tower mode shape of the bridge in longitudinal direction cannot be identified from the modal analysis of the FE model in the first fifty mode shapes. As expected, no longitudinal mode frequency is determined from the acceleration data as shown in Figures 6.54-55. The outcomes from these sensors are pertained to the deck vertical mode shapes since the longitudinal response of the towers directly affects the vibration of the deck.

Table 6.8 : Modal identification of longitudinal modes of the bridge.

Mode Type	Mode Number	Mode Shape	Experimental (Longitudinal Direction)						Graphical Presentation
			During		After		Change (%)		
			Period [s]	Freq. [Hz]	Period [s]	Freq. [Hz]	Period [s]	Freq. [Hz]	
Deck Modes	Mode-1	1st L_{sym}							No Graphical Presentation
	Mode-2	1st V_{asym}							
	Mode-3	1st V_{sym}	6.250	0.160	6.250	0.160	-	-	
	Mode-4	1st L_{asym}							
	Mode-5	2nd V_{sym}	4.525	0.221	4.525	0.221	-	-	
	Mode-6	1st T							
	Mode-7	2nd V_{asym}							
Tower Modes	Mode-8	1st L_{sym}							
	Mode-9	1st L_{asym}							

L_{sym}: Lateral symmetric; L_{asym}: Lateral asymmetric;V_{sym}:Vertical symmetric; V_{asym}:Vertical asymmetric; T: Torsional

Accordingly, Mode-3 (1st Deck V_{symm}) and Mode-5 (2nd Deck V_{asymm}) are identified from the both ranges. As revealed in Figures 6.54-55, it is also worth to note that the obtained PSD values from two accelerometers for each range are the same. All identification results are summarized in Table 6.8. The mean frequency values of the data for each range are taken into account in Table 6.8. The outcomes demonstrate that no % change in Mode-3 and Mode-5 is obtained due to same results from each range.

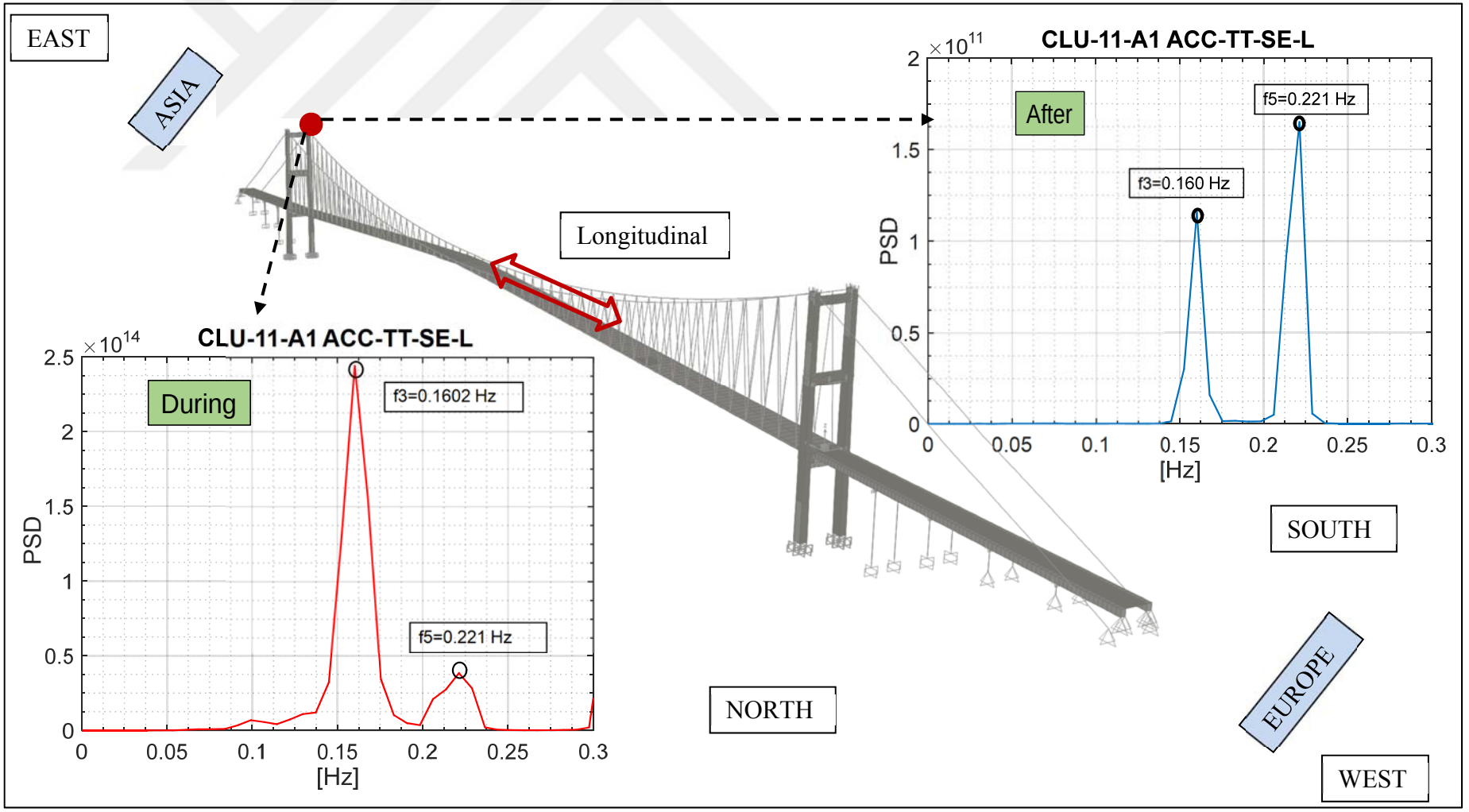

Figure 6.54 : Power Spectral Density (PSD) of the acceleration data at tower-top-south-east in longitudinal direction.

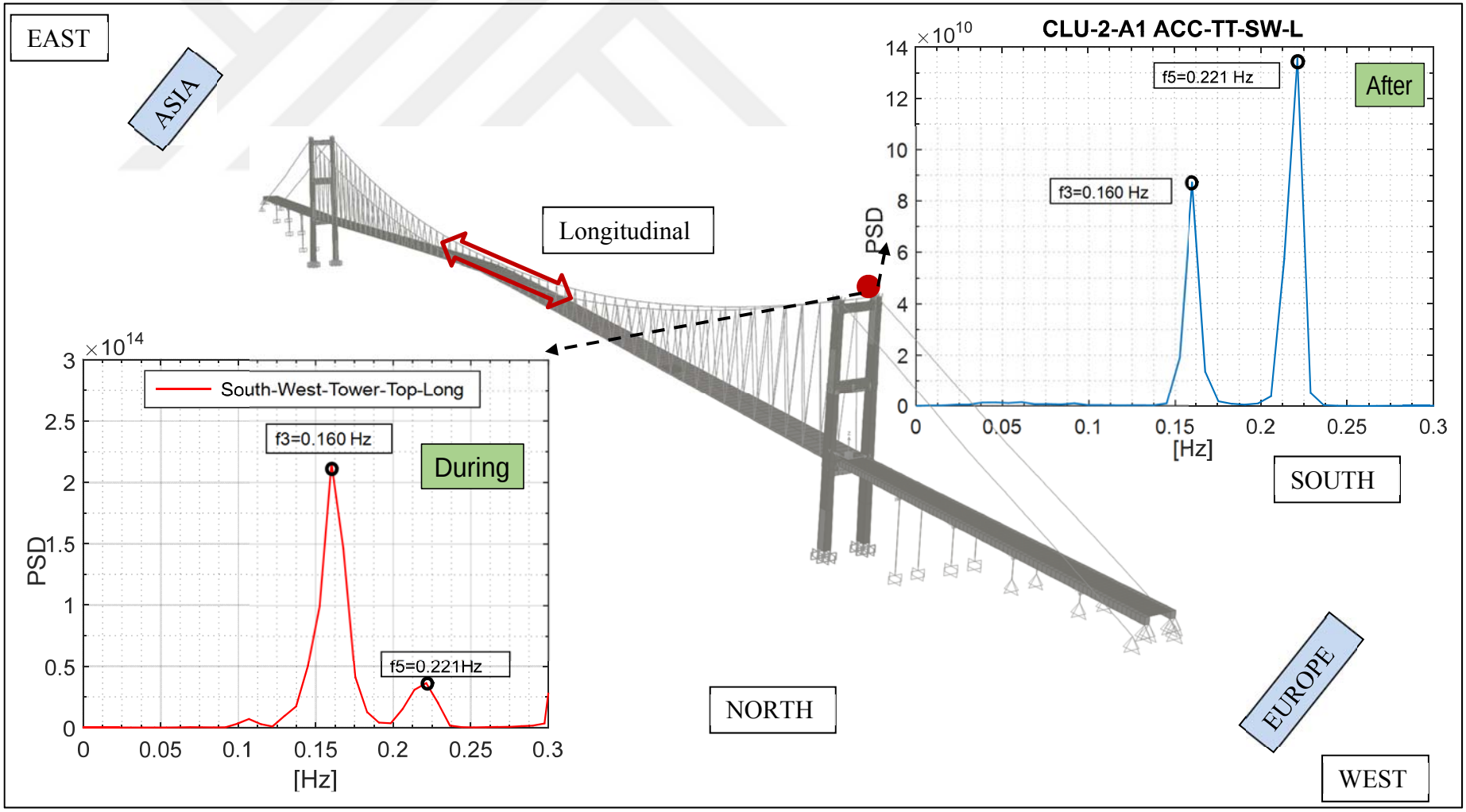

Figure 6.55 : Power Spectral Density (PSD) of the acceleration data at tower-top-south-west in longitudinal direction.

6.4 Calibration of FE Models of the Bridge

As stated in the previous sections, the results from "After" range can be considered as natural vibration characteristics of the bridge. In addition to the other studies in literature, "After" range provides opportunity to make calibration of the developed FE models with inclined hangers. Therefore, the comparison of the outcomes from "After" with those from the developed FE models are made as given in Table 6.9 for the spine-beam FE model and in Table 6.10 for the full-scale shell FE model.

Table 6.9 : Comparison of the spine-beam FE model with the experimental results.

Mode Type	Mode Number	Mode Shape	Comparison (Spine-beam FE model and Experimental)						Graphical Presentation
			Frame Model		After (Experimental)		Change (%)		
			Period [s]	Freq. [Hz]	Period [s]	Freq. [Hz]	Period [s]	Freq. [Hz]	
Deck Modes	Mode-1	1st L_{sym}	12.984	0.077	12.766	0.078	1.707	**-1.679**	
	Mode-2	1st V_{asym}	7.217	0.139	8.065	0.124	-10.505	**11.738**	
	Mode-3	1st V_{sym}	6.453	0.155	6.250	0.160	3.251	**-3.149**	
	Mode-4	1st L_{asym}	4.926	0.203	4.967	0.201	-0.819	**0.825**	
	Mode-5	2nd V_{sym}	4.561	0.219	4.525	0.221	0.809	**-0.803**	
	Mode-6	1st T	3.806	0.263	3.546	0.282	7.329	**-6.738**	
	Mode-7	2nd V_{asym}	3.759	0.266	3.542	0.282	6.129	**-5.785**	
Tower Modes	Mode-8	1st L_{sym}	3.309	0.302	3.319	0.301	-0.289	**0.304**	
	Mode-9	1st L_{asym}	3.222	0.310	2.855	0.350	12.841	**-11.380**	

L_{sym}: Lateral symmetric; L_{asym}: Lateral asymmetric;V_{sym}:Vertical symmetric; V_{asym}:Vertical asymmetric; T: Torsional

According to % change in Table 6.9, the maximum error % is obtained for Mode-2 and Mode-9 with approximately 11%. For the other modes, the error is in the range of 0-7.0 %. As mentioned in the previous section, Mode-2 is identified only from "During" range instead of "After" range considered for ambient vibration. Therefore, such high error in Mode-2 is dependent on that the mode is not be identified from "After" range. Generally, the error range for the first nine mode shapes of the bridge is allowable level. These conclusions revel that the considerations utilized in FE modeling of the Bosphorus Bridge are estimated well and are properly implemented.

Similar consequences are also determined for the comparison between the full-scale shell FE models and "After" range. As presented in Table 6.10, the error % change ranges from 1.16 % to 12.01 %. The maximum value is obtained with 12.01 % for

Mode-2. This is related to the reason mentioned above. Compared to the results from the spine-beam FE model, Mode-9 is identified very well by the full-scale shell FE mode due to five times lower error % than that of the spine-beam model. This yield to a conclusion that the considerations for the full-scale shell FE model of the towers are more realistic than those of the spine-beam FE model.

Table 6.10 : Comparison of the full-scale FE model with the experimental results.

Mode Type	Mode Number	Mode Shape	Comparison (Full-scale FE model and Experimental)						Graphical Presentation
			Shell Model		After (Experimental)		Change (%)		
			Period [s]	Freq. [Hz]	Period [s]	Freq. [Hz]	Period [s]	Freq. [Hz]	
Deck Modes	Mode-1	1st L_{sym}	13.090	0.076	12.766	0.078	2.538	**-2.979**	
	Mode-2	1st V_{asym}	7.220	0.139	8.065	0.124	-10.472	**12.097**	
	Mode-3	1st V_{sym}	6.481	0.154	6.250	0.160	3.696	**-3.750**	
	Mode-4	1st L_{asym}	5.020	0.199	4.967	0.201	1.069	**-1.159**	
	Mode-5	2nd V_{sym}	4.620	0.216	4.525	0.221	2.102	**-2.262**	
	Mode-6	1st T	3.834	0.261	3.546	0.282	8.119	**-7.509**	
	Mode-7	2nd V_{asym}	3.588	0.279	3.542	0.282	1.301	**-1.284**	
Tower Modes	Mode-8	1st L_{sym}	3.453	0.290	3.319	0.301	4.050	**-3.893**	
	Mode-9	1st L_{asym}	2.920	0.342	2.855	0.350	2.264	**-2.214**	

L_{sym}: Lateral symmetric; L_{asym}: Lateral asymmetric;V_{sym}:Vertical symmetric; V_{asym}:Vertical asymmetric; T: Torsional

The results from the two comparisons indicates that the established FE models are reliably verified not only with the study in literature but also with the SHM data recorded during strong wind. Based on the calculated error changes in the first nine mode frequencies/periods, the reliability of the FE models are acceptable level for utilizations of the bridge, such as earthquake, heavy traffic analyses etc. Therefore, no further considerations are adopted for the model updating. The estimated structural specifications are also identified well according to comparative outcomes.

6.5 Influence of the Extreme Wind Event on the Modal Characteristics of the Bridge

Strong wind effects on dynamic response of the Bosphorus Bridge is investigated. For this aim, the investigation procedure mentioned above in detail is summarized for Mode-1 in Figure 6.56. Thus, the first consecutive effective singular modes of the deck and tower are identified separately for “During” and “After”. These modal frequencies are determined depending on investigating considerable change in the total mass

participation of interest direction. The results from "After" range provides to find the natural vibration frequencies of the bridge and to compare to those from "During" range. Thus, the effects of the extreme wind load on the modal characteristics of the bridge are determined in terms of % change in the period/frequency as given in Table 6.11.

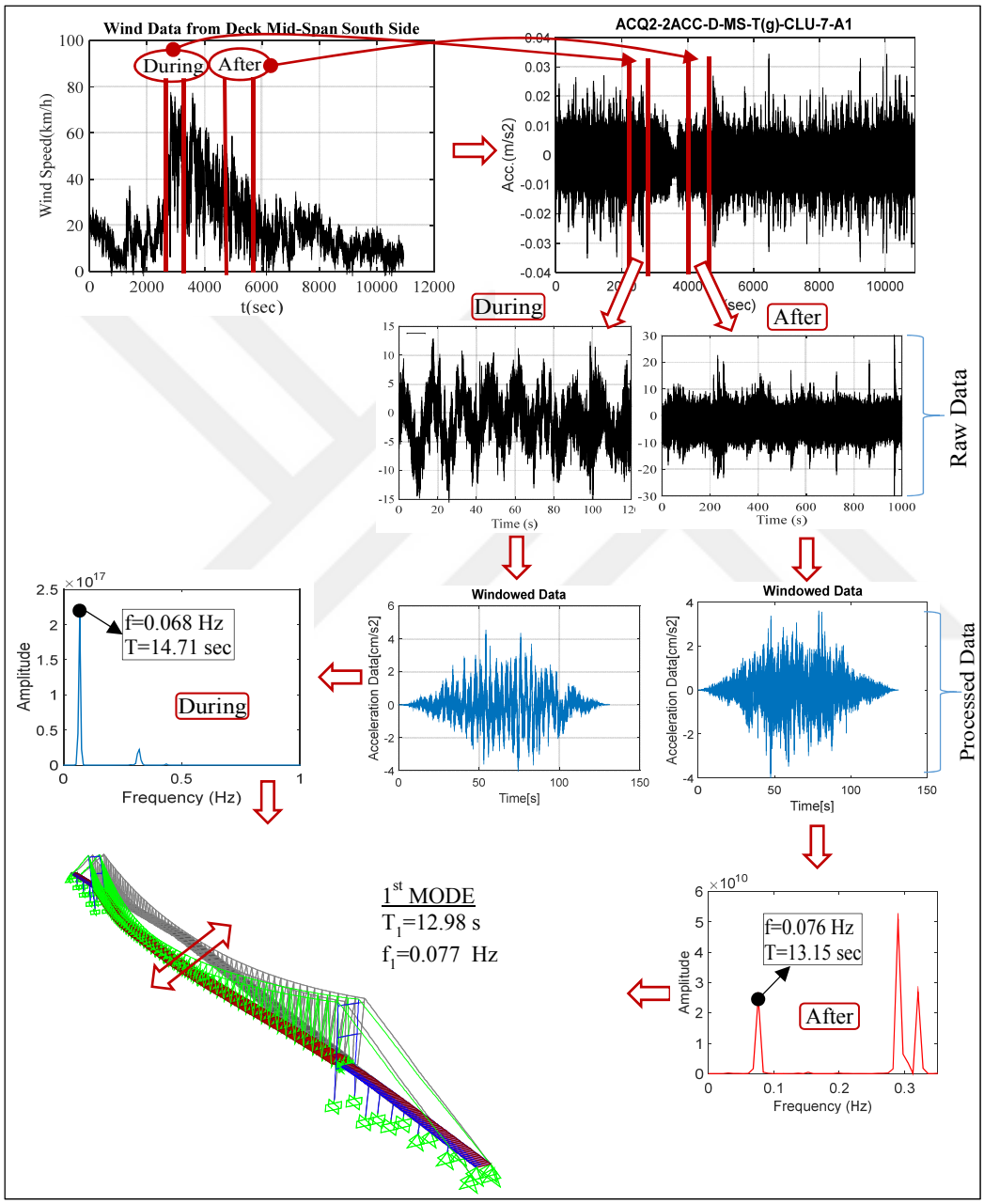

Figure 6.56 : The influence of the extreme wind on the modal features of the bridge.

From Table 6.11, maximum change in the modal frequencies of the bridge is obtained under for Mode-1 (1st Deck L_{symm}) with 15.20 % increase in the period or 13.20 % decrease in the frequency. The other modes, except for Mode-3 (1st V_{symm}) and Mode-

4 (1st L_{asymm}), are identified not to be affected from the strong wind event due to % change equal to or less than 1.0. Mode-3 and Mode-4 are also affected from the extreme wind with 2.5 % increase in the frequency. Based on these conclusions, the strong wind considerably excites the bridge in the transverse direction and leads to high movement in this direction. Moreover, the vibration characteristics of the bridge are determined to return to the natural vibration frequencies after the extreme wind load. This means that the bridge continues its service without damage. The qualitative comparison between the "During" and "After" ranges also indicates that the damping capacity of the bridge increased. This increase is estimated to result from the friction at the expansion joints and the change in the boundary conditions of the rocker bearings restrained for lateral direction.

Table 6.11 : Comparison of "After" with "During".

Mode Type	Mode Number	Mode Shape	Experimental (Comparison)						Graphic
			During		After		Change (%)		
			Period [s]	Freq. [Hz]	Period [s]	Freq. [Hz]	Period [s]	Freq. [Hz]	
Deck Modes	Mode-1	1st L_{sym}	14.706	0.068	12.766	0.078	15.196	**-13.191**	
	Mode-2	1st V_{asym}	8.065	0.124	8.065	0.124	0.000	**0.000**	
	Mode-3	1st V_{sym}	6.096	0.164	6.250	0.160	-2.469	**2.531**	
	Mode-4	1st L_{asym}	4.854	0.206	4.967	0.201	-2.265	**2.318**	
	Mode-5	2nd V_{sym}	4.561	0.219	4.525	0.221	0.798	**-0.792**	
	Mode-6	1st T	3.591	0.279	3.546	0.282	1.257	**-1.241**	
	Mode-7	2nd V_{asym}	3.591	0.279	3.542	0.282	1.376	**-1.358**	
Tower Modes	Mode-8	1st L_{sym}	3.405	0.294	3.319	0.301	2.611	**-2.544**	
	Mode-9	1st L_{asym}	2.837	0.353	2.855	0.350	-0.647	**0.651**	

L_{sym}: Lateral symmetric; L_{asym}: Lateral asymmetric;V_{sym}:Vertical symmetric; V_{asym}:Vertical asymmetric; T: Torsional

7. UTILIZATION, INTERPRETATION AND DECISION FOR PERFORMANCE PREDICTION: MULTI-POINT EARTHQUAKE ANALYSIS

One of the most significant events for all structures is earthquake excitation because of the various uncertainties in terms of seismology and response of structures to this event. Seismological properties of earthquakes, such as fault mechanism, seismic hazard and risk assessment etc. have been identified well utilizing the probabilistic and deterministic approaches. The response of structures to earthquake event; however, has still been studied by researchers in the field of structural engineering although many significant provisions are proposed by seismic codes, experimentally and theoretically conducted studies. With the help of field-reconnaissance and post-earthquake assessment after from destructive earthquakes, various methods and philosophies for earthquake analysis and earthquake-resistant design have been accurately developed, especially for the building structures. For seismic structural analysis of large-scale structures, such as long-span suspension or cable-stayed bridges, such advances are partially acceptable due to the complexity of these structures, which means that there is no general codes or standards for large-scale bridges. Therefore, special efforts for seismic analysis and design of long-span bridges need to be made by identifying its current structural properties and site soil conditions properly.

In the seismic analysis of structures, it is general assumption that earthquake induces structures uniformly, which means that the effects of site soil conditions are not considered. This idealization can be taken into account for building and short-span structures; however, for large-scale structures whose supports are likely to have different soil conditions, a special attention to these bridges needs to be paid. Therefore, various investigations and studies have been conducted in literature to identify the earthquake behavior of suspension bridges and cable-stayed bridges. For numerical analysis of suspension bridges, several idealizations and assumptions were made by Abdel-Ghaffar (1976) and Abdel-Ghaffar (1978). They proposed a method

including certain steps considering the theory of a linearized and the finite element. Abdel-Ghaffar and Rubin (1982) conducted a study on the multi-support earthquake analysis of suspension bridges. For this aim, they defined suitable ground motions performing finite Fourier Transform of real earthquake motion records. Abdel-Ghaffar and Rubin (1983) and Ahmed and Lawrance (1983a) also studied the vertical and lateral response of the Golden Gate Suspension Bridge to multi-support earthquake motions. They exhibited that more realistic response of suspension bridges could be obtained considering a number of modes and that uniform-support excitation did not yield to reliable results for the extended structures due to not having the ability to find out the most unfavorable case. In order to identify the nonlinear behavior of suspension bridges, an approach was proposed by Abdel-Ghaffar and Rubin (1983b) and Abdel-Ghaffar and Rubin (1983c), and they indicated the applicability of this approach considering the Golden Gate Bridge and the Vincent Thomas Bridge. A good relationship between experimental and numerical results was obtained by Ahmed and Robert (1985a) and Ahmed and Robert (1985b). A new method was proposed by Kiureghian and Neuenhofer (1992) for the multi-support earthquake analysis of structures under spatially varying earthquake excitations accounting for wave passage, coherency and local soil condition effects. Dumanoglu and Soyluk (2003) conducted a study on stochastic response of cable-stayed bridge under spatially varying seismic motions. In that study, dynamic behavior of long-span bridges was demonstrated to be relatively affected from spatially varying ground motions. Therefore, they concluded that the varying earthquake motions should be considered in the analysis of large-scale structures. Site-specific ground motions were utilized for stochastic earthquake analysis of a cable-supported bridge. From the analysis, the supports of the bridge were relatively affected under spatially varying earthquake motions (Dumanoglu and Severn, 1990; Dumanoglu and Soyluk, 2003). Recently conducted studies from Alexander (2008), Karmakar et al. (2012), Soyluk and Sicacik (2012), Wang et al. (2009) and Zhao et al. (2015) were also focused on the investigation of the effects of multi-support earthquake excitation on existing long-span bridges.

After from the destructive earthquakes in last two decades in Turkey, Izmit (1999) and Duzce (1999) earthquakes, the public awareness of structural earthquake safety and performance of the existing structures in Turkey has increased progressively. General Directorate of Turkish State Highways (KGM) conducted a number of rehabilitation

projects (JBSI 2004) for the most critical long-span bridges in Turkey, the Bosphorus and the Fatih Sultan Mehmet Bridges. Besides, researchers in bridge engineering carried out important studies for these bridges. The first informative and prominent studies were conducted by Brownjohn et al. (1992), Brownjohn et al. (1989), Dumanoglu et al. (1992), Dumanoglu and Severn (1990) and Erdik and Uckan (1989) on system identification of the bridges based on the experimental results. Ambient vibration test was performed by Brownjohn et al. (1989) and Erdik and Uckan (1989) to extract the vibration properties of the Bosphorus Bridge using monitoring data. They resulted in these studies with a closure agreement between experimental outcomes and those from numerical analysis. Brownjohn et al. (1992) conducted a much more comprehensive study on full-scale dynamic testing of the Fatih Sultan Mehmet Bridge to identify experimental and theoretical dynamic characteristics of the bridge. Utilizing data recorded from the reference accelerometers installed on the critical points at the deck and the towers of the bridge, lateral, vertical, torsional and longitudinal mode shapes and associated frequencies were extracted. In other studies from Brownjohn et al. (1992) and Dumanoglu et al. (1992), dynamic properties of the Fatih Sultan Mehmet Bridge and earthquake-induced behavior of the bridge were also investigated. Recently new studies were also conducted for these bridges by Apaydin (2002), Apaydin (2010), Erdik and Apaydın (2007) and Kosar (2003). In order to determine natural vibration characteristics of the Bosphorus Bridge and to verify experimental results with those from the other studies in literature, ambient vibration survey was utilized and finite element model-FE of the bridge was established by Kosar (2003). Relatively detailed investigation was performed for the 2nd Bosphorus Bridge by Apaydin (2002). Along with experimental testing study, this study investigated the earthquake behavior of the bridge considering uniform-support excitation. Travelling earthquake analysis was also conducted for determining the effects on seismic response of the bridge to this event. Seismic performance evaluation of two approach viaducts of the Bosphorus Bridge was investigated by Bas (2011) to indicate the efficiency of the performance-based assessment and design code of TSC-R (2008). The outcomes obtained from the study showed good relationship between the provisions of (TSC-R 2008) and CalTrans (2001). Depending on the performance of the viaducts, retrofitting investigation was made for their columns. Consequently, this study has revealed that performance evaluation of the side-span including damage investigation of potential structural elements is necessary for reliable retrofitting of the

bridge although no plastic deformation need to be considered for the main span of the bridge. Detailed study on the earthquake behavior and retrofit needs for the Fatih Sultan Mehmet Bridge and the Bosphorus Bridge was carried out by Apaydin (2010). For this purpose, realistic uniform earthquake motion records generated according to the seismic demand of the bridges given in KGM (2004) were utilized considering site-soil properties of the located region of the bridges and the earthquake scenario M_w=7.4 for active Marmara Fault. This study also presented the considerations for FE model of the bridges. Based on the results from the uniform-support earthquake analysis, the need for considering the multi-support earthquake analysis was stated for long-span bridges. Moreover, dampers replaced to the tower-deck points close to the rocker bearings was recommended so as to reduce longitudinal translation of the deck. Apaydin et al. (2016) conducted recently new study on the performance prediction of the Fatih Sultan Mehmet Bridge under site-specific spatially varying multi-support earthquake excitation. They utilized specifically generated strong ground motions for the earthquake analysis. The comparative outcomes from the study indicated that the multi-support earthquake analysis should be considered for long-span suspension bridge to reliably identify structural behavior of the bridge and thus to determine the most suitable retrofit project for the bridge.

As mentioned in the references, either no or limited elaborate investigations on structural performance of the Bosphorus Bridge were made. Particularly, there is no specific study for the multi-point earthquake analysis (Mp) of the bridge in the literature. The related studies in literature were basically focused on the uniform-point (Up) analysis of the bridge. Therefore, the Mp analysis is required to better understand the seismic behavior of the Bosphorus Bridge. Considering these recommendations, this chapter of the dissertation aims at determining the effects of spatially varying earthquake motion on the Bosphorus Bridge, at presenting the practice-oriented multi-point earthquake analysis procedure for the bridge, and at offering more reliable results from the multi-point earthquake analysis to recommend the most suitable retrofit strategy for the bridge. For this objective, spatially varying site-specific earthquake motion records are generated taking the geographic coordinates and site-specific conditions of the bridge's supports of the anchorage and tower at each side into account. In order to make earthquake analysis of the bridge, the developed spine-beam FE model is used. In addition, practice-oriented multi-point earthquake analysis

procedure easily implementable for long-span structures is proposed. Utilizing the advanced FE model of the bridges and proposed analysis method, the results obtained from the Mp are presented and are compared with those from the uniform-point earthquake analysis (Up) to demonstrate the effect of the Mp on the seismic performance prediction of the bridge. Moreover, similar efforts are made for the bridge with vertical hanger. Thus, the effects of the change in hanger form on the earthquake response of the bridge are also identified. Along with the simulation of the scenario earthquake, spectrum compatible earthquake records are also generated according to the DD-1 earthquake level spectrum given in the new Turkish Seismic Code. Based on the comparative outcomes, the most critical bridge's components in terms of structural rehabilitation are determined. Certain recommendations are given for these critical elements of the bridge.

7.1 Spatially Varying Site-Specific Earthquake Motions

In order to simulate site-specific ground motions, geographic coordinates of the bridge's support points has firstly to be determined. As indicated in Figure 7.1, the support coordinates of the bridge are obtained depending on the general coordinates of the bridge. Figure 7.1 also presents the general considerations of the practice-oriented multi-point earthquake analysis of the bridge. Utilizing these coordinates of the bridge, the stochastic modeling technique proposed by Boore (1983) is used to generate earthquake ground motions. This technique that considers the earthquake as a point source was then extended by Beresnev and Atkinson (1997) and Beresnev and Atkinson (1998). They divided the fault plane into small rectangular subfaults treating as point source. The subdivided faults featured separated point sources. This extended new version having stochastic character was programmed, FINSIM (FINite fault SIMulation program), by Beresnev and Atkinson (1998). Taking the scenario earthquake of M_w=7.4 predicted to occur with the probability of 70 % in next 30 years in Istanbul into consideration, the FINSIM was modified and adapted by Böse (2006) to develop early-warning system for Istanbul estimating site-specific ground motions. Further explanations for these considerations could be found in Böse (2006). Another important step to produce site-specific earthquake ground motion for the bridge is to specify very well the parameters to be used in the modified FINSIM. For this purpose, the detailed study of Ansal et al. (2009) is utilized. The parameters that are determined

for the loss estimation in Istanbul and that reflect deterministically the seismicity of Istanbul are given in Table 7.1. Besides, these simulation parameters are determined from a number of scientific reseach projects and studies conducted for the Izmit (1999) earthquake that is the most destructive recent earthquake in the history of Istanbul. Since the FINSIM simulation requires aforementioned deterministic earthquake parameters, the Kocaeli EQ (1999) is adopted for the simulation. On the other hand, the simulated multi-point earthquake motions are used to produce design spectrum compatible earthquake records.

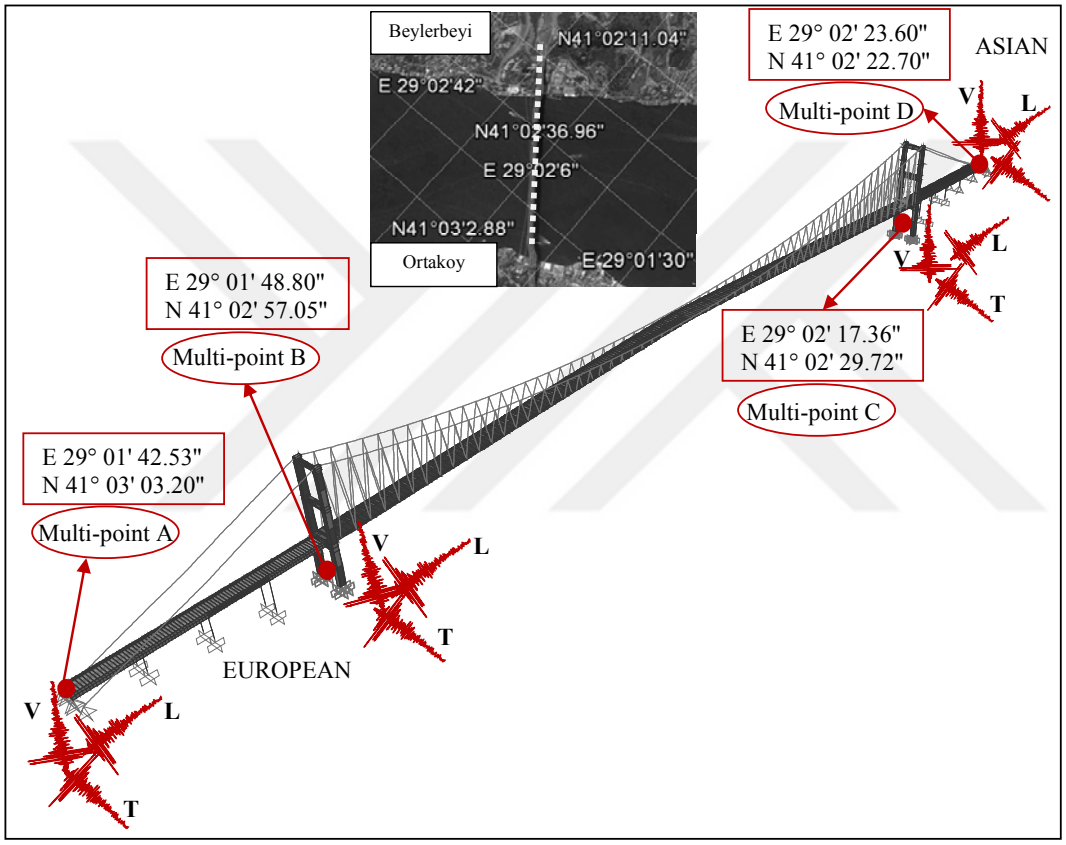

Figure 7.1 : Description of geographic coordinates of the support points of the bridge.

Depending on the comparison of the acceleration response spectra of the scenario multi-point earthquake motions with those corresponding to the DD-1 and DD-2 earthquake levels defined in the new Turkish Seismic Code (TSC, 2007) which design spectrum will be utilized is determined for this aim. Therefore, three different multi-point earthquake simulations are estimated to be conducted: (i) scenario multi-point earthquake motion (ii) DD-1 spectrum compatible multi-point earthquake motion (iii) DD-2 spectrum compatible multi-point earthquake motion. Details for these earthquake motions are given in the following sections.

Table 7.1 : The parameters for simulation of ground motions.

Parameter	Parameter value
Fault orientation	Strike 81.5°, Dip 90°
Fault dimensions along strike and dip (km)	108 by 20
Stress parameter (bars)	100
Subfault dimensions (km)	10 by 10
Moment (dyn·cm)	1.7×10^{27}
Moment magnitude	7.4
Inelastic attenuation Q(f)	$180 \cdot f^{0.45}$
Geometric spreading	$1/R \leq 30$km $1/R^{0.4}$ 30-60 $1/R^{0.6}$ 60-90 $1/R^{0.8}$ 90-100 $1/R^{0.5} > 100$
Windowing function	Saragoni-Hart
Crustal-shear wave velocity (km/sec)	3.3
Crustal density (g/cm^3)	2.7
Focal mechanism	Strike slip

7.1.1 Scenario multi-point earthquake records

Stochastic simulation is conducted using the well-known parameters of the Kocaeli Earthquake (1999) given in Table 7.1. The code for Finite-Fault Simulation (FINSIM) is utilized for the simulation. Due to fact that the effective mode periods of the Bosphorus Bridge are generally higher than T=1.0 s, multi-point earthquake records are determined by matching long-period (T>1.0 s) part of the response spectrum of the records with that of the design response spectrum of DD-1 earthquake level according to the new Turkish Seismic Code TSC (2017). The DD-1 earthquake level with a 2 % probability of exceedance in 50 years corresponding to return period of 2475 years is the maximum earthquake to be considered in earthquake resistant design of structures. As given in Table 7.2, general specifications of DD-1 earthquake are determined for the Bosphorus Bridge. Considering these parameters, plotting parameters are also calculated using the equations 7.1-4. These calculated parameters are then used to plot response spectrum whose characteristics are presented in Figure 7.2.

Table 7.2 : General specifications of DD-1 design response spectrum.

DD-1 Earthquake Level Spectrum		
S_s	Short period spectral acceleration constant =	1.50
S_1	T=1.0 s period spectral acceleration constant =	0.40
F_s	Local site effect coefficient for S_s=	1.00
F_1	Local site effect coefficient for S_1=	1.00
γ_F	Near-fault constant=	1.20

$$S_{DS} = S_S F_S = 1.50 \cdot 1.00 = 1.50 \quad (7.1)$$

$$S_{D1} = S_1 \gamma_F F_1 = 0.40 \cdot 1.20 \cdot 1.00 = 0.48 \quad (7.2)$$

$$T_A = 0.20 \frac{S_{D1}}{S_{DS}} = 0.20 \frac{0.48}{1.50} = 0.064 \quad (7.3)$$

$$T_B = \frac{S_{D1}}{S_{DS}} = \frac{0.48}{1.50} = 0.32; T_L = 6.0 \text{ s} \quad (7.4)$$

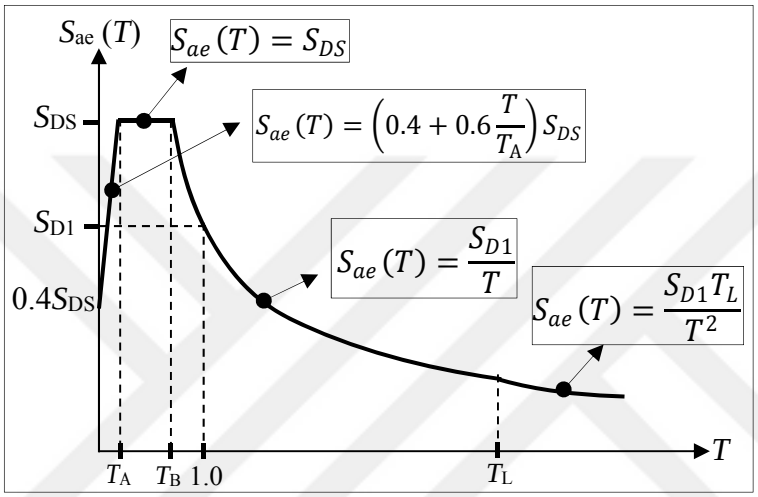

Figure 7.2: General curve for response spectrums in TSC (2017).

where;

S_{ae}=Elastic design spectral acceleration (g)

S_{DS}= Design spectral acceleration constant for short period range.

S_{D1}= Design spectral acceleration constant for 1.0 sec period range.

Based on these considerations, the simulation process for scenario multi-point earthquake motion is performed and the acceleration ground motion time-histories (ATH) show in Figure 7.3 are generated for the Bosphorus Bridge. Although the process yields to the ATHs, the displacement ground motion time histories (DTH) need to be obtained for the multi-point earthquake analyses. Therefore, the scenario DTHs are presented in Figure 7.4. As shown in Figure 7.4, the triple-direction (two horizontals and one vertical) ground motions are generated for the each considered multi-point, A, B, C and D revealed in Figure 7.1. Total number of twelve ground motions were defined for the analysis. The process of base-line correction and

detrending is also performed to obtain relatively precise displacement ground motions and thus results from the multi-point earthquake analyses.

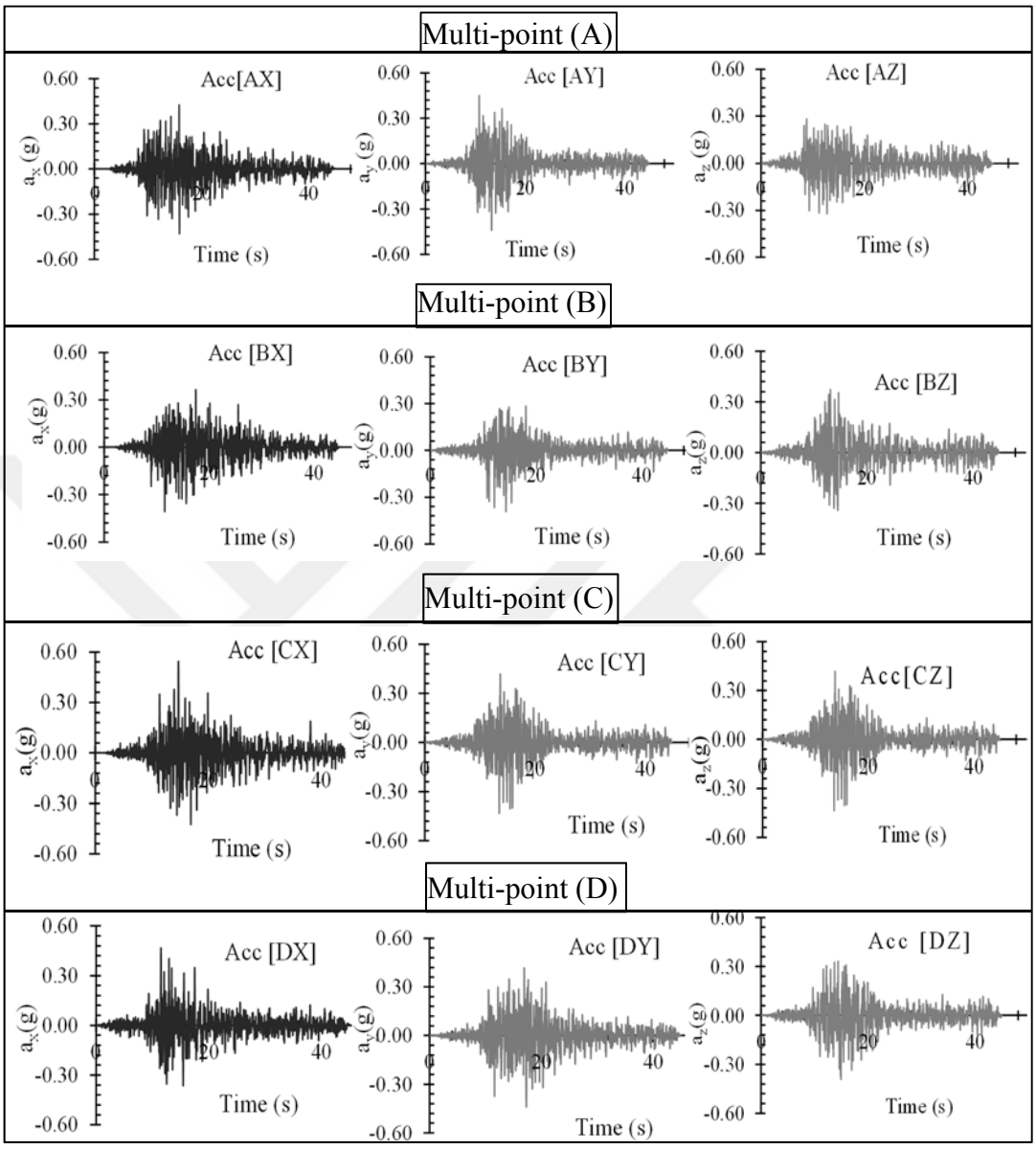

Figure 7.3 : Scenario multi-point acceleration earthquake time-histories.

In addition to the Mp earthquake analyses, the Up earthquake analysis that is well-known general earthquake analysis is carried out to compare the effects of the Mp earthquake motions with uniform-support motions on the basis of critical section force and movement capacity of the bridge. In an attempt to make Up analysis, the mean acceleration earthquake records obtained with arithmetic averaging of the scenario Mp earthquake motion in three directions are considered. These Up earthquake motions are given with blue line (mean) in Figure 7.4. From the comparative depiction given

in Figure 7.4, the Mp earthquake motions are observed to be relatively higher than the Up earthquake motions.

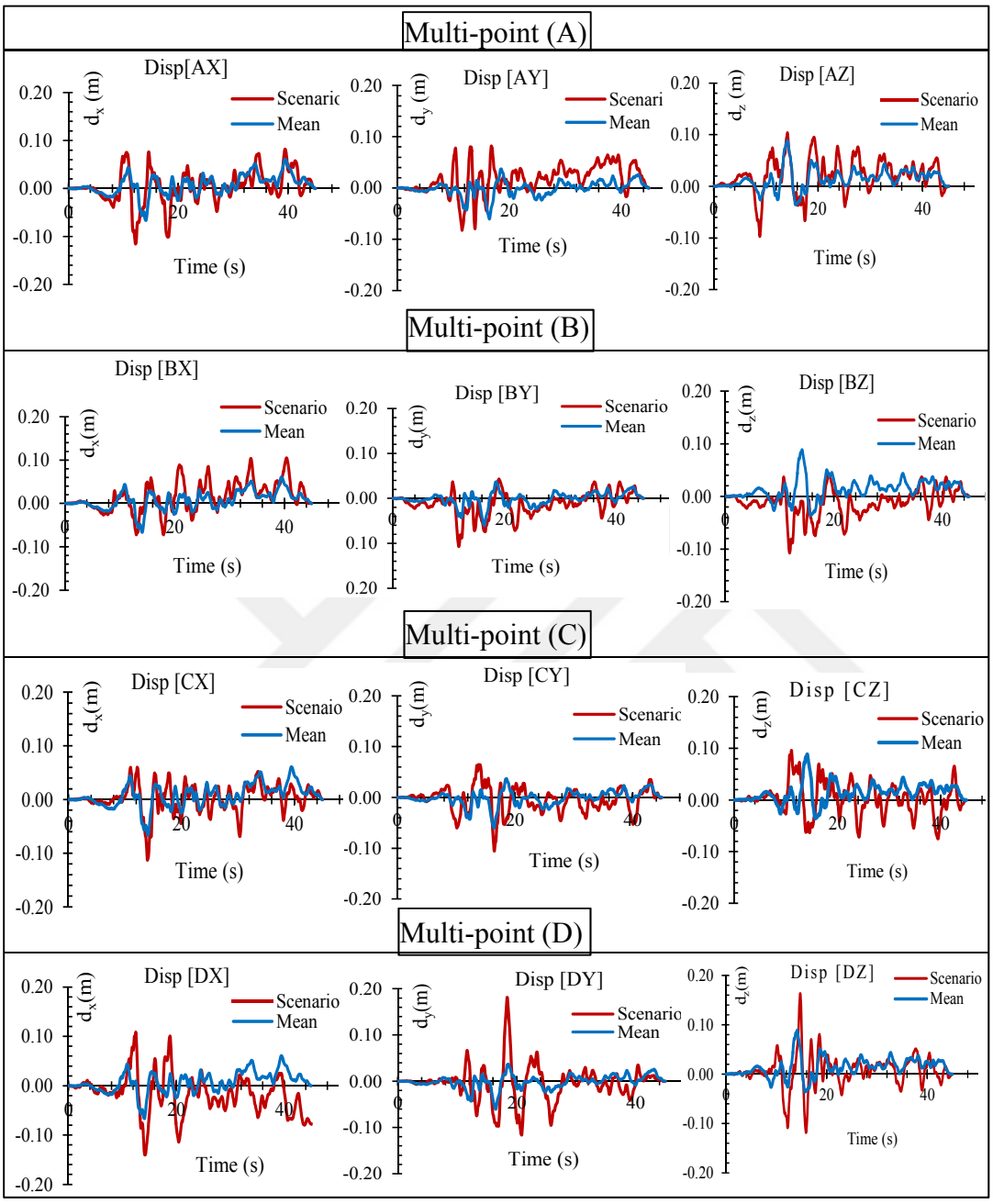

Figure 7.4 : Scenario multi-point and uniform-point displacement earthquake time-histories.

The simulation, as mentioned above, is performed in a compatible with the long-period part (T>1.0 s) of DD-1 design spectrum. The compatibility of acceleration response spectra of the simulated scenario multi-point earthquake motions are indicated in Figures 7.5-6. From these figures, a good agrrement is provided for long period region.

However, the spectral matching needs to be considered not only in long-period range but also in all periods due to high difference in the other periods (T<1.0 s). Based on this conclusion, fully DD-1 spectrum compatible multi-point earthquake records are decided to be generated considering the scenario multi-point earthquake records as source/reference earthquakes. Accordingly, the Mp analysis is also conducted for these simulated earthquakes.

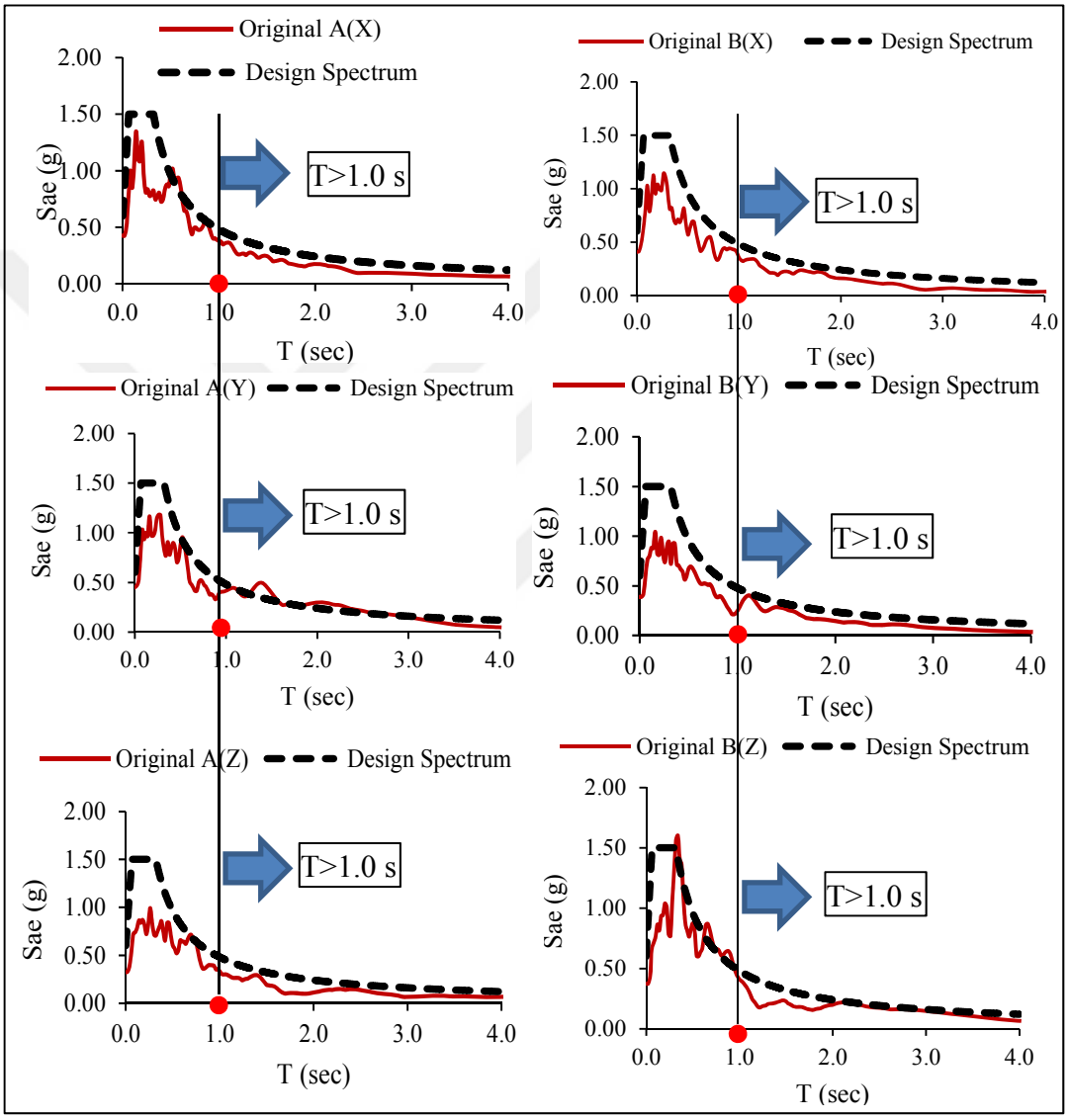

Figure 7. 5 : Comparison of the response spectrum of the scenario A and B multi-point earthquakes with DD-1earthquake level design spectrum.

In order to determine the earthquake level of the simulated scenario records, the response spectra of the scenario earthquakes are also compared with DD-1 and DD-2 design spectra. The DD-2 earthquake level features a 10 % probability of exceedance in 50 years corresponding to return period of 475 years. For this aim, plotting parameters of the DD-2 earthquake are determined using equations 7.1-4, and they are

summarized in Table 7.3. Thus, response spectra of the scenario earthquake for each multi-point in triple directions are depicted with the design response spectra in Figure 7.7.

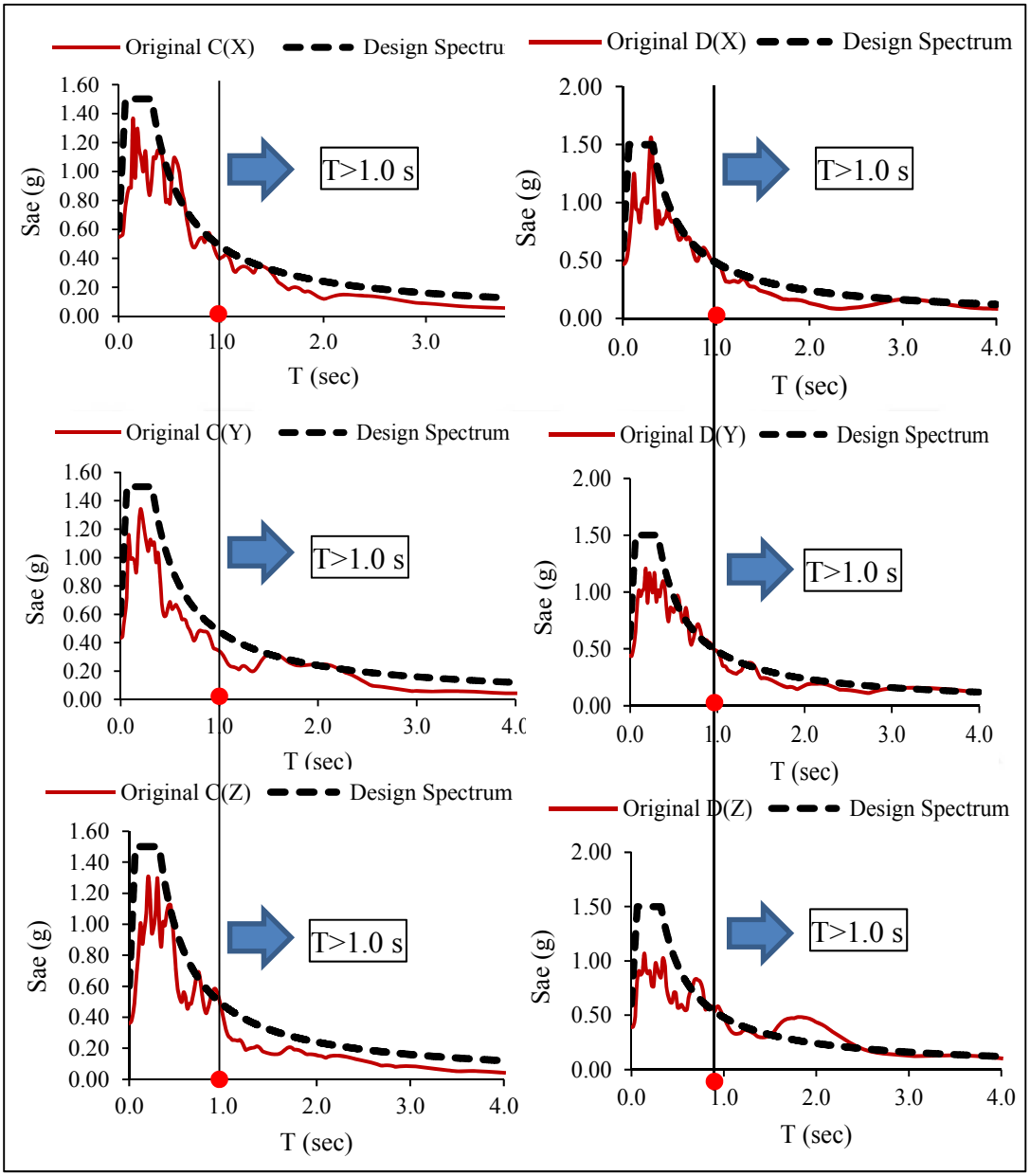

Figure 7.6 : Comparison of the response spectrum of the scenario C and D multi-point earthquakes with DD-1earthquake level design spectrum.

The response spectra of the scenario earthquakes are obtained as mean spectra of the design spectra, which means that the DD-1 and DD-2 design spectrums are the max. and min. limits of the scenario earthquake response spectra, respectively. Before the simulation process, the DD-1 and DD-2 design spectrum are estimated to be adopted for design spectrum compatible earthquake motions. As shown in Figure 7.7, nevertheless, the spectral values of the DD-2 are relatively lower than those of the

scenario earthquake motions. Therefore, the DD-2 spectrum compatible multi-point earthquake motions are decided not to be generated for the Mp analysis. From this conclusion, analysis results obtained from the DD-2 spectrum compatible earthquake are also estimated readily not to be critical in terms of the performance prediction of the bridge compared to those from the scenario earthquake.

Table 7.3 : General specifications of DD-2 design response spectrum.

DD-2 Earthquake Level Spectrum		
S_s	Short period spectral acceleration constant =	0.80
S_1	T=1.0 s period spectral acceleration constant =	0.20
F_s	Local soil-site effect coefficient for S_s=	1.00
F_1	Local soil-site effect coefficient for S_1=	1.00
γ_F	Near-fault effect constant=	1.20

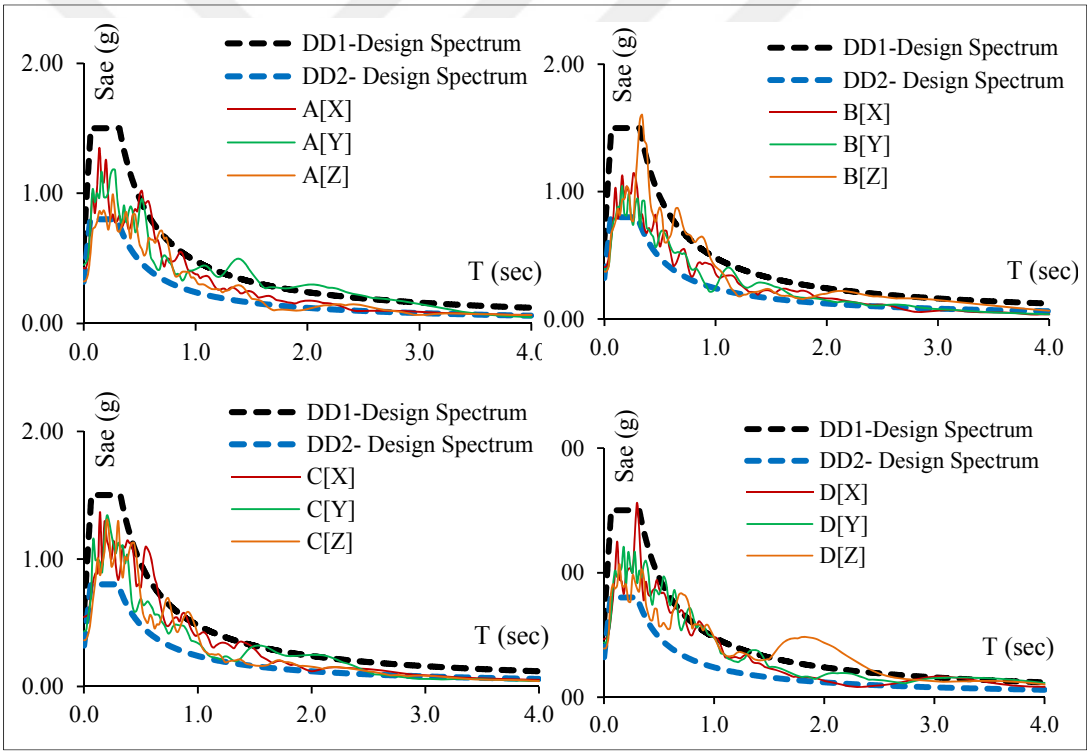

Figure 7.7 : Comparison of the reponse spectra of the sceanario earthquake records with the design spectrum of the DD-1 and DD-2 earthquake levels.

7.1.2 DD-1 design spectrum compatible multi-point earthquake records

Depending on the outcomes from the comparison as shown in Figure 7.7, new multi-point earthquake motions are obtained by fully matching with the DD-1 design spectra in all periods. For this objective, stochastically generated scenario earthquake records are considered as source earthquakes in order to feature the all parameters adopted in

the FINSIM simulation. In Figure 7.8, the matched multi-point earthquake motions are given with the scenario earthquakes in order to realize the difference between two simulations. Displacement obtained from the matched earthquake is relatively higher than that from the scenario earthquake. Thus, results from the Mp analyses under the matched multi-point earthquake motions are estimated to be more critical than those from the scenario multi-point earthquake motions that are generated in compatible with the long-period range of the design spectrum.

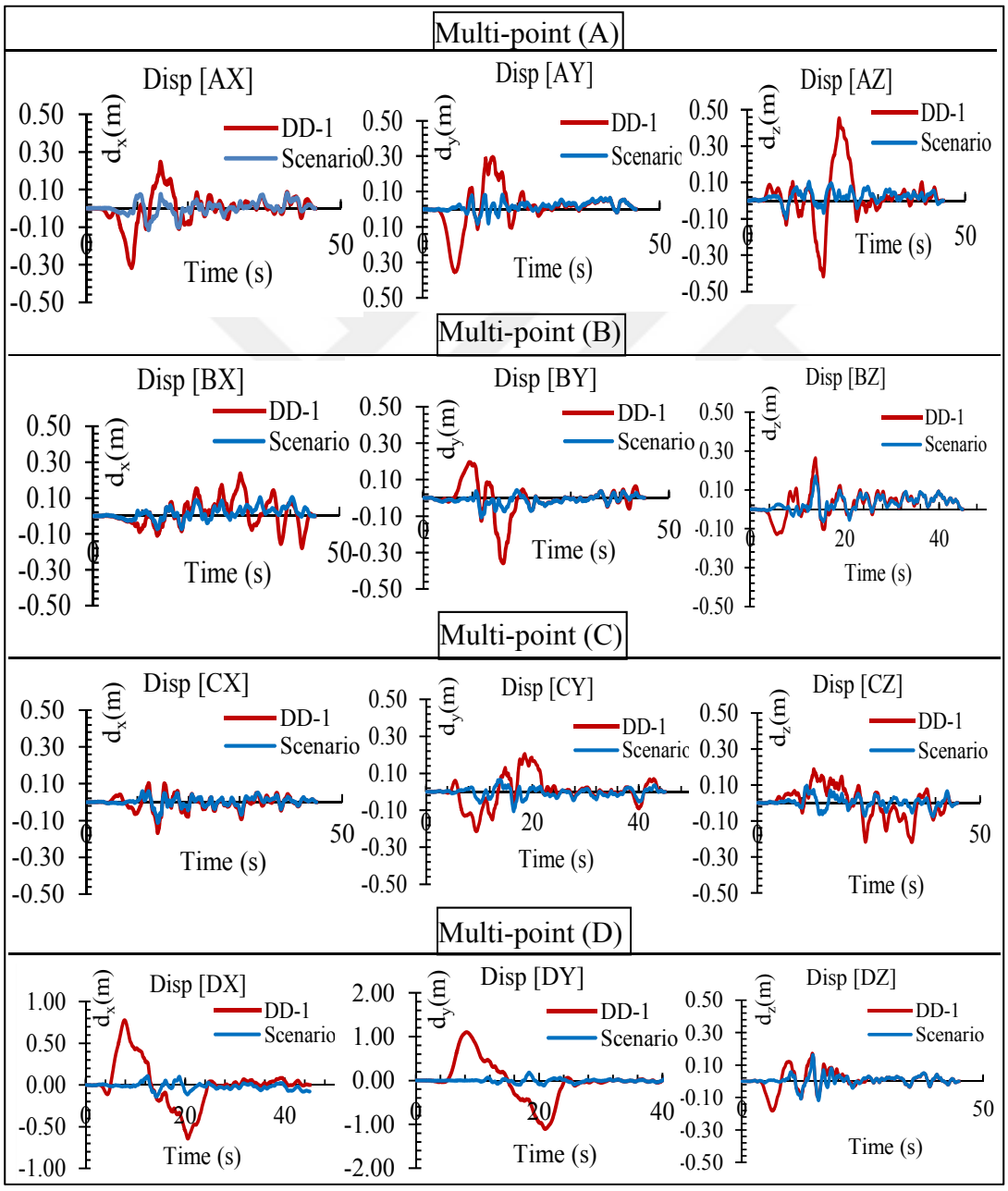

Figure 7.8 : The DD-1 spectrum compatible and scenario spatially varying site–specific multi-point displacement earthquake time-histories.

For the accuracy of the matching process, original, matched and the design spectrum are shown in one figure for each multi-point records as indicated in Figures 7.9-12. Based on the matching, relatively high compatible earthquake records with the design spectrum are obtained for the Mp analysis. Defining these EQ records, the Mp analysis is also conducted for two bridge models with inclined and vertical hangers.

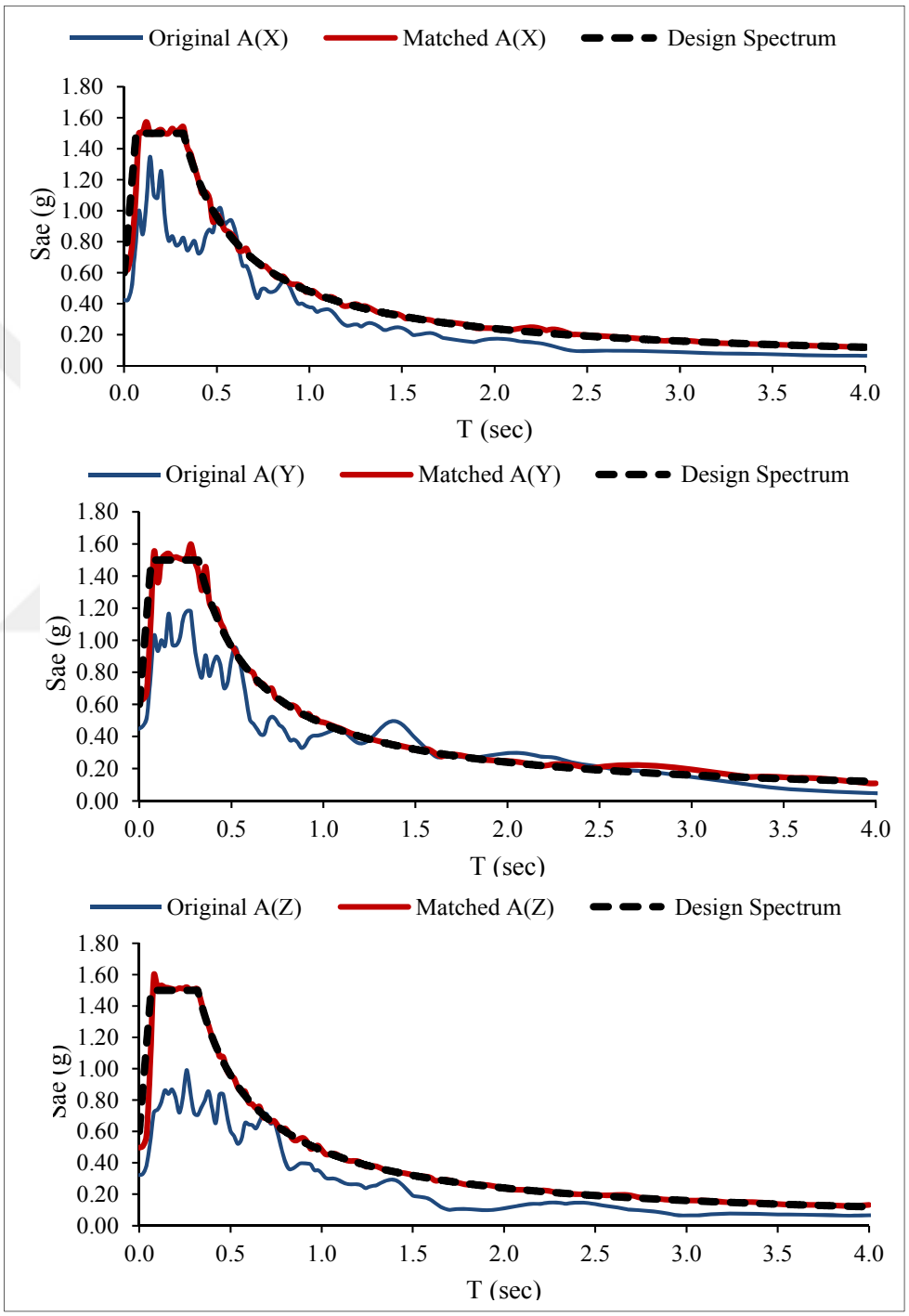

Figure 7.9 : Comparison of original, matched and DD-1 design spectrum for Multi-point (A).

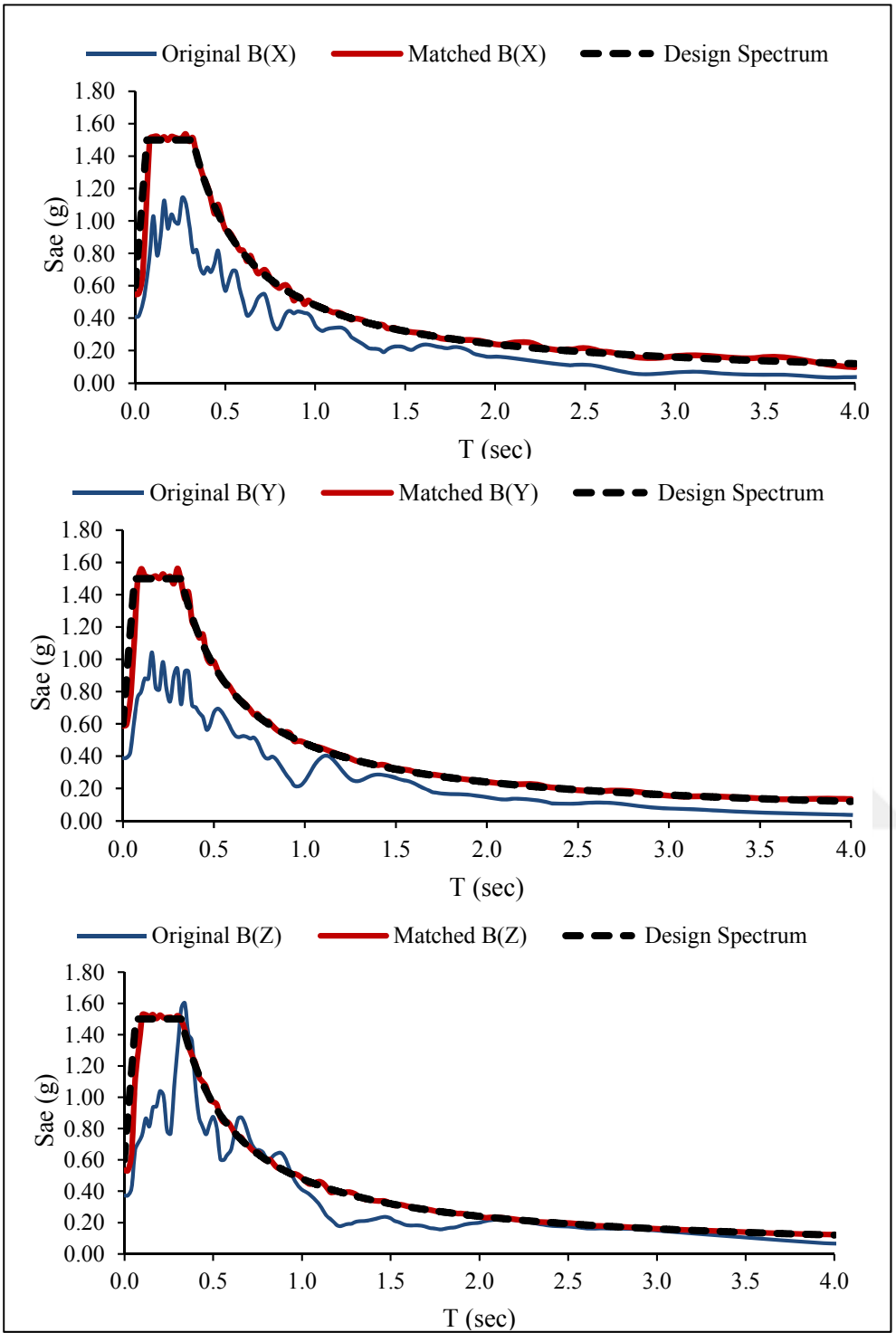

Figure 7.10 : Comparison of original, matched and DD-1 design spectrum for Multi-point (B).

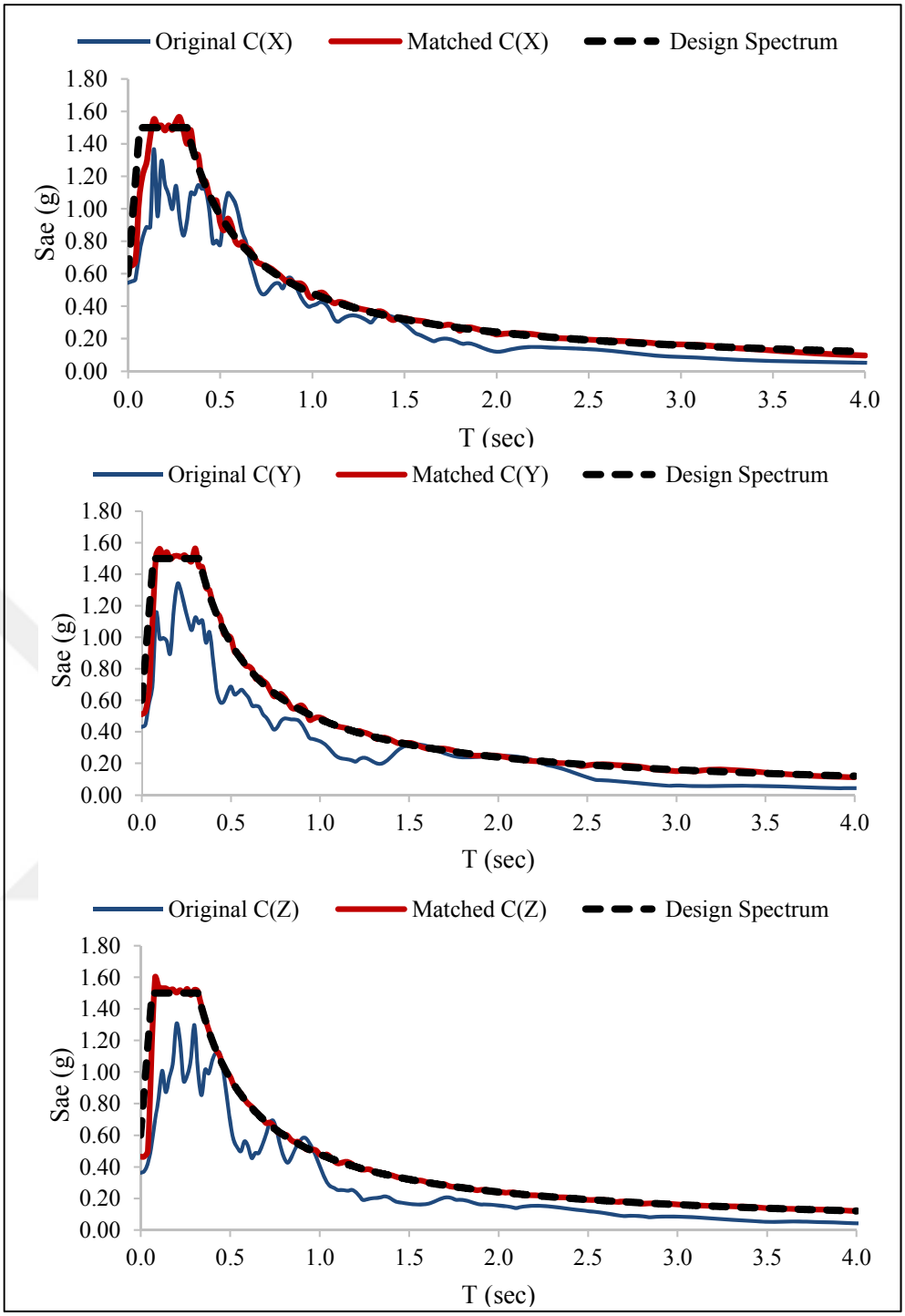

Figure 7.11 : Comparison of original, matched and DD-1 design spectrum for Multi-point (C).

For the Up analysis, uniform displacement time-histories that are determined from the average of the matched multi-point earthquake accelerations are taken into account. The obtained mean displacement time-histories are given in Figure 7.13. In order to make a comparison, the matched multi-point earthquake records are also presented in this figure. As demonstrated in Figure 7.13, the matched earthquakes have high

displacement values compared to the mean earthquakes; therefore, the Mp analysis results under the matched earthquakes are predicted to be higher than those under the mean earthquakes.

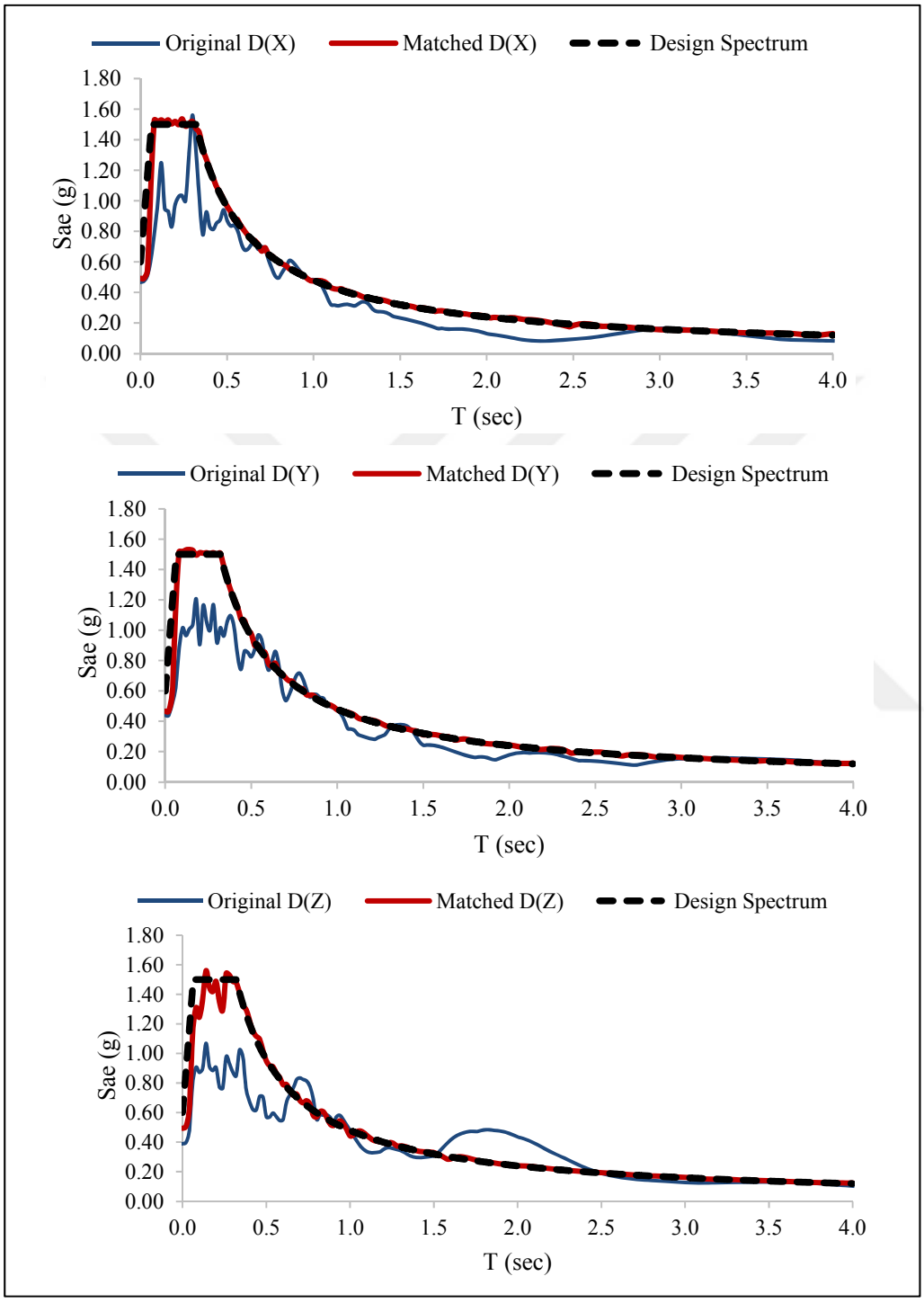

Figure 7.12 : Comparison of original, matched and DD-1 design spectrum for Multi-point (D).

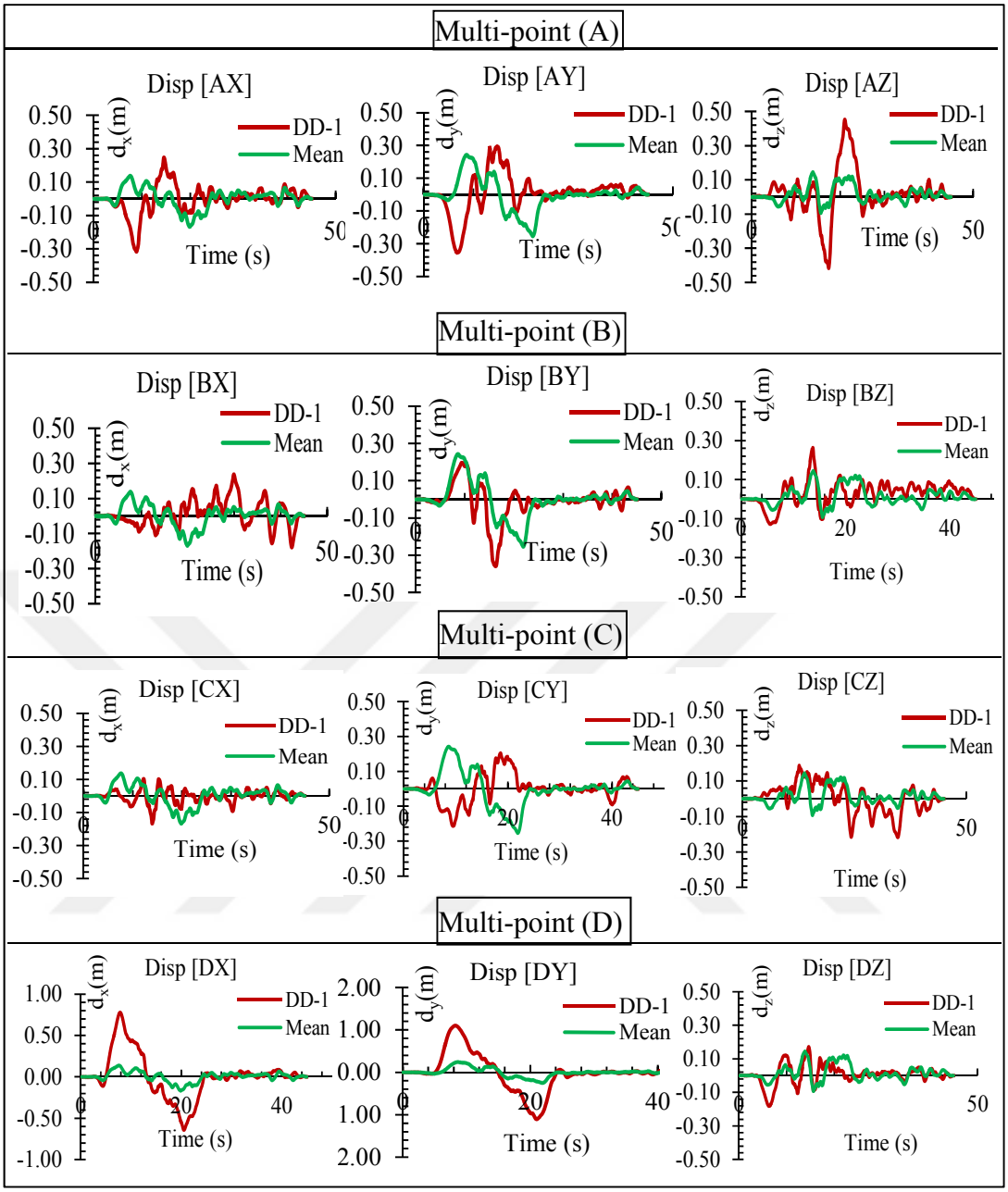

Figure 7.13 : DD-1 spectrum-compatible multi-point and uniform-point (mean) spatially varying site–specific multi-point displacement earthquake records.

Thus, total number of two simulated multi-point earthquake motions: (i) scenario multi-point earthquake motion (ii) DD-1 spectrum compatible multi-point earthquake motion, are taken into account for the Mp and Up analyses.

7.2 Earthquake Analysis

Considering the produced spatially varying site-specific ground motions, the non-linear geometric time-history analysis of the bridge is performed through the SAP2000 (SAP2000, 2016) software. Large displacement option that is relatively significant for

large-scale slender structures is also considered in the programme for the Mp analysis of the bridge. Since the Bosphorus Bridge has currently been in operation only for cars, truck lanes are not taken into account for the live-load (LL). Therefore, only standard car loads are adopted in the time-history analysis. For this objective, H30-S24 truck load is adopted for live-load consideration. According to the Technical Specifications for Highways Bridges (KGM, 1982), lane traffic load for standard cars can be considered as 1/3 of AASHTO (AASHTO-LRFD, 2007) H30-S24 truck load of 9.0 kN/m. As shown in Figure 7.14, each lane of the bridge is loaded with uniformly distributed lane traffic load of 3.0 kN/m. Thus, total uniform load of 18.0 kN/m is considered for the live-load of the Bosphorus Bridge.

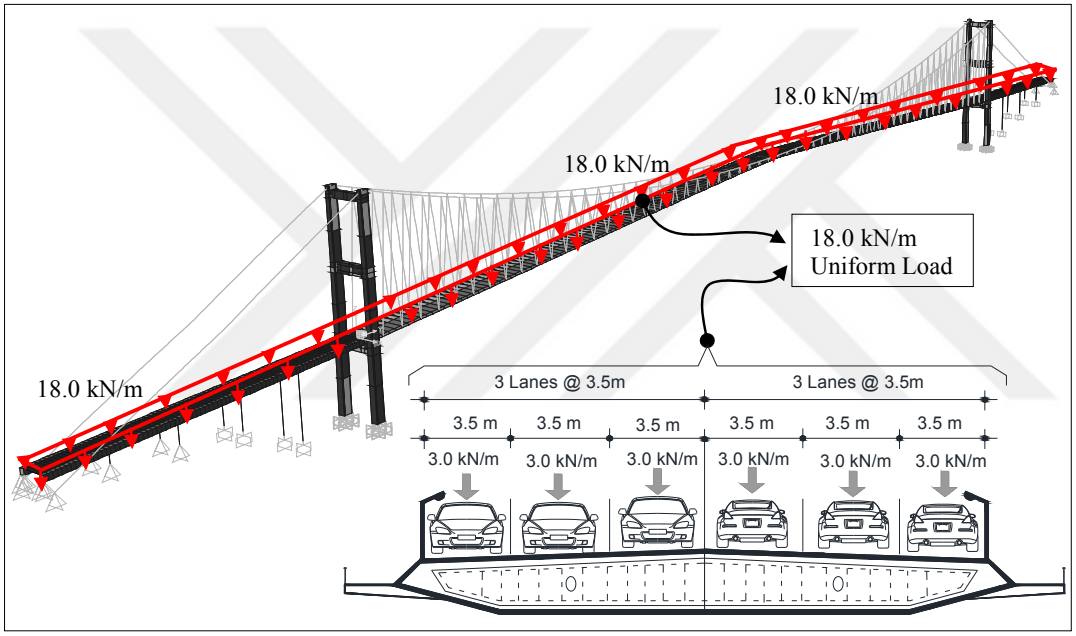

Figure 7.14 : Live-load consideration for the Mp and Up analyses.

Moreover, modal damping ratio of ξ=0.02 is considered to calculate the proportional structural damping proposed by Rayleigh (1945) using the equations 7.5-6 since the bridge was made of structural steel. In this approach, as shown in equation 7.5, the damping matrix [c] of a structural system is presented as linear combination of the mass [m] and stiffness [k] matrices with the constants of a_0 and a_1. However, the most common use of the proportional damping in the non-linear direct-integration response history analysis is the formulation given in equation 7.6 even though certain drawbacks of this approach that leads to "spurious" damping force due to the consideration of specific number of modes were drawn by Chopra and McKenna (2016). The constants of a_0 and a_1 can be easily determined by substituting the specific two modal angular

frequencies (ω_i and ω_j) and the corresponding modal damping ratios (ζ_i and ζ_j) into equation 7.6.

$$[c] = a_0[m] + a_1[k] \tag{7.5}$$

$$\xi = \frac{a_0}{2}\frac{1}{\omega_n} + \frac{a_1}{2}\omega_n \tag{7.6}$$

The modal frequencies (ω_i and ω_j) to define proportional damping in the time-history analyses were separately selected for the bridge with inclined and vertical hanger according to the dominant modes of the test structure in the horizontal and vertical directions: the 1st dominant horizontal mode (1st Deck L_{asymm}) and the 1st dominant vertical mode (1st Deck Mode-1 V_{asymm}). Corresponding modal damping ratio for these specified modes were considered as $\zeta_1=\zeta_2=2.0$ % that is well-known value for steel structures. Thus, calculated proportional damping coefficients were defined to the SAP2000 for two FE models of the bridge.

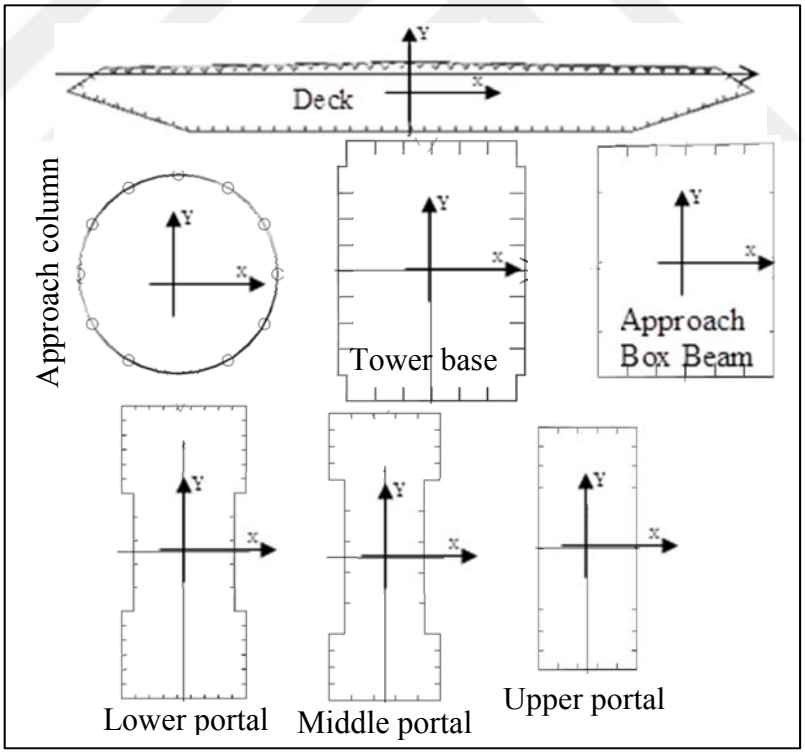

Figure 7.15 : Critical components to be compared with the Mp and Up analyses.

In order to make comparison of the results from the Mp and Up with the sectional capacity of the critical components of the bridge, elaborate sectional analysis of the bridge's components is first carried out and, their yield and plastic moment capacity

are obtained from the sectional analysis. Axial force capacity is also determined, especially for the tower section. Sectional capacity of these critical sections is given in Table 7.4 according to the axes depicted in Figure 7.15.

Table 7.4 : Sectional capacity of critical components of the bridge.

Component		Axial Force (P_c -kN)	Bending Moment (M_b-kNm)			
			X-Direction		Y-Direction	
			M_{xy}	M_{xp}	M_{yy}	M_{yp}
Deck		773198	216894	373643	2988888	6357806
Tower	Base section	235767	449159	708195	389111	586221
	Retrofitted	385959	687623	1118541	597314	931794
Portal Beam	Lower	129257	329203	536176	178963	272077
	Middle	85268	167210	272083	70926	113603
	Upper	66975	97125	150370	62890	92646
Approach viaduct	Box beam	82447	109964	169883	59381	98954
	Column	48460	22580	29037	22580	29037
Cable	Main cable	273247	-	-	-	-
	Back-stay	292417	-	-	-	-
	Hanger	15920	-	-	-	-

7.2.1 Multi-point earthquake analysis (Mp)

The multi-points of the bridge as shown in Figure 7.1 are utilized to make the multi-point earthquake analysis (Mp). For this aim, the practice-oriented procedure is developed as schematically summarized in Figure 7.16. Although general assumption for the earthquake analysis is to utilize acceleration ground motion time-history (ATH), the developed Mp analyses procedure requires to use displacement ground motion time-history (DTH) instead of ATH. Based on this consideration, unit support displacement (d=1.0 m) is separately defined in three directions for each multi-point (A, B, C and D). Accordingly, displacement of the bridge's support is provided to be changed in time in accordance with given DTH for the multi-point C. After definition of this load case for each support of the bridge, total number of twelve separated time-history load cases are synchronically combined in one time-history load case. These steps can be easily implemented with the help of a structural analysis software, such as SAP2000, Open Sees etc.

The multi-point earthquake analysis is carried out for two FE modes of the bridge: (i) inclined hanger and (ii) vertical hanger. Besides, the scenario and DD-1 compatible multi-point earthquake motions are considered for the Mp analyses.

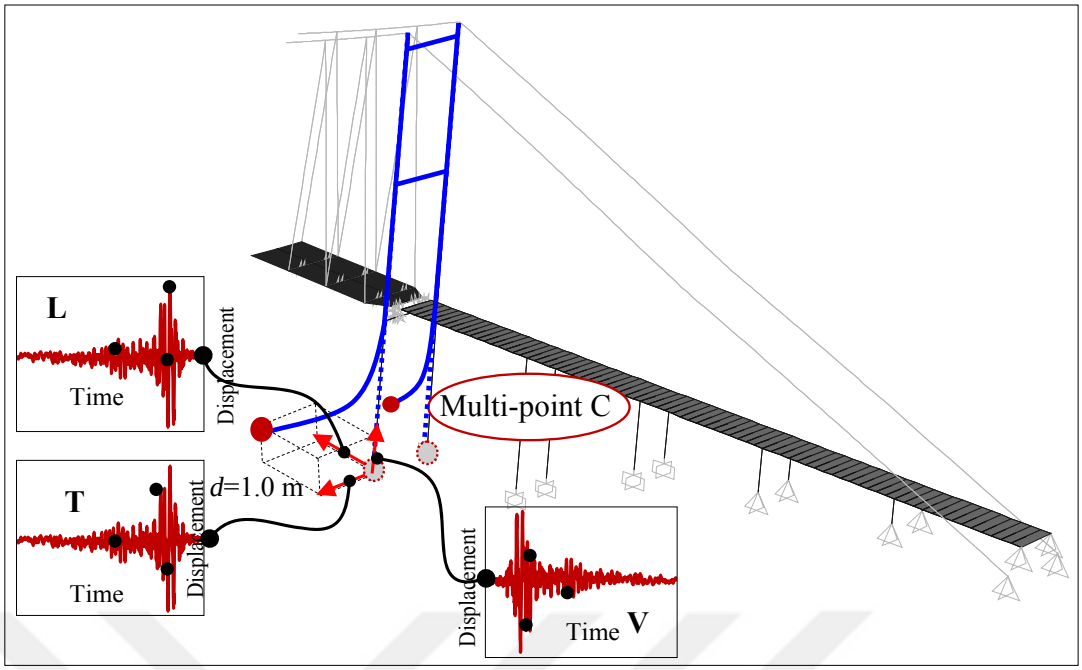

Figure 7.16 : Multi-point earthquake analysis procedure.

7.2.1.1 The Mp analysis under the scenario multi-point earthquake motion

Considering the requirements in the previous section, the first Mp analysis is conducted under the scenario multi-point earthquakes. According to Table 7.5, no increase in the cable elements is obtained due to vertical hanger arrangement. For the main and back-stay cables, no change can be considered with 1.86 % and 0.96 % decrease in the tensile force; however, the tensile force of the hanger elements relatively increases as 71.3 % in case of vertical hanger arrangement. The condition necessary for geometric stability of the bridge is thus provided by no tensile force change in the main and back-stay cables at the top-saddle. High decrease in the tensile force of hanger is directly pertinent to no horizontal component of vertical hanger.

Table 7.5 : Cable elements results from the Mp analysis for the bridge with inclined and vertical hanger under the scenario earthquake.

Cable Elements Tensile Force	Multi-point analysis		Change (%)	Capacity	Capacity Ratio	
	Inclined	Vertical		Max. Tensile	Inclined/Max. Tensile	Vertical/Max. Tensile
Main Cable (kN) (max.)	227656.41	223413.97	**-1.86**	273247.47	**83.32**	**81.76**
Back-Stay (kN) (max)	238801.88	236512.09	**-0.96**	292417.03	**81.66**	**80.88**
Hanger (kN (max)	8391.31	2409.40	**-71.29**	15920.48	**52.71**	**15.13**

Despite of low decrease in the main and back-stay cables of the bridge with vertical hangers, their use of the sectional capacity is relatively higher than that of the hanger element. With the capacity ratio of 80-83 % for both two models, the scenario earthquake demands high sectional force from the main and back-stay cables compared to 15-53 % capacity ratio of the hanger element.

As to the main deck of the bridge, the vertical hanger arrangement leads to decrease in the shear force, the bending moment and the compressive axial force with percentage decrease of 10.14 %, 6.33 % and 83.86 %, respectively. According to Table 7.6, the compressive axial force relatively decreases in case the vertical hanger arrangement. Such a high decrease is based on no horizontal component of the vertical hanger along the bridge's axis. As given in Table 7.6, the capacity ratios of the main deck section are also considerably low for the bridge models with inclined and vertical hangers. Therefore, no effects on the structural performance of the main deck are concluded from the scenario multi-point earthquake analysis of the bridge with vertical hangers.

As given in Table 7.7, similar outcomes are also obtained for the portal beams. For the lower portal beam, only compressive axial force decreases as 2.32 % in case vertical hanger and the other sectional forces are obtained to be higher for vertical hanger than inclined hanger. The increase in the shear force and the bending moment of the lower portal beam results from the viscous damper and the wind tongue. For the middle portal beam, all sectional forces increase with low percentage increase. Hence, the upper portal beam is not affected from the vertical hanger. It is also interesting outcome that the capacity ratios increase from lower to upper portal beam as indicated in Table 7.7. Besides, the use of the sectional capacity is obtained to be higher for vertical hanger than for inclined hanger.

According to Table 7.8, the tower base section actions of the shear force, bending moment and axial compressive force increased as 14.16 %, 17.20 % and 0.05 %, respectively, under the scenario multi-point earthquake of the bridge with vertical hanger. In Table 7.8, the yield and plastic capacities of the section at the tower-base are separately given for inclined and vertical hanger due to fact that in the hanger replacement project, the tower base-section was strengthened with the additional stiffener elements of doubly symmetric I-beam W530x123 as shown in Figure 7.17.

Table 7.6 : The main deck results from the Mp analysis for the bridge with inclined and vertical hanger under the scenario earthquake.

Deck	Multi-point analysis		Change (%)	Capacity		Capacity Ratio			
	Inclined	Vertical		Yield	Plastic	Inclined/Yield	Vertical/Yield	Inclined/Plastic	Vertical/Plastic
Shear Force (kN) (max.)	5297.24	4760.18	**-10.14**	**-**	**-**	-	-	-	-
Bending Moment (kNm) (max)	265595.42	248771.30	**-6.33**	2988888.00	6357806.00	**8.89**	**8.32**	**4.18**	**3.91**
Compressive Axial Force (kN) (max)	69234.00	11174.54	**-83.86**	773198.00	773198.00	**8.95**	**1.45**	**0.09**	**0.01**

Table 7.7 : Portal beams results from the Mp analysis for the bridge with inclined and vertical hanger under the scenario earthquake.

Portal Beam		Multi-point analysis		Change (%)	Capacity		Capacity Ratio			
		Inclined	Vertical		Yield	Plastic	Inclined/Yield	Vertical/Yield	Inclined/Plastic	Vertical/Plastic
Lower Portal	Shear Force (kN) (max.)	13447.16	15349.43	**14.15**	**-**	**-**	**-**	**-**	**-**	**-**
	Bending Moment (kNm) (max)	84620.97	91638.15	**8.29**	329203.00	536175.83	**25.70**	**27.84**	**15.78**	**17.09**
	Compressive Axial Force (kN) (max)	2407.43	2351.47	**-2.32**	129257.00	129257.00	**1.86**	**1.82**	**1.86**	**1.82**
Middle Portal	Shear Force (kN) (max.)	4003.98	4393.48	**9.73**	-	-	**-**	**-**	**-**	**-**
	Bending Moment (kNm) (max)	58711.31	63933.47	**8.89**	167210.00	272082.55	**35.11**	**38.24**	**21.58**	**23.50**
	Compressive Axial Force (kN) (max)	185.39	213.45	**15.13**	85268.00	85268.00	**0.22**	**0.25**	**0.22**	**0.25**
Upper Portal	Shear Force (kN) (max.)	2499.26	2387.72	**-4.46**	-	-	**-**	**-**	**-**	**-**
	Bending Moment (kNm) (max)	34541.40	33090.10	**-4.20**	97125.00	150369.53	**35.56**	**34.07**	**22.97**	**22.01**
	Compressive Axial Force (kN) (max)	1430.47	1454.82	**1.70**	66975.00	66975.00	**2.14**	**2.17**	**2.14**	**2.17**

Moreover, the increase in the shear force and the bending moment is based on additional longitudinal force from the viscous damper and the wind tongue mounted at the expansion joints. The capacity ratios are also determined as high for the bridge with inclined and vertical hangers; however, these ratios indicate that the tower base-section is estimated to remain elastic under the scenario earthquake.

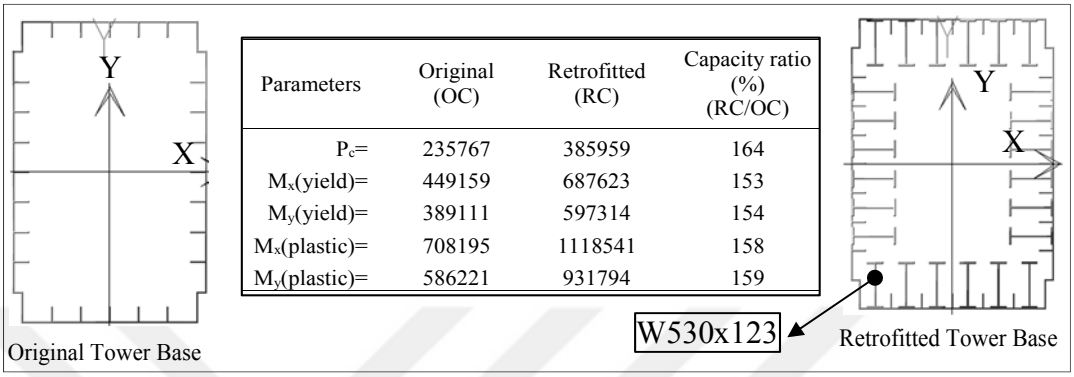

Figure 7.17 : Retrofitting of the tower base-section in the hanger replacement project.

The approach box-beam is relaxed with the vertical hanger arrangement as given in Table 7.9 with 2.17 % increase in the shear force and 26.66 % and 50. 24 % decrease in the bending moment and compressive axial force, respectively. Such high decrease in these elements is based on low force concentration on the viscous dampers located at the expansion joints of the bridge. Moreover, the conclusion is also estimated to be related to the earthquake level, which means that the triggering level might be high to obtain an increase in these sectional forces of the approach box-beam. These estimations can also be proved by displacement-time history of the expansion joints. Consequently, the approach box-beam is not influenced by the vertical hanger arrangement.

The results from the approach column are presented in Table 7.10. 14.17 % and 5.71 % increase in the bending moment and compressive axial force, respectively. The increase in these sectional actions is predicted to be result from additional force at the wind tongue in vertical and horizontal directions. Besides, the decrease in the shear force of the approach column is directly related to the decrease in the compressive axial force of the approach box-beam as shown in Table 7.9. Depending on the capacity ratios given in Table 10, the approach column is determined not to be affected from the vertical hanger arrangement.

Table 7.8 : Tower base-section results from the Mp analysis for the bridge with inclined and vertical hanger under the scenario earthquake.

Tower Base Section	Multi-point analysis		Change (%)	Capacity				Capacity Ratio			
				Yield		Plastic					
	Inclined	Vertical		Inclined	Vertical	Inclined	Vertical	Inclined/ Yield	Vertical/ Yield	Inclined/ Plastic	Vertical/ Plastic
Shear Force (kN) (max.)	10618.72	12122.69	**14.16**	-	-	-	-	-	-	-	-
Bending Moment (kNm)(max)	331269.55	388237.03	**17.20**	449159.00	687623.00	708195.00	1118541.00	**73.75**	**56.46**	**46.78**	**34.71**
Compressive Axial Force (kN) (max)	200058.29	200160.00	**0.05**	385959.00	385959.00	385959.00	385959.00	**51.83**	**51.86**	**51.83**	**51.86**

Table 7.9 : Approach box results from the Mp analysis for the bridge with inclined and vertical hanger under the scenario earthquake.

Approach Box	Multi-point analysis		Change (%)	Capacity		Capacity Ratio			
	Inclined	Vertical		Yield	Plastic	Inclined/Yield	Vertical/Yield	Inclined/Plastic	Vertical/Plastic
Shear Force (kN) (max.)	3881.57	3965.87	**2.17**	-	-	-	-	-	-
Bending Moment (kNm) (max)	72482.49	53156.22	**-26.66**	109964.00	169883.10	**65.91**	**48.34**	**42.67**	**31.29**
Compressive Axial Force (kN) (max)	26291.76	13081.81	**-50.24**	82447.00	82447.00	**31.89**	**15.87**	**31.89**	**15.87**

Table 7.10 : Approach column results from the Mp analysis for the bridge with inclined and vertical hanger under the scenario earthquake.

Approach Column	Multi-point analysis		Change (%)	Capacity		Capacity Ratio			
	Inclined	Vertical		Yield	Plastic	Inclined/Yield	Vertical/Yield	Inclined/Plastic	Vertical/Plastic
Shear Force (kN) (max.)	208.42	199.98	**-4.05**	-	-	-	-	-	-
Bending Moment (kNm) (max)	2866.62	3272.75	**14.17**	22580.00	29036.50	**12.70**	**14.49**	**9.87**	**11.27**
Compressive Axial Force (kN) (max)	8232.36	8702.30	**5.71**	48460.00	48460.00	**16.99**	**17.96**	**16.99**	**17.96**

Along with the sectional forces, displacement-time history at critical points of the deck mid-span in three directions, the expansion joint and the tower top-saddle is presented in Figures 7.18-23. As shown in Figure 7.18 and Figure 7.20, no change in horizontal and vertical directions at the deck mid-span is obtained. The same behavior in horizontal direction at this point for the bridge with inclined and vertical hangers is based on the scenario earthquake level, which means that the viscous dampers at the expansion joints are not forced enough to reduce the movement of the deck in horizontal direction. The vertical movement of the deck mid-span is obtained as expected since no change in vertical direction should be due to the geometry and stability requirement of the bridge.

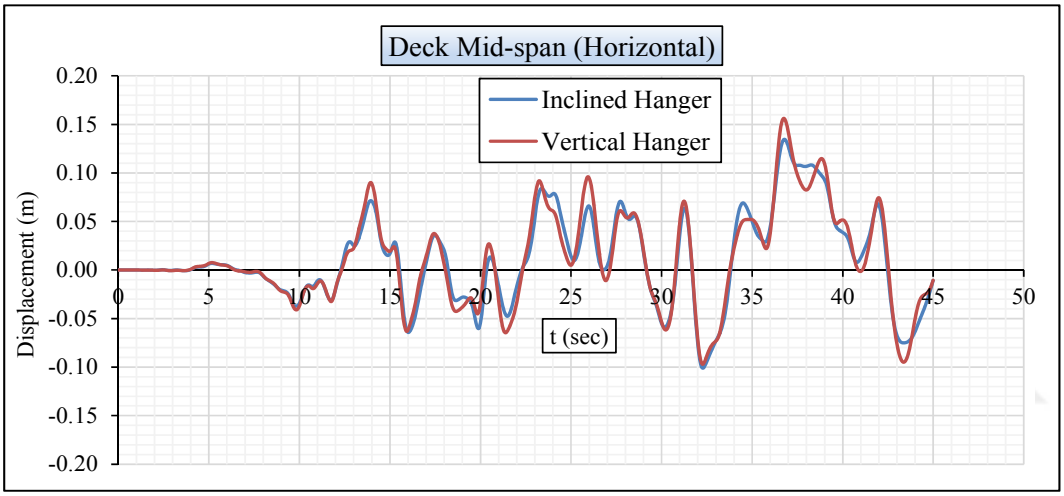

Figure 7.18 : Deck mid-span (horizontal) displacement results from the Mp analysis for the bridge with inclined and vertical hanger under the scenario earthquake.

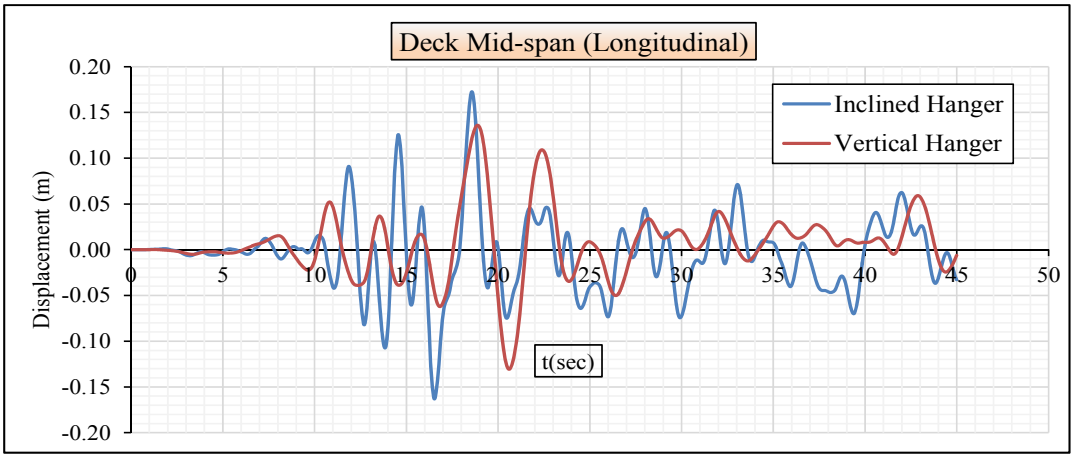

Figure 7.19 : Deck mid-span (longitudinal) displacement results from the Mp analysis for the bridge with inclined and vertical hanger under the scenario earthquake.

The other important result is longitudinal displacement of the deck at the mid-span. The movement in this direction for the bridge with inclined hanger is clear to obtain less than that of the bridge with vertical hanger due to the viscous dampers that is aimed to reduce displacement of the deck in longitudinal direction. As seen in Figure 7.19, the reducing effect of the viscous damper on the longitudinal movement of the deck is determined. Similar behavior is also expected for the displacement-time history of the expansion joints. From Figure 7.21, the displacement of the bridge with vertical hanger decreases compared to that of the bridge with inclined hanger due to the viscous damper.

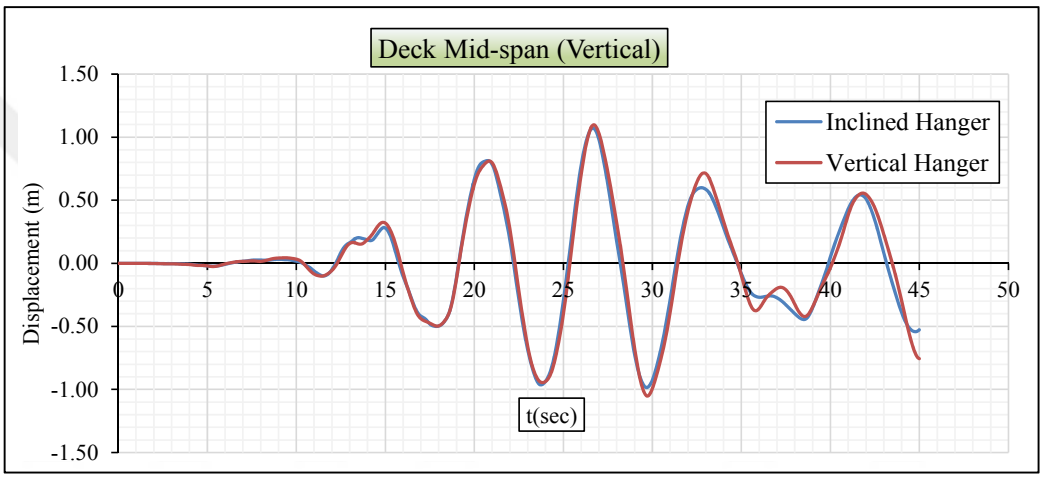

Figure 7. 20 : Deck mid-span (vertical) displacement results from the Mp analysis for the bridge with inclined and vertical hanger under the scenario earthquake.

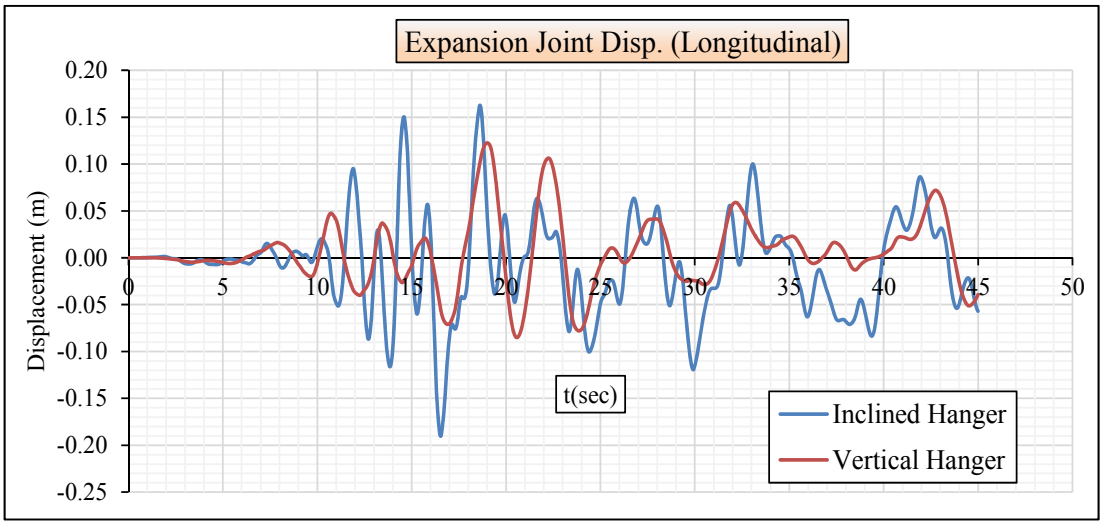

Figure 7.21 : Expansion joint displacement results from the Mp analysis for the bridge with inclined and vertical hanger under the scenario earthquake.

When it comes to the tower top-saddle, no change in longitudinal and horizontal direction is obtained in case of vertical hanger. The outcomes are expected because geometry and stability of the bridge with vertical hangers should be provided by no change in the tower displacement at the top-saddle. In terms of the structural response, the Bosphorus Bridge is obtained not to be influenced by the vertical hanger arrangement.

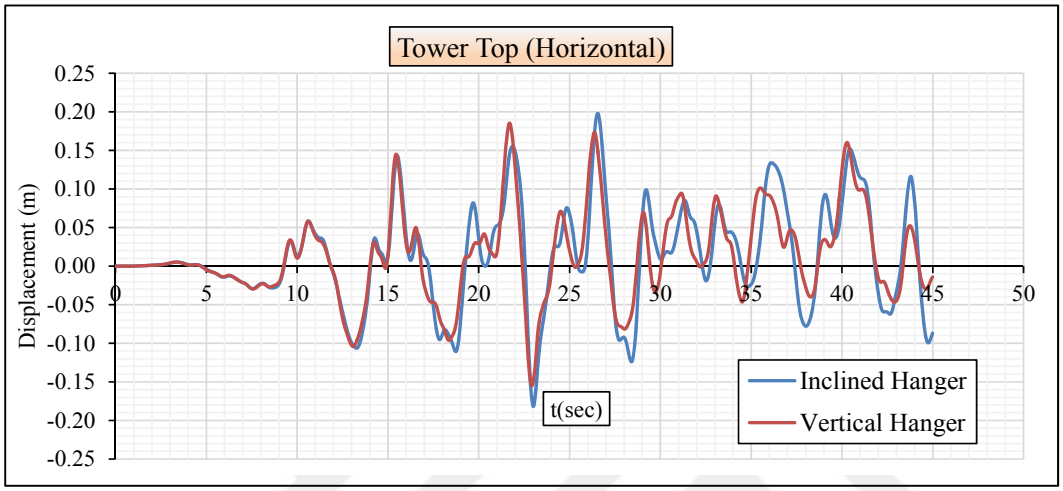

Figure 7.22 : Tower top (horizontal) displacement results from the Mp analysis for the scenario earthquake.

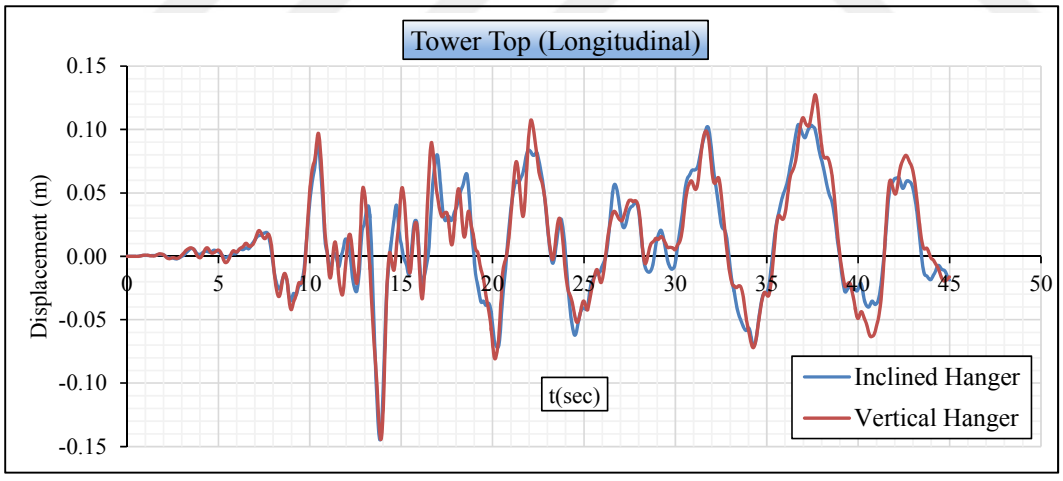

Figure 7.23 : Tower top (longitudinal) displacement results from the Mp analysis for the scenario earthquake.

7.2.1.2 The Mp analysis under the DD-1 multi-point earthquake motion

Defining these EQ records, the Mp analysis is conducted for two bridge models with inclined and vertical hangers and the results are comparatively given in Tables 7.11-18. From Table 7.11, the tensile force of the cable elements of the main, backstay and hanger decreased as 1.41 %, 0.03 % and 75.66 %, respectively for the bridge with

vertical hanger under the DD-1 multi-point earthquake excitation. For the stability of the bridge, no change in the main and backstay cables is estimated before the analysis. Approximately no decrease in these elements under multi-point earthquake excitation proves this estimation. However, percentage decrease for the hanger elements is obtained relatively higher than the main and backstay cables. Such a high decrease pertains to no lateral force component of vertical hanger when compared to inclined hanger with the diagonal tensile force consisting of not only vertical component but also lateral component. The reason is raised for higher decrease in the hanger elements than the main and backstay cables.

Table 7.11 : Cable elements results from the Mp analysis for the bridge with inclined and vertical hanger under the DD-1 earthquake.

Cable Elements Tensile Force	Multi-point analysis		Change (%)	Capacity	Capacity Ratio	
	Inclined	Vertical		Max. Tensile	Inclined/Max. Tensile	Vertical/Max. Tensile
Main Cable (kN) (max.)	252693.40	249125.03	**-1.41**	273247.47	**92.48**	**91.17**
Back-Stay (kN) (max)	265474.15	265382.15	**-0.03**	292417.03	**90.79**	**90.75**
Hanger (kN (max)	12456.30	3031.78	**-75.66**	15920.48	**78.24**	**19.04**

The comparison with the capacity ratio also reveals that the main and back-stay cables almost use almost their capacities under the DD-1 earthquake motions. However, the hanger cables are obtained to be relaxed with vertical arrangement due to noticeable percentage decrease of 59.20 %. These outcomes also prove that geometric and stability conditions of the bridge are provided under low stress with vertical hangers. Based on these remarks, the vertical hanger arrangement is obviously obtained to be more suitable for the Bosphorus Bridge in terms of stress decrement that leads to decrease in the possibility of fatigue problem.

According to Table 7.12, the tower base section actions of the shear force, bending moment and axial compressive force increased as 13.12 %, 20.85 % and 3.48 %, respectively, under DD-1 multi-point earthquake of the bridge with vertical hangers. Moreover, the increase in the shear force and the bending moment is based on the additional longitudinal force from the viscous damper and the wind tongue mounted at the expansion joints. Thus, the increase is compared with the yield and plastic capacity of the section and only bending moment action is obtained higher than the capacity. In addition, the section of the bridge with inclined hangers did not provide

its bending moment capacity. Particularly, the bending moment yield capacity of the section is noticeably lower than the analysis results from two bridge models. When compared to the plastic capacity, the results from the analyses are also obtained to be high. This means that the capacity of not only the retrofitted but also project tower base section cannot provide the demand for the DD-1 multi- point earthquake and a damage at the section is also estimated. Due to the damage estimation at the retrofitted section, new doubly symmetric I-beam of W1100x499 is selected as shown in Figure 7.24 to provide the yield capacity of the new tower base section higher than the analysis results. As given in Table 7.13, the new retrofitted section has higher capacity than the demand for multi-point earthquake.

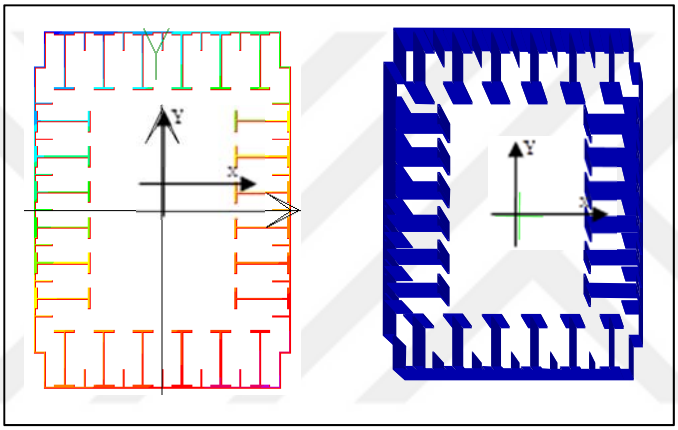

Figure 7.24 : New retrofitted tower base-section with W1100x499 I-beam.

As given in Table 7.14 and 7.15 for the main deck and the portal beams, respectively, these structural components provided the demand for the multi-point earthquake. Hence, no damage is estimated for them. Under the earthquake motion, the sectional actions of the bridge with vertical hanger generally decreased for these components. Only bending moment increased in the main deck. This increase is related to the contribution of the additional force at the damper to the bending moment. The outcome can be also verified by the decrease in the displacement of the deck ends in the longitudinal direction of the bridge with vertical hanger. The comparison for the use of capacity of the section reveals that no change in the bending moment is determined for two bridge models. Nevertheless, the compressive axial force of the main deck can be more critical for the bridge with inclined hanger due to ten times higher use of the capacity.

Table 7.12 : Tower base-section results from the Mp analysis for the bridge with inclined and vertical hanger under the DD-1 earthquake.

Tower Base Section	Multi-point analysis		Change (%)	Capacity				Capacity Ratio			
				Yield		Plastic					
	Inclined	Vertical		Inclined	Vertical	Inclined	Vertical	Inclined/ Yield	Vertical/ Yield	Inclined/ Plastic	Vertical/ Plastic
Shear Force (kN) (max.)	31862.00	36040.74	**13.12**	-	-	-	-	**-**	**-**	**-**	**-**
Bending Moment (kNm)(max)	1252816.64	1514042.15	**20.85**	449159.00	687623.00	708195.00	1118541.00	**278.92**	**220.18**	**176.90**	**135.36**
Compressive Axial Force (kN) (max)	223437.82	231213.41	**3.48**	385959.00	385959.00	385959.00	385959.00	**57.89**	**59.91**	**57.89**	**59.91**

Table 7.13 : Retrofitted tower base-section results from the Mp analysis for the bridge with inclined and vertical hanger under the DD-1 earthquake.

Tower Base Section	Multi-point analysis		Change (%)	Capacity				Capacity Ratio			
				Yield		Plastic					
	Inclined	Vertical		Inclined	Vertical	Inclined	Vertical	Inclined/ Yield	Vertical/ Yield	Inclined/ Plastic	Vertical/ Plastic
Shear Force (kN) (max.)	31862.00	36040.74	**13.12**	-	-	-	-	**-**	**-**	**-**	**-**
Bending Moment (kNm)(max)	1252816.64	1514042.15	**20.85**	1554868.00	1554868.00	2022392.10	2022392.10	**80.57**	**97.37**	**61.95**	**74.86**
Compressive Axial Force(kN) (max)	223437.82	231213.41	**3.48**	759872.51	759872.51	759872.51	759872.51	**29.40**	**30.43**	**29.40**	**30.43**

When it comes to the portal beams as presented in Table 7.15, 9.80 % and 12.74 % increase in the shear force and the compressive axial force of the lower portal beam are obtained in the bridge with vertical hanger. Such increase in these components is directly related to wind tongue with elastomeric restrictions in vertical, longitudinal and lateral directions at the mid-span of the lower portal beam at the deck ends and. Limitation of the deck ends in lateral direction leads to additional lateral force transferring to the lower portal beam as compressive axial force. Similar load transfer is pertinent to the increase in the shear force. Therefore, it is underlined that additional devices of the damper and wind tongue for the structural safety are accompanied with additional force to the portal beams. However, the capacity ratios are almost same for both inclined and vertical hangers. This means that the response of the portal beams of the bridge with vertical hanger to earthquake motion is relatively similar to that of the bridge with inclined hanger. Therefore, installing the damper and wind tongue are predicted not to affect the seismic performance of the portal beams.

As for the rectangular box-beam of the approach viaduct, no increase in the shear force and bending moment is obtained, which in turn they are determined lower for vertical hanger than inclined hanger. However, the compressive axial force increased as 7.65 % as shown in Table 7.16. This increase is related to force resulting from the viscous damper and wind tongue in longitudinal direction. On other hand, it is also interesting outcomes for the bridge with inclined and vertical hangers that the box-beam has low bending moment capacity upon compared to the results from the analysis. Therefore, structural rehabilitation needs to be conducted so as to increase the yield and plastic bending moment capacity of the section. In order to be no interruption in the operational service of the bridge, retrofitting strategy is determined to easily mount doubly symmetric I-beam of W530x123 stiffener elements to the interior surface of the rectangular box-beam. Based on the results from of the analysis of the retrofitted section given in Table 7.17, the retrofitted box-beam with additional stiffeners provided the demand for the DD-1 multi-point earthquake. The yield bending moment capacity-to-inclined hanger ratio is approximately equal to one and the plastic bending moment ratio is less than one. For the bridge with vertical hanger, these ratios are 12-13 % lower than those of inclined hanger.

Table 7.14 : The main deck results from the Mp analysis for the bridge with inclined and vertical hanger under the DD-1earthquake.

Deck	Multi-point analysis		Change (%)	Capacity		Capacity Ratio			
	Inclined	Vertical		Yield	Plastic	Inclined/Yield	Vertical/Yield	Inclined/Plastic	Vertical/Plastic
Shear Force (kN) (max.)	6822.00	5587.18	**-18.10**	-	-	**-**	**-**	**-**	**-**
Bending Moment (kNm) (max)	406831.55	432207.23	**6.24**	2988888.00	6357806.00	**13.61**	**14.46**	**6.40**	**6.80**
Compressive Axial Force (kN) (max)	81827.52	43575.38	**-46.75**	773198.00	773198.00	**10.58**	**0.06**	**0.11**	**0.06**

Table 7.15 : Portal beams results from the Mp analysis for the bridge with inclined and vertical hanger under the DD-1 earthquake.

Portal Beam		Multi-point analysis		Change (%)	Capacity		Capacity Ratio			
		Inclined	Vertical		Yield	Plastic	Inclined/Yield	Vertical/Yield	Inclined/Plastic	Vertical/Plastic
Lower Portal	Shear Force (kN) (max.)	37531.87	41208.71	**9.80**	-	-	**-**	**-**	**-**	**-**
	Bending Moment (kNm) (max)	221286.25	216271.43	**-2.27**	329203.00	536175.83	**67.22**	**65.70**	**41.27**	**40.34**
	Compressive Axial Force (kN) (max)	3171.03	3575.04	**12.74**	129257.00	129257.00	**2.45**	**2.77**	**2.45**	**2.77**
Middle Portal	Shear Force (kN) (max.)	4814.95	4760.83	**-1.12**	-	-	**-**	**-**	**-**	**-**
	Bending Moment (kNm) (max)	70471.44	67714.56	**-3.91**	167210.00	272082.55	**42.15**	**40.50**	**25.90**	**24.89**
	Compressive Axial Force (kN) (max)	220.67	214.20	**-2.93**	85268.00	85268.00	**0.26**	**0.25**	**0.26**	**0.25**
Upper Portal	Shear Force (kN) (max.)	3217.35	3051.64	**-5.15**	-	-	**-**	**-**	**-**	**-**
	Bending Moment (kNm) (max)	44998.16	42004.94	**-6.65**	97125.00	150369.53	**46.33**	**43.25**	**29.93**	**27.93**
	Compressive Axial Force (kN) (max)	1674.37	1677.53	**0.19**	66975.00	66975.00	**2.50**	**2.50**	**2.50**	**2.50**

Table 7.16 : Approach box results from the Mp analysis for the bridge with inclined and vertical hanger under the DD-1 earthquake.

Approach Box	Multi-point analysis		Change (%)	Capacity		Capacity Ratio			
	Inclined	Vertical		Yield	Plastic	Inclined/Yield	Vertical/Yield	Inclined/Plastic	Vertical/Plastic
Shear Force (kN) (max.)	6198.61	5758.44	**-7.10**	-	-	-	-	-	-
Bending Moment (kNm) (max)	224092.91	196101.56	**-12.49**	109964.00	169883.10	**203.79**	**178.33**	**131.91**	**115.43**
Compressive Axial Force (kN) (max)	39433.22	42449.79	**7.65**	82447.00	82447.00	**47.83**	**51.49**	**47.83**	**51.49**

Table 7.17 : Retrofitted approach box results from the Mp analysis for the bridge with inclined and vertical hanger under the DD-1earthquake.

Approach Box	Multi-point analysis		Change (%)	Capacity		Capacity Ratio			
	Inclined	Vertical		Yield	Plastic	Inclined/ Yield	Vertical/ Yield	Inclined/ Plastic	Vertical/ Plastic
Shear Force (kN) (max.)	6198.61	5758.44	**-7.10**	-	-	-	-	-	-
Bending Moment (kNm) (max)	224092.91	196101.56	**-12.49**	225093.00	248745.50	**99.56**	**87.12**	**90.09**	**78.84**
Compressive Axial Force (kN) (max)	39433.22	42449.79	**7.65**	146817.10	146817.10	**26.86**	**28.91**	**26.86**	**28.91**

Table 7.18 : Approach column results from the Mp analysis for the bridge with inclined and vertical hanger under the DD-1 earthquake.

Approach Column	Multi-point analysis		Change (%)	Capacity		Capacity Ratio			
	Inclined	Vertical		Yield	Plastic	Inclined/ Yield	Vertical/ Yield	Inclined/ Plastic	Vertical/ Plastic
Shear Force (kN) (max.)	430.78	785.07	**82.24**	-	-	-	-	-	-
Bending Moment (kNm) (max)	12540.59	16417.65	**30.92**	22580.00	29036.50	**55.54**	**72.71**	**43.19**	**56.54**
Compressive Axial Force (kN) (max)	10994.80	10821.09	**-1.58**	48460.00	48460.00	**22.69**	**22.33**	**22.69**	**22.33**

These conclusions demonstrated that the proposed retrofitting schema is suitable for the rectangular box-beam. Hence, this type of retrofit intervention is selected. For this aim, additional stiffener elements of doubly symmetric I-beam W530x123 are recommended as demonstrated in Figure 7.25.

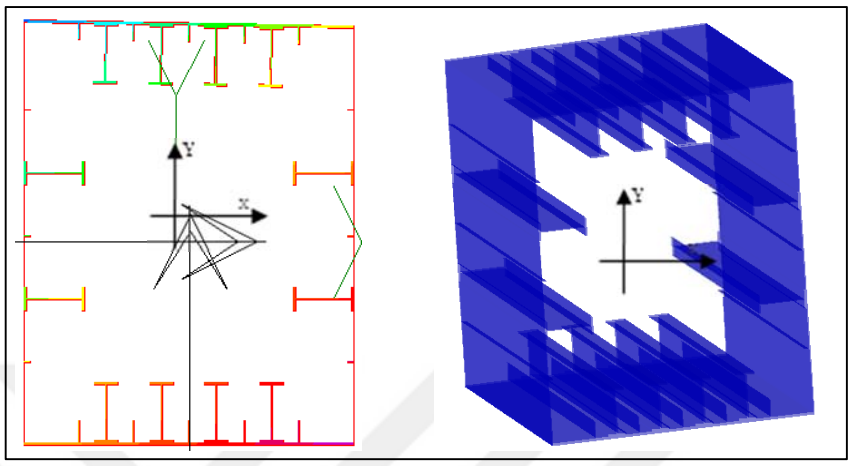

Figure 7.25 : New retrofitted approach viaduct box-beam with W1100x499 I-beam.

Despite of 82.24 % and 30.92 % increase in the shear force and bending moment of the circular box-columns of the bridge with vertical hanger, a damage is not predicted to be observed according to Table 7.18. Under DD-1 multi-point earthquake excitation, only compressive axial force decreased as 1.58 % not effective for the change of the structural behavior of the bridge. The results showed that the circular-box columns of the approach viaducts have higher sectional capacity than the demand for the earthquake and thus, the substructure of the approach-viaducts are not affected by the vertical hanger arrangement of the bridge. Moreover, the increase in the shear force and bending moment of the approach column is estimated to result from the additional force from the damping device and wind tongue along the bridge's axis.

In addition to the sectional force of the bridge, the displacements of the critical points of the bridge, deck mid-span, expansion joint and tower top-saddle are compared during earthquake time as indicated in Figures 7.26-28, respectively. The variation of the displacement at the deck mid-span is obtained in three directions of horizontal, longitudinal and vertical. Under the DD-1 multi-point earthquake motion, the results from inclined hanger are generally higher than vertical hanger. Horizontal displacement obtained at the deck mid-span is somewhat affected with vertical hanger.

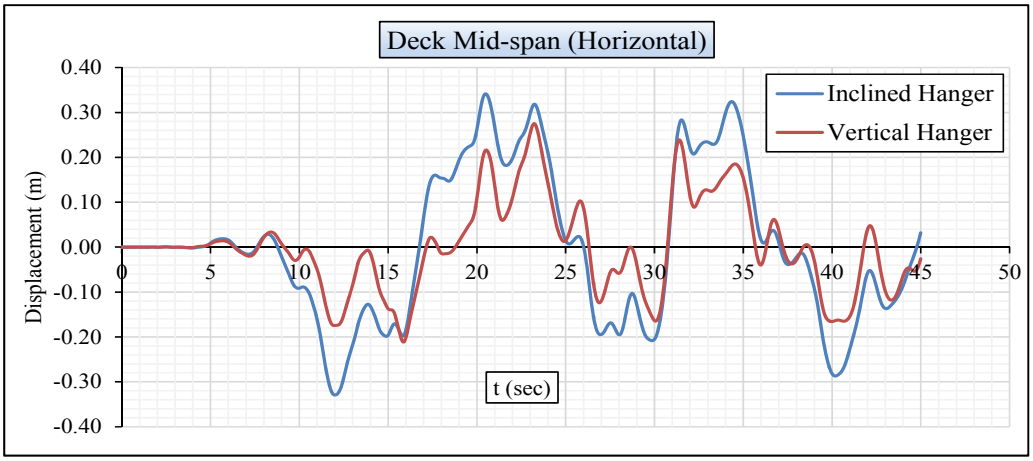

Figure 7.26 : Deck mid-span (horizontal) displacement results from the Mp analysis for the bridge with inclined and vertical hanger under the DD-1 earthquake.

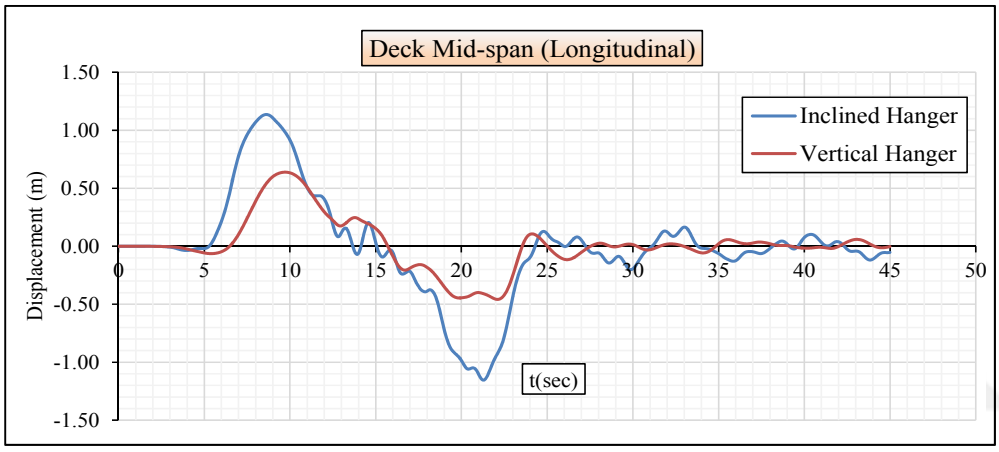

Figure 7.27 : Deck mid-span (longitudinal) displacement results from the Mp analysis for the bridge with inclined and vertical hanger under the DD-1 earthquake.

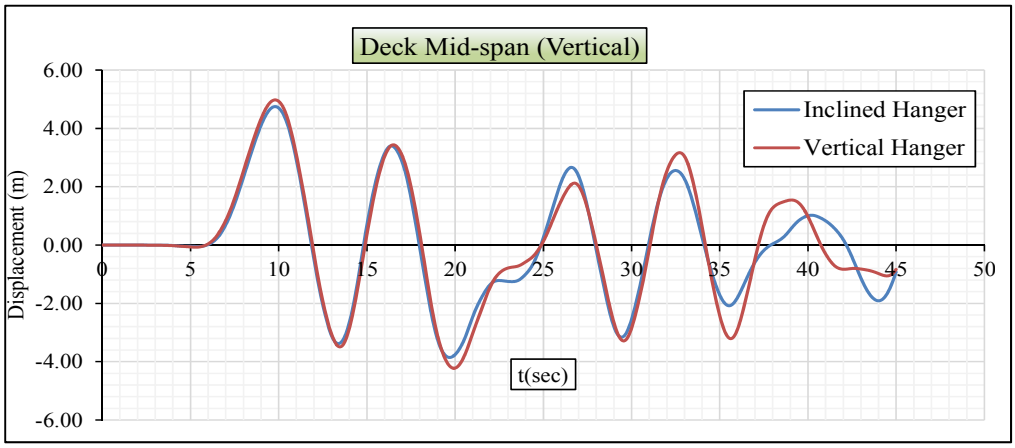

Figure 7.28 : Deck mid-span (vertical) displacement results from the Mp analysis for the bridge with inclined and vertical hanger under the DD-1 earthquake.

Due to the high rigidity of the wind–tongue, almost fully limitation of the deck ends in horizontal direction leads to lower displacement for vertical hanger than that for inclined hanger. Rather than vertical hanger arrangement, such outcome is mostly

based on the wind tongue and viscous damper at the deck ends. As depicted in Figure 7.28, approximately no change in vertical displacement at the deck mid-span is obtained. This result pertains that the geometry of the main deck with a chamber length of 8.0 m and the tower top-saddle points should be same as that of inclined hanger. However, longitudinal displacement at the deck mid-span of the bridge with vertical hanger relatively decreased as 50 % compared to inclined hanger. As mentioned on the investigation of the cable elements, no lateral force component of vertical hanger causes to be low longitudinal displacement. Another reason for such a decrease is directly relevant to the viscous damper located at the expansion joints. Owing to higher axial rigidity of the main deck and the results from vertical displacement of the deck mid-span, displacement-time history of the expansion joints in longitudinal direction is expected to be similar to that of the deck mid-span. As shown in Figure 7.29, this prediction is observed and longitudinal displacement is influenced by vertical hanger arrangement. Consequently, almost 50 % decrease is obtained compared to inclined hanger. The consequence is directly based on the viscous dampers and no lateral component of vertical hanger.

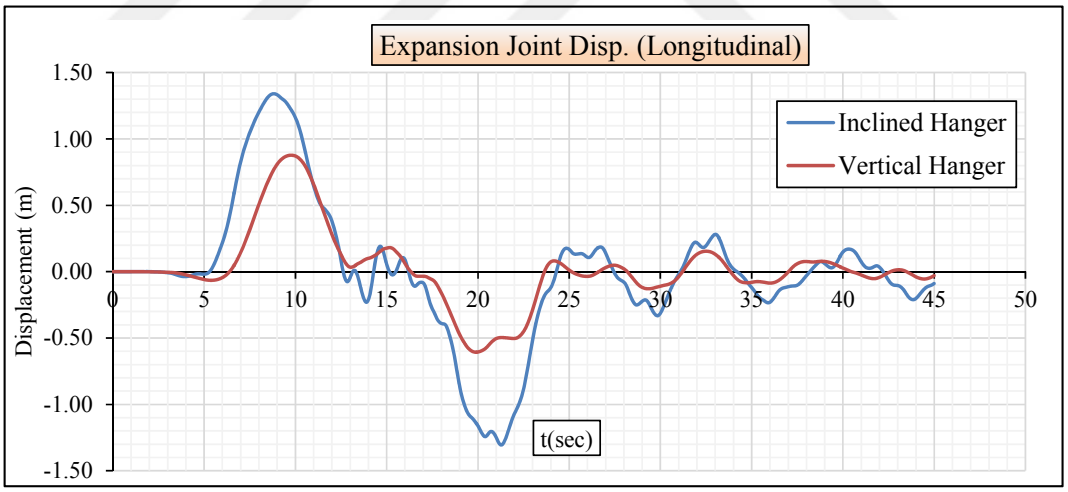

Figure 7.29 : Expansion joint displacement results from the Mp analysis for the DD-1 earthquake.

The decrease in longitudinal displacement of the main deck leads to increase in the bending moment and shear force of the tower base section. As given in Table 7.12, these sectional actions are increased. The main reason for this result is that the concentrated load at the viscous damper is transferred to the towers. Another important outcome is also obtained that displacement capacity of 1.07 m of the expansion joints is not provided for inclined hanger arrangement. In order to make the excessive

movement of approximately 1.5 m lower than the capacity displacement of 1.07 m as given in Figure 7.29, damper elements need to be located on the expansion joints at the both sides. The inclusion of the viscous dampers in the hanger replacement project meets all needs for this task, which means that no further effort is necessary for this aim.

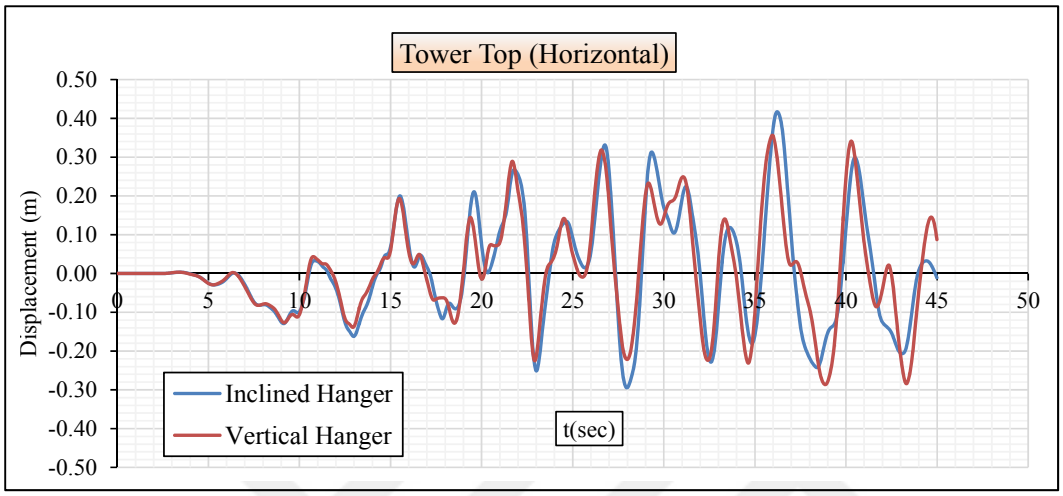

Figure 7.30 : Tower top (horizontal) displacement results from the Mp analysis for the DD-1 earthquake.

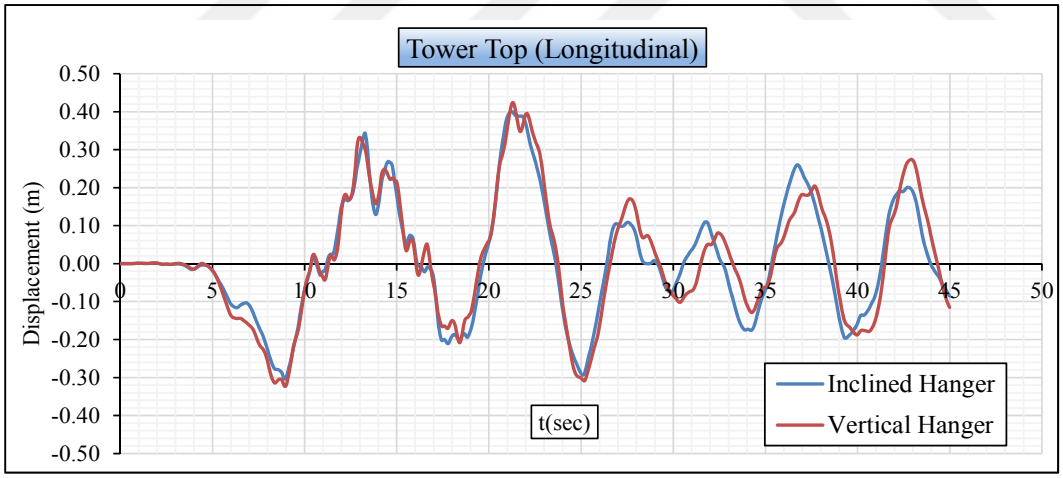

Figure 7.31 : Tower top (longitudinal) displacement results from the Mp analysis for the DD-1 earthquake.

The other significant point is to investigate displacement-time history of the tower top-saddle. For the stability of the tower, no high increase in tensile force of the main cable and the back-stay cable at the tower top-saddle should be obtained due to vertical hanger arrangement. Based on almost no change in these cable elements as indicated in Table 7.12, the variation of displacement in the earthquake duration are estimated to be approximately same before the analysis. As expected, no change in these cables

is obtained as given in Figures 7.30-31. Thus, the tower top-saddle points are concluded not to be affected by vertical hanger arrangement.

7.2.2 Uniform-Point Earthquake Analysis (Up)

The uniform-point earthquake analysis (Up) is the same as the well-known unified earthquake analysis of structures. This approach differs from the Mp analysis with an aspect that the same earthquake motions excite all supports points of the bridge. General assumption for the unified earthquake analysis is to use acceleration time-history. The use of displacement time-history corresponding to acceleration time-history is also true for this analysis. For this aim, similar procedure to the Mp analysis in which same displacement time-history obtained by two times integration of acceleration time-history is acted on all support points of the bridges considered as depicted in Figure 7.16. In other words, different time-history records as in the Mp analysis are not considered for each support point of the bridge. Therefore, one of the important step of the Up analysis is how displacement-time histories to be utilized in the analyses are generated. For this aim, three displacement time-histories are obtained from the integration of the average acceleration time-histories that are calculated by averaging the simulated multi-point earthquake records for each direction. These uniform-point ground motions are given as mean earthquake in Figures 7.4 and Figure 7.13 for the scenario and DD-1 earthquake motions, respectively.

7.2.2.1 The Up analysis under the scenario multi-point earthquake motion

In order to determine the effect of the Mp analysis on the bridge, the Up analyses are conducted for the bridge with inclined and vertical hangers under the scenario multi-point earthquake motions. The results from the cable elements are given in Table 7.19.

Table 7.19 : Cable elements results from the Up analysis for the bridge with inclined and vertical hanger under the scenario earthquake.

Cable Elements Tensile Force	Uniform-point analysis		Change (%)	Capacity	Capacity Ratio	
	Inclined	Vertical		Max. Tensile	Inclined/Max. Tensile	Vertical/Max. Tensile
Main Cable (kN) (max.)	218659.71	213970.91	**-2.14**	273247.47	**80.02**	**78.31**
Back-Stay (kN) (max)	229620.56	227359.63	**-0.98**	292417.03	**78.53**	**77.75**
Hanger (kN (max)	6564.02	2281.40	**-65.24**	15920.48	**41.23**	**14.33**

The tensile force of the main, back-stay and hanger cables decrease as 2.14 %, 0.98 and 65.24 %, respectively. Due to no horizontal component of vertical hanger, such a high decrease in the hanger elements is obtained for the bridge with vertical hanger. As mentioned in the Mp analysis, almost no change in the tensile force of the main and back-stay cablese is estimated before the analyses so as to remain the geometry and stability of the bridge with vertical hanger to be same as that of the bridge with inclined hanger that is selected according to the original design specifications of the bridge. The expected outcomes are provided with 2.14 % change for the main cable and 0.98 % change for the back-stay cable.

As given in Table 7.20 and Table 7.21 for the main deck and the portal beams, respectively, these structural components provided the demand from the scenario multi-point earthquake. Hence, no damage is estimated for them. Under the earthquake motion, the sectional actions of the bridge with vertical hanger generally increase for these components. Only compressive axial force decreases in the main deck and middle portal beam. As given in Table 7.20, 87.5 % decrease in the main deck is related to low axial stress due to no horizontal component of vertical hangers in the longitudinal direction. The comparison for the use of capacity of these sections reveals that no change in the bending moment is determined for two bridge models. Nevertheless, the compressive axial force of the main deck can be more critical for the bridge with inclined hanger due to high use of the capacity compared to vertical hanger. The decrease in the bending moment and the shear force the tower base-section as presented in Table 7.22 is based on the high decease in the compressive axial force of the main deck show in Table 7.20. This outcome is also related to relatively low movement at the deck mid-span and expansion joints in the longitudinal direction. Similar conclusions are also stated for the decrease in the bending moment and the compressive axial force of the approach box-beam as given in Table 7.23. Besides, no damage is estimated for the main deck and the approach box-beam due to low capacity ratios of them. As presented in Table 7.24, the sectional forces of the approach column increase as 4.83 %, 10.32 % and 3.68 % in the shear force, the bending moment and the compressive axial force, respectively. The increase in the bending moment and the compressive axial force of the section is related to the increase in the shear force of the approach box-beam and in the compressive axial force of the towers. Based on the capacity ratios of this section, no damage is estimated for the approach column.

Table 7.20 : The main deck results from the Up analysis for the bridge with inclined and vertical hanger under the scenario earthquake.

Deck	Uniform-point analysis		Change (%)	Capacity		Capacity Ratio			
	Inclined	Vertical		Yield	Plastic	Inclined/Yield	Vertical/Yield	Inclined/Plastic	Vertical/Plastic
Shear Force (kN) (max.)	4413.84	4425.16	**0.26**	-	-	**-**	**-**	**-**	**-**
Bending Moment (kNm) (max)	125341.00	139632.02	**11.40**	2988888.00	6357806.00	**4.19**	**4.67**	**1.97**	**2.20**
Compressive Axial Force (kN) (max)	51932.72	6526.41	**-87.43**	773198.00	773198.00	**6.72**	**0.01**	**0.07**	**0.01**

Table 7.21 : Portal beams results from the Up analysis for the bridge with inclined and vertical hanger under the scenario earthquake.

Portal Beam		Uniform-point analysis		Change (%)	Capacity		Capacity Ratio			
		Inclined	Vertical		Yield	Plastic	Inclined/Yield	Vertical/Yield	Inclined/Plastic	Vertical/Plastic
Lower Portal	Shear Force (kN) (max.)	7424.05	7781.20	**4.81**	-	-	**-**	**-**	**-**	**-**
	Bending Moment (kNm) (max)	56888.94	60408.18	**6.19**	329203.00	536175.83	**17.28**	**18.35**	**10.61**	**11.27**
	Compressive Axial Force (kN) (max)	1627.00	1687.73	**3.73**	129257.00	129257.00	**1.26**	**1.31**	**1.26**	**1.31**
Middle Portal	Shear Force (kN) (max.)	2588.25	2735.43	**5.69**	-	-	**-**	**-**	**-**	**-**
	Bending Moment (kNm) (max)	35882.97	37228.39	**3.75**	167210.00	272082.55	**21.46**	**22.26**	**13.19**	**13.68**
	Compressive Axial Force (kN) (max)	138.40	135.14	**-2.36**	85268.00	85268.00	**0.16**	**0.16**	**0.16**	**0.16**
Upper Portal	Shear Force (kN) (max.)	1513.84	1564.81	**3.37**	-	-	**-**	**-**	**-**	**-**
	Bending Moment (kNm) (max)	20722.64	21338.41	**2.97**	97125.00	150369.53	**21.34**	**21.97**	**13.78**	**14.19**
	Compressive Axial Force (kN) (max)	1324.28	1349.87	**1.93**	66975.00	66975.00	**1.98**	**2.02**	**1.98**	**2.02**

Table 7.22 : Tower base-section results from the Up analysis for the bridge with inclined and vertical hanger under the scenario earthquake.

Tower Base Section	Uniform-point analysis		Change (%)	Capacity				Capacity Ratio			
				Yield		Plastic					
	Inclined	Vertical		Inclined	Vertical	Inclined	Vertical	Inclined/ Yield	Vertical/ Yield	Inclined/ Plastic	Vertical/ Plastic
Shear Force (kN) (max.)	5667.81	5360.42	**-5.42**	-	-	-	-	**-**	**-**	**-**	**-**
Bending Moment (kNm)(max)	190122.31	85026.73	**-55.28**	449159.00	687623.00	708195.00	1118541.00	**42.33**	**12.37**	**26.85**	**7.60**
Compressive Axial Force (kN) (max)	187255.89	193822.25	**3.51**	385959.00	385959.00	385959.00	385959.00	**48.52**	**50.22**	**48.52**	**50.22**

Table 7.23 : Approach box results from the Up analysis for the bridge with inclined and vertical hanger under the scenario earthquake.

Approach Box	Uniform-point analysis		Change (%)	Capacity		Capacity Ratio			
	Inclined	Vertical		Yield	Plastic	Inclined/Yield	Vertical/Yield	Inclined/Plastic	Vertical/Plastic
Shear Force (kN) (max.)	3243.78	3297.87	**1.67**	-	-	**-**	**-**	**-**	**-**
Bending Moment (kNm) (max)	48860.43	42570.71	**-12.87**	109964.00	169883.10	**44.43**	**38.71**	**28.76**	**25.06**
Compressive Axial Force (kN) (max)	13633.54	9208.56	**-32.46**	82447.00	82447.00	**16.54**	**11.17**	**16.54**	**11.17**

Table 7.24 : Approach column results from the Up analysis for the bridge with inclined and vertical hanger under the scenario earthquake.

Approach Column	Uniform-point analysis		Change (%)	Capacity		Capacity Ratio			
	Inclined	Vertical		Yield	Plastic	Inclined/Yield	Vertical/Yield	Inclined/Plastic	Vertical/Plastic
Shear Force (kN) (max.)	107.13	112.31	**4.83**	-	-	**-**	**-**	**-**	**-**
Bending Moment (kNm) (max)	1495.82	1650.23	**10.32**	22580.00	29036.50	**6.62**	**7.31**	**5.15**	**5.68**
Compressive Axial Force (kN) (max)	7331.86	7601.81	**3.68**	48460.00	48460.00	**15.13**	**15.69**	**15.13**	**15.69**

As indicated in Figure 7.32 and Figure 7.34, the displacement of the deck mid-span in horizontal and vertical directions is obtained not to be affected by the vertical hanger arrangement. No change in the movement of the deck in the horizontal direction as depicted in Figure 7.32 can be related to the viscous dampers and the earthquake level. For the vertical direction as shown in Figure 7.34, providing same geometry and stability of the bridge with vertical hangers as that of the bridge with inclined hangers is the main reason why no change is obtained in this direction.

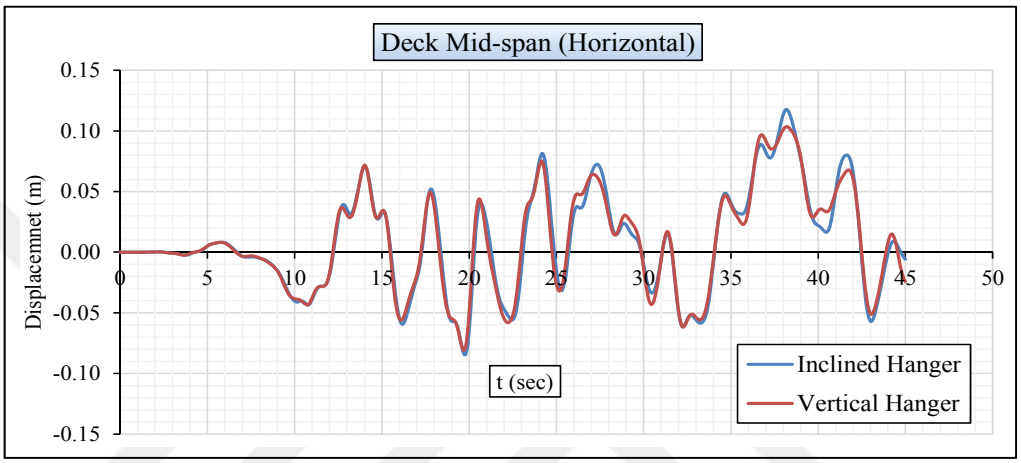

Figure 7.32 : Deck mid-span (horizontal) displacement results from the Up analysis for the bridge with inclined and vertical hanger under the scenario earthquake.

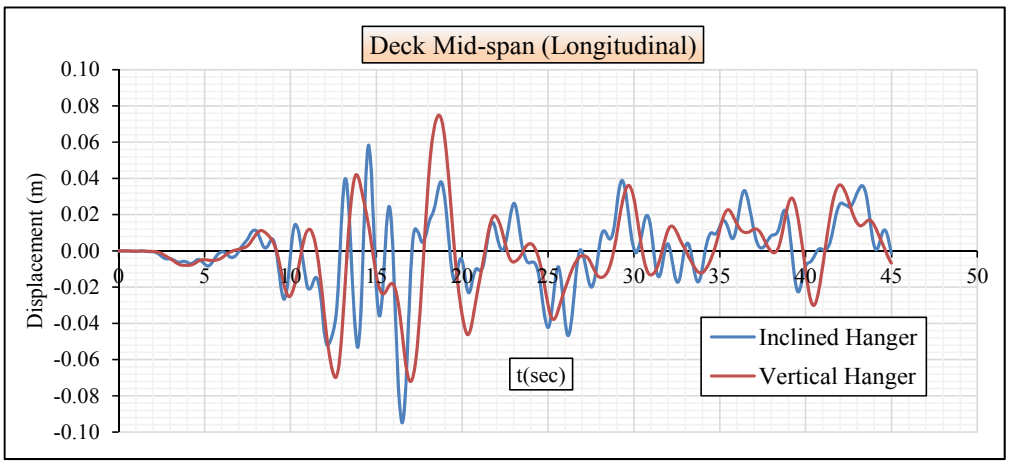

Figure 7.33 : Deck mid-span (longitudinal) displacement results from the Up analysis for the bridge with inclined and vertical hanger under the scenario earthquake.

Due to higher axial rigidity of the deck section, same displacement-time behavior is expected for both the deck mid-span and the expansion joints at the deck ends in the longitudinal direction. Upon comparing Figure 7.33 with Figure 7.35, this estimation is verified. These figures also show that almost no change is obtained. Therefore, the

viscous damper is estimated not to be active under the scenario uniform-point earthquake. Moreover, relatively low movement of the deck mid-span and expansion joints proves this prediction.

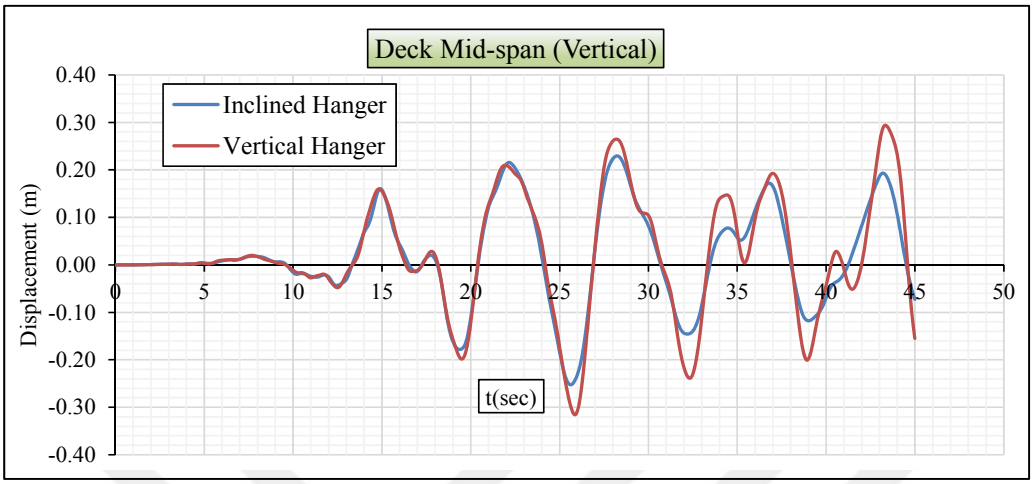

Figure 7.34 : Deck mid-span (vertical) displacement results from the Up analysis for the bridge with inclined and vertical hanger under the scenario earthquake.

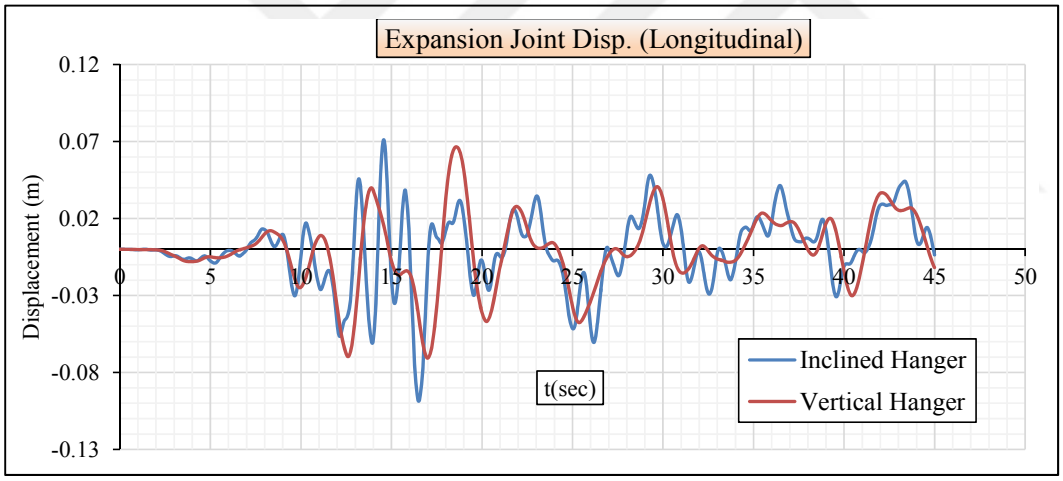

Figure 7.35 : Expansion joint displacement results from the Up analysis for the scenario earthquake.

In order to provide the original project geometry of the bridge with inclined hangers, no displacement change in horizontal and longitudinal displacement of the tower at top-saddles should be obtained from the Up analysis. As demonstrated in Figures 7.36-37, this prediction is obtained. Based on these outcomes, the Bosphorus Bridge is estimated to be elastic under the scenario uniform-point earthquake motion.

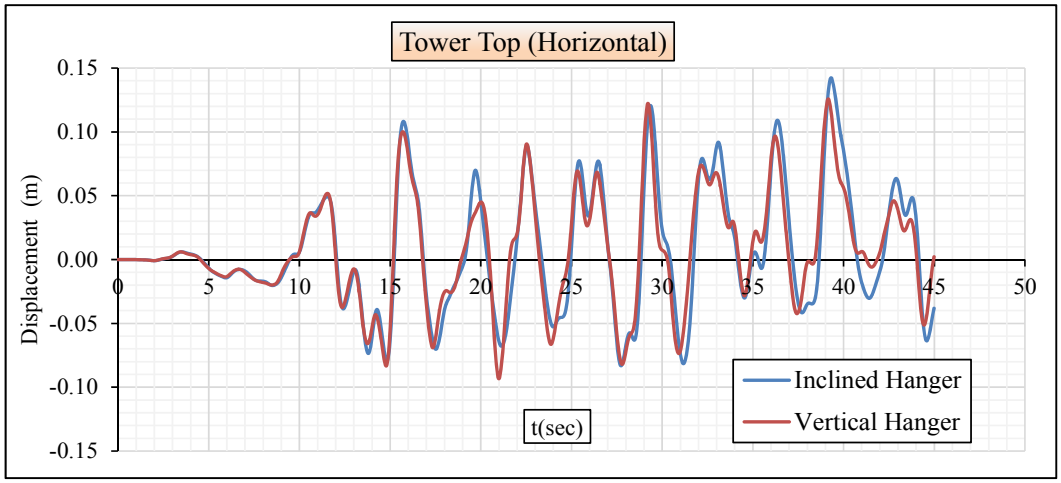

Figure 7.36 : Tower top (horizontal) displacement results from the Up analysis for the scenario earthquake.

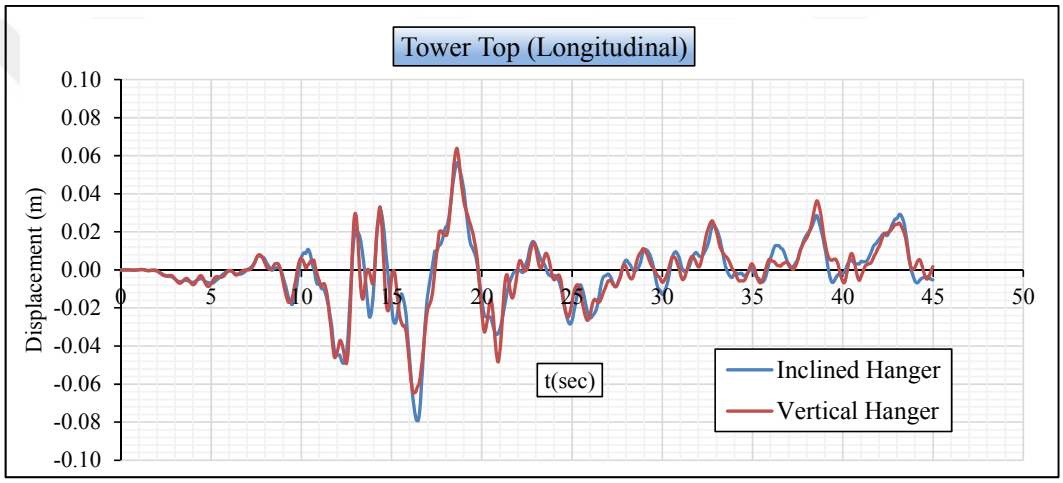

Figure 7.37 : Tower top (longitudinal) displacement results from the Up analysis for the scenario earthquake.

7.2.2.2 The Up analysis under the DD-1 multi-point earthquake motion

According to Table 7.25, the tensile force of the cable elements decreases in case of vertical hanger. The highest decrease of 65.37 % is obtained as 65.37 for the hanger elements. For the main and back-stay cables, almost no change can be considered with 1.41 % and 0.13 %, respectively. This outcome is necessary to remain the geometry and stability of the bridge with vertical hangers same as the bridge with inclined hangers. The balanced force of the main and back-stay cables at the tower top-saddle should be provided in case of the bridge with vertical hanger. As in the other analyses, such a high decrease in the hanger elements are based on no component of vertical hangers in the longitudinal direction of the bridge. Low stress/axial force on the main deck is also estimated according to this result. The demand from the DD-1 multi-point earthquake for the cable elements are given with the capacity ratios presented in Table

7.25. Based on the results, the main and back-stay cables use approximately their capacities of 80 % for the bridge with inclined and vertical hangers, which means that the DD-1 uniform-point earthquake relatively forces the Bosphorus Bridge.

Table 7.25 : Cable elements results from the Up analysis for the bridge with inclined and vertical hanger under the DD-1 earthquake.

Cable Elements Tensile Force	Uniform-support analysis		Change (%)	Capacity	Capacity Ratio	
	Inclined	Vertical		Max. Tensile	Inclined/Max. Tensile	Vertical/Max. Tensile
Main Cable (kN) (max.)	220814.04	217709.73	**-1.41**	273247.47	**80.81**	**79.67**
Back-Stay (kN) (max)	231934.55	231635.61	**-0.13**	292417.03	**79.32**	**79.21**
Hanger (kN (max)	6752.76	2338.38	**-65.37**	15920.48	**42.42**	**14.69**

The analysis results from the main deck and the portal beams are given in Table 7.26 and Table 7.27, respectively. Approximately no change in the bending moment of the main deck is obtained in case of vertical hanger. For the shear force and the compressive axial force, 3.76 % and 83.50 % decrease are determined and this outcome is directly based on decrease in the tensile force of the hanger elements. As for the capacity ratios, the main deck provides the demand from the DD-1 earthquake. The highest change in the portal beams is determined for the lower portal beam as shown in Table 7.27. The percentage change decreases from the lower beam to the upper beam. This means that the lower portal beam is forced at the expansion joints. The increase in the shear force, the bending moment and the compressive axial force of the lower portal beam is pertinent to the wind tongue or the viscous dampers located on the expansion joints. Same conclusion is also stated for the middle portal beam. The compressive axial force of the upper portal beam is only affected from the vertical hanger. No change is obtained for the other sectional force the upper portal beam. In addition, the main deck and the portal beam are estimated not to be damaged under the uniform-point DD-1 earthquake according to the calculated capacity ratios given in Table 7.26 and Table 7.27. The decrease in the shear force and the bending moment of the tower base-section is directly related to the decrease in the bending moment and compressive axial force of the approach box-beam. The decrease in the shear force of the tower base section leads to the decrease in the bending moment of the approachbox-beam. Similar relationships is also obtained between the bending moment of the main deck and the compressive axial force of the approach box-beam

Table 7.26 : The main deck results from the Up analysis for the bridge with inclined and vertical hanger under the DD-1earthquake.

Deck	Uniform-point analysis		Change	Capacity		Capacity Ratio			
	Inclined	Vertical	(%)	Yield	Plastic	Inclined/Yield	Vertical/Yield	Inclined/Plastic	Vertical/Plastic
Shear Force (kN) (max.)	4712.83	4535.51	**-3.76**	-	-	**-**	**-**	**-**	**-**
Bending Moment (kNm) (max)	192112.51	192932.58	**0.43**	2988888.00	6357806.00	**6.43**	**6.45**	**3.02**	**3.03**
Compressive Axial Force (kN) (max)	56725.31	9360.31	**-83.50**	773198.00	773198.00	**7.34**	**0.01**	**0.07**	**0.01**

Table 7.27 : Portal beams results from the Up analysis for the bridge with inclined and vertical hanger under the DD-1 earthquake.

Portal Beam		Uniform-point analysis		Change	Capacity		Capacity Ratio			
		Inclined	Vertical	(%)	Yield	Plastic	Inclined/Yield	Vertical/Yield	Inclined/Plastic	Vertical/Plastic
Lower Portal	Shear Force (kN) (max.)	7939.36	8747.73	**10.18**	-	-	**-**	**-**	**-**	**-**
	Bending Moment (kNm) (max)	74555.96	83016.44	**11.35**	329203.00	536175.83	**22.65**	**25.22**	**13.91**	**15.48**
	Compressive Axial Force (kN) (max)	1893.50	2079.48	**9.82**	129257.00	129257.00	**1.46**	**1.61**	**1.46**	**1.61**
Middle Portal	Shear Force (kN) (max.)	3958.89	4136.36	**4.48**	-	-	**-**	**-**	**-**	**-**
	Bending Moment (kNm) (max)	54801.66	57348.89	**4.65**	167210.00	272082.55	**32.77**	**34.30**	**20.14**	**21.08**
	Compressive Axial Force (kN) (max)	142.68	154.85	**8.53**	85268.00	85268.00	**0.17**	**0.18**	**0.17**	**0.18**
Upper Portal	Shear Force (kN) (max.)	2263.54	2267.57	**0.18**	-	-	**-**	**-**	**-**	**-**
	Bending Moment (kNm) (max)	30582.83	30519.25	**-0.21**	97125.00	150369.53	**31.49**	**31.42**	**20.34**	**20.30**
	Compressive Axial Force (kN) (max)	1327.74	1378.26	**3.80**	66975.00	66975.00	**1.98**	**2.06**	**1.98**	**2.06**

as presented in Table 7. 28 and Table 7.29. The increase in the compressive axial force of the tower base-section and the shear force of the approach box-beam is based on the wind tongue at the mid-point of deck ends. Besides, no damage is estimated for these components depending on the capacity ratios.

As given in Table 7.30 for the approach box column, 6.50 % limited increase in the shear force and the compressive axial force is relevant to the increase in the shear force of the approach box-beam. This conclusion is also directly related to the increase in the sectional force of the lower portal beam as given in Table 7.27. The bending moment of the section increases with the increase in the shear force of the approach box column. According to the capacity ratios, the approach box column provides the demand from the uniform-point DD-1 earthquake.

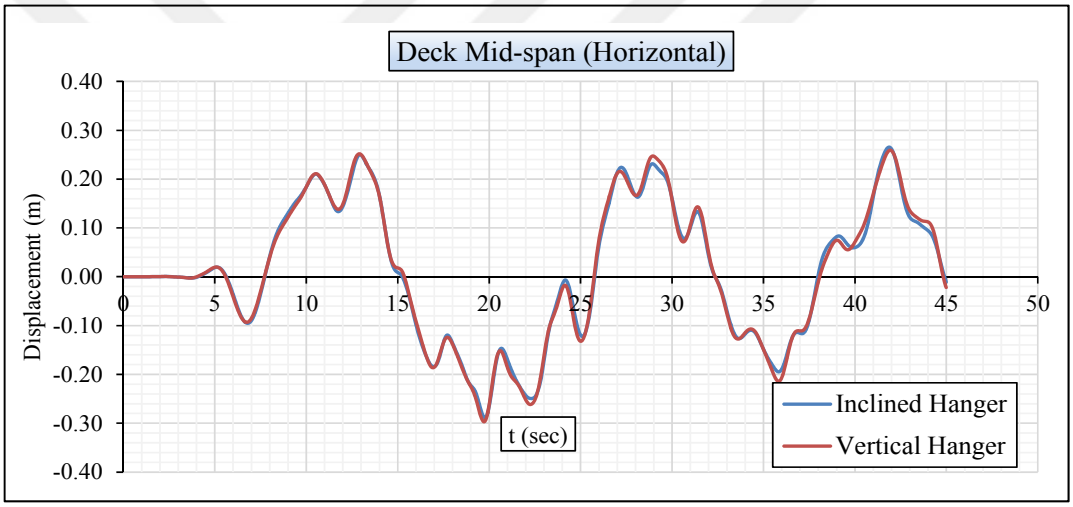

Figure 7.38 : Deck mid-span (horizontal) displacement results from the Up analysis for the bridge with inclined and vertical hanger under the DD-1 earthquake.

The displacement-time histories of the critical points are also presented in Figures 7.38-43. Although a decrease in the horizontal displacement at the deck mid-span shown in Figure 7.38 is expected for the bridge with vertical hanger due to the viscous dampers and the wind tongue, almost similar displacement response is obtained for the bridge with inclined and vertical hangers. This outcome is based on the earthquake excitation type. In order to provide the geometry and stability of the bridge with inclined hanger to be same for the bridge with vertical hanger, no change in the displacement in the vertical direction is estimated before the Up analysis. This estimation is provided as depicted in Figure 7.39.

Table 7.28 : Tower base-section results from the Up analysis for the bridge with inclined and vertical hanger under the DD-1earthquake.

Tower Base Section	Uniform-point analysis		Change (%)	Capacity				Capacity Ratio			
	Inclined	Vertical		Yield		Plastic					
				Inclined	Vertical	Inclined	Vertical	Inclined/ Yield	Vertical/ Yield	Inclined/ Plastic	Vertical/ Plastic
Shear Force (kN) (max.)	5903.36	5555.59	**-5.89**	-	-	-	-	**-**	**-**	**-**	**-**
Bending Moment (kNm)(max)	196205.48	92409.89	**-52.90**	449159.00	687623.00	708195.00	1118541.00	**43.68**	**13.44**	**27.71**	**8.26**
Compressive Axial Force (kN) (max)	189647.31	196852.95	**3.80**	385959.00	385959.00	385959.00	385959.00	**49.14**	**51.00**	**49.14**	**51.00**

Table 7.29 : Approach box results from the Up analysis for the bridge with inclined and vertical hanger under the DD-1 earthquake.

Approach Box	Uniform-point analysis		Change (%)	Capacity		Capacity Ratio			
	Inclined	Vertical		Yield	Plastic	Inclined/Yield	Vertical/Yield	Inclined/Plastic	Vertical/Plastic
Shear Force (kN) (max.)	3469.74	3576.14	**3.07**	-	-	**-**	**-**	**-**	**-**
Bending Moment (kNm) (max)	51578.40	46018.10	**-10.78**	109964.00	169883.10	**46.90**	**41.85**	**30.36**	**27.09**
Compressive Axial Force (kN) (max)	14502.82	10508.05	**-27.54**	82447.00	82447.00	**17.59**	**12.75**	**17.59**	**12.75**

Table 7.30 : Approach column results from the Up analysis for the bridge with inclined and vertical hanger under the DD-1 earthquake.

Approach Column	Uniform-point analysis		Change (%)	Capacity		Capacity Ratio			
	Inclined	Vertical		Yield	Plastic	Inclined/ Yield	Vertical/ Yield	Inclined/ Plastic	Vertical/ Plastic
Shear Force (kN) (max.)	110.30	113.85	**3.22**	-	-	**-**	**-**	**-**	**-**
Bending Moment (kNm) (max)	1511.16	1667.69	**10.36**	22580.00	29036.50	**6.69**	**7.39**	**5.20**	**5.74**
Compressive Axial Force (kN) (max)	7889.62	8418.70	**6.71**	48460.00	48460.00	**16.28**	**17.37**	**16.28**	**17.37**

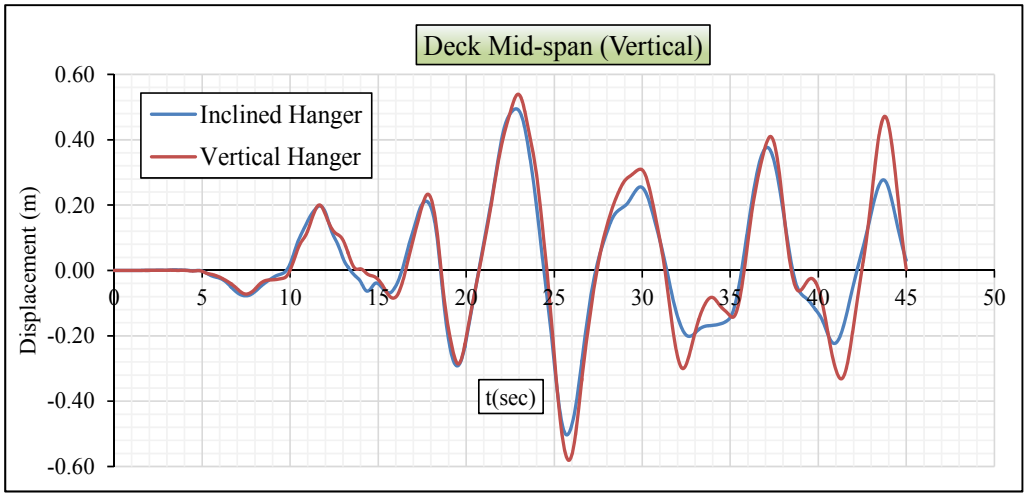

Figure 7.39 : Deck mid-span (vertical) displacement results from the Up analysis for the bridge with inclined and vertical hanger under the DD-1earthquake.

The most important direction to show the effects of the vertical hanger arrangement on the displacement response history is the longitudinal direction at the deck mid-span. As indicated in Figure 7.40, almost similar displacement response is obtained despite of estimating reduced longitudinal displacement in case of vertical hanger. This conclusion pertains to the earthquake excitation type, the uniform-point earthquake.

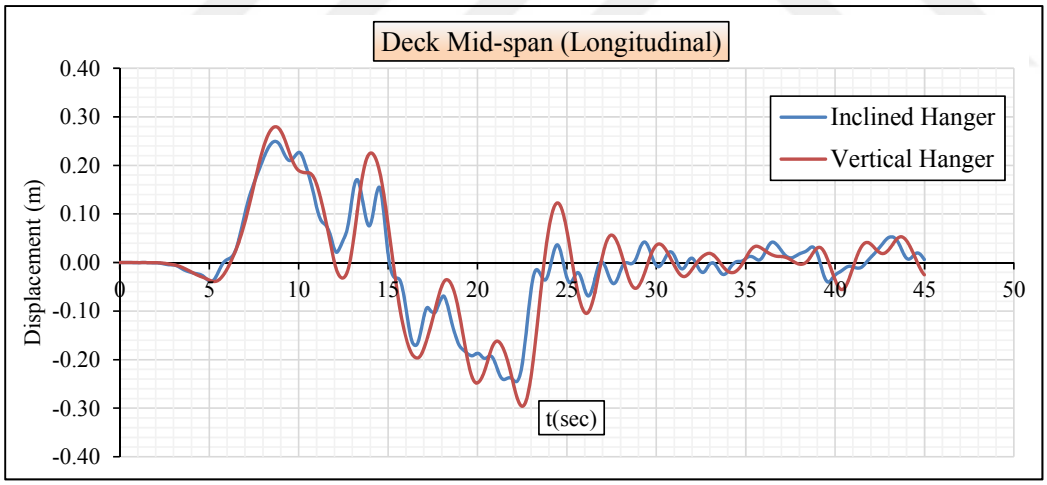

Figure 7.40: Deck mid-span (longitudinal) displacement results from the Up analysis for the bridge with inclined and vertical hanger under the DD-1 earthquake.

Due to very high rigidity in longitudinal direction of the main deck, the displacement-time histories of the expansion joints are expected to be same as that of the deck mid-span. This expectation is obtained as indicated in Figure 7.41. Based on this outcome, the viscous dampers and wind tongue are determined not to be effective to decrease in the displacement in longitudinal direction.

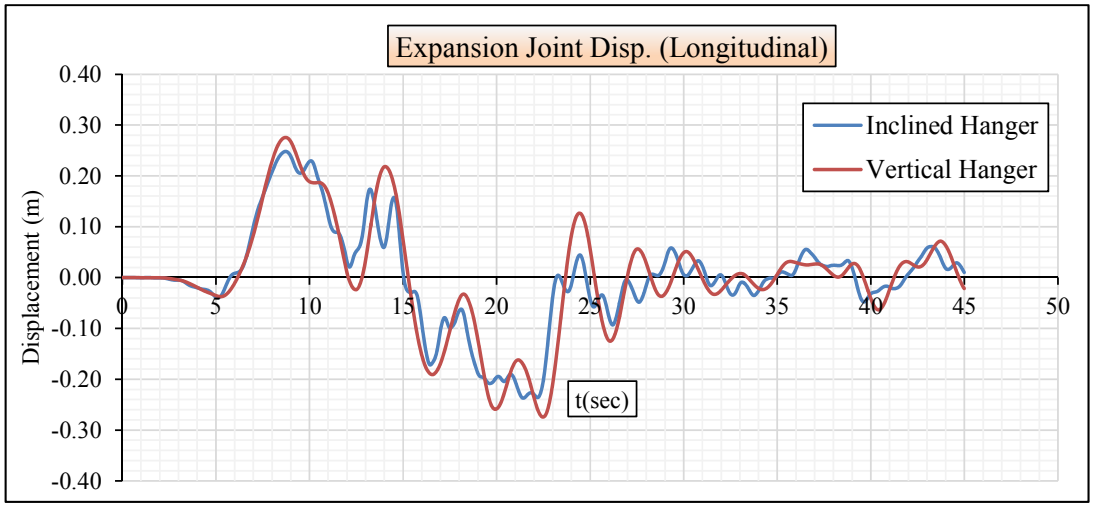

Figure 7.41 : Expansion joint displacement results from the Up analysis for the DD-1 earthquake.

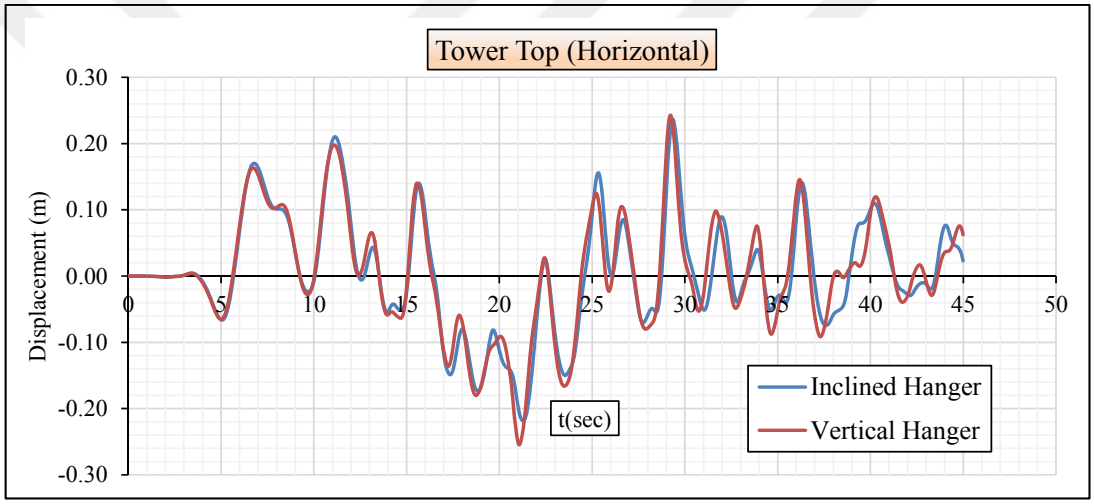

Figure 7.42 : Tower top (horizontal) displacement results from the Up analysis for the DD-1 earthquake.

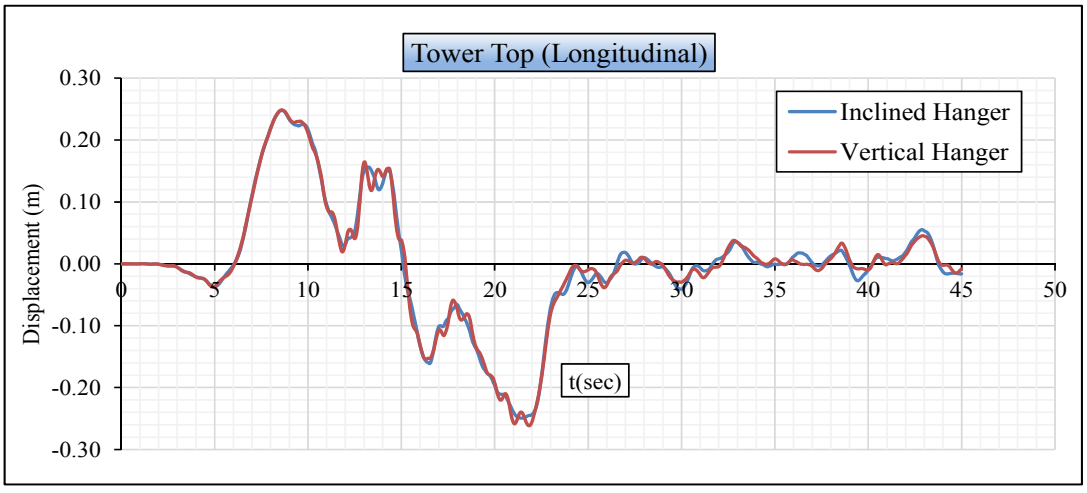

Figure 7.43 : Tower top (longitudinal) displacement results from the Up analysis for the DD-1 earthquake.

In order to provide the geometric and stability features of the bridge with vertical hanger to be same as those of the bridge with inclined hanger, the results from displacement of the tower top-saddle of the bridge with vertical hanger are estimated not to be different from that of the bridge with inclined hanger. The analysis results reveal no change in displacement-time history in horizontal and longitudinal directions at the tower-top saddle as presented in Figures 7.42-43.

Consequently, the uniform-point earthquake analysis (Up) is carried out for two FE models of the bridge: (i) inclined hanger and (ii) vertical hanger. Besides, the scenario and DD-1 compatible multi-point earthquake motions are considered for the Mp analyses.

7.3 Comparison

The main aim of the earthquake analysis of the Bosphorus Bridge is to identify the effects of the hanger arrangement on structural performance prediction of the bridge. Therefore, the Mp and Up analysis results are separately given in the former section with the tables on the basis of comparison of inclined hanger with vertical hanger. In addition, two different analysis methods (Mp and Up) and earthquake levels (scenario and DD-1) are also considered for this purpose. However, a comparison between the scenario and DD-1 multi-point earthquake motions is not made in the analysis section. Similarly, the effects of the earthquake excitation type: Mp and Up on the structural response of the bridge with inclined and vertical hangers are not specified with comparison. Accordingly, the following comparisons are presented in this section of the dissertation.

- Earthquake level comparison (Scenario and DD-1)
- Analysis method comparison (Mp and Up)

7.3.1 Earthquake level comparison (Scenario and DD-1)

7.3.1.1 Comparison for the Up analysis

The comparison results for the earthquake level under uniform-point earthquake motions are presented in detail in Tables 7.31-35 and Figures 7.44-49. According to Table 7.31, the cable elements are not relatively affected from the earthquake level for both hanger arrangements. Even though higher increase in the cable elements is

expected, the capacity ratio of them reaching to 90% indicates that the obtained results are in the allowable value. This means that the cable elements are using their capacity regardless of the earthquake levels considered. Therefore, two earthquake levels are critical for the cable elements. On the other hand, these outcomes can be based on the analysis method (Up) comparing to those from the Mp analysis, which yields to expectation for higher results from the Mp analysis. Consequently, the highest increase in the tensile force is obtained for the hanger elements as 2.50 %- 2.90 % in two hanger arrangements.

As given in Table 7.32, the bending moment and the compressive axial force of the lower portal beam are relatively influenced from the earthquake level for both hanger arrangements. Based on the increase in these actions, the bridge with vertical hanger is affected more than the bridge with inclined hanger due to the wind tongue and the viscous dampers at the expansion joints. For the middle and upper portal beams, the highest increase for two models is obtained in the shear force and the bending moment. Similar results are also obtained for the upper portal. The link beam function of the portal beams between two tower legs are proved with this conclusion.

The tower base section is obtained not to be affected from the earthquake level under the uniform-point earthquake motions as presented in Table 7.33. The low increase is related to the Up analysis methods. Under the multi-point earthquake motions, percentage increase is estimated to be higher than the Up motions.

Earthquake level noticeably affects only the bending moment of the main deck of the bridge with inclined hanger. For the bridge with vertical hanger, the bending moment and the compressive axial force are obtained to be affected from the earthquake level as given in Table 7.34. Depending on these outcomes, the bridge with vertical hanger is more sensitive than the bridge inclined hanger in terms of the compressive axial force. This conclusion is based on the viscous dampers and wind tongues.

According to Table 7.35, the box-beam and column of the approach viaduct are determined not to be more sensitive to the earthquake level. The highest increase is obtained in the compressive axial force of the box-beam of the bridge with vertical hanger. This conclusion indicates that the viscous dampers and wind tongues are effective as the earthquake level increases.

Table 7.31: Earthquake level comparison under uniform-point earthquake for the cable elements.

Cable Elements Tensile Force	Results				Change			
	Scenario EQ		DD-1 EQ		Inclined		Vertical	
	Inclined	Vertical	Inclined	Vertical	%	Graphic	%	Graphic
Main Cable (kN) (max.)	218659.71	213970.91	220814.04	217709.73	**0.99**		**1.75**	
Back-Stay (kN) (max)	229620.56	227359.63	231934.55	231635.61	**1.01**		**1.88**	
Hanger (kN (max)	6564.02	2281.40	6752.76	2338.38	**2.88**		**2.50**	

Table 7.32 : Earthquake level comparison under uniform-point earthquake for the portal beams.

Portal Beam		Results				Change			
		Scenario EQ		DD-1 EQ		Inclined		Vertical	
		Inclined	Vertical	Inclined	Vertical	%	Graphic	%	Graphic
Lower Portal	Shear Force (kN) (max.)	7424.05	7781.20	7939.36	8747.73	**6.94**		**12.42**	
	Bending Moment (kNm) (max)	56888.94	60408.18	74555.96	83016.44	**31.06**		**37.43**	
	Compressive Axial Force (kN) (max)	1627.00	1687.73	1893.50	2079.48	**16.38**		**23.21**	
Middle Portal	Shear Force (kN) (max.)	2588.25	2735.43	3958.89	4136.36	**52.96**		**51.21**	
	Bending Moment (kNm) (max)	35882.97	37228.39	54801.66	57348.89	**52.72**		**54.05**	
	Compressive Axial Force (kN) (max)	138.40	135.14	142.68	154.85	**3.09**		**14.59**	
Upper Portal	Shear Force (kN) (max.)	1513.84	1564.81	2263.54	2267.57	**49.52**		**44.91**	
	Bending Moment (kNm) (max)	20722.64	21338.41	30582.83	30519.25	**47.58**		**43.02**	
	Compressive Axial Force (kN) (max)	1324.28	1349.87	1327.74	1378.26	**0.26**		**2.10**	

Table 7.33 : Earthquake level comparison under uniform-point earthquake for the tower base section.

Tower Base Section	Results				Change			
	Scenario EQ		DD-1 EQ		Inclined		Vertical	
	Inclined	Vertical	Inclined	Vertical	%	Graphic	%	Graphic
Shear Force (kN) (max.)	5667.81	5360.42	5903.36	5555.59	**4.16**		**3.64**	
Bending Moment (kNm) (max)	190122.31	85026.73	196205.48	92409.89	**3.20**		**8.68**	
Compressive Axial Force (kN) (max)	187255.89	193822.25	189647.31	196852.95	**1.28**		**1.56**	

Table 7.34 : Earthquake level comparison under uniform-point earthquake for the main deck.

Deck	Results				Change			
	Scenario EQ		DD-1 EQ		Inclined		Vertical	
	Inclined	Vertical	Inclined	Vertical	%	Graphic	%	Graphic
Shear Force (kN) (max.)	4413.84	4425.16	4712.83	4535.51	**6.77**		**2.49**	
Bending Moment (kNm) (max)	125341.00	139632.02	192112.51	192932.58	**53.27**		**38.17**	
Compressive Axial Force (kN) (max)	51932.72	6526.41	56725.31	9360.31	**9.23**		**43.42**	

Table 7.35 : Earthquake level comparison under uniform-point earthquake for the box-beam and column of the approach viaduct.

Approach		Results				Change			
		Scenario EQ		DD-1 EQ		Inclined		Vertical	
		Inclined	Vertical	Inclined	Vertical	%	Graphic	%	Graphic
Beam	Shear Force (kN) (max.)	3243.78	3297.87	3469.74	3576.14	**6.97**		**8.44**	
	Bending Moment (kNm) (max)	48860.43	42570.71	51578.40	46018.10	**5.56**		**8.10**	
	Compressive Axial Force (kN) (max)	13633.54	9208.56	14502.82	10508.05	**6.38**		**14.11**	
Column	Shear Force (kN) (max.)	107.13	112.31	110.30	113.85	**2.97**		**1.38**	
	Bending Moment (kNm) (max)	1495.82	1650.23	1511.16	1667.69	**1.03**		**1.06**	
	Compressive Axial Force (kN) (max)	7331.86	7601.81	7889.62	8418.70	**7.61**		**10.75**	

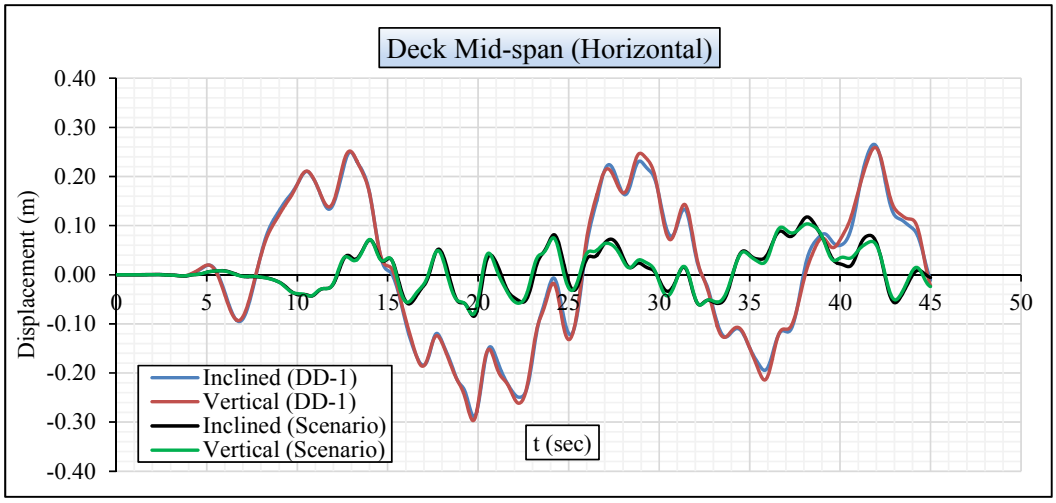

Figure 7.44 : Earthquake level comparison under uniform-point earthquake for the displacement from the deck mid-span in horizontal direction.

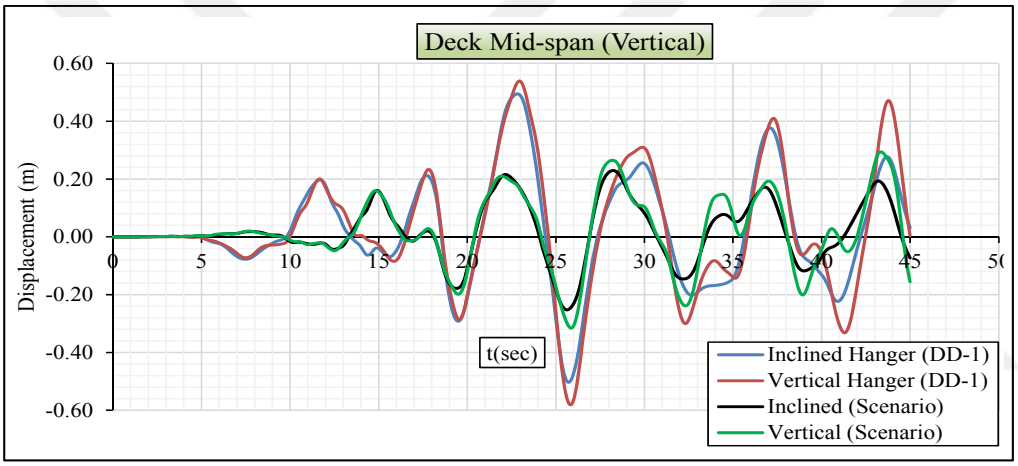

Figure 7.45 : Earthquake level comparison under uniform-point earthquake for the dispclacement from the deck mid-span in vertical direction.

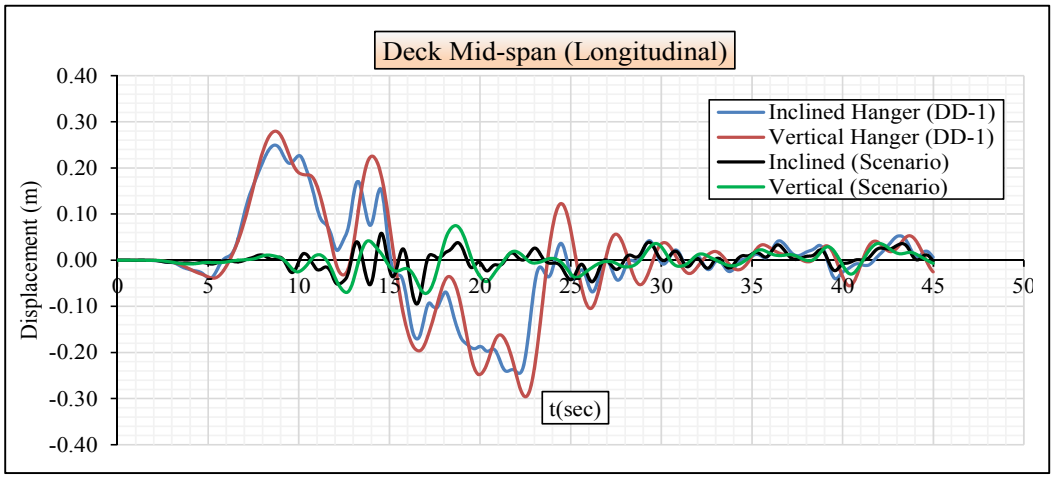

Figure 7.46 : Earthquake level comparison under uniform-point earthquake for the displacement from the deck mid-span in longitudinal direction.

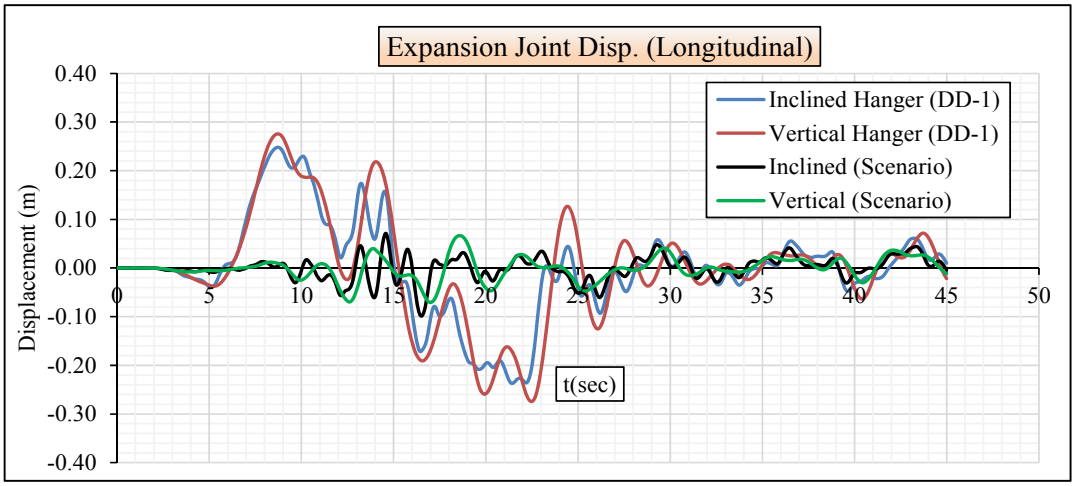

Figure 7.47 : Earthquake level comparison under uniform-point earthquake for the displacement from the expansion joint in longitudinal direction.

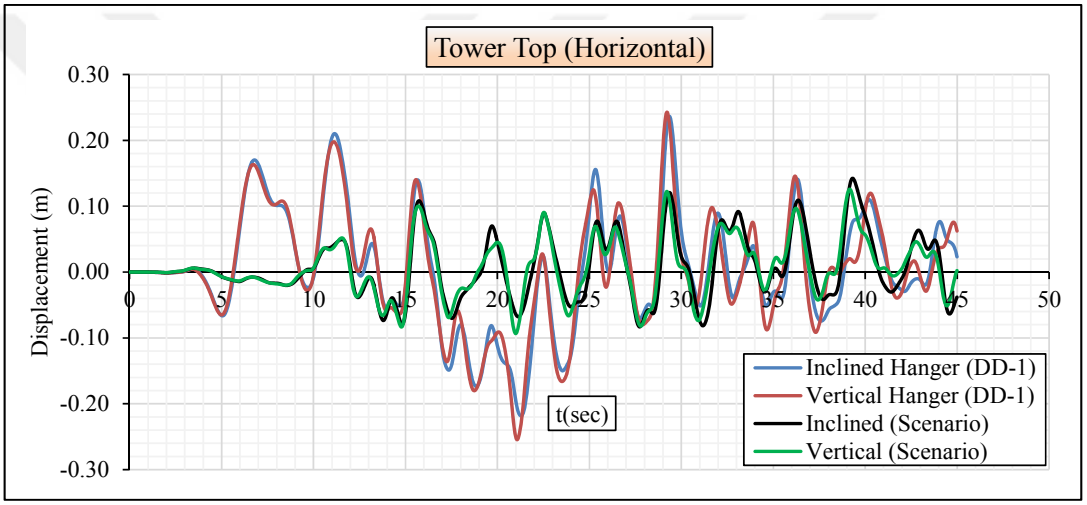

Figure 7.48 : Earthquake level comparison under uniform-point earthquake for the displacement from the tower top-saddle in horizontal direction.

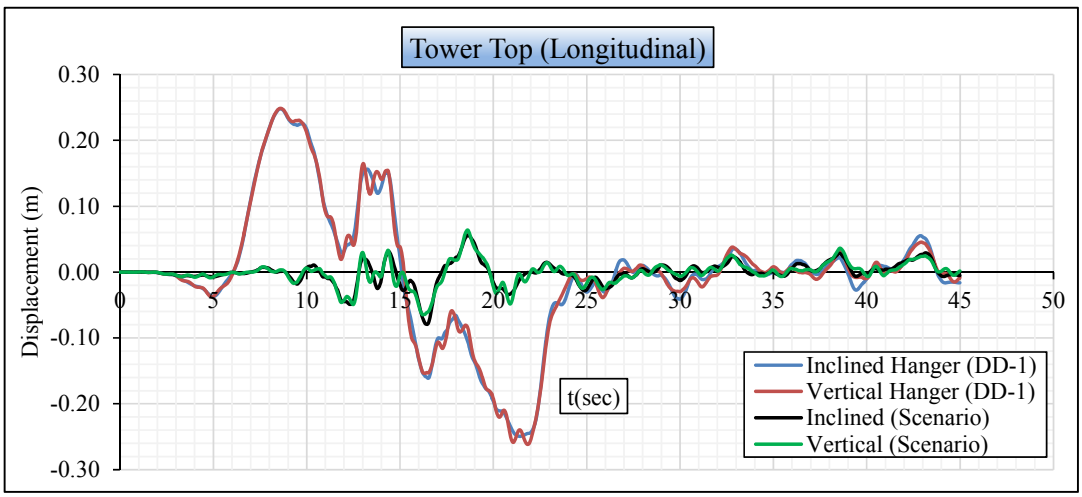

Figure 7.49 : Earthquake level comparison under uniform-point earthquake for the displacement from the tower top-saddle in longitudinal direction.

The comparison is also made for displacement time-history of the critical points of the bridge in Figures 7.44-49. From the all figures, displacement response of the bridge increases under the DD-1 uniform-point earthquake. Moreover, the vertical hanger arrangement is obviously determined to affect the structural response of the Bosphorus Bridge.

Consequently, the results from the earthquake level comparison conclude that the sectional force value is affected less than estimated value under the uniform-point earthquake. The highest increase in the sectional force is obtained for the portal beams and the main deck that directly pertinent to the viscous damper and the wind tongues. Hence, the viscous damper and the wind tongues are determined to be more sensitive to the earthquake level. The low increase in the sectional force of the bridge is predicted to be related to the analysis method (Up).

7.3.1.2 Comparison for the Mp analysis

According to the comparison for the cable elements as presented in Table 7.36, 10 %-12 % increase in the tensile force of the main and back-stay cables is obtained. The increase in the hanger elements reaches to 48 % for the bridge with inclined hanger and to 26 % for the bridge with vertical hanger. Such a high difference is based on the no horizontal component of vertical hanger. Thus, the cable elements are obtained to be affected from the earthquake level under the multi-point earthquake.

As given in Table 7.37, the highest increase is determined for the lower portal beam. Particularly, the shear force and the bending moment increase as 136 % - 180 %. The bridge with inclined hanger is determined to be more sensitive to the earthquake level than the bridge with vertical hanger under the multi-point earthquake motions. For the other portal beams, the percentage increase is lower than that of the lower portal beam. These conclusions depict that the portal beam are affected from the multi-point earthquake level due to its support function for the main deck and the approach viaducts.

As expected from the high increase in the lower portal beams, the bending moment and the shear force of the tower base-section are increased as 200%-290%. The increase in these forces is based on the additional force from the viscous dampers and the wind tongues at the expansion joints. Moreover, the additional forces from these devices require high movement in longitudinal direction at the expansion joints.

Table 7.36 : Earthquake level comparison under multi-point earthquake for the cable elements.

Cable Elements Tensile Force	Results				Change			
	Scenario EQ		DD-1 EQ		Inclined		Vertical	
	Inclined	Vertical	Inclined	Vertical	%	Graphic	%	Graphic
Main Cable (kN) (max.)	227656.41	223413.97	252693.40	249125.03	**11.00**		**11.51**	
Back-Stay (kN) (max)	238801.88	236512.09	265474.15	265382.15	**11.17**		**12.21**	
Hanger (kN (max)	8391.31	2409.40	12456.30	3031.78	**48.44**		**25.83**	

Table 7.37 : Earthquake level comparison under multi-point earthquake for the portal beams.

Portal Beam		Results				Change			
		Scenario EQ		DD-1 EQ		Inclined		Vertical	
		Inclined	Vertical	Inclined	Vertical	%	Graphic	%	Graphic
Lower Portal	Shear Force (kN) (max.)	13447.16	15349.43	37531.87	41208.71	**179.11**		**168.47**	
	Bending Moment (kNm) (max)	84620.97	91638.15	221286.25	216271.43	**161.50**		**136.01**	
	Compressive Axial Force (kN) (max)	2407.43	2351.47	3171.03	3575.04	**31.72**		**52.03**	
Middle Portal	Shear Force (kN) (max.)	4003.98	4393.48	4814.95	4760.83	**20.25**		**8.36**	
	Bending Moment (kNm) (max)	58711.31	63933.47	70471.44	67714.56	**20.03**		**5.91**	
	Compressive Axial Force (kN) (max)	185.39	213.45	220.67	214.20	**19.03**		**0.35**	
Upper Portal	Shear Force (kN) (max.)	2499.26	2387.72	3217.35	3051.64	**28.73**		**27.81**	
	Bending Moment (kNm) (max)	34541.40	33090.10	44998.16	42004.94	**30.27**		**26.94**	
	Compressive Axial Force (kN) (max)	1430.47	1454.82	1674.37	1677.53	**17.05**		**15.31**	

Table 7.38 : Earthquake level comparison under multi-point earthquake for the tower base section.

Tower Base Section	Results				Change			
	Scenario EQ		DD-1 EQ		Inclined		Vertical	
	Inclined	Vertical	Inclined	Vertical	%	Graphic	%	Graphic
Shear Force (kN) (max.)	10618.72	12122.69	31862.00	36040.74	**200.06**		**197.30**	
Bending Moment (kNm) (max)	331269.55	388237.03	1252816.64	1514042.15	**278.19**		**289.98**	
Compressive Axial Force (kN) (max)	200058.29	200160.00	223437.82	231213.41	**11.69**		**15.51**	

Table 7.39 : Earthquake level comparison under multi-point earthquake for the main deck.

Deck	Results				Change			
	Scenario EQ		DD-1 EQ		Inclined		Vertical	
	Inclined	Vertical	Inclined	Vertical	%	Graphic	%	Graphic
Shear Force (kN) (max.)	5297.24	4760.18	6822.00	5587.18	**28.78**		**17.37**	
Bending Moment (kNm) (max)	265595.42	248771.30	406831.55	432207.23	**53.18**		**73.74**	
Compressive Axial Force (kN) (max)	69234.00	11174.54	81827.52	43575.38	**18.19**		**289.95**	

Table 7.40 : Earthquake level comparison under multi-point earthquake for the box-beam and column of the approach viaduct.

Approach		Results				Change			
		Scenario EQ		DD-1 EQ		Inclined		Vertical	
		Inclined	Vertical	Inclined	Vertical	%	Graphic	%	Graphic
Beam	Shear Force (kN) (max.)	3881.57	3965.87	6198.61	5758.44	59.69		45.20	
	Bending Moment (kNm) (max)	72482.49	53156.22	224092.91	196101.56	209.17		268.92	
	Compressive Axial Force (kN) (max)	26291.76	13081.81	39433.22	42449.79	49.98		224.49	
Column	Shear Force (kN) (max.)	208.42	199.98	430.78	785.07	106.69		292.57	
	Bending Moment (kNm) (max)	2866.62	3272.75	12540.59	16417.65	337.47		401.65	
	Compressive Axial Force (kN) (max)	8232.36	8702.30	10994.80	10821.09	33.56		24.35	

The displacement time-history of the critical points of the bridge is also presented to identify the earthquake level effects on the displacement response of the bridge. Total number of three points in three directions are considered and the results are given in Figures 7.50-7.55. For all points, considerable diffrerence between the earthquakes considered is determined under the multi-point earthquake.

As a result, the earthquake level comparison is relatively effective under the multi-point earthquake motion compared to the uniform-point earthquake motion. Along with the DD-1 earthquake, the multi-point earthquake analysis is obtained to be an important parameter for reliable earthquake analysis of the bridge.

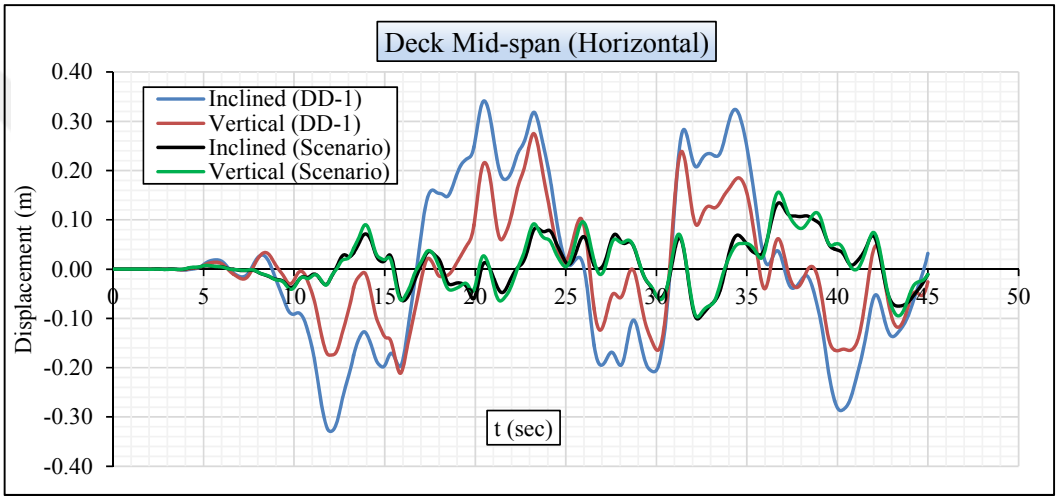

Figure 7.50 : Earthquake level comparison under multi-point earthquake for the displacement from the deck mid-span in horizontal direction.

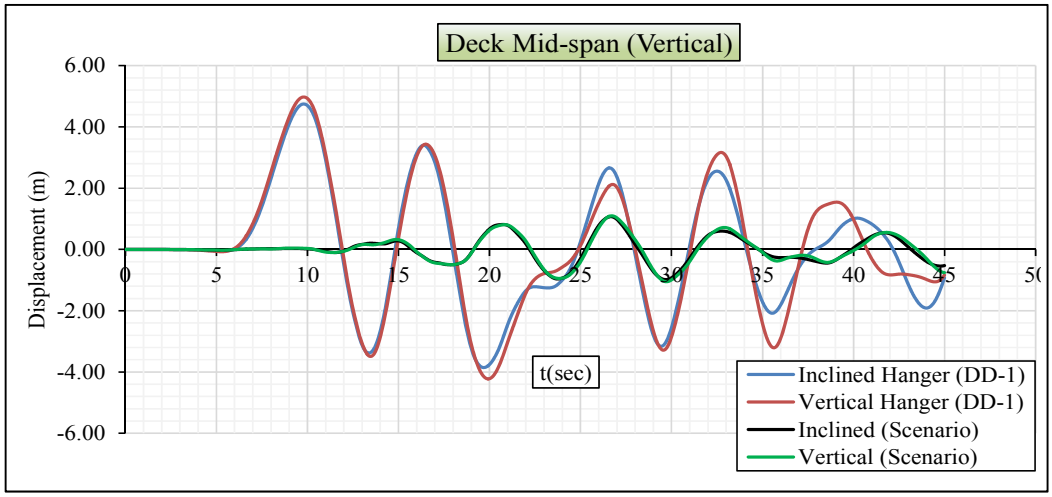

Figure 7.51 : Earthquake level comparison under multi-point earthquake for the displacement from the deck mid-span in vertical direction.

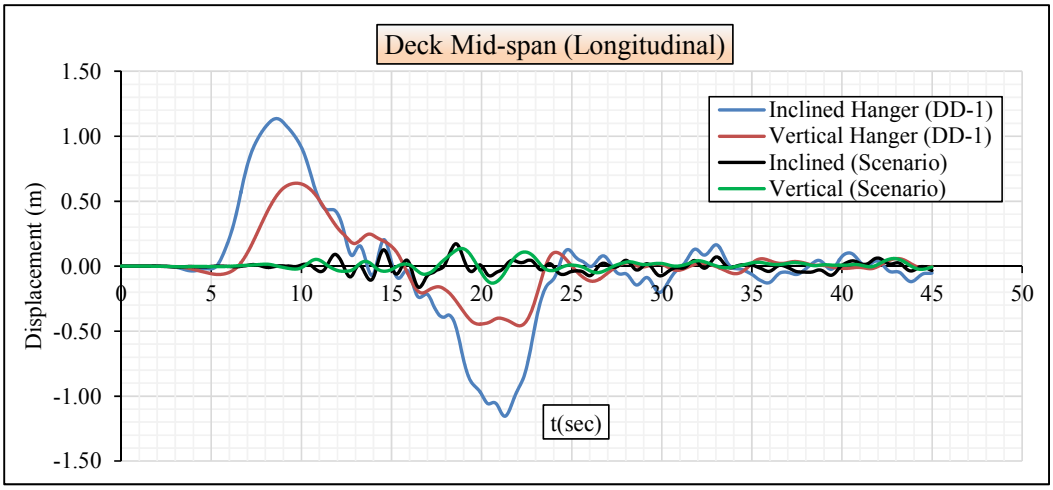

Figure 7.52 : Earthquake level comparison under multi-point earthquake for the displacement from the deck mid-span in longitudinal direction.

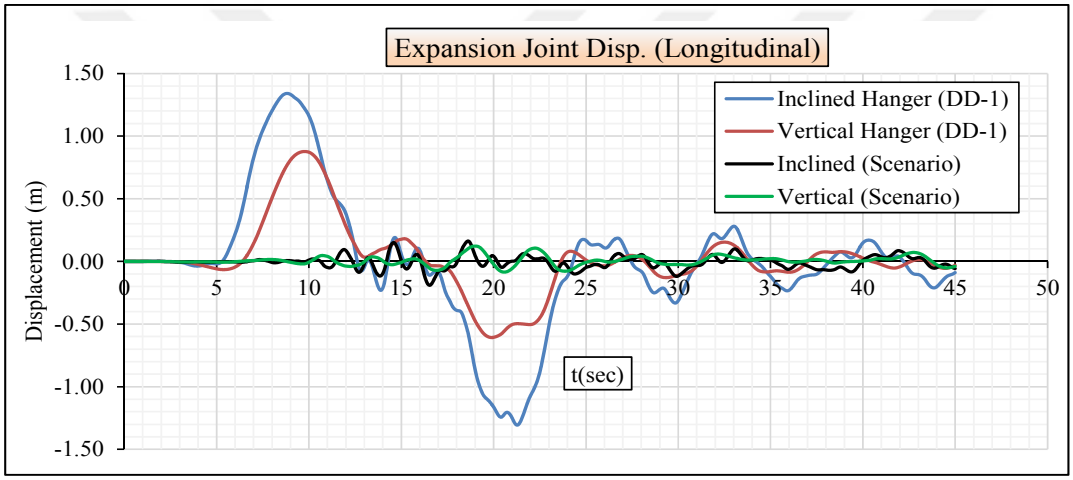

Figure 7.53 : Earthquake level comparison under multi-point earthquake for the displacement from the expansion joint in longitudinal direction.

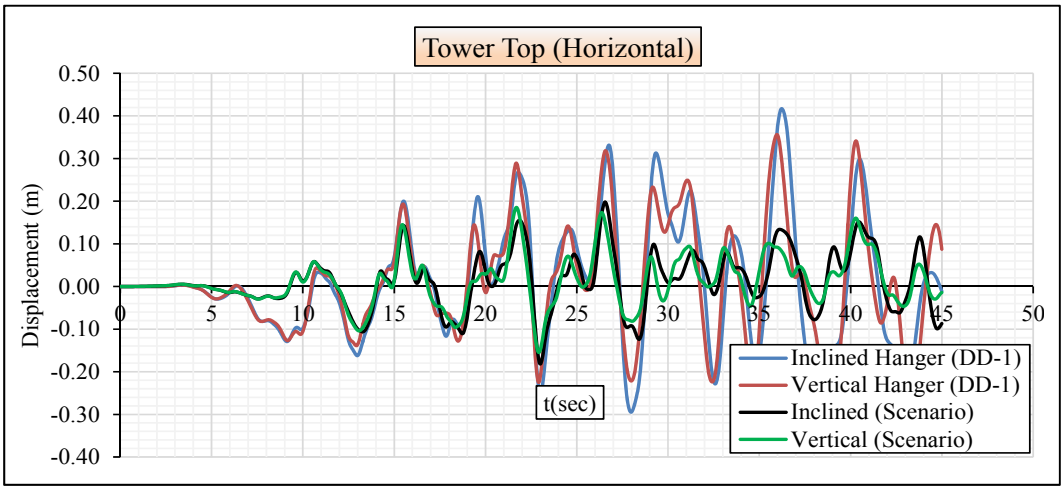

Figure 7.54 : Earthquake level comparison under uniform-point earthquake for the displacement from the tower top-saddle in horizontal direction.

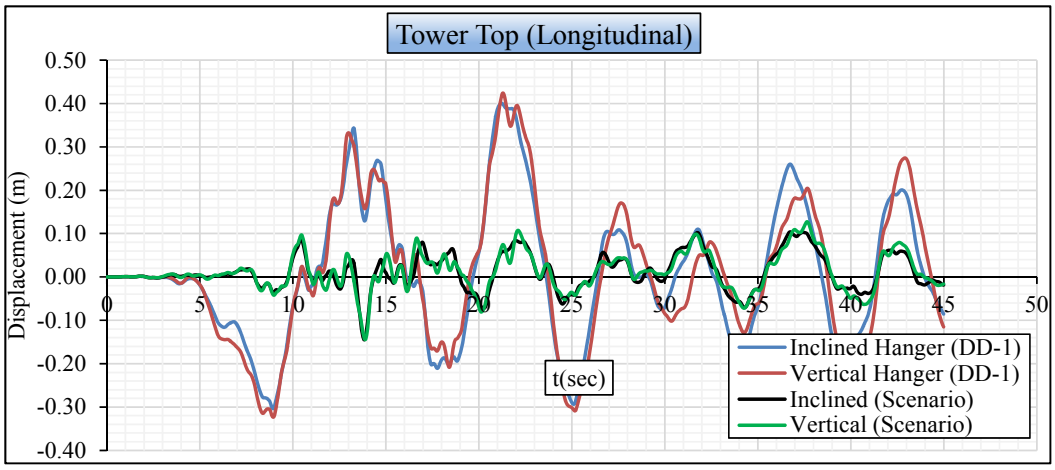

Figure 7.55 : Earthquake level comparison under uniform-point earthquake for the displacement from the tower top-saddle in longitudinal direction.

7.3.2 Earthquake analysis method comparison (Mp and Up)

7.3.2.1 Comparison for the scenario earthquake

According to Table 7.41, the highest increase in tensile force of the cable elements is obtained for the hanger elements. The others increase relatively less than the hangers. The difference between the inclined and the vertical hangers is directly pertinent to no horizontal component of the vertical hanger. Besides, the scenario earthquake is estimated not to be effective for the Mp analysis. Based on the results given in Table 7.42, the shear force and the bending moment increase in all portal beams. The percentage increase is decreasing from the lower portal beam to the upper portal beam. Moreover, the percentage values of the lower and middle portal beams of the bridge with vertical hanger are higher than those of the bridge with inclined hanger. Accordingly, the sectional forces of the portal beams are affected from the earthquake analysis method (Mp analysis).For the tower base-section as presented in Table 7.43, relatively high increase is obtained for the shear force and the bending moment. The percentage values of the bridge with vertical hanger are also higher than those of the bridge with inclined hanger. This increase is based on the additional force from the viscous dampers and wind tongues. Similarly, all sectional forces increase in the main deck given in Table 7.44. From the difference between the compressive axial forces of the bridge with inclined and vertical hangers, the displacement at the expansion joints estimated to be high under the scenario multi-point earthquake motion. As shown in Table 7.45, similar increase in all sectional forces is obtained for the approach viaducts.

Table 7.41 : Earthquake analysis method comparison under scenario earthquake for the cable elements.

Cable Elements Tensile Force	Results				Change			
	Up		Mp		Inclined		Vertical	
	Inclined	Vertical	Inclined	Vertical	%	Graphic	%	Graphic
Main Cable (kN) (max.)	218659.71	213970.91	227656.41	223413.97	**4.11**		**4.41**	
Back-Stay (kN) (max)	229620.56	227359.63	238801.88	236512.09	**4.00**		**4.03**	
Hanger (kN (max)	6564.02	2281.40	8391.31	2409.40	**27.84**		**5.61**	

Table 7.42 : Earthquake analysis method comparison under scenario earthquake for the portal beams.

Portal Beam		Results				Change			
		Up		Mp		Inclined		Vertical	
		Inclined	Vertical	Inclined	Vertical	%	Graphic	%	Graphic
Lower Portal	Shear Force (kN) (max.)	7424.05	7781.20	13447.16	15349.43	**81.13**		**97.26**	
	Bending Moment (kNm) (max)	56888.94	60408.18	84620.97	91638.15	**48.75**		**51.70**	
	Compressive Axial Force (kN) (max)	1627.00	1687.73	2407.43	2351.47	**47.97**		**39.33**	
Middle Portal	Shear Force (kN) (max.)	2588.25	2735.43	4003.98	4393.48	**54.70**		**60.61**	
	Bending Moment (kNm) (max)	35882.97	37228.39	58711.31	63933.47	**63.62**		**71.73**	
	Compressive Axial Force (kN) (max)	138.40	135.14	185.39	213.45	**33.95**		**57.95**	
Upper Portal	Shear Force (kN) (max.)	1513.84	1564.81	2499.26	2387.72	**65.09**		**52.59**	
	Bending Moment (kNm) (max)	20722.64	21338.41	34541.40	33090.10	**66.68**		**55.07**	
	Compressive Axial Force (kN) (max)	1324.28	1349.87	1430.47	1454.82	**8.02**		**7.77**	

Table 7.43 : Earthquake analysis method comparison under scenario earthquake for the tower base-section.

Tower Base Section	Results				Change			
	Up		Mp		Inclined		Vertical	
	Inclined	Vertical	Inclined	Vertical	%	Graphic	%	Graphic
Shear Force (kN) (max.)	5667.81	5360.42	10618.72	12122.69	**87.35**		**126.15**	
Bending Moment (kNm) (max)	190122.31	85026.73	331269.55	388237.03	**74.24**		**356.61**	
Compressive Axial Force (kN) (max)	187255.89	193822.25	200058.29	200160.00	**6.84**		**3.27**	

Table 7.44 : Earthquake analysis method comparison under scenario earthquake for the main deck.

Deck	Results				Change			
	Up		Mp		Inclined		Vertical	
	Inclined	Vertical	Inclined	Vertical	%	Graphic	%	Graphic
Shear Force (kN) (max.)	4413.84	4425.16	5297.24	4760.18	**20.01**		**7.57**	
Bending Moment (kNm) (max)	125341.00	139632.02	265595.42	248771.30	**111.90**		**78.16**	
Compressive Axial Force (kN) (max)	51932.72	6526.41	69234.00	11174.54	**33.31**		**71.22**	

Table 7.45 : Earthquake analysis method comparison under scenario earthquake for the box-beam and column of the approach viaduct.

Approach		Results				Change			
		Up		Mp		Inclined		Vertical	
		Inclined	Vertical	Inclined	Vertical	%	Graphic	%	Graphic
Beam	Shear Force (kN) (max.)	3243.78	3297.87	3881.57	3965.87	**19.66**		**20.26**	
	Bending Moment (kNm) (max)	48860.43	42570.71	72482.49	53156.22	**48.35**		**24.87**	
	Compressive Axial Force (kN) (max)	13633.54	9208.56	26291.76	13081.81	**92.85**		**42.06**	
Column	Shear Force (kN) (max.)	107.13	112.31	208.42	199.98	**94.56**		**78.07**	
	Bending Moment (kNm) (max)	1495.82	1650.23	2866.62	3272.75	**91.64**		**98.32**	
	Compressive Axial Force (kN) (max)	7331.86	7601.81	8232.36	8702.30	**12.28**		**14.48**	

Earthquake analysis method comparison under the scenario earthquake motion is also made according to the displacement time-histories of the critical points of the bridge. Generally, the Mp analysis amplifies the displacement values according to Figures 7.56-61.

Depending on the results from the Mp-Up comparison under the scenario earthquake, the Mp analysis yields to higher sectional force and displacement response than the Up analysis. Therefore, the Mp analysis method is determined to be considered for long-span bridges.

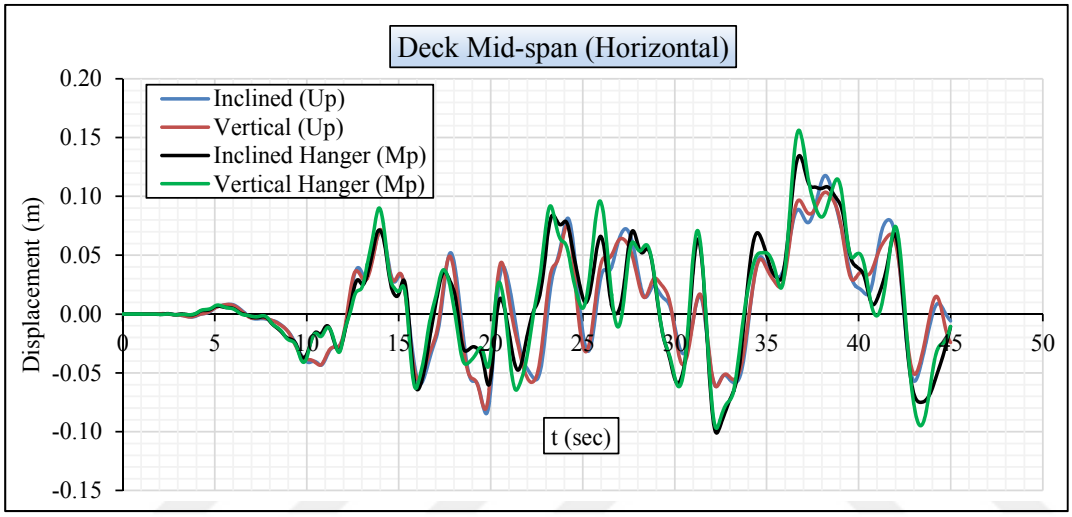

Figure 7.56 : Earthquake analysis method comparison under the scenario earthquake for displacement from the deck mid-span in horizontal direction.

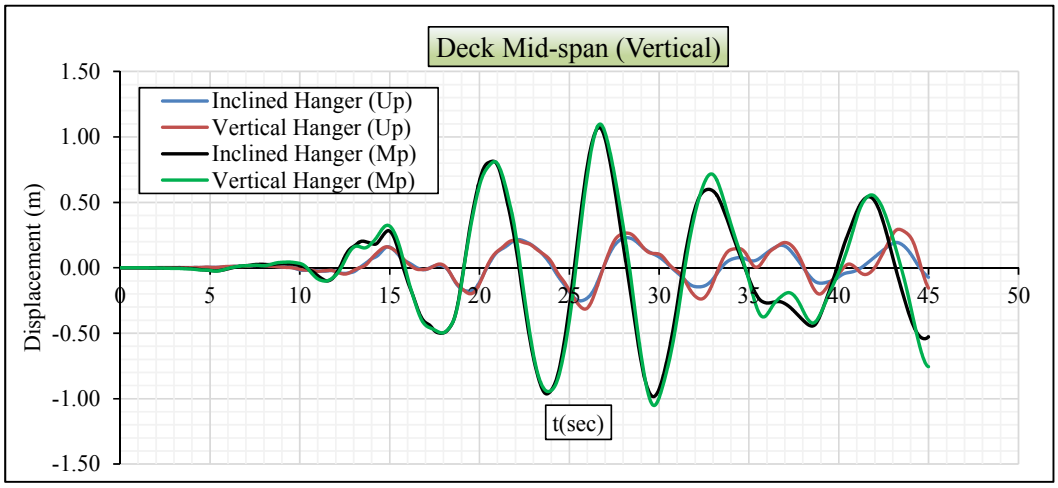

Figure 7.57 : Earthquake analysis method comparison under the scenario earthquake for displacement from the deck mid-span in vertical direction.

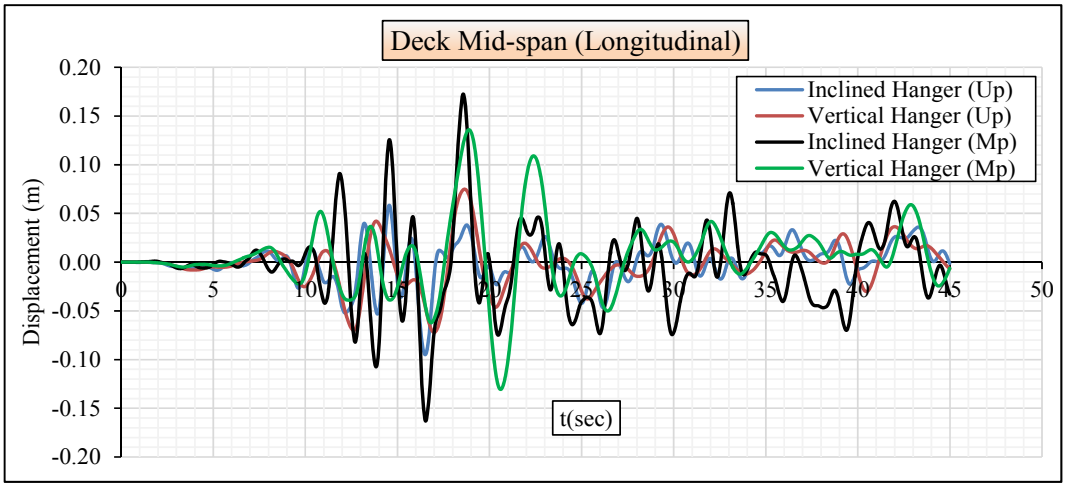

Figure 7.58 : Earthquake analysis method comparison under the scenario earthquake for displacement from the deck mid-span in longitudinal direction.

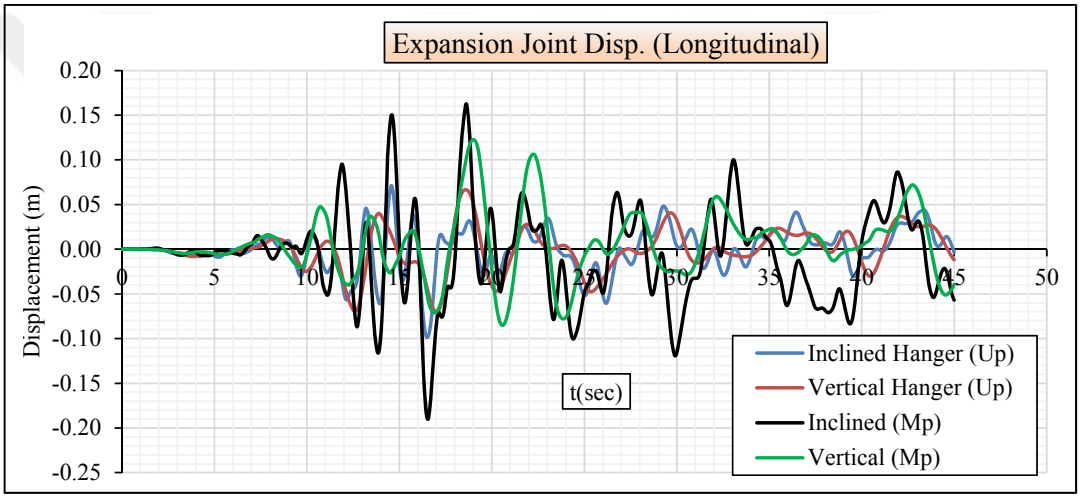

Figure 7.59 : Earthquake analysis method comparison under the scenario earthquake for displacement from the expansion joint in longitudinal direction.

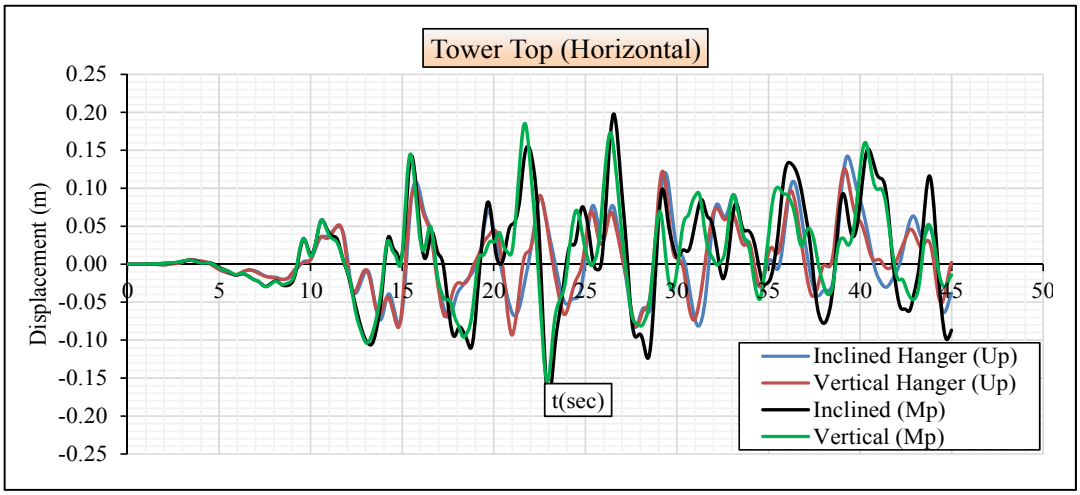

Figure 7.60 : Earthquake analysis method comparison under the scenario earthquake for displacement from the tower-top in horizontal direction.

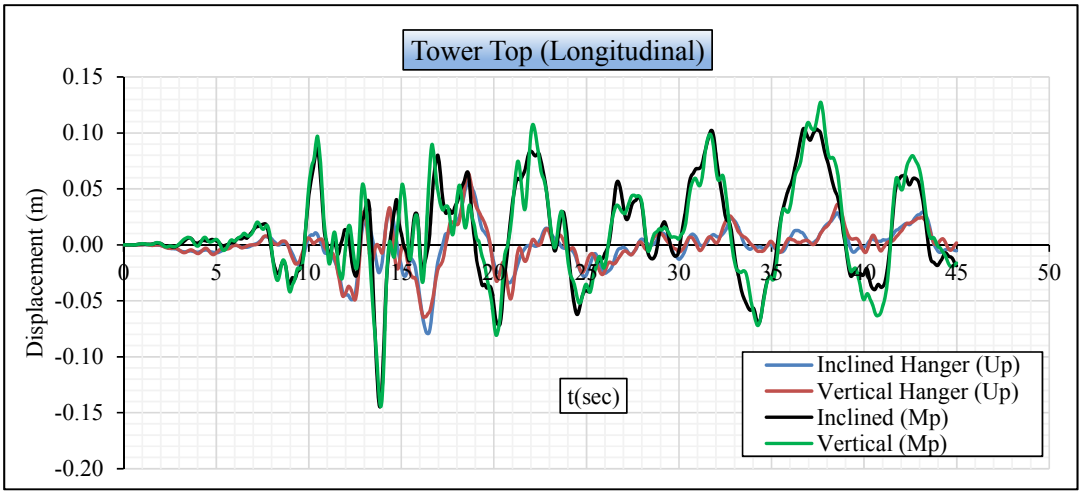

Figure 7.61 : Earthquake analysis method comparison under the scenario earthquake for displacement from the tower-top in longitudinal direction.

7.3.2.2 Comparison for the DD-1 earthquake

Under the DD-1 earthquake motion, the hanger tensile force for the bridge with inclined and vertical hangers is obtained to be affected from the Mp analysis as depicted in Table 7.46. The percentage increase of the bridge with vertical hanger is lower than that of the bridge with inclined hanger. This outcome is pertinent to the absence of the horizontal component of the vertical hanger. As for the main and back-stay cables, 15 % increase in the tensile force is determined.According to Table 7.47 for the portal beams, the highest percentage increase in the sectional forces is determined for the lower portal beam. This conclusion is related to support function of the lower beam for the main deck and the approach viaduct. Approximately 20 % - 50 % increase in the sectional forces is obtained for the middle and lower portal beams. The tower base-section is highly affected from the both the DD-1 earthquake level and the Mp analysis according to Table 7.48. With 15 and 5 times higher increase in the bending moment and the shear force, respectively, the performance of the tower is clearly estimated to be changed under the DD-1 multi-point earthquake motions. Moreover, the increase in the lower portal beam is directly related to such increase in the tower base section. As given in Table 7.49, the highest increase in the section forces of the main deck is obtained as the bending moment for the bridge with inclined hanger and as the compressive axial force for the bridge with vertical hanger. For the bridge with vertical hanger, 365 % increase in the compressive axial force is based on the additional force from the viscous dampers and the wind tongues. In general, the main deck is considerably influenced from the DD-1 multi-point earthquake motion.

Table 7.46 : Earthquake analysis method comparison under the DD-1 earthquake for the cable elements.

Cable Elements Tensile Force	Results				Change			
	Up		Mp		Inclined		Vertical	
	Inclined	Vertical	Inclined	Vertical	%	Graphic	%	Graphic
Main Cable (kN) (max.)	220814.04	217709.73	252693.40	249125.03	**14.44**		**14.43**	
Back-Stay (kN) (max)	231934.55	231635.61	265474.15	265382.15	**14.46**		**14.57**	
Hanger (kN (max)	6752.76	2338.38	12456.30	3031.78	**84.46**		**29.65**	

Table 7.47 : Earthquake analysis method comparison under the DD-1 earthquake for the portal beam.

Portal Beam		Results				Change			
		Up		Mp		Inclined		Vertical	
		Inclined	Vertical	Inclined	Vertical	%	Graphic	%	Graphic
Lower Portal	Shear Force (kN) (max.)	7939.36	8747.73	37531.87	41208.71	**372.73**		**371.08**	
	Bending Moment (kNm) (max)	74555.96	83016.44	221286.25	216271.43	**196.81**		**160.52**	
	Compressive Axial Force (kN) (max)	1893.50	2079.48	3171.03	3575.04	**67.47**		**71.92**	
Middle Portal	Shear Force (kN) (max.)	3958.89	4136.36	4814.95	4760.83	**21.62**		**15.10**	
	Bending Moment (kNm) (max)	54801.66	57348.89	70471.44	67714.56	**28.59**		**18.07**	
	Compressive Axial Force (kN) (max)	142.68	154.85	220.67	214.20	**54.66**		**38.32**	
Upper Portal	Shear Force (kN) (max.)	2263.54	2267.57	3217.35	3051.64	**42.14**		**34.58**	
	Bending Moment (kNm) (max)	30582.83	30519.25	44998.16	42004.94	**47.14**		**37.63**	
	Compressive Axial Force (kN) (max)	1327.74	1378.26	1674.37	1677.53	**26.11**		**21.71**	

Table 7.48 : Earthquake analysis method comparison under the DD-1 earthquake for the tower base-section.

Tower Base Section	Results				Change			
	Up		Mp		Inclined		Vertical	
	Inclined	Vertical	Inclined	Vertical	%	Graphic	%	Graphic
Shear Force (kN) (max.)	5903.36	5555.59	31862.00	36040.74	**439.73**		**548.73**	
Bending Moment (kNm) (max)	196205.48	92409.89	1252816.64	1514042.15	**538.52**		**1538.40**	
Compressive Axial Force (kN) (max)	189647.31	196852.95	223437.82	231213.41	**17.82**		**17.45**	

Table 7.49 : Earthquake analysis method comparison under the DD-1 earthquake for the main deck.

Deck	Results				Change			
	Up		Mp		Inclined		Vertical	
	Inclined	Vertical	Inclined	Vertical	%	Graphic	%	Graphic
Shear Force (kN) (max.)	4712.83	4535.51	6822.00	5587.18	**44.75**		**23.19**	
Bending Moment (kNm) (max)	192112.51	192932.58	406831.55	432207.23	**111.77**		**124.02**	
Compressive Axial Force (kN) (max)	56725.31	9360.31	81827.52	43575.38	**44.25**		**365.53**	

Table 7.50 : Earthquake analysis method comparison under the DD-1 earthquake for the box-beam and columns of approach viaducts.

Approach		Results				Change			
		Up		Mp		Inclined		Vertical	
		Inclined	Vertical	Inclined	Vertical	%	Graphic	%	Graphic
Beam	Shear Force (kN) (max.)	3469.74	3576.14	6198.61	5758.44	**78.65**		**61.02**	
	Bending Moment (kNm) (max)	51578.40	46018.10	224092.91	196101.56	**334.47**		**326.14**	
	Compressive Axial Force (kN) (max)	14502.82	10508.05	39433.22	42449.79	**171.90**		**303.97**	
Column	Shear Force (kN) (max.)	110.30	113.85	430.78	785.07	**290.54**		**589.55**	
	Bending Moment (kNm) (max)	1511.16	1667.69	12540.59	16417.65	**729.86**		**884.46**	
	Compressive Axial Force (kN) (max)	7889.62	8418.70	10994.80	10821.09	**39.36**		**28.54**	

The box-beam and column of the approach viaduct is obtained to be more sensitive to the multi-point earthquake analysis. As presented in Table 7.50, the percentage increase in the bending moment becomes 800 %, which reveals that performance prediction of the bridge can be considered.

Along with the sectional forces, displacement time-history response of the bridge is also investigated to identify the effects of the Mp analysis under the DD-1 earthquake. The outcomes are presented in Figures 7.62-67. From the displacement response, the Mp analysis and the DD-1 earthquake level are obtained to be the most effective considerations for earthquake performance prediction of the bridge.

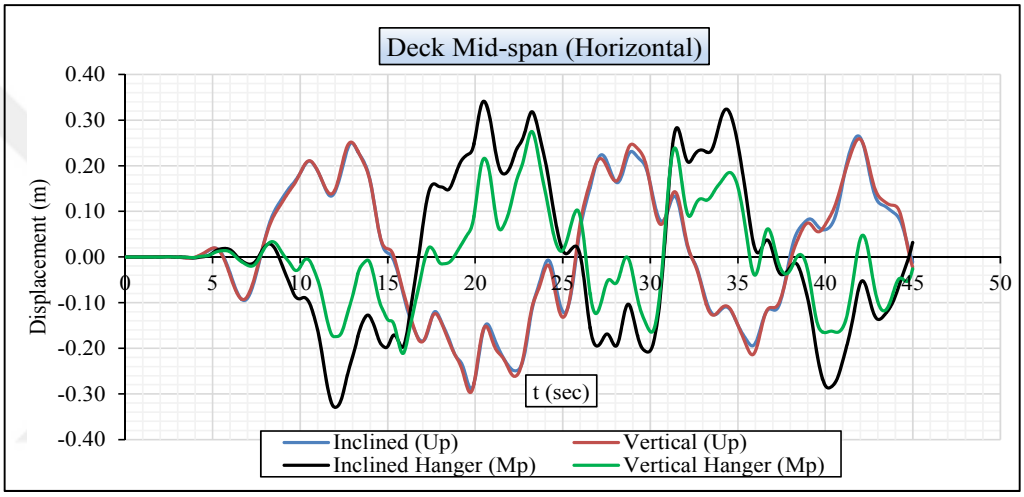

Figure 7.62 : Earthquake analysis method comparison under the DD-1 earthquake for displacement from the deck mid-span in horizontal direction.

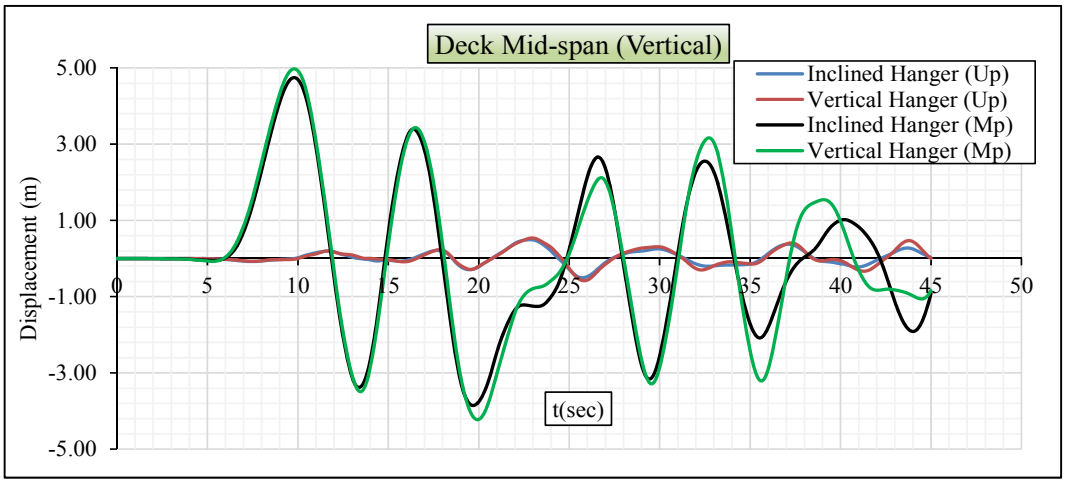

Figure 7.63 : Earthquake analysis method comparison under the DD-1 earthquake for displacement from the deck mid-span in vertical direction.

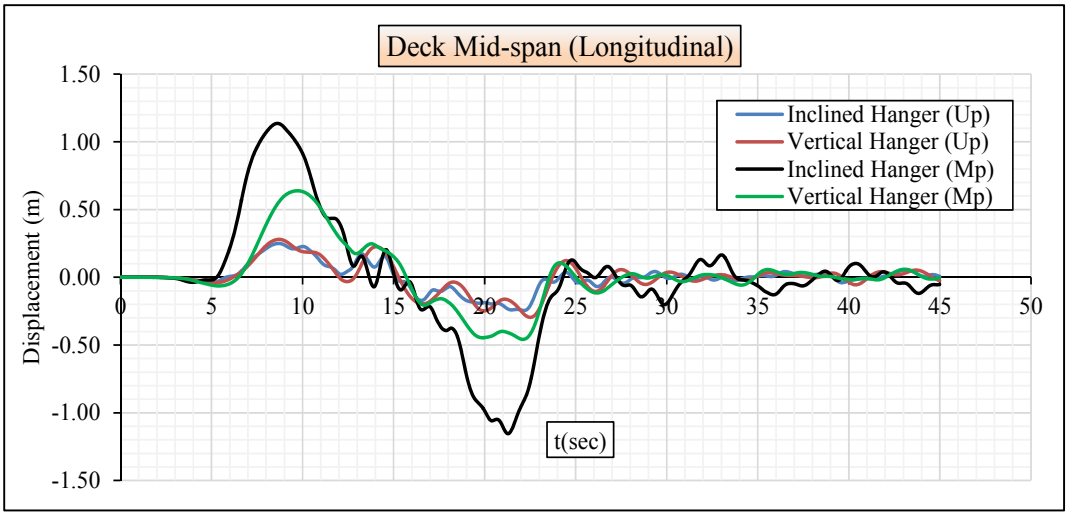

Figure 7.64 : Earthquake analysis method comparison under the DD-1 earthquake for displacement from the deck mid-span in longitudinal direction.

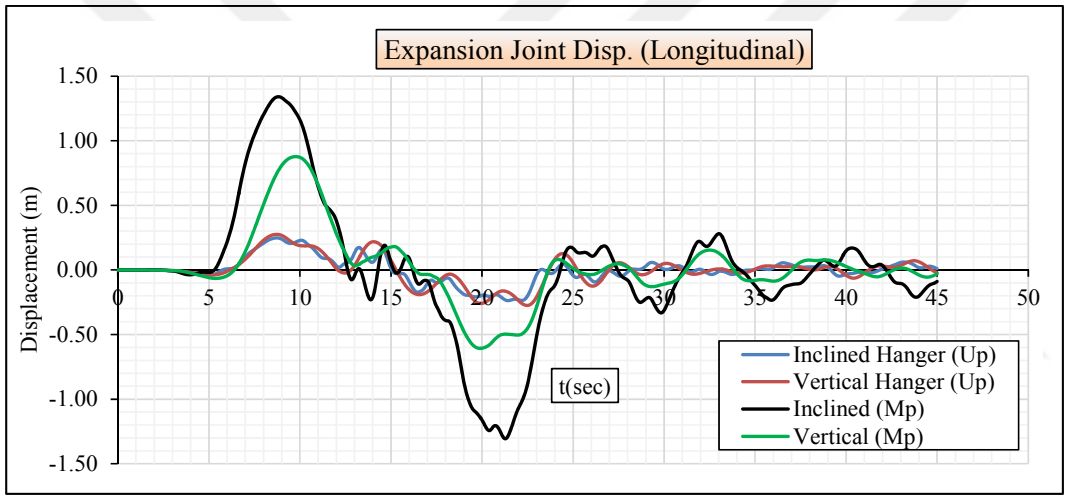

Figure 7.65 : Earthquake analysis method comparison under the DD-1 earthquake for displacement from the expansion joint in longitudinal direction.

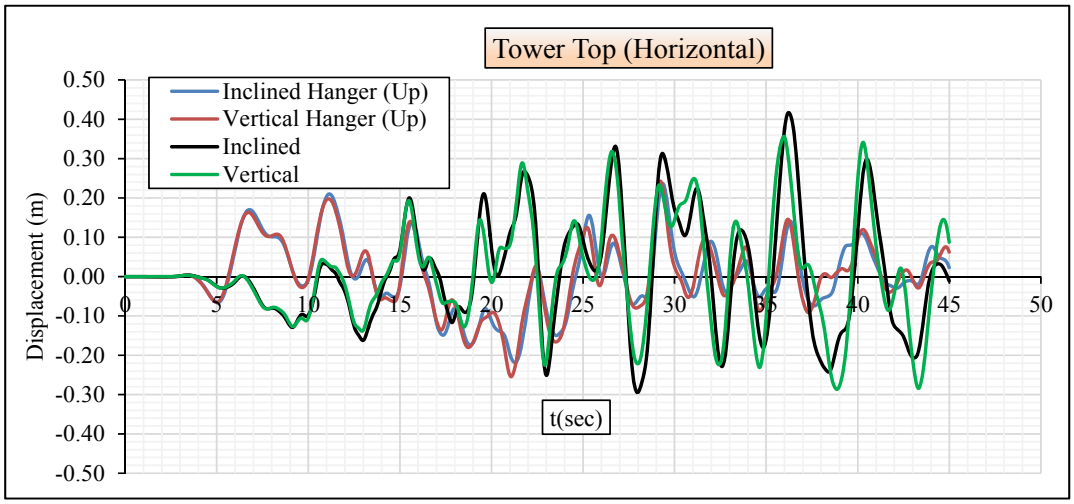

Figure 7.66 : Earthquake analysis method comparison under the DD-1 earthquake for displacement from the tower top-saddle in horizontal direction.

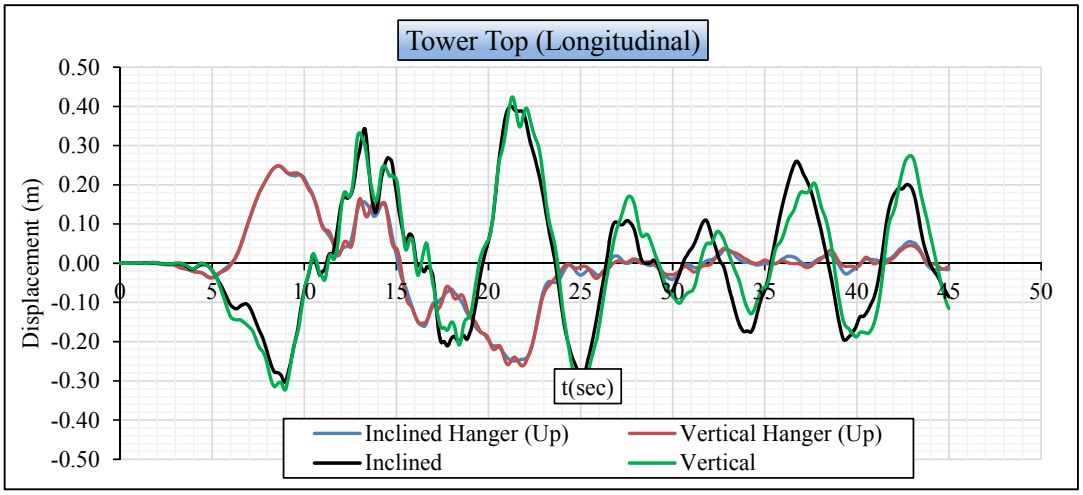

Figure 7.67 : Earthquake analysis method comparison under the DD-1 earthquake for displacement from the tower top-saddle in longitudinal direction.

7.4 Earthquake-Based Structural Identification

Based on relatively low deck mid-span horizontal displacement value range of 0.15-0.35 m under the scenario and the DD-1 multi-point earthquakes as shown in Figure 7.56 and Figure 7.62, the towers are expected to move oppositely in each other in transverse direction. For this aim, maximum displacements at the tower top-saddle are obtained in transverse and longitudinal directions for inclined and vertical hangers. These results are given in Table 7.51. From Table 7.51, the towers' opposite movements that are approximately equal to each other are determined for transverse and longitudinal directions. Thus, small displacement at the center of the deck under the scenario and the DD-1 multi-point earthquake motions is considerably related to the movement behavior of the towers.

Table 7.51 : Maximum displacement of the tower top-saddle from the Mp analysis.

Location	Transverse (m)				Longitudinal (m)			
	Vertical		Inclined		Vertical		Inclined	
	Scenario	DD-1	Scenario	DD-1	Scenario	DD-1	Scenario	DD-1
European	0.189	0.381	0.199	0.418	0.127	0.401	0.113	0.415
Asian	-0.221	-0.348	-0.228	-0.386	-0.136	-0.475	-0.138	-0.521

As indicated in Figure 7.57 and 7.63, vertical displacement of the deck at the mid-span is determined as a range from 1.0 m to 5.0 m for the scenario and the DD-1 earthquakes. Along with the cause to high increase in the sectional forces of the critical elements, such high displacement in vertical direction of the deck also leads to

approaching the Asian tower to the European tower. As depicted in Table 7.51, this conclusion can be easily estimated with the opposite displacement of each tower in longitudinal direction.

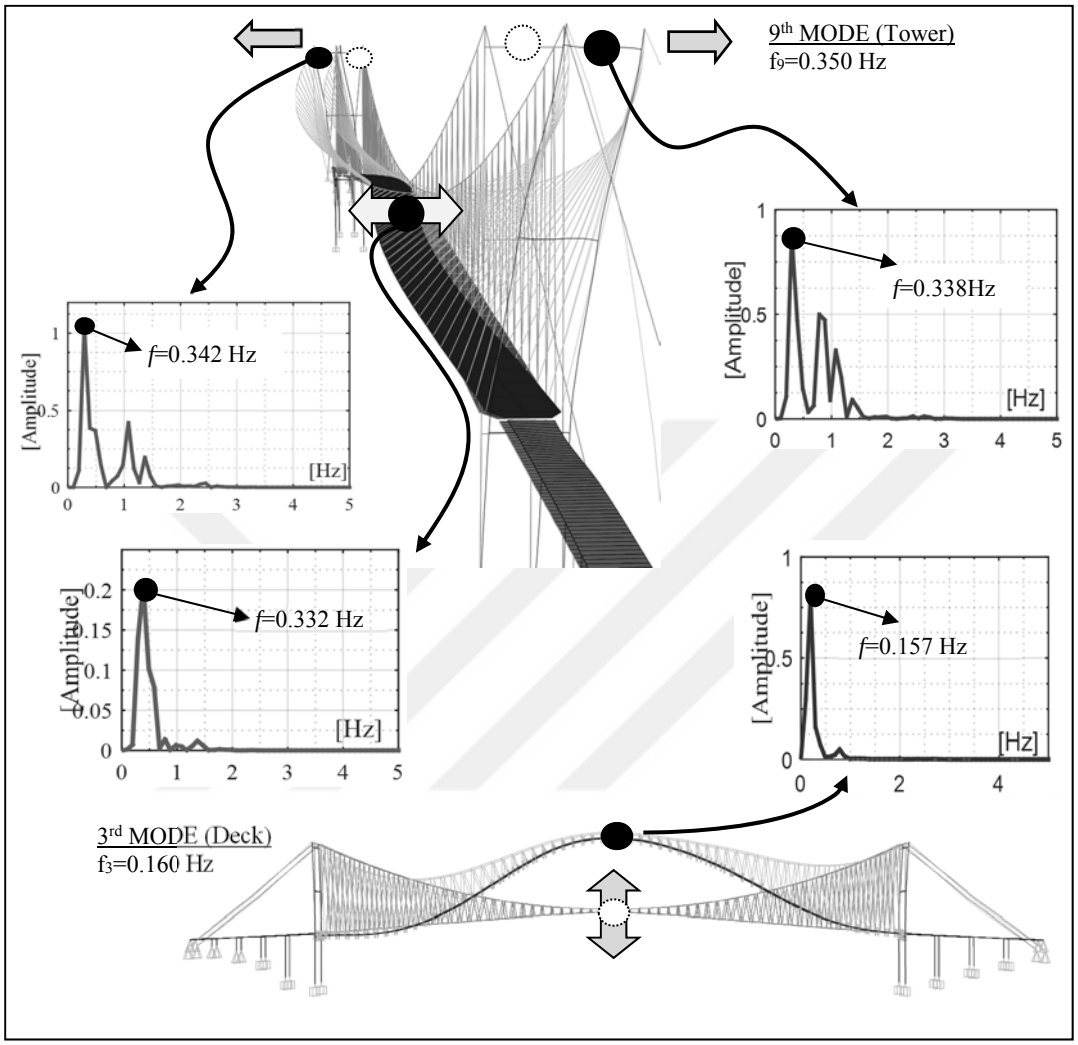

Figure 7.68 : Relationship between critical displacements and modal response of the bridge.

The high vertical displacement of the deck mid-span and the opposite movement of the towers in each other in transverse and longitudinal directions are estimated to be mostly pertinent to modal response of the bridge. As shown in Figure 7.68, the 9th mode of the bridge (1st L_{asymm} Tower mode) is found to be related to the opposite movement of the tower. In addition, there is a similarity between this mode and small displacement at the center of the deck in transverse direction. In order to show this relation, the frequency-domain analysis of the FFT is performed considering the acceleration data obtained from these points under the multi-point earthquake. As depicted in Figure 7.68, the FFT analysis of the European and Asian tower top-saddle

acceleration data in transverse direction results in the dominant frequency of 0.338 Hz and 0.342 Hz, respectively. Similarly, this analysis is also performed for the deck mid-span acceleration data in transverse direction and the dominant frequency of 0.332 Hz is obtained. Compared the experimental 1st L_{asymm} tower mode (9th mode) frequency of 0.350 Hz identified from the 'After' range of the extreme wind event with the obtained frequencies, very close agreement is determined. Therefore, the tower mode of the bridge is concluded to be also relatively effective in addition to the deck mode under the multi-point motion. As mentioned previously, the high displacement is obtained at the deck mid-span in vertical direction. This high displacement value is estimated to be related to the 3rd mode (1st V_{symm} deck) of the bridge. Performing the FFT analysis of the deck mid-span acceleration data in vertical direction, the dominant frequency of 0.157 Hz were obtained. Since this frequency is very close to experimentally obtained 3rd vertical symmetric mode frequency of 0.160 Hz, this mode is determined to be the most influential on the vertical displacement. All details and results are presented and summarized in Figure 7.68 and Table 7.52. The difference between the experimental frequency and the response acceleration frequency are also given in the table. According to the results, the multi-point earthquake response of the bridge is clearly identified to be highly pertinent to the Mode-3 and Mode-9.

Table 7.52 : Comparison of the results from FFT with those from the modal analysis.

Mode number	Mode shape	Frequency [Hz]			
		Experimental (f_e)	FFT		Δ (%) $[(f_r-f_e)/f_e]$
			Point	(f_r)	
Mode-3	1st V_{symm} Deck	0.160	Deck mid-span	0.157	-0.02
Mode-9	1st L_{asymm} Tower	0.350	Tower top saddle	0.338 (Europe)	-0.03
				0.342 (Asia)	-0.02
			Deck mid-span	0.332	-0.05

V_{symm} : Vertical symmetric; L_{asymm} : Lateral asymmetric

Consequently, the earthquake reponse of the bridge under relatively high complex multi-point earthquake motions is identified based on the natural vibration frequencies of 1st $V_{sym\ Deck}$ and 1st $L_{asym\ Tower}$ modes. Since experimental data during earthquake motion are not recorded with the SHM system of the bridge or controlled earthquake vibration testing bridge is not possible for the in-service Bosphorus, this investigation enables to make a prediction for the bridge response to the possible earthquake in Istanbul.

8. CONCLUSIONS

The main objective of the dissertation is to make a comprehensive investigation on structural response of the long-span bridges in Turkey adopting the integrated approach of St-Id. For this aim, the Boshporus Suspension Bridge is considered as a real-life civil infrastructure in this dissertation. From the consequences of the Bosphorus Bridge, it is also aimed to present a framework for integrated solution to safety and proper structural condition assessment of other existing or newly constructing long-span bridges in Turkey.

The dissertation is mainly can be divided into three integrated parts:

In the first part of the dissertation, the first two steps of St-Id, which are visualization / conceptualization and priori modeling, are carried out. For this aim, original project drawings, retrofit projects and experiences from the bridge's official authority KGM (General Directorate of Turkish State Highways) are identified properly. Taking these documents and experiences into consideration, elaborate study is conducted to establish priori finite element model (FEM) of the bridge. Based on the conclusions from the priori model, more advanced FE models of improved spine-beam and 3-D full-scale shell are developed for further investigations on the bridge. In this section of the dissertation, similar efforts are also made for FE modeling of the bridge with vertical hangers. Thus, the hanger replacement project considerations that also include certain retrofitting works are specified. Accordingly, improved spine-beam and 3-D full-scale shell FE model of the Bosphorus Bridge with inclined and vertical hangers are prepared to perform the modal analysis. Making a comparison between the results of the FE models, correction for the models and vertical hanger effects are determined in terms of natural vibration frequency.

In the second part of this dissertation, the SHM system of the Bosphorus Bridge is identified in detail in accordance with the requirements of St-Id approach in order to conduct the second two steps of St-Id: experimentation and data analysis. General design considerations, monitoring objectives and parameters of the SHM system are clarified depending on the bridge's own characteristics. The monitoring specifications

of the bridge are also determined to be relatively close agreement with those of the well-known long-span bridges in Hong Kong and Japan. Considering these specifications and recommendations of the KGM, critical points and components to be monitored are specified and preliminary performance criteria is proposed for the Bosphorus Bridge. For data analysis, the extreme wind event is considered. Before the data analysis, this event is accurately identified. Depending on the preliminary results, the need to developing a new code for averaging extreme wind data is stated. The frequency-domain results are then obtained to be clearer and the first nine dominant (deck and tower modes) modes of the bridge are identified. Moreover, influence of the extreme wind event on the bridge is determined on the basis of its dynamic properties through SHM data.

The last part of the dissertation includes the calibration/verification of the developed FE models with the experimental frequencies obtained from the extreme wind event through the SHM system, and the utilization and decision making for seismic performance prediction of the bridge under the multi-point scenario earthquake motion.

The following contributions and key points are obtained from the dissertation and given below;

- The importance of the St-Id for a combined structural assessment concept of the Bosphorus Bridge is underlined. Besides, the concept is stated to be considered not only for structural assessment but also for maintenance, operational performance control, management and safety of the bridge.
- High compatibility of SHM system specifications of the bridge with those of the important long-span bridges in Hong-Kong and Japan is obtained based on monitoring objectives and parameters. Thus, SHM-based operational performance criteria approach is proposed for the Bosphorus Bridge.
- The bridge with inclined and vertical hangers is modeled using two well-known FEM techniques: spine beam (global) and multi-scale (local and global). For this aim, elaborate modelling specifications are determined for the bridge.
- A very close agreement with the previous experimental studies for the bridge with inclined hanger, which is an error lower than 10 % in the first five modes,

is determined. The deck and tower modes are identified as the most effective modes of the bridge.

- As expected for the effect of vertical hanger arrangement on vertical dynamic behavior of the bridge, high change in the vertical deck modes of the bridge with vertical hanger, which is 10-24 % in vertical deck modes and less than 1.0 % for lateral deck and other modes (tower and cable modes), is obtained.
- The key elements for operational and extreme events of the bridge are specified as the towers, deck and expansion-joints. In order to monitor these critical elements, physical parameters are identified: movements in bridge axis, fatigue/traffic effect and bridge response.
- The limit events, limit states and corresponding preventions are proposed for developing operational performance criteria of the Bosphorus Bridge.
- With the SHM data recorded during strong wind events on the bridge, the first effective single modes (decks and towers) are obtained. The spine-beam and 3-D shell FE models of the bridge with inclined hangers with the wind data that is an error less than 10 % are verified/updated.
- Rather than other modes, high influence of the extreme wind on the 1st lateral symmetric deck modes is determined as the 15 % increase as in the modal period. Elastic behavior of the bridge is likely to be under extreme wind load case.
- An approach for the earthquake performance prediction of the Bosphorus Bridge, Multi-point Earthquake Analysis (Mp), is proposed.
- Site-specific earthquake records considering possible earthquake scenario in Istanbul, which is Scenario and DD-1 compatible EQ motions, are generated.
- The most vulnerable components of the bridge are obtained as tower, approach-viaduct column and expansion joints.
- No increase in the main and back-stay cables and relatively low decrease in hanger cables for vertical hanger are determined. Decrease in axial force of the main deck for vertical hanger arrangement and high increase in the tower base-section and approach column forces for vertical hanger are obtained.

- Sectional force values from the Mp analysis are obtained to be higher than those of the Up. Therefore, the importance of the Mp analysis is stated to be utilized for long-span suspension bridge.
- Under the scenario earthquakes for from the multi-point and uniform-point earthquake analyses of the bridge, the bridge with both inclined and vertical hangers is not likely to be damaged and no repair and strengthening intervention can be required for the bridge. Under the DD-1 spectrum compatible earthquakes, damage is estimated for the tower base-section and approach viaduct box-section of the bridge with both inclined and vertical hangers. For retrofit strategy, sectional capacity is recommended to be increased with additional longitudinal stiffener of doubly symmetric W100x499 I-beam.

Based on the summarized key points above, the followings are presented as recommandations/future works;

- Updating and redefining the monitoring parameters of the bridge.
- Optimum new sensor configuration based on the monitoring parameters: experimental and numerical studies.
- Structural Identification (St-Id)-based integrated health monitoring system.
- Detailed wind simulation of the bridge.
- Quantifying of performance criteria for operational and extreme events through SHM data.
- A comprehensive SHM center for the long-span bridges in Istanbul.
- Connection of the earthquake early warning system with the SHM system

REFERENCES

AASHTO-LRFD Bridge Design Specifications. (2007). American Association of State Highway and Transportation Officials (AASHTO). Washington, D.C.

ABAQUS [ABAQUS Documentation]. Dassault Systèmes. USA: RI.

Abdel-Ghaffar, A. M. (1978). Free lateral vibrations of suspension bridges, *Journal of the Structural Division*, *104* (3), 503-525.

Abdel-Ghaffar, A. M. (1976). *Dynamic analyses of suspension bridge structures and some related topics*. (PhD thesis). California Institute of Technology, CA, USA.

Abdel-Ghaffar, A. M., and Rubin, L. I. (1982). Suspension bridge response to multiple-support excitations, *ASCE Journal of Engineering Mechanics Divisions*, *108* (2), 419-435.

Abdel-Ghaffar, A. M. and Rubin, L. I. (1983). Vertical seismic behaviour of suspension bridges, *Earthquake Engineering and Structural Dynamics*, *11* (1), 1-19.

Abdel-Ghaffar, A. M. and Rubin, L. I. (1983a). Nonlinear free vibrations of suspension bridges: application, *Journal of Engineering Mechanic*s, *109* (1), 330-345.

Abdel-Ghaffar, A. M. and Rubin, L. I. (1983b). Nonlinear free vibrations of suspension bridges: theory, Journal *of Engineering Mechanics*, *109* (1), 313-329.

Abe, K. and Amano, K. (1998). Monitoring system of the Akashi Kaikyo Bridge (Vol. 22, pp. 29-34). Japan: Honshi Technical Report.

Agbabian, M. S., Masri, S. F., Miller, R. K. and Caughey, T. K. (1991). System identification approach to detection of structural changes, *Journal of Engineering Mechanics*, *117* (2), 370-390.

Ahmed, M. A. G. and Lawrence, I. R. (1983). Lateral earthquake response of suspension bridges, *Journal of Structural Engineering*, *109* (3), 664-675.

Ahmed, M. A. G. and Robert, H. S. (1985a). Ambient vibration studies of Golden Gate Bridge: I. suspended structure, *Journal of Engineering Mechanics, 111* (4), 463-482.

Ahmed, M. A. G. and Robert, H. S. (1985b). Ambient vibration studies of Golden Gate Bridge: II. Pier-tower structure, *Journal of Engineering Mechanics*, *111* (4), 483-499.

Aktan, A., Grimmelsman, K., Barrish, R., Catbas, F. and Tsikos, C. (2000). Structural identification of a long-span truss bridge, *Transportation*

Research Record: Journal of the Transportation Research Board, *1696*, 210-218.

Aktan, A. E., Catbas, F. N., Grimmelsman, K. A. and Pervizpour, M. (2002). Development of a model health-monitoring guide for major bridges. USA: FHWA Rep. Dev.

Aktan, A. E., Catbas, F. N., Grimmelsman, K. A. and Tsikos, C. J. (2000). Issues in infrastructure health monitoring for management, *Journal of Engineering Mechanics*, *126* (7), 711-724.

Aktan, A. E., Farhey, D. N., Helmicki, A. J., Brown, D. L., Hunt, V. J., Lee, K. L., Levi, A. (1997). Structural identification for condition assessment: experimental arts, *Journal of Structural Engineering (ASCE)*, *123* (12), 1674-1684.

Aktan, A. E. and Yao, J. T. P. (1996). On structural identification of constructed facilities. *Proceeding of Structures Congress XIV*. New York, N.Y.

Aktan, E., Çatbaş, N., Türer, A. and Zhang, Z. (1998). Structural identification: analytical aspects, *Journal of Structural Engineering*, *124* (7), 817-829.

Alexander, N. A. (2008). Multi-support excitation of single span bridges, using real seismic ground motion recorded at the SMART-1 array, *Computers and Structures*, *86* (1–2), 88-103.

Ansal, A., Akinci, A., Cultrera, G., Erdik, M., Pessina, V., Tönük, G., and Ameri, G. (2009). Loss estimation in Istanbul based on deterministic earthquake scenarios of the Marmara Sea region (Turkey), *Soil Dynamics and Earthquake Engineering*, *29* (4), 699-709.

ANSYS (12-0-1) [User's Manual, Revision]. USA: Swanson Analysis System.

Apaydin, N., Bas, S. and Catbas, N. (2015). Long-span bridges: behavior under operational and extreme wind loads, *The Third International Conference on Smart Monitoring, Assessment and Rehabilitation of Civil Structures (SMAR2015)*, Antalya, Turkey, September 7-9.

Apaydin, N. and Erdik, M. (1999). Structural Vibration Monitoring System for the Bosphorus Suspension Bridges. In M. Ö. Erdik, M. Çelebi, V. Mihailov and N. Apaydin (Eds.), *Strong Motion Instrumentation for Civil Engineering Structures* (pp. 605). Netherlands: Springer.

Apaydin, N. M. (2010). Earthquake performance assessment and retrofit investigations of two suspension bridges in Istanbul, *Soil Dynamics and Earthquake Engineering*, *30* (8), 702-710.

Apaydın, N. M. (2002). *Seismic analysis of Fatih Sultan Mehmet Suspension Bridge*. (Ph.D. thesis). Kandilli Observatory and Earthquake Engineering Res earch Institute, Bogazici University, ISTANBUL.

Apaydin, N. M., Bas, S. and Harmandar, E. (2016). Response of the Fatih Sultan Mehmet Suspension Bridge under spatially varying multi-point earthquake excitations, *Soil Dynamics and Earthquake Engineering*, *84*, 44-54.

Apaydın, N. M., Kaya, Y., Şafak, E. and Alçık, H. (2012). Vibration characteristics of a suspension bridge under traffic and no traffic conditions, *Earthquake Engineering and Structural Dynamics*, *41* (12), 1717-1723.

ASCE (2013). 2013 Report card for America's infrastructure. Reston, VA, USA: American Society of Civil Engineers.

Asgari, B., Osman, S. A. and Adnan, A. (2013). Three-dimensional finite element modelling of long-span cable-stayed bridges, *The IES Journal Part A: Civil & Structural Engineerin*g, *6* (4), 258-269.

Bas, S. (2011).*Dynamic analysis and seismic performance assessment of the approach viaducts of the Bosphorus Bridge*. (M.Sc.Thesis). Istanbul Technical University, Istanbul.

Bas, S., Apaydin, N., Ilki, A. and Catbas, F. N. (2016). Structural health monitoring system-SHMs of the long span bridges in Turkey, *The 8th International Conference on Bridge Maintenance, Safety and Management* (IABMAS 2016*)*, Foz da Iguacu, Brazil, June 26-30.

Bas, S., Apaydin, N. M. and Celep, Z. (2016). Earthquake performance of the two approach viaducts of the bosphorus suspension bridge, *Earthquakes and Structures*, *11* (3), 387-406.

Bas, S., Apaydin, N. M., and Celep, Z. (2016). Free Vibration Analysis and Seismic Performance Assessment of Two Approach Viaducts of Bosphorus Suspension Bridge. In A. Caner, P. Gülkan & K. Mahmoud (Eds.), D*evelopments in International Bridge Engineering: Selected Papers from Istanbul Bridge Conference 2014* (pp. 65-75). Cham: Springer International Publishing.

Beresnev, I. A. and Atkinson, G. M. (1997). Modeling finite-fault radiation from the ωn spectrum, *Bulletin of the Seismological Society of America*, *87* (1), 67-84.

Beresnev, I. A. and Atkinson, G. M. (1998). FINSIM--a FORTRAN program for simulating stochastic acceleration time histories from finite faults, *Seismological Research Letters*, *69* (1), 27-32.

Beyen, K., Uckan, E. and Erdik, M. (1994). Ambient vibration investigation of the Bogazici Suspension Bridge. *Proceeding of the Earthqueke Resistant Construction and Design*, Rotterdam.

Bodeux, J. B. and Golinval, J. C. (2001). Application of ARMAV models to the identification and damage detection of mechanical and civil engineering structures, *Smart Materials and Structures*, *10* (3), 479.

Boller, C., Chang, F.-K. and Fujino, Y. (2009). *Encyclopedia of Structural Health Monitoring*. Wiley.

Boore, D. M. (1983). Stochastic simulation of high frequency ground motions based on seismological models of the radiated spectra, *Bulletin of the Seismological Society of America*, *73* (6A), 1865-1894.

Böse, M. (2006). *Earthquake early warning for Istanbul using artificial neural networks*. (Ph.D. Thesis).Universität Karlsruhe (TH), Germany.

Brownjohn, J., Dumanoglu, A. A., Severn, R. T. and Blakeborough, A. (1989). Ambient vibration survey of the Bosphorus Suspension Bridge, *Earthquake Engineering and Structural Dynamics*, *18* (2), 263-283.

Brownjohn, J. M. and Pan, T.-C. (2008). Identifying loading and response mechanisms from ten years of performance monitoring of a tall building, *Journal of Performance of Constructed Facilities*, *22* (1), 24-34.

Brownjohn, J. M. W. (1994). Observations on non-linear dynamic characteristics of suspension bridges, *Earthquake Engineering and Structural Dynamics*, *23* (12), 1351-1367.

Brownjohn, J. M. W. (2003). Ambient vibration studies for system identification of tall buildings, *Earthquake Engineering and Structural Dynamics*, *32* (1), 71-95.

Brownjohn, J. M. W., Dumanoglu, A. A. and Severn, R. T. (1992). Ambient vibration survey of The Fatih Sultan Mehmet (Second Bosporus) Suspension Bridge, *Earthquake Engineering and Structural Dynamics*, *21* (10), 907-924.

Brownjohn, J. M. W., Dumanoglu, A. A. and Severn, R. T. (1992). Full-scale dynamic testing of the 2nd Bosporus Suspension Bridge, *The 10th World Conference on Earthquake Engineering*, Spain.

Brownjohn, J. M. W., Dumanoglu, A. A., Severn, R. T. and Blakeborough, A. (1989). Ambient vibration survey of the Bosphorus Suspension Bridge, *Earthquake Engineering and Structural Dynamics*, *18* (2), 263-283.

Brownjohn, J. M. W., Moyo, P., Omenzetter, P. and Lu, Y. (2003). Assessment of highway bridge upgrading by dynamic testing and finite-element model updating, *Journal of Bridge Engineering*, *8* (3), 162-172.

Brownjohn, J. M. W. and Xia, P.-Q. (2000). Dynamic assessment of curved cable-stayed bridge by model updating, *Journal of Structural Engineering*, *126* (2), 252-260.

BS-968 on high yield stress structural steel. (1968). U.K.: British Standards Institution.

CalTrans. (2001). *Guide Specification for Seismic Design of Steel Bridges*. California US: Department of Tansportation (DOT), State of California.

Catbas, F. N., Burkett, M., J. and Basharat, A. (2004). Challenges in structural health monitoring. *Proceedings of the 4th International Workshop on Structural Control*, New York, USA.

Catbas, F. N., Ciloglu, S. K., Grimmelsman, K. A., Pan, Q., Pervizpour, M. and Aktan, A. E. (2003). Limitations in structural identification of long span bridges. *The Keynote Presentation and Proceedings of the International Workshop on Structural Health Monitoring of Bridges/Colloquium on Bridge Vibration*. Japan: Kitami Institute of Technology.

Chan, T. H. T., Guo, L. and Li, Z. X. (2003). Finite element modelling for fatigue stress analysis of large suspension bridges, *Journal of Sound and Vibration*, *261* (3), 443-464.

Chang, C. C., Chang, T. Y. P. and Zhang, Q. W. (2001). Ambient vibration of long-span cable-stayed bridge, *Journal of Bridge Engineering*, *6* (1), 46-53.

Charles, R. F. and David, A. J. (1998). Comparative study of damage identification algorithms applied to a bridge: I. Experiment, *Smart Materials and Structures*, *7* (5), 704.

Chopra, A. K. (2012). *Dynamics of Structures: Theory and Applications to Earthquake Engineering*. Upper Saddle River, New Jersey, USA: Prentice-Hall International Series in Civil Engineering and Engineering Mechanics.

Chopra, A. K. and McKenna, F. (2016). Modeling viscous damping in nonlinear response history analysis of buildings for earthquake excitation, *Earthquake Engineering and Structural Dynamics*, *45* (2), 193-211.

Catbas, F. N., Kijewski-Correa, T. and Aktan, A. E. (2013). *Structural Identification of Constructed Systems: Approaches, Methods, and Technologies for Effective Practice of St-Id*. American Society of Civil Engineers,

David, F. M. and John, T. D. (1990). Experimental study of bridge monitoring technique, *Journal of Structural Engineerin*g, *116* (9), 2532-2549.

Doebling, S. W., Farrar, C. R. and Prime, M. B. (1998). A summary review of vibration-based damage identification methods, *Shock and vibration digest*, *30* (2), 91-105.

Doebling, S. W., Farrar, C. R., Prime, M. B. and Shevitz, D. W. (1996). Damage identification and health monitoring of structural and mechanical systems from changes in their vibration characteristics: a literature review. USA: Los Alamos National Laboratory.

Duan, Y. F., Xu, Y. L., Fei, Q. G., Wong, K. Y., Chan, K. W. Y., Ni, Y. Q. and Ng, C. L. (2011). Advanced finite element model of Tsing Ma Bridge for structural health monitoring, *International Journal of Structural Stability and Dynamics*, *11* (02), 313-344.

Dumanoglu, A. A., Brownjohn, J. M. W. and Severn, R. T. (1992). Seismic analysis of the Fatih Sultan Mehmet (Second Bosporus) Suspension Bridge, *Earthquake Engineering and Structural Dynamics*, *21* (10), 881-906.

Dumanoglu, A. A. and Severn, R. T. (1990). Stochastic response of suspension bridges to earthquake forces, *Earthquake Engineering and Structural Dynamics*, *19* (1), 133-152.

Dumanoglu, A. A. and Soyluk, K. (2003). A stochastic analysis of long span structures subjected to spatially varying ground motions including the site-response effect, *Engineering Structures*, *25* (10), 1301-1310.

Erdik, M. and Apaydın, N. (2007). Earthquake Response of Suspension Bridges. In E. İnan & A. Kırış (Eds.), *Vibration Problems ICOVP 2005* (pp. 181-194). Dordrecht: Springer Netherlands.

Erdik, M. and Uckan, E. (1989). Ambient vibration survey of the Bogazici Suspension Bridge. Istanbul-Turkey: Kandilli Observatory and Earthquake Research Institute, Bogazici University.

Eurocode (1994). *Structural design of construction works in the European Union-EU*. Brussels, Belgium: European Committee for Standardization.

Flint, A. R., McFadyen, A. N., Lau, C. K., and Wong, K. Y. (1995). Wind and structural health monitoring system for lantau fixed crossing, part 2: performance requirement of on-structure instrumentation system, *The International Conference*, *'Bridges into 21st Century'*, Hong Kong.

Freeman-Fox-Partners (1968a). Bosporus Bridge calculations: File No: 1, 2, 3, 4, 5, SW.1. Westminster, London.

Freeman-Fox-Partners (1968b). Bosporus Bridge towers, suspended structures, cables, anchorage drawings, SW.1. Westminster, London.

Fujino, Y., Murata, M., Okano, S. and Takeguchi, M. (2000). Monitoring system of the Akashi Kaikyo Bridge and displacement measurement using GPS. *Proceedings of SPIE 3995, Nondestructive Evaluation of Highways, Utilities, and Pipelines IV*. Newport Beach, CA, 06 March.

Gimsing, N. J. and Georgakis, C. T. (2011). *Cable Supported Bridges: Concept and Design*. Wiley.

Gokce, H. B. (2012). *Structural identification through monitoring, modeling, and predictive analysis under uncertainty*. (Ph.D. Thesis). University of Central Florida, Orlando, FL, USA.

Gokce, H. B., Catbas, F. N., Gul, M. and Frangopol, D. M. (2013). Structural identification for performance prediction considering uncertainties: case study of a movable bridge, *Journal of Structural Engineering*, *139* (10), 1703-1715.

Gul, M. and Catbas, F. N. (2011). Structural health monitoring and damage assessment using a novel time series analysis methodology with sensor clustering, *Journal of Sound and Vibration*, *330* (6), 1196-1210.

Gurley, K. and Kareem, A. (1999). Applications of wavelet transform in earthquake, wind and ocean engineering, *Engineering Structures*, *21* (2), 149-167.

Hae-Bum, Y. and Sami, F. M. (2009). Stochastic change detection in uncertain nonlinear systems using reduced-order models: classification, *Smart Materials and Structures*, *17* (1).

Hart, G. C. and Yao, J. T. P. (1977). System identification in structural dynamics, *Journal of Engineering Mechanics*, *103* (6), 1089-1104.

Highways-Department (2002). Wind and structural health monitoring system: appendix w33 of the particular specification for the construction of Hong Kong – Shenzhen Western Corridor. Hong Kong SAR: the Government of the Hong Kong SAR.

Hong, A. L., Ubertini, F. and Betti, R. (2011). Wind analysis of a suspension bridge: identification and finite-element model simulation, *Journal of Structural Engineering*, *137* (1), 133-142.

Hou, Z., Noori, M. and Amand, R. S. (2000). Wavelet-based approach for structural damage detection, *Journal of Engineering Mechanics*, *126* (7), 677-683.

Jaishi, B. and Ren, W.-X. (2005). Structural finite element model updating using ambient vibration test results, *Journal of Structural Engineering*, *131* (4), 617-628.

Jan-Ming, K. and Ni, Y.-Q. (2005). Technology developments in structural health monitoring of large-scale bridges, *Engineering Structures*, *27* (12), 1715-1725.

JBSI. (2004). Seismic reinforcement of large-scale bridges in Istanbul. Ankara, Turkey: Japanese Bridge and Structure Institute.

Jiang, X. and Adeli, H. (2005). Dynamic wavelet neural network for nonlinear identification of highrise buildings, *Computer-Aided Civil and Infrastructure Engineering*, *20* (5), 316-330.

JSCE. (1998). The Akashi-Kaikyo Bridge design and construction of the world's longest bridge. Japan: Honshu-Shikoku Bridge Authority.

Karmakar, D., Ray-Chaudhuri, S. and Shinozuka, M. (2012). Seismic response evaluation of retrofitted Vincent Thomas Bridge under spatially variable ground motions, *Soil Dynamics and Earthquake Engineering*, *42*, 119-127.

Kashima, S., Yanaka, Y., Suzuki, S., and Mori, K. (2001). Monitoring the Akashi Kaikyo Bridge: first experiences, *Structural Engineering International*, *11* (2), 120-123.

KGM. (1973). Record Book: İstanbul Boğaziçi Köprüsü (Bosphorus Suspension Bridge). Ankara/Turkey: General Directorate of Turkish State Highways.

KGM. (1982). Technical specifications for highway bridges. Ankara, Turkey: General Directorate of Highways.

KGM. (2004). Specifications for seismic reinforcement structures, Report 2: Design principle and earthquake waves for the project entitled ''Seismic Reinforcement of Large Scale Bridges in Istanbul. Istanbul, Turkey: General Directorate of Turkish State Highways.

KGM. (2008a). The Bosphorus Birdge monitoring handbook. Ankara, Turkey: General Directorate of Turksih State Highways.

KGM. (2008b). The Bosphorus Birdge monitoring user manual. Ankara, Turkey: General Directorate of Turkish State Highways.

KGM. (2015). Project drawings: the maintenance, repiar, structural reinforcement, engineering works and consultancy services of Bogazici Bridge. Ankara, Turkey: General Directorate of Turkish State Highways.

Kijewski, T. and Kareem, A. (2003). Wavelet transforms for system identification in civil engineering, *Computer-Aided Civil and Infrastructure Engineering*, *18* (5), 339-355.

Kiureghian, A. D. and Neuenhofer, A. (1992). Response spectrum method for multi-support seismic excitations, *Earthquake Engineering and Structural Dynamics*, *21* (8), 713-740.

Ko, J. M. and Ni, Y. Q. (2005). Technology developments in structural health monitoring of large-scale bridges, *Engineering Structures*, *27* (12), 1715-1725

Kosar, U. (2003). *System identification of Bogazici Suspension Brid*ge. (M.Sc. Thesis). Bogazici University, Istanbul.

Lau, C. K., Wong, K. Y., Chan, W. Y. K. and Man, K. L. D. (1999). The structural health monitoring system and structural health monitoring of cable-supported bridges, *International (ICE) Conference on Current and Future Trends in Bridge Design, Construction and Maintenance*.

Liu, S. C. and Yao, J. T. P. (1978). Structural identification concept, *Journal of Structural Engineering*, *104* (12), 1845-1858.

M. Karbhari, V. and Ansari, F. (2009). *Structural Health Monitoring of Civil Infrastructure Systems*. Woodhead Publishing.

Maeck, J. and De Roeck, G. (2003). Damage assessment using vibration analysis on the Z24-Bridge, *Mechanical Systems and Signal Processing*, *17* (1), 133-142.

Masri, S. F., Nakamura, M., Chassiakos, A. G. and Caughey, T. K. (1996). Neural network approach to detection of changes in structural parameters, *Journal of Engineering Mechanics*, *122* (4), 350-360.

Masri, S. F., Smyth, A. W., Chassiakos, A. G., Caughey, T. K. and Hunter, N. F. (2000). Application of neural networks for detection of changes in nonlinear systems, *Journal of Engineering Mechanics*, *126* (7), 666-676.

Apaydin, N. (2010). Earthquake performance assessment and retrofit investigations of two suspension bridges in Istanbul, *Soil Dynamics and Earthquake Engineering*, *30* (8), 702-710.

Messervey, T. and Frangopol, D. (2007). Bridge Live Load Effects Based on Statistics of Extremes Using on-site Load Monitoring. In D.M Frangopol, M.Kawatani, C-W. Kim (Eds.), *Reliability and Optimization of Structural Systems: Assessment, Design, and Life-Cycle Performance* (pp. 173-180): CRC Press.

Moon, F. L. and Aktan, A. E. (2006). Structural identification of constructed systems and the impact of epistemic uncertainty. *The Proceedings of the 3rd International Conference on Bridge Maintenance, Safety, and Management* (IABMAS), Porto, Portugal.

Mottershead, J. E. and Friswell, M. I. (1993). Model updating in structural dynamics: a survey, *Journal of Sound and Vibration*, *167* (2), 347-375.

Mufti, A. A. (2001). Guidelines for Structural Health Monitoring. Canada: ISIS

Mustafa, G. and Catbas, F. N. (2011). Damage assessment with ambient vibration data using a novel time series analysis methodology, *Journal of Structural Engineering*, *137* (12), 1518-1526.

Nakamura, M., Masri, S. F., Chassiakos, A. G. and Caughey, T. K. (1998). A method for non-parametric damage detection through the use of neural

networks, *Earthquake Engineering and Structural Dynamics*, *27* (9), 997-1010.

NASTRAN [Multidisciplinary Structural Analysis]. Newport Beach, CA, USA: MSC Software.

Natke, H. G., Cottin, N. and Prells, U. (1994). Problems and Related Counter-Measures in Mathematical Model Improvement. In G. I. Schueller, M. Shinozuka & J. T. P. Yao (Eds.), *Structural Safety and Reliability* (pp. 821-827). Rotterdam: Balkemea.

Natke, H. G. and Yao, J. T. P. (1988). System identification approaches in structural safety evaluation structural safety evaluation based on system identification approaches. Proceedings of the Workshop (pp. 460-473). Wiesbaden: Vieweg+Teubner Verlag.

Nigbor, R. L., Abdel-Ghaffar, A. M. and Masri, S. F. (1991). Dynamic Monitoring of suspension bridges. *The International Workshop of Technologies for Hong Kong's Infrastructures*, Hong Kong.

Patran [Complete FEA Modeling Solution]. Newport Beach, CA, USA: MSC software.

Petrovski, J. P., Paskalov, T., Stojkovich, A. and Jurokovski, D. (1974). Vibration studies of Istanbul Bogazici Suspension Bridge. Skopje. Yugoslavia: Eaarthquake Engineering and Engineering Seismology (IZIIS).

Rayleigh, L. (1945). *Theory of Sound*. Dover: New York, NY, USA.

Ren, W.-X., Harik, I. E., Blandford, G. E., Lenett, M. and Basehart, T. M. (2004). Roebling suspension bridge. II: Ambient testing and live-load response, Journal of Bridge Engineering, *9* (2), 119-126.

SAP2000 (v17). [Structural software for analysis and design]: Computers and Structures Inc.

Shinozuka, M. and Ghanem, R. (1995). Structural system identification II: experimental verification, *Journal of Engineering Mechanic, 121* (2), 265-273.

Sohn, H., Farrar, C. R., Hemez, F. M., Shunk, D. D., Stinemates, D. W., Nadler, B. R. and Czarnecki, J. J. (2003). A review of structural health monitoring literature: 1996–2001. New Mexico: Los Alamos National Laboratory.

Soyluk, K. and Sicacik, E. A. (2012). Soil–structure interaction analysis of cable-stayed bridges for spatially varying ground motion components, *Soil Dynamics and Earthquake Engineering*, *35*, 80-90.

Susoy, M., Catbas, F. N. and Frangopol, D. M. (2008). Evaluation of time-variant bridge reliability using structural health monitoring. *The 2008 IMAC-XXVI: Conference & Exposition on Structural Dynamics*, Orlando, FL, USA.

Tezcan, S., Ipek, M., Petrovski, J., Paskalov, T. and Durgunoglu, T. (1975). Ambient and forced vibration survey of Istanbul Bogazici Suspension Bridge, *The fifth European Conference on Earthquake Engineering*.

TSC-R. (2008). *Turkish Seismic Code for Coastal, Horbor, Railway and Transpoatation Structures*. Ankara: Ministry of Transport, Maritime Affairs and Communications.

TSC (2017). *Turkish Seismic Code*. Ankara: Republic of Turkey Prime Ministry Disaster and Emergency Management Authority.

Wang, H., Li, A. and Li, J. (2010). Progressive finite element model calibration of a long-span suspension bridge based on ambient vibration and static measurements, *Engineering Structures*, *32* (9), 2546-2556.

Wang, J., Carr, A. J., Cooke, N. and Moss, P. J. (2009). The response of a 344 m long bridge to non-uniform earthquake ground motions, *Engineering Structures*, *31* (11), 2554-2567.

Wenzel, H. (2009). *Health Monitoring of Bridge*s. Wiley.

Wong, K.-Y. (2007). Design of a structural health monitoring system for long-span bridges, *Structure and Infrastructure Engineerin*g, *3* (2), 169-185.

Wong, K. Y. (2001). Tsing Ma Bridge bearing Investigation, a memorandum to chief engineer of Tsing Ma control area regarding the investigation results. Hong Kong: Weather and Structural Health Monitring System (WASHMS).

Wong, K. Y., Lau, C. K. and Flint, A. R. (2000). Planning and implementation of the Structural Health Monitoring system for cable supported bridges in Hong- Kong, *The Nondestructive Evaluation of Highways, Utilities and Pipelines IV*, Newport Beach, CA, March 6.

Worden, K. (1997). Structural fault detection using a novelty measure, *Journal of Sound and Vibration*, *201* (1), 85-101.

Worden, K., Allen, D., Sohn, H. and Farrar, C. (2002). Extreme value statistics for damage detection in mechanical structures. Los Alamos, NM: Los Alamos National Laboratory.

Xu, Y.-L. and Xia, Y. (2011). *Structural Health Monitoring of Long-Span Suspension Bridges*. CRC Press.

Xu, Y. L. (2008). Making good use of structural health monitoring systems: Hong Kong's experience, T*he Second International Forum on Advances in Structural Engineering, Structural Disaster, Prevention, Monitoring and Control*, Dalian, China.

Yamada, H., Katsuchi, H. and Kitagawa, M. (2000). Field Measurement of wind property at Ohnaruto Bridge and the Akashi Kaikyo Bridge, The Workshop on Research and Monitoring of Long Span Bridges.

Yeung, C. K., Lau, C. K., Wong, K. Y., Flint, A. R. and McFadyen, A. N. (1995). Wind and Structural Health Monitoring System for Lantau Fixed Crossing, Part 1: system planning and design, *International Conference, 'Bridges into 21st Century*', Hong Kong.

Yun, H.-B., Masri, S. F., Wolfe, R. W. and Benzoni, G. (2009). Data-driven methodologies for change detection in large-scale nonlinear dampers with noisy eamsurements, *Journal of Sound and Vibration*, *322* (1–2), 336-357.

Zhao, B., Wang, Y., Chen, Z., Shi, Y., Jiang, Y. and Wang, Y. (2015). Research on the random seismic response analysis for multi- and large-span structures to multi-support excitations, E*arthquake Engineering and Engineering Vibration*, *14* (3), 527-538.

Zhu, Q., Xu, Y. L. and Xiao, X. (2015). Multiscale modeling and model updating of a cable-stayed bridge. I: modeling and influence line analysis, *Journal of Bridge Engineering*, *20* (10).

CURRICULUM VITAE

Name Surname **:** Selçuk BAŞ

Place and Date of Birth **:** Ankara/15.05.1986

E-Mail **:** selcukbas@itu.edu.tr

EDUCATION **:**

- **M.Sc (2009-2011)** **:** Istanbul Technical University, Structural Engineering
  Supervisor: Prof. Dr. Zekai CELEP
  Co-Supervisor: Assoc. Prof. Dr. Nurdan APAYDIN
- **Ph.D (2012-2017)** **:** Istanbul Technical University, Structural Engineering

PROFESSIONAL EXPERIENCE AND REWARDS:

- 2011-Continue, Research Assistant. at the Department of Civil Engineering, Bartın University
- Turkish Raod Association, The best journal paper in 2017, General Directorate of Turkish State Highways, Ankara, Turkey.
- Scientific Performance Awards in 2016 (Natural and Applied Science), Bartın University.
- Turkish Raod Association, The best M.Sc. Thesis in 2011, General Directorate of Turkish State Highways, Ankara, Turkey
- 2011 Completed M.Sc.at Istanbul Technical University

PUBLICATIONS, PRESENTATIONS AND PATENTS ON THE THESIS:

Journal

- **Bas, S., Apaydin N.M, Ilki A. and Catbas F.N.** (2017). Structural health monitoring system of the long-span bridges in Turkey, *Structure and Infrastructure Engineering* (Accepted).

Conference Paper/Proceeedings

- **Bas, S., Apaydin N. and Catbas, F.N.** (2017). Wind-induced modal identification of the Bosphorus Bridge using shm-structural health monitoring data, *The 39th IABSE Symposium-Engineering the Future*, Vancouver, B.C., Canada, Sep. 19-23. (Accepted).
- **Bas, S., Apaydin, N., Ilki, A. and Catbas, F. N.** (2017). Wind analysis of the Bosphorus Suspension Bridge: numerical and experimental investigation, *The 4th International Conference on Smart Monitoring, Assessment and Rehabilitation of Civil Structures,* Zurich, Switzerland, Sep. 13-15. (Accepted).
- **Bas, S., Apaydin, N., Ilki, A. and Catbas, F. N.** (2016). Structural health monitoring system-shms of the long-span bridges in Turkey, *The 8th International Conference on Bridge Maintenance, Safety and Management* (IABMAS 2016), Foz do Iguaçu, Brazil, June 26-30.
- **Bas, S., Apaydin N. and Catbas, F.N.** (2016). Considerations for finite element modeling of the Bosphorus Suspension Bridge, *Istanbul Bridge Conference 2016*, Istanbul, Turkey, August 8-10.
- **Bas, S., Apaydin N. and Catbas, F.N.** (2015). Long-span bridges: behavior under operational and extreme wind loads, *The 3rd Conference on Smart Monitoring, Assessment and Rehabilitation of Civil Structures*, Antalya, Turkey, Sept.7-9.